

VOLUME 76

JANUARY 20, 1972

NUMBER 2

JPCHAX

THE JOURNAL OF

PHYSICAL
CHEMISTRY

PUBLISHED BIWEEKLY BY THE AMERICAN CHEMICAL SOCIETY

THE JOURNAL OF PHYSICAL CHEMISTRY

BRYCE CRAWFORD, Jr., *Editor*

STEPHEN PRAGER, *Associate Editor*

ROBERT W. CARR, Jr., FREDERIC A. VAN-CATLEDGE, *Assistant Editors*

EDITORIAL BOARD: A. O. ALLEN (1970-1974), J. R. BOLTON (1971-1975), F. S. DAINTON (1972-1976), M. FIXMAN (1970-1974), H. S. FRANK (1970-1974), R. R. HENTZ (1972-1976), J. R. HUIZENGA (1969-1973), W. J. KAUFMANN (1969-1973), R. L. KAY (1972-1976), W. R. KRIGBAUM (1969-1973), R. A. MARCUS (1968-1972), W. J. MOORE (1969-1973), J. A. POPLE (1971-1975), B. S. RABINOVITCH (1971-1975), H. REISS (1970-1974), S. A. RICE (1969-1975), F. S. ROWLAND (1968-1972), R. L. SCOTT (1968-1972), R. SEIFERT (1968-1972), W. A. ZISMAN (1972-1976)

CHARLES R. BERTSCH, *Manager, Editorial Production*

AMERICAN CHEMICAL SOCIETY, 1155 Sixteenth St., N.W., Washington, D. C. 20036

FREDERICK T. WALL, *Executive Director*

Books and Journals Division

JOHN K. CRUM, *Director (Acting)*

JOSEPH H. KUNEY, *Head, Business Operations Department*

RUTH REYNARD, *Assistant to the Director*

©Copyright, 1972, by the American Chemical Society. Published biweekly by the American Chemical Society at 20th and Northampton Sts., Easton, Pa. 18042. Second-class postage paid at Washington, D. C., and at additional mailing offices.

All manuscripts should be sent to *The Journal of Physical Chemistry*, Department of Chemistry, University of Minnesota, Minneapolis, Minn. 55455.

Additions and Corrections are published once yearly in the final issue. See Volume 75, Number 26 for the proper form.

Extensive or unusual alterations in an article after it has been set in type are made at the author's expense, and it is understood that by requesting such alterations the author agrees to defray the cost thereof.

The American Chemical Society and the Editor of *The Journal of Physical Chemistry* assume no responsibility for the statements and opinions advanced by contributors.

Correspondence regarding accepted copy, proofs, and reprints should be directed to Editorial Production Office, American Chemical Society, 20th and Northampton Sts., Easton, Pa. 18042. Manager: CHARLES R. BERTSCH. Assistant Editor: EDWARD A. BORGER. Editorial Assistant: WILLIAM T. BOYD.

Advertising Office: Century Communications Corporation, 142 East Avenue, Norwalk, Conn. 06851.

Business and Subscription Information

Remittances and orders for subscriptions and for single copies,

notices of changes of address and new professional connections, and claims for missing numbers should be sent to the Subscription Service Department, American Chemical Society, 1155 Sixteenth St., N.W., Washington, D. C. 20036. Allow 4 weeks for changes of address. Please include an old address label with the notification.

Claims for missing numbers will not be allowed (1) if received more than sixty days from date of issue, (2) if loss was due to failure of notice of change of address to be received before the date specified in the preceding paragraph, or (3) if the reason for the claim is "missing from files."

Subscription rates (1972): members of the American Chemical Society, \$20.00 for 1 year; to nonmembers, \$60.00 for 1 year. Those interested in becoming members should write to the Admissions Department, American Chemical Society, 1155 Sixteenth St., N.W., Washington, D. C. 20036. Postage to Canada and countries in the Pan-American Union, \$5.00; all other countries, \$6.00. Single copies for current year: \$3.00. Rates for back issues from Volume 56 to date are available from the Special Issues Sales Department, 1155 Sixteenth St., N.W., Washington, D. C. 20036.

This publication and the other ACS periodical publications are now available on microfilm. For information write to: MICROFILM, Special Issues Sales Department, 1155 Sixteenth St., N.W., Washington, D. C. 20036.

THE JOURNAL OF PHYSICAL CHEMISTRY

Volume 76, Number 2 January 20, 1972

JPCHAx 76(2) 143-284 (1972)

Thermal Decomposition of 3,4-Dimethylhexane, 2,2,3-Trimethylpentane, <i>tert</i> -Butylcyclohexane, and Related Hydrocarbons	Wing Tsang	143
Electron Spin Resonance Study of the $\text{SO}_2^{\cdot -}$ Formation in the Thermal Decomposition of Sodium Dithionite, Sodium and Potassium Metabisulfite, and Sodium Hydrogen Sulfite	Edward G. Janzen	157
Transfer Diffusion. III. Kinetics and Mechanism of the Triiodide-Iodide Exchange Reaction	I. Ruff, V. J. Friedrich, and K. Csillag	162
The Photochemistry of Benzene in Oxygenated Aqueous Solution in the $^1\text{B}_{2u}$ First Excited Singlet State	Menahem Luria and Gabriel Stein	165
Chlorophyll-Poly(vinylpyridine) Complexes. IV. Transfer of Energy to a Complex of Pyrochlorophyll with DTNB	G. R. Seely	172
The Photolysis of Hydroxylamine in Aqueous Solution	D. Behar, D. Shapira, and A. Treinin	180
Electronegativity Effects in T-for- CH_2X Substitutions for Recoil Tritium Reactions with <i>n</i> -Propyl Fluoride	Thomas Smal, Bartyra Arezzo, and F. S. Rowland	187
Temperature Dependence of the Reaction Yields from Recoil Tritium Reactions. II. Tritium Atom Addition to 1-Butene and <i>cis</i> -2-Butene	Richard Kushner and F. S. Rowland	190
Measurement of Excited Singlet Yields in γ Radiolysis of Benzene and Ketones. The Radiation-Induced "Type-II" Elimination of 4-Methyl-4-phenyl-2-pentanone	Bizhan M. Zarnegar and David G. Whitten	198
Pulse Radiolysis of Sodium Metaphosphate Glasses	Aaron Barkatt, Michael Ottolenghi, and Joseph Rabani	203
Stereochemistry of the Silver-Catalyzed Epoxidation of Olefins	W. F. Richey	213
Temperature Dependence of the Kerr Constant of Water	Yeong-jgi Chen and William H. Orttung	216
The External Heavy Atom Effect on the Phosphorescence Spectra of Some Halonaphthalenes	Linda G. Thompson and S. E. Webber	221
The Triplet States of Biphenylene	F. Peradejordi, C. Tétreau, and D. Lavalette	225
A Molecular Orbital Calculation of Chemically Interacting Systems. Bimolecular Nucleophilic Substitution	Kenichi Fukui, Hiroshi Fujimoto, and Shinichi Yamabe	232
Low Pressure Ultrafiltration of Sucrose and Raffinose Solutions with Anisotropic Membranes	R. W. Baker, F. R. Eirich, and H. Strathmann	238
Standard Potential of the Ferrocene-Ferricinium Electrode in Pyridine. Evaluation of Proton Medium Effect	L. M. Mukherjee	243
A Nuclear Magnetic Resonance Study of Acid-Base Interactions for the Chloranil Electrode System in Acetonitrile	N. F. Hepfinger, R. P. T. Tomkins, and P. J. Turner	246
Effect of Pressure on Charge-Transfer Complexes in Solution. II. Complexes Formed between Ions and between Ions and Neutral Molecules	A. H. Ewald and J. A. Scudder	249
Dilatometric Studies of Counterion Binding by Polycarboxylates	A. James Begala and Ulrich P. Strauss	254
Infrared Optical Constants and Absorption Intensities of Naphthalene Single Crystal	Koji Tsuji and Haruka Yamada	260
Mass Spectrometric Study of the Reaction of Dicyanoacetylene with Oxygen Atoms	Clifford W. Hand and Ralph H. Obenauf, Jr.	269
Transitions in Mesophase-Forming Systems. III. Transformation Kinetics and Textural Changes in Cholesteryl Nonanoate	Fraser P. Price and Joachim H. Wendorff	276

NOTES

- Carbon-13 Nuclear Magnetic Resonance Relaxation in Hemimellitene and Isodurene
 Terry D. Alger, David M. Grant, and Robin K. Harris 281

COMMUNICATIONS TO THE EDITOR

- Rate Constants, Threshold Energies, and Energy Partitioning for Three and Four Centered Hydrogen Chloride
 Elimination Reactions of 1,1,2-Trichloroethane-1-*d*₁ K. C. Kim and D. W. Setser 283

AUTHOR INDEX

- | | | | | |
|--|--|---|---|---|
| Alger, T. D., 281
Arezzo, B., 187

Baker, R. W., 238
Barkatt, A., 203
Begala, A. J., 254
Behar, D., 180

Chen, Y., 216
Csillag, K., 162

Eirich, F. R., 238
Ewald, A. H., 249
Friedrich, V. J., 162 | Fujimoto, H., 232
Fukui, K., 232

Grant, D. M., 281

Hand, C. W., 269
Harris, R. K., 281
Hepfinger, N. F., 246

Janzen, E. G., 157

Kim, K. C., 283
Kushner, R., 190 | Lavalette, D., 225
Luria, M., 165

Mukherjee, L. M., 243

Obenauf, R. H., Jr., 269
Orttung, W. H., 216
Ottolenghi, M., 203

Peradejordi, F., 225
Price, F. P., 276

Rabani, J., 203
Richey, W. F., 213 | Rowland, F. S., 187, 190
Ruff, I., 162

Scudder, J. A., 249
Seely, G. R., 172
Setser, D. W., 283
Shapira, D., 180
Smail, T., 187
Stein, G., 165
Strathmann, H., 238
Strauss, U. P., 254

Tétreau, C., 225
Thompson, L. G., 221 | Tomkins, R. P. T., 246
Treinin, A., 180
Tsang, W., 143
Tsuji, K., 260
Turner, P. J., 246

Webber, S. E., 221
Wendorff, J. H., 276
Whitten, D. G., 198

Yamabe, S., 232
Yamada, H., 260
Zarnegar, B. M., 198 |
|--|--|---|---|---|

In papers with more than one author the name of the author to whom inquiries about the paper should be addressed is marked with an asterisk in the by-line.

Thermal Decomposition of 3,4-Dimethylhexane, 2,2,3-Trimethylpentane, *tert*-Butylcyclohexane, and Related Hydrocarbons

by Wing Tsang

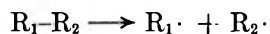
National Bureau of Standards, Washington, D. C. 20234 (Received August 2, 1971)

Publication costs assisted by National Bureau of Standards

3,4-Dimethylhexane, 2,2,3-trimethylpentane, and *tert*-butylcyclohexane have been decomposed in a single-pulse shock tube. Rate expressions for the main bond-breaking steps are: $k(sec-C_4H_9-sec-C_4H_9 \rightarrow 2sec-C_4H_9\cdot) = 10^{16.24} \exp(-37,900/T) \text{ sec}^{-1}$; $k(sec-C_4H_9-tert-C_4H_9 \rightarrow sec-C_4H_9\cdot + tert-C_4H_9\cdot) = 10^{16.20} \exp(-36,400/T) \text{ sec}^{-1}$; and $k(tert-C_4H_9-c-C_6H_{11} \rightarrow tert-C_4H_9\cdot + c-C_6H_{11}\cdot) = 10^{16.31} \exp(-37,300/T) \text{ sec}^{-1}$. They lead to $\Delta H_{f,300}(sec-C_4H_9\cdot) = 55 \text{ kJ/mol}$ (13.2 kcal/mol), $\Delta H_{f,300}(tert-C_4H_9\cdot) = 39 \text{ kJ/mol}$ (9.3 kcal/mol), and $\Delta H_{f,300}(c-C_6H_{11}\cdot) = 66 \text{ kJ/mol}$ (15.8 kcal/mol). Rate expressions for the decomposition of all hydrocarbons formed from *sec*-butyl or cyclohexyl radicals and methyl, ethyl, isopropyl, *tert*-butyl, *tert*-amyl, allyl, 1-methylallyl, propynyl, and benzyl radicals have been calculated. Estimates are given for the rates of decomposition of hydrocarbons formed from *n*-propyl radicals and any of the compounds listed above. The accumulated single-pulse shock tube data can now give quantitative information on the initial cracking patterns of almost all aliphatic hydrocarbons. The *A* factors determined in this study provide striking confirmation for the earlier observation that this value, per C-C bond, for alkanes is a constant. On this basis, it appears that $D(tert-C_5H_{11}-H) - D(tert-C_4H_9-H) = 5.4 \text{ kJ/mol}$; $D(sec-C_4H_9-H) - D(i-C_3H_7-H) = 3.5 \text{ kJ/mol}$; $D(n-C_3H_7-H) - D(C_2H_5-H) \sim -1.5 \text{ kJ/mol}$. The absolute magnitude of the *A* factors are all at least a factor of 10 lower than expected. It is demonstrated that recent chemical activation and very low pressure pyrolysis studies support the shock tube results.

Introduction

This is the sixth^{1,2} of a series of papers on hydrocarbon decomposition. Previous investigations have determined the rate constants and parameters for the reaction



where $R_1\cdot$ and $R_2\cdot$ may be any of the following radicals: methyl, ethyl, isopropyl, *tert*-butyl, *tert*-amyl, allyl, 1-methylallyl, benzyl, and propynyl. This has led to a determination of the heats of formation of these radicals. In addition, it appears that the preexponential factors or entropies of activation for all the alkanes studied are constant ($\sim 10^{16.2} \text{ sec}^{-1}$) and are considerably lower than expected.^{1,2} The present study is concerned with the mechanism and rates of decomposition

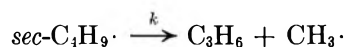
of 3,4-dimethylhexane, 2,3,3-trimethylpentane, and *tert*-butylcyclohexane. Primary attention will be focused in the reactions that form *sec*-butyl and cyclohexyl radicals. Their heats of formation as well as rate parameters for bond breaking of all the hydrocarbons formed from either of these two species and any of the radicals listed above can then be determined. Comparisons with the earlier results on 2,3-dimethylbutane and 2,2,3-trimethylbutane decomposition will lead to additional information on the effects of β -methylation on carbon-carbon bond strength. Also of interest will be the relative importance of the various modes of decomposition of *sec*-butyl and cyclohexyl radicals. Fi-

(1) W. Tsang, *J. Chem. Phys.*, **43**, 352 (1965); **44**, 4283 (1966); **46**, 2187 (1966).

(2) W. Tsang, *Int. J. Chem. Kinet.*, **1**, 245 (1969); **2**, 23 (1970).

nally, the heat of formation of *tert*-butyl radicals will be redetermined.

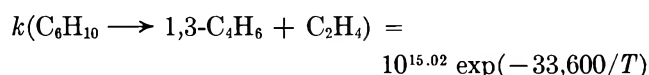
There have been no previous studies on the thermal decomposition of 3,4-dimethylhexane, 2,2,3-trimethylpentane, and *tert*-butylcyclohexane. The heat of formation of *sec*-butyl radical has been determined by Chekhov, Tsulingol's, and Ioffe³ using an iodination technique. Their results have been interpreted by Golden and Benson⁴ as consistent with $\Delta H_{f,300}(\text{sec-C}_4\text{H}_9\cdot) = 54.3 \text{ kJ/mol}$ (with an uncertainty of 5–10 kJ). For cyclohexyl radicals, Kerr⁵ gives $\Delta H_{f,300}(\text{C}_6\text{H}_{11}\cdot) = 54 \pm 13 \text{ kJ/mol}$. This is based on the abstraction of hydrogen atom from cyclohexane by methyl radical⁵ and a Polanyi plot. Lin and Laidler⁶ have shown that at temperatures below 600°K the predominant mode of *sec*-butyl radical decomposition is *via* the reaction



where $k = 10^{14} \exp(-16,300/T) \text{ sec}^{-1}$. No previous work on the mechanism and rate of decomposition of cyclohexyl radicals can be found.

Experimental Section

All of the studies have been carried out in a single-pulse shock tube. The experimental equipment and procedure have been described in earlier communications.⁷ Quantitative data are obtained from the comparative rate technique using the decyclization reaction of cyclohexene⁸



as the standard.⁹ This method involves the simultaneous decomposition of two compounds by the same reflected shock wave and the determination of the respective rate constants for decomposition. From a series of experiments, a relationship between the two sets of rate constants can be derived. If the rate parameters of one of these processes are well known, the other set of values can be easily determined. Thus, the usual uncertainty in shock tube temperature is eliminated. In addition, the extremely short residence time (<1 msec) and the low concentrations of the substances to be pyrolyzed ($\leq 0.02\%$), together with the presence of toluene (1%) ensure the suppression of all possible chain or cross reaction processes. A more quantitative discussion of these factors can be found in earlier communications.^{1,2}

The 2,2,3-trimethylpentane, 3,4-dimethylhexane, and *tert*-butylcyclohexane are all of a stated purity of 99% or better and have been purchased from Chemical Samples Co.¹⁰ "Chromatoquality" grade cyclohexene, "Research" grade toluene, and "Ultrahigh Purity" argon and all the other chemicals have been used without further purification. Gas chromatographic analysis are carried out with 12-ft ethylhexasebacate and β,β' -

oxidipropionitrile columns (at 30 and 0°, respectively) with hydrogen flame ionization detection.

Results

(a) *2,2,3-Trimethylpentane*. The initial experiments have been carried out with a 0.01% mixture in the absence of the standard compound but with 1% toluene present. The results are given in Table I. Large quantities of methane, C₂ hydrocarbons, and benzene are also present. Except for ethylene, these compounds are by-products of the primary decomposition reaction. Their modes of formation have been discussed in detail in earlier communications and need not be considered further. For the present purposes the data in Table I can be accounted for by the reaction mechanism given in Figure 1. The main reaction involves the cleavage of the most highly substituted carbon-carbon bond with the resulting formation of *sec*-butyl and *tert*-butyl radicals. Almost all of the latter decomposes into isobutene and a hydrogen atom. The primary mode of *sec*-butyl radical decomposition is to produce propylene and methyl radical. It is about 11–12 times faster than the processes which involve the ejection of a hydrogen atom. For the latter reaction, removal of a secondary hydrogen atom is favored over that of a primary hydrogen by a factor of about 3. Aside from these numbers, the quality of the data does not permit a meaningful determination of the temperature dependence between the concurrent processes.

Two secondary processes the ejection of a tertiary methyl radical and a secondary ethyl radical are also of some importance. Unfortunately, since their possible reaction products are for the most part similar, it is not possible to distinguish between the two processes. All that can be said is that the sum total rate of these two processes is about one-fifth as fast as the primary reaction.

The results of comparative rate studies between 2,2,3-trimethylpentane and cyclohexene are summarized in Figure 2. The rate constant for cyclohexene decomposition is derived from the expression

(3) E. E. Chekhov, A. L. Tsulingol's, and I. I. Ioffe, *Neftekhimiya*, **7**, 717 (1967); *Chem. Abstr.*, **67**, 48759k (1968).

(4) D. M. Golden and S. W. Benson, *Chem. Rev.*, **69**, 125 (1969).

(5) J. A. Kerr, *ibid.*, **66**, 469 (1966).

(6) M. C. Lin and K. J. Laidler, *Can. J. Chem.*, **45**, 1315 (1967).

(7) W. Tsang, *J. Chem. Phys.*, **40**, 1171, 2487 (1964).

(8) W. Tsang, *ibid.*, **42**, 1805 (1965).

(9) In a recent study, using the decyclization reaction of ethylcyclobutane as a standard cyclohexene decomposition rate has been found to be $k(\text{C}_6\text{H}_{10} \rightarrow 1,3\text{-C}_4\text{H}_6 + \text{C}_2\text{H}_4) = 10^{15.30} \exp(-33,690/T) \text{ sec}^{-1}$. The present value is based on an isopropyl bromide dehydrobromination standard and has been used in all previous studies. It is employed here purely for the sake of consistency.

(10) Certain commercial materials and equipment are identified in this paper in order to specify adequately the experimental procedure. In no case does such identification imply recommendation or endorsement by the National Bureau of Standards, nor does it necessarily imply that the material or equipment identified is necessarily the best available for the purpose.

Table I: Distribution of Higher Hydrocarbons Formed during 2,2,3-Trimethylpentane Decomposition (0.01% 2,2,3-trimethylpentane in 1% toluene and argon)

$\frac{100[\text{C}_8\text{H}_{18}]_t}{[\text{C}_8\text{H}_{18}]_i}$	$\frac{100[i\text{-C}_4\text{H}_8]_t^a}{[\text{C}_8\text{H}_{18}]_i}$	$\frac{100[\text{tert-C}_4\text{H}_8\text{-}2]_t}{[\text{C}_8\text{H}_{18}]_i}$	$\frac{100[c\text{-C}_4\text{H}_8\text{-}2]_t}{[\text{C}_8\text{H}_{18}]_i}$	$\frac{100[\text{C}_6\text{H}_{10}]_t^b}{[\text{C}_8\text{H}_{18}]_i}$	$\frac{100[\text{C}_6\text{H}_{12}]_t^c}{[\text{C}_8\text{H}_{18}]_i}$	$\frac{100[\text{C}_8\text{H}_{18}]_t}{[\text{C}_8\text{H}_{18}]_i}$	t , μsec	$k(\text{C}_8\text{H}_{18})$, sec^{-1}	T , ^d $^\circ\text{K}$	ρ , ^d mm (NTP)
41.3	43.5	1.3	0.8	8.1			800	800	1180	455
9.5	10.5	0.3	0.2				800	145	1116	432
1.7	1.8	0.04	0.03				850	22	1057	413
1.4	1.5	0.05	0.03				800	19	1051	385
7.3	7.9	0.27	0.18				850	94	1102	1230
23.2	25.0	0.80	0.53	4.3			850	360	1150	1250
25.6	27.5			4.6	0.9	66	850	406	1157	448
4.3	4.7			0.8	0.17	96	850	57	1084	420
35.0	37.5			6.5	1.2	54	850	610	1165	450
4.9	5.3			0.8			850	64	1090	425
21.6	23.3			3.8	0.8	67	750	380	1160	1260

^a Also include small quantity of 1-butene. ^b 2-Methylbutene-2. ^c 2-Methylpentene-2. ^d Temperature was calculated assuming $k(\text{C}_8\text{H}_{18}) = 10^{16.30} \exp(-36,400/T) \text{ sec}^{-1}$. Density was calculated using the temperature and the gas dynamic properties of the system.

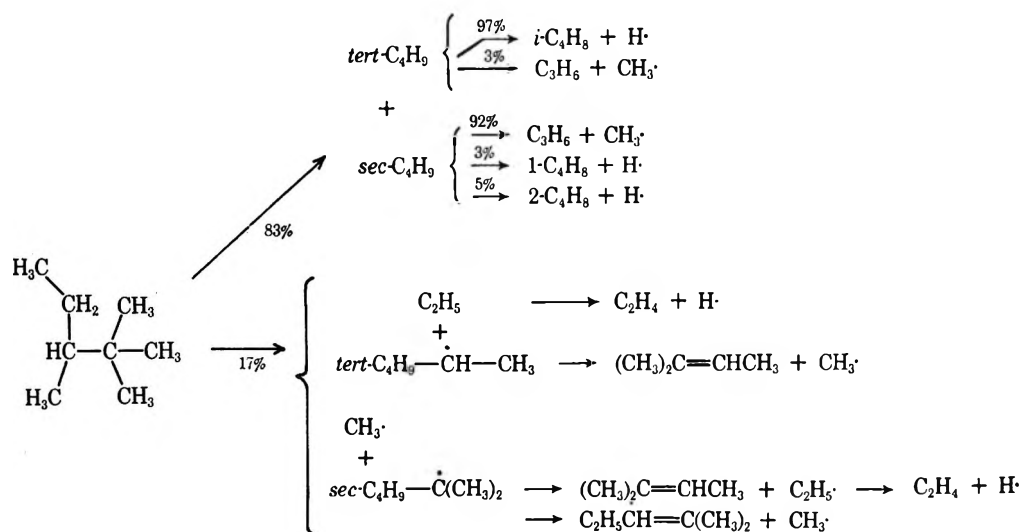


Figure 1. Mechanism for the decomposition of 0.01% 2,2,3-trimethylpentane in 1% toluene and argon at 1100°K. Percentages represent estimated importance of reaction pathway.

$$-k(\text{C}_8\text{H}_{10} \rightarrow 1,3\text{-C}_4\text{H}_8 + \text{C}_2\text{H}_4) = \frac{1}{t} \ln \left\{ 1 - \frac{[1,3\text{-C}_4\text{H}_8]_t}{[\text{C}_8\text{H}_{10}]_i} \right\}$$

while the appropriate equation for the main reaction in 2,2,3-trimethylpentane decomposition is

$$-k(\text{tert-C}_4\text{H}_9\text{-sec-C}_4\text{H}_9 \rightarrow \text{tert-C}_4\text{H}_9\cdot + \text{sec-C}_4\text{H}_9\cdot) = \frac{1}{tX} \ln \left\{ 1 - 1.03 \frac{[i\text{-C}_4\text{H}_8]_t}{[\text{C}_8\text{H}_{18}]_i} X \right\}$$

where $X = 1 + (\text{C}_6\text{H}_{10})_t / 1.03(i\text{-C}_4\text{H}_8)_t + (\text{C}_6\text{H}_{12})_t / 1.03(i\text{-C}_4\text{H}_8)_t \sim 1.2$. In these expressions $k(\)$ is the rate constant, t is the residence time, $(\)_t$ is the final concentration, and $(\)_i$ is the initial concentration. The number 1.03 takes into account the earlier obser-

vation that about 3% of the decomposition products of *tert*-butyl radicals are due to propylene and methyl radical formation. A least-squares analysis of the data resulted in the following rate relationship

$$\log k(\text{tert-C}_4\text{H}_9\text{-sec-C}_4\text{H}_9 \rightarrow \text{tert-C}_4\text{H}_9\cdot + \text{sec-C}_4\text{H}_9\cdot) = (1.083 \pm 0.004)$$

$$\log k(\text{C}_8\text{H}_{10} \rightarrow 1,3\text{-C}_4\text{H}_8 + \text{C}_2\text{H}_4) + (0.082 \pm 0.006)$$

Using the rate expression for cyclohexene decomposition given earlier, this leads to

$$k(\text{tert-C}_4\text{H}_9\text{-sec-C}_4\text{H}_9 \rightarrow \text{tert-C}_4\text{H}_9\cdot + \text{sec-C}_4\text{H}_9\cdot) = 10^{16.30 \pm 0.07} \exp(-36,400 \pm 140/T) \text{ sec}^{-1}$$

The uncertainties are least-squares deviations. The actual estimated error limits are more of the order of

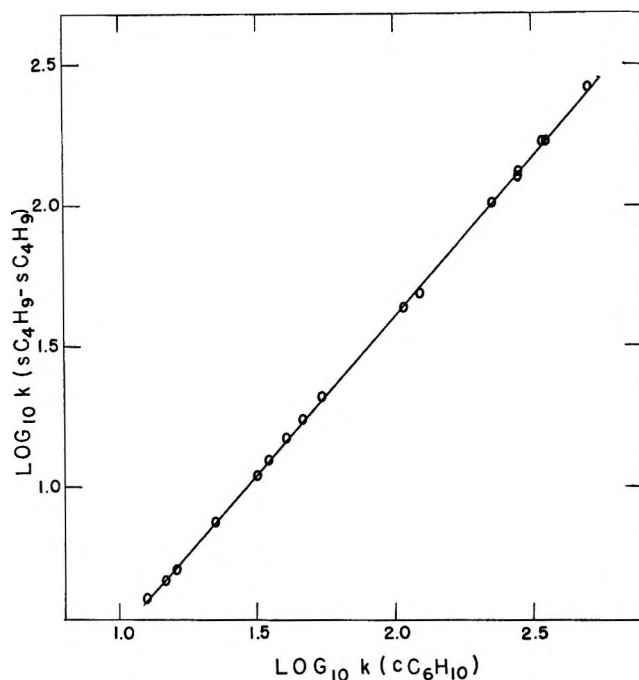
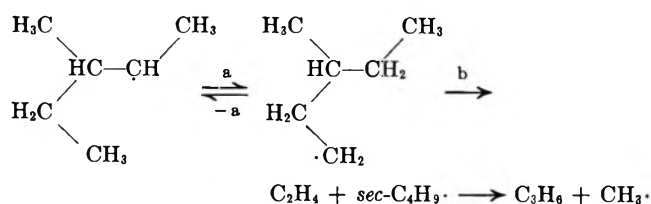


Figure 2. Comparative rate study of the thermal decomposition of 2,2,3-trimethylpentane (0.01%) and cyclohexene (0.01%) in 1% toluene and argon.

$10^{\pm 0.3} \text{ sec}^{-1}$ in the preexponential factor and 6 kJ in activation energy. As noted previously, this includes the uncertainties in the rate expression for the standard reaction.

(b) *3,4-Dimethylhexane*. The pyrolysis of a mixture of 0.02% 3,4-dimethylhexane in 1% toluene and argon results in the product distribution as given in Table II. As before, large quantities of methane and C_2 hydrocarbons can be detected but will not be considered in the present analysis on the basis of the reasons given earlier. The mechanism which is in accord with such results can be found in Figure 3. Once again, scission of the most highly substituted carbon-carbon bond is followed by the rapid decomposition of the newly formed *sec*-butyl radicals into propylene (main product) and the butenes. Two side reactions, the ejection of secondary methyl and ethyl radicals, have also been observed. It is not possible to distinguish between these two processes. Together, the sum of their rates is about 60% of the main mode of decomposition. Note that in this analysis the possibility of intramolecular hydrogen atom transfer has been neglected. This is a source of uncertainty. For example, in 3-methylpentyl-2 radical decomposition the following reaction sequence is possible



Since propylene concentration is used as the measure of the extent of the main reaction, such neglect will tend to exaggerate its importance. On the other hand, if the results of Lin and Laidler⁶ for *sec*-butyl radical decomposition given above and those of Endrenyi and LeRoy¹¹ on the isomerization of *n*-pentyl radicals

$$k(n\text{-C}_5\text{H}_{11} \cdot \longrightarrow \text{sec-C}_5\text{H}_{11} \cdot) = 10^{7.2} \exp(-540/T) \text{ sec}^{-1}$$

can be taken as representative of the processes of interest, this will mean that the bond-breaking reaction of 3-methylpentyl-2 radical is about 100 times faster than the isomerization process. Furthermore, this is likely to be a conservative estimate since for the isomerization reaction the reverse process ($-a$) is probably faster. Thus, errors introduced by the present procedure are probably not important.

The results of comparative rates studies between the principal mode of decomposition of 3,4-dimethylhexane and cyclohexene are summarized in Figure 4. The rate expression for cyclohexene pyrolysis is as given earlier. For the other system the appropriate expression is

$$-k = \frac{1}{t(X)} \ln \left(1 - \frac{1.08(\text{C}_3\text{H}_6)_f}{2(\text{C}_8\text{H}_{18})_i} X \right)$$

where

$$X = 1 + \frac{2(\text{C}_4\text{H}_8-2)_f'}{1.08(\text{C}_3\text{H}_6)_f} + \frac{2(\text{C}_5\text{H}_{10})_f}{1.08(\text{C}_3\text{H}_6)_f} + \frac{2(\text{C}_6\text{H}_{10})_f}{1.08(\text{C}_3\text{H}_6)_f} \sim 1.6$$

Note that in the present case $(\text{C}_4\text{H}_8-2)_f'$ refers to the butene-2 compounds that originate from the secondary reaction. The factors 1.08 and 2 reflect the fact that the decomposition of *sec*-butyl radicals result in the formation of small amounts of the butenes and that two *sec*-butyl radicals are formed from the decomposition of each 3,4-dimethylhexane molecule. All the other expressions are as defined earlier. A least-squares analysis of the data yields the following rate relationship.

$$\log k(\text{sec-C}_4\text{H}_9\text{-sec-C}_4\text{H}_9 \longrightarrow$$

$$2\text{sec-C}_4\text{H}_9 \cdot) = (1.131 \pm 0.005) \times$$

$$\log k(\text{C}_6\text{H}_{10} \longrightarrow 1,3\text{-C}_4\text{H}_6 + \text{C}_2\text{H}_4) - (0.648 \pm 0.009)$$

From the previously determined expression for $k(\text{C}_6\text{H}_{10})$, this leads to

$$k(\text{sec-C}_4\text{H}_9 \cdot)_2 \longrightarrow 2\text{sec-C}_4\text{H}_9 \cdot =$$

$$10^{16.34 \pm 0.08} \exp(-37,900 + 160/T) \text{ sec}^{-1}$$

The uncertainty limits are as given earlier.

(c) *tert*-Butylcyclohexane. The shock induced decomposition of a mixture of 0.02% *tert*-butylcyclohexane in 1% toluene and argon results in the formation of large quantities of isobutene and 1,3-butadiene.

(11) L. Endrenyi and D. J. LeRoy, *J. Phys. Chem.*, **70**, 4081 (1966).

Table II: Distribution of Higher Hydrocarbons Formed during 3,4-Dimethylhexane Decomposition (0.02% 3,4-dimethylhexane in 1% toluene and argon)

$100[\text{C}_2\text{H}_6]_f$ [C_2H_6] _i	$100[t\text{-C}_4\text{H}_{10}]_f$ [C_4H_{10}] _i	100- [$\text{tert-C}_4\text{H}_9$] _f [C_4H_9] _i	100- [$c\text{-C}_4\text{H}_9$] _f [C_4H_9] _i	100[$c,tert\text{-C}_6\text{H}_{10-2}$] _f [C_6H_{10}] _i	100[$c,tert\text{-C}_6\text{H}_{10-2}$] _f [C_6H_{10}] _i	100[C_8H_{18}] _f [C_8H_{18}] _i	t , μsec	$k(\text{C}_8\text{H}_{18})$	T_1^a , $^\circ\text{K}$	ρ_1^a , mm Hg (STP)
4.0	0.14	0.56	0.38	0.37	~0.08		900	24.3	1100	429
2.4	0.08	0.34	0.24	0.22			900	14.4	1088	425
20.2	0.60	3.0	2.2	2.1	~0.3		900	133	1161	451
4.2	0.12	0.6	0.4	0.41			900	24.8	1100	429
1.4	0.06	0.2	0.14	0.12			900	8.4	1070	1250
2.2	0.08	0.36	0.28	0.25			900	13.0	1084	1190
13.8	0.46	2.2	1.5	1.5			900	86.5	1141	1160
0.76	0.03	0.12	0.08	0.07			850	4.9	1052	410
30.0	0.94	4.6	3.2	3.3	~0.5	76	800	234	1180	462
0.52	0.02	0.08	0.05	0.06			900	3.1	1040	408
2.62	0.08	0.38	0.26	0.22			900	15.7	1090	425
7.6	0.20	1.08	0.78	0.77			900	46.8	1125	437
11.4	0.34	1.68	1.18	1.18	~0.14	92	900	71	1135	440

^a Temperature was calibrated assuming $k(\text{C}_8\text{H}_{18}) = 10^{16.34} \exp(-37,900/T) \text{ sec}^{-1}$. Density was calculated from the temperature and gas dynamic properties of the system.

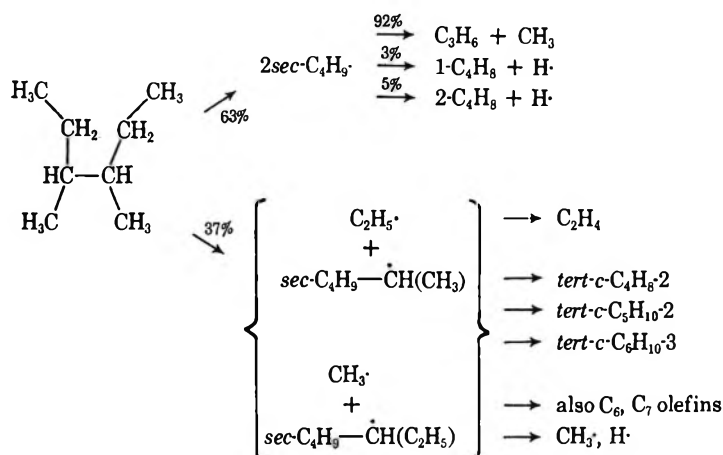
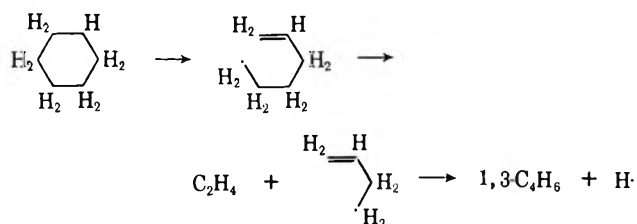


Figure 3. Mechanism for the decomposition of 0.02% 3,4-dimethylhexane in 1% toluene and argon at 1100°K. Percentages represent estimated importance of reaction pathway.

Aside from sizable amounts of methane, C_2 hydrocarbons, and benzene which are mostly secondary products (see earlier discussions) and are of no kinetic consequence in the present content, smaller quantities of propylene, isoprene, and cyclohexene are detectable. Traces of various pentadienes and methylated cyclopentenes are probably also present. Unfortunately at the time of these experiments the absence of the necessary standards prevented positive identification or quantification. Nevertheless, it is clear that the concentration of these substances is considerably lower than that of isoprene and cyclohexene (between a factor of 3 to 5) and thus can be ignored in the quantitative analysis of the main reaction process. The relevant data are summarized in Table III.

A mechanism which is in accord with the above results is given in Figure 5. The main reaction is once again the cleavage of the most highly substituted car-

bon-carbon bond. *tert*-Butyl and cyclohexyl radicals are formed. The former decomposes rapidly into isobutene and trace quantities of propylene (~3%). Thus, a determination of the rate of isobutene formation serves as an excellent marker for the rate of the main reaction. The principal decomposition product of cyclohexyl radical is 1,3-butadiene. This must arise for the most part from the following process



The direct hydrogen atom expulsion reaction, resulting in the formation of cyclohexene can also produce 1,3-

Table III: Distribution of Higher Hydrocarbons Formed during Tetrabutylcyclohexane Decomposition (0.02% *tert*-butylcyclohexane in 1% toluene and argon)

$\frac{100[\text{C}_6\text{H}_6]_f}{[\text{C}_{10}\text{H}_{20}]_i}$	$\frac{100[i\text{-C}_4\text{H}_8]_f}{[\text{C}_{10}\text{H}_{20}]_i}$	$\frac{100[1,3\text{-C}_4\text{H}_6]_f}{[\text{C}_{10}\text{H}_{20}]_i}$	$\frac{100[\text{isoprene}]_f}{[\text{C}_{10}\text{H}_{20}]_i}$	$\frac{100[c\text{-C}_6\text{H}_{10}]_f}{[\text{C}_{10}\text{H}_{20}]_i}$	$t, \mu\text{sec}$	$k[\text{C}_{10}\text{H}_{20}]$	$T, ^\circ\text{K}$	$\rho, \text{mm Hg (STP)}$
2.63	20.8	13.2	0.7	1.7	850	285	1170	460
0.34	2.8	1.6			850	34	1095	425
1.58	12.6	7.9	0.4	1.3	850	163	1148	445
0.37	3.0	1.7	~0.06	0.3	850	37	1100	430
4.75	35.4	25.5	1.6	1.8	850	540	1192	465
0.45	4.25	2.35	1.0	0.4	900	50	1110	1300
0.06	0.33	0.17			850	4	1031	405

^a Temperature was calculated assuming $k(\text{C}_{10}\text{H}_{20}) = 10^{16.31} \exp(-37,300/T) \text{ sec}^{-1}$. Density was calculated from the temperature and gas dynamic properties of the system.

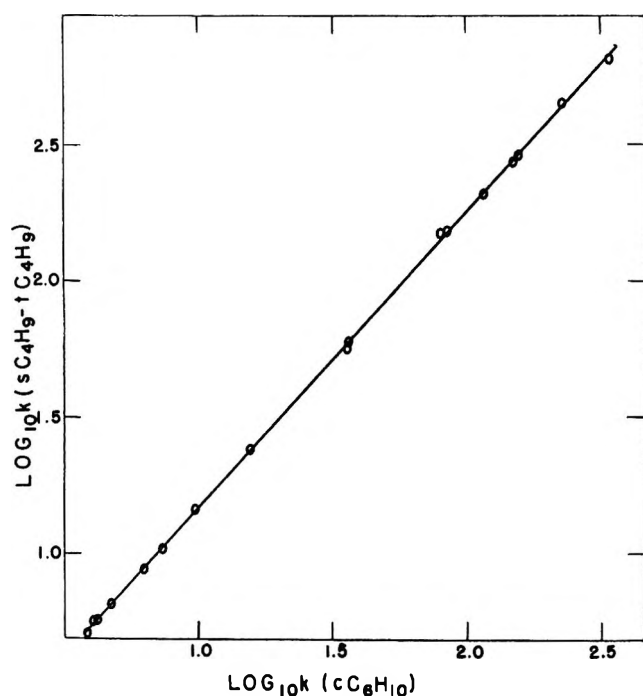
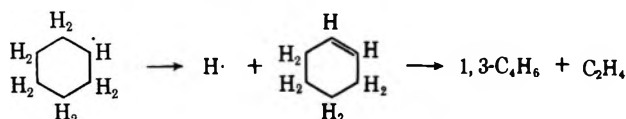


Figure 4. Comparative rate study of the thermal decomposition of 3,4-dimethylhexane (0.01%) and cyclohexene (0.01%) in 1% toluene and argon.

butadiene. The reaction sequence is



Fortunately, the rate constants for cyclohexene decomposition are precisely the numbers being used as "standards" for these studies and thus are extremely reliable. From the subsequent results on *tert*-butylcyclohexane decomposition it can be seen that the two sets of rate constants are almost equal. Thus, at low extent of *tert*-butylcyclohexane pyrolysis most of the newly formed cyclohexene molecules are not decomposed. At higher temperatures the decyclization reaction is of

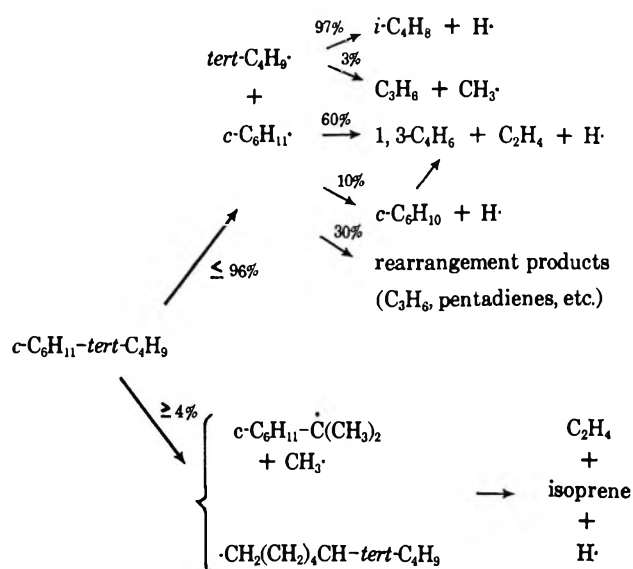
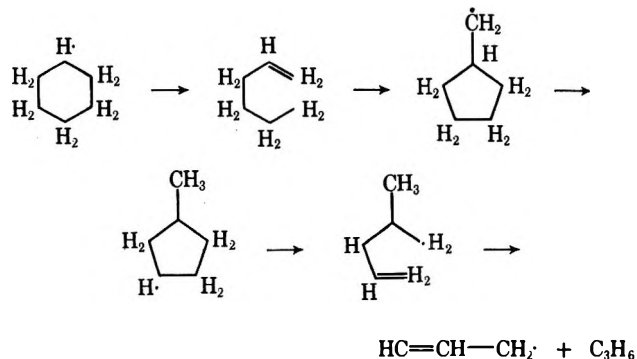


Figure 5. Mechanism for the decomposition of 0.02% *tert*-butylcyclohexane in 1% toluene and argon at 1100°K. Percentages represent estimated importance of reaction pathway.

major importance. Nevertheless, the sum of the cyclohexene and butadiene concentration remain at all times less than the isobutene concentration. This is evidence that some cyclohexyl radicals survive the reaction period and/or that some undergo a variety of other decomposition processes. One such possibility is as follows



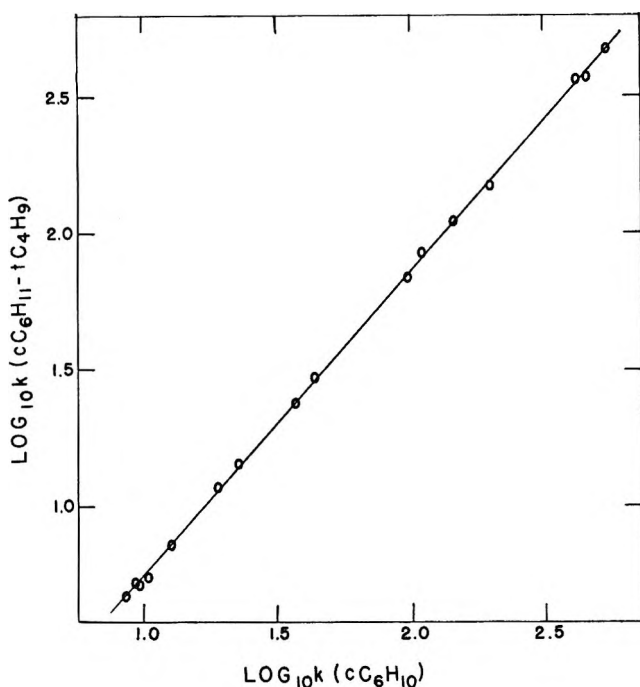


Figure 6. Comparative rate study of the thermal decomposition of *tert*-butylcyclohexane (0.01%) and cyclohexene (0.01%) in 1% toluene and argon.

Making the further assumption that the heat capacity of *sec*-butyl radicals is intermediate between that of 1-butene and *n*-butane gives $(\Delta H_f^{sec-C_4H_9})_{300} = 55$ kJ/mol (13.2 kcal/mol), in excellent agreement with the number quoted earlier. A similar calculation from 2,2,3-trimethylpentane decomposition results give ΔH -(reaction) = E (activation energy) = 302 kJ = $(\Delta H_f^{sec-C_4H_9})_{1100} + (\Delta H_f^{tert-C_4H_9})_{1100} - (\Delta H_f^{2,2,3-C_5H_{18}})_{1100}$. From $(\Delta H_f^{2,2,3-C_5H_{18}})_{1100} = -262$ kJ¹³ and $(\Delta H_f^{sec-C_4H_9})_{1100} = 28$ kJ kcal this leads to $(\Delta H_f^{tert-C_4H_9})_{1100} = 11.7$ kJ/mol. This is in striking agreement with earlier determinations.^{1,2} Thus, from hexamethylethane decomposition $(\Delta H_f^{tert-C_4H_9})_{1100} = 10.9$ kJ/mol while the results of 2,2,3-trimethylbutane decomposition yields $(\Delta H_f^{tert-C_4H_9})_{1100} = 9.6$ kJ/mol (using $(\Delta H_f^{i-C_3H_7})_{1100} = 50.5$ kJ as derived from shock tube data and in good agreement with accepted values^{1,2}). Aside from demonstrating the consistency and reproducibility of comparative rate single-pulse shock tube studies, the present number confirms the earlier conclusion¹⁴ that the generally accepted value for the heat of formation of *tert*-butyl radical is in error. From the present study and assuming the heat capacity of *tert*-butyl radicals to be intermediate between isobutene and isobutane this gives $(\Delta H_f^{tert-C_4H_9})_{300} = 39$ kJ/mol (9.3 kcal/mol). This is 2.5 kcal higher than the accepted value of 6.8 kcal/mol.⁵

For *tert*-butylcyclohexane, the same procedure as that employed earlier yields

$$\Delta H(\text{reaction}) = E(\text{activation energy}) = 309 \text{ kJ} = (\Delta H_f^{tert-C_4H_9})_{1100} + (\Delta H_f^{c-C_6H_{11}})_{1100} - (\Delta H_f^{c-C_{10}H_{20}})_{1100}$$

The heat of formation of *tert*-butylcyclohexane has never been determined. For the present purposes, an estimate has been made, using as a basis, the enthalpies of related molecules. This should be fairly satisfactory and results in $(\Delta H_f^{c-C_{10}H_{20}})_{1100} = -262 \pm 2$ kJ/mol. Combining this with $(\Delta H_f^{tert-C_4H_9})_{1100} = 11.7$ kJ/mol as determined previously, this gives $(\Delta H_f^{c-C_6H_{11}})_{1100} = 34.7$ kJ/mol. Assuming that the heat capacity of cyclohexyl radical is intermediate between that of cyclohexane and cyclohexene this gives $(\Delta H_f^{c-C_6H_{11}})_{300} = 66$ kJ/mol (15.8 kcal/mol). This is higher than the value recommended by Kerr, 55 ± 12 kJ/mol, although still within the error limits. The present number is the result of a direct determination while the suggested value is from a Polanyi plot. Note that the use of the literature value for the heat of formation of *tert*-butyl radical in the present context will make $(\Delta H_f^{c-C_6H_{11}})_{300} = 76$ kJ/mol. This is unacceptably high since it implies a carbon-hydrogen bond energy in cyclohexane of 99 kcal/mol which is equal to that for ethane.

(b) *Derived Rate Parameters.* In previous communications^{1,2} it has been demonstrated the rate constants and parameters for decomposition of hydrocarbon molecules AA, BB, AB, CC, and BC (where A, B, and C are radicals) are related to each other on the basis of their thermodynamic properties. The only necessary condition is that the value of the appropriate cross-combination to combination ratio, $(k_r^2(AB)/k_r(AA)k_r(BB))^{1/2}$ where k_r is the combination rate, be known. Experimentally, this number is quite easy to measure and in every case it has turned out to be near 2. On this basis the following equations have been derived

$$\nu_{AB} = 2(\nu_{AA}\nu_{BB})^{1/2} \exp [(1/2R)(S_{AA} + S_{BB} - 2S_{AB})]$$

$$E_{AB} = 1/2(H_{AA} + H_{AB} - 2H_{AB}) + 1/2(E_{AA} + E_{BB})$$

and for cases where the kinetic and thermal parameters for the decomposition of BB are not known

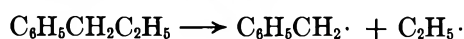
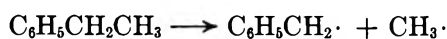
$$\nu_{AB}/\nu_{BC} = (\nu_{AA}/\nu_{CC})^{1/2} \times \exp \left[(1/R) \left(\frac{S_{AA} - S_{CC}}{2} - (S_{AB} - S_{BC}) \right) \right]$$

$$E_{AB} - E_{BC} = 1/2(H_{AA} - H_{CC}) - (H_{AB} - H_{BC}) + 1/2(E_{AA} - E_{CC})$$

where ν and E are the appropriate frequency factor and activation energy for unimolecular decomposition. This procedure is superior to the usual means by which hydrocarbon bond-breaking reactions are calculated, since properties of alkyl radicals and the recombination rate (k_r) are not required. A direct confirmation has been offered in an earlier communication² where rate constants for the reactions

Table IV: Rate Expressions for the Thermal Decomposition of Hydrocarbons, Involving the Formation of *sec*-Butyl and Cyclohexyl Radicals
$$\begin{aligned}
 k(\text{sec-C}_4\text{H}_9\text{-CH}_3(\text{isopentane}) \rightarrow \text{sec-C}_4\text{H}_9\cdot + \text{CH}_3\cdot) &= 10^{16.4} \exp(-42,100/T) \text{ sec}^{-1} \\
 k(\text{sec-C}_4\text{H}_9\text{-C}_2\text{H}_5(3\text{-methylpentane}) \rightarrow \text{sec-C}_4\text{H}_9\cdot + \text{C}_2\text{H}_5\cdot) &= 10^{16.7} \exp(-40,000/T) \text{ sec}^{-1} \\
 k(\text{sec-C}_4\text{H}_9\text{-}i\text{-C}_3\text{H}_7(2,3\text{-dimethylpentane}) \rightarrow \text{sec-C}_4\text{H}_9\cdot + i\text{-C}_3\text{H}_7\cdot) &= 10^{16.1} \exp(-38,400/T) \text{ sec}^{-1} \\
 k(\text{sec-C}_4\text{H}_9\text{-tert-C}_4\text{H}_9(2,2,3\text{-trimethylpentane}) \rightarrow \text{sec-C}_4\text{H}_9\cdot + \text{tert-C}_4\text{H}_9\cdot) &= 10^{16.35} \exp(-36,300/T) \text{ sec}^{-1} \\
 [k(\text{sec-C}_4\text{H}_9\text{-tert-C}_4\text{H}_9(2,2,3\text{-trimethylpentane}) \rightarrow \text{sec-C}_4\text{H}_9\cdot + \text{tert-C}_4\text{H}_9\cdot) &= 10^{16.3} \exp(-36,400/T) \text{ sec}^{-1}]^a \\
 k(\text{sec-C}_4\text{H}_9\text{-tert-C}_6\text{H}_{11}(3,3,4\text{-trimethylhexane}) \rightarrow \text{sec-C}_4\text{H}_9\cdot + \text{tert-C}_6\text{H}_{11}\cdot) &= 10^{16.2} \exp(-35,200/T) \text{ sec}^{-1} \\
 k(\text{sec-C}_4\text{H}_9\text{-}c\text{-C}_6\text{H}_{11}(\text{sec-butylcyclohexane}) \rightarrow \text{sec-C}_4\text{H}_9\cdot + c\text{-C}_6\text{H}_{11}\cdot) &= 10^{16.2} \exp(-38,800/T) \text{ sec}^{-1} \\
 k(\text{sec-C}_4\text{H}_9\text{-C}_3\text{H}_5(4\text{-methylhexene-1}) \rightarrow \text{sec-C}_4\text{H}_9\cdot + \text{C}_3\text{H}_5\cdot(\text{allyl})) &= 10^{16.7} \exp(-34,600/T) \text{ sec}^{-1} \\
 k(\text{sec-C}_4\text{H}_9\text{-C}_4\text{H}_7(3,4\text{-dimethylhexene-1}) \rightarrow \text{sec-C}_4\text{H}_9\cdot + \text{C}_4\text{H}_7\cdot(\text{methylallyl})) &= 10^{16.9} \exp(-32,000/T) \text{ sec}^{-1} \\
 k(\text{sec-C}_4\text{H}_9\text{-CH}_2\text{C}_6\text{H}_5(3\text{-methylbutylbenzene}) \rightarrow \text{sec-C}_4\text{H}_9\cdot + \text{C}_6\text{H}_5\text{CH}_2\cdot(\text{benzyl})) &= 10^{16.4} \exp(-34,200/T) \text{ sec}^{-1} \\
 k(\text{sec-C}_4\text{H}_9\text{-C}_3\text{H}_3(4\text{-methylhexene-1}) \rightarrow \text{sec-C}_4\text{H}_9\cdot + \text{C}_3\text{H}_3\cdot(\text{propynyl})) &= 10^{15.5} \exp(-34,200/T) \text{ sec}^{-1} \\
 k(c\text{-C}_6\text{H}_{11}\text{-CH}_3(\text{methylcyclohexane}) \rightarrow c\text{-C}_6\text{H}_{11}\cdot + \text{CH}_3\cdot) &= 10^{16.3} \exp(-42,900/T) \text{ sec}^{-1} \\
 k(c\text{-C}_6\text{H}_{11}\text{-C}_2\text{H}_5(\text{ethylcyclohexane}) \rightarrow c\text{-C}_6\text{H}_{11}\cdot + \text{C}_2\text{H}_5\cdot) &= 10^{16.3} \exp(-40,500/T) \text{ sec}^{-1} \\
 k(c\text{-C}_6\text{H}_{11}\text{-}i\text{-C}_3\text{H}_7(\text{isopropylcyclohexane}) \rightarrow c\text{-C}_6\text{H}_{11}\cdot + i\text{-C}_3\text{H}_7\cdot) &= 10^{16.1} \exp(-39,300/T) \text{ sec}^{-1} \\
 k(c\text{-C}_6\text{H}_{11}\text{-tert-C}_6\text{H}_{11}(\text{tert-amylcyclohexane}) \rightarrow c\text{-C}_6\text{H}_{11}\cdot + \text{tert-C}_6\text{H}_{11}\cdot + \text{tert-C}_6\text{H}_{11}\cdot) &= 10^{15.1} \exp(-36,300/T) \text{ sec}^{-1} \\
 k(c\text{-C}_6\text{H}_{11}\text{-}c\text{-C}_6\text{H}_{11}(\text{dicyclohexane}) \rightarrow 2c\text{-C}_6\text{H}_{11}\cdot) &= 10^{16.1} \exp(-39,800/T) \text{ sec}^{-1} \\
 k(c\text{-C}_6\text{H}_{11}\text{-C}_3\text{H}_5(\text{allylcyclohexane}) \rightarrow c\text{-C}_6\text{H}_{11}\cdot + \text{C}_3\text{H}_5\cdot(\text{allyl})) &= 10^{16.7} \exp(-35,000/T) \text{ sec}^{-1} \\
 k(c\text{-C}_6\text{H}_{11}\text{-C}_4\text{H}_7(\text{methylallylcyclohexane}) \rightarrow c\text{-C}_6\text{H}_{11}\cdot + \text{C}_4\text{H}_7\cdot(1\text{-methylallyl})) &= 10^{16.7} \exp(-33,100/T) \text{ sec}^{-1} \\
 k(c\text{-C}_6\text{H}_{11}\text{-CH}_2\text{C}_6\text{H}_5(\text{benzylcyclohexane}) \rightarrow c\text{-C}_6\text{H}_{11}\cdot + \text{C}_6\text{H}_5\text{CH}_2\cdot(\text{benzyl})) &= 10^{15.2} \exp(-35,500/T) \text{ sec}^{-1} \\
 k(c\text{-C}_6\text{H}_{11}\text{-C}_3\text{H}_3(\text{propynylcyclohexane}) \rightarrow c\text{-C}_6\text{H}_{11}\cdot + \text{C}_3\text{H}_3\cdot(\text{propynyl})) &= 10^{15.5} \exp(-36,000/T) \text{ sec}^{-1}
 \end{aligned}$$

^a Expression in brackets is from experimental results.



have been calculated from the shock tube results on the decomposition of isobutylbenzene, 2,3-dimethylbutane, neopentane, 2,2,3,3-tetramethylbutane, 3,3-dimethylpentane, and 2,3,3-trimethylpentane, and shown to be quantitative agreement with experimental values in the literature derived from other methods.

Thus, the data generated from the present investigation can be combined with earlier results to generate a rather large number of rate parameters for a variety of other interesting processes. The numbers are summarized in Table IV. It will be noted that for the present purposes one or the other set of data involving the formation of *sec*-butyl radicals is redundant since from either set of rate parameters all the relevant information can be derived. The "excess" of data does permit another check of the consistency of these shock tube results. This is the reason for the two sets of rate parameters for 2,2,3-trimethylpentane decomposition. The calculated numbers are from the data on hexamethylethane and 3,4-dimethylhexane decomposition, while the experimental values are from the present study. There is excellent agreement. Even more striking is the concordance in rate constants

$$k^{1100}_{\text{calcd}}(2,2,3\text{-trimethylpentane}) = 86 \text{ sec}^{-1}$$

and

$$k^{1100}_{\text{exptl}}(2,2,3\text{-trimethylpentane}) = 73 \text{ sec}^{-1}$$

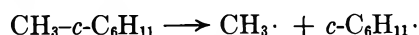
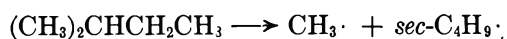
A considerable amount of the necessary thermal data necessary for the present calculations are not available. These have been estimated, using as a basis, properties

Table V: Estimated Thermal Values Used in Present Study

	ΔH_{100} , kJ/mol	ΔS_{100} , J/mol K
3,3,4-Trimethylhexane	-273 (-65.7) ^a	950 (228) ^b
<i>sec</i> -Butylcyclohexane	-258 (-62.0)	945 (227)
Isopropyl cyclohexane	-239 (-57.5)	850 (204)
<i>tert</i> -Butylcyclohexane	-262 (-63.0)	915 (220)
<i>tert</i> -Amylcyclohexane	-275 (-66.0)	1025 (245)
Dicyclohexane	-259 (-62.1)	1015 (243)
4,4-Dimethylpentene-1	-114 (-27.4)	729 (175)
3,4-Dimethylpentene-1	-115 (-27.6)	745 (179)
3-Methylhexene-1	-105 (-25.2)	759 (182)
4-Methylhexene-1	-112 (-26.6)	750 (180)
3,4-Dimethylhexene-1	-133 (-31.9)	833 (200)
Allylcyclohexane	-112 (-26.6)	829 (199)
Methylallylcyclohexane	-133 (-32.0)	915 (219)
4-Methylpentene-1	86.5 (20.7)	629 (150)
4-Methylhexene-1	108 (25)	710 (170)
Propynylcyclohexane	108 (25)	794 (190)
3-Methylbutylbenzene	-77.5 (-18.6)	915 (220)
Benzylcyclohexane	-80 (-19.2)	990 (238)

^a (kcal/mol). ^b (cal/mol K).

of similar molecules. The relevant numbers may be found in Table V. Finally, the two reactions which



form methyl radicals have been calculated using the following expression for neopentane decomposition

$$k(\text{C}(\text{CH}_3)_4 \rightarrow \text{CH}_3\cdot + \text{tert-C}_4\text{H}_9\cdot) = 10^{16.8} \exp(-41,100/T) \text{ sec}^{-1}$$

This is the revised expression given in the previous

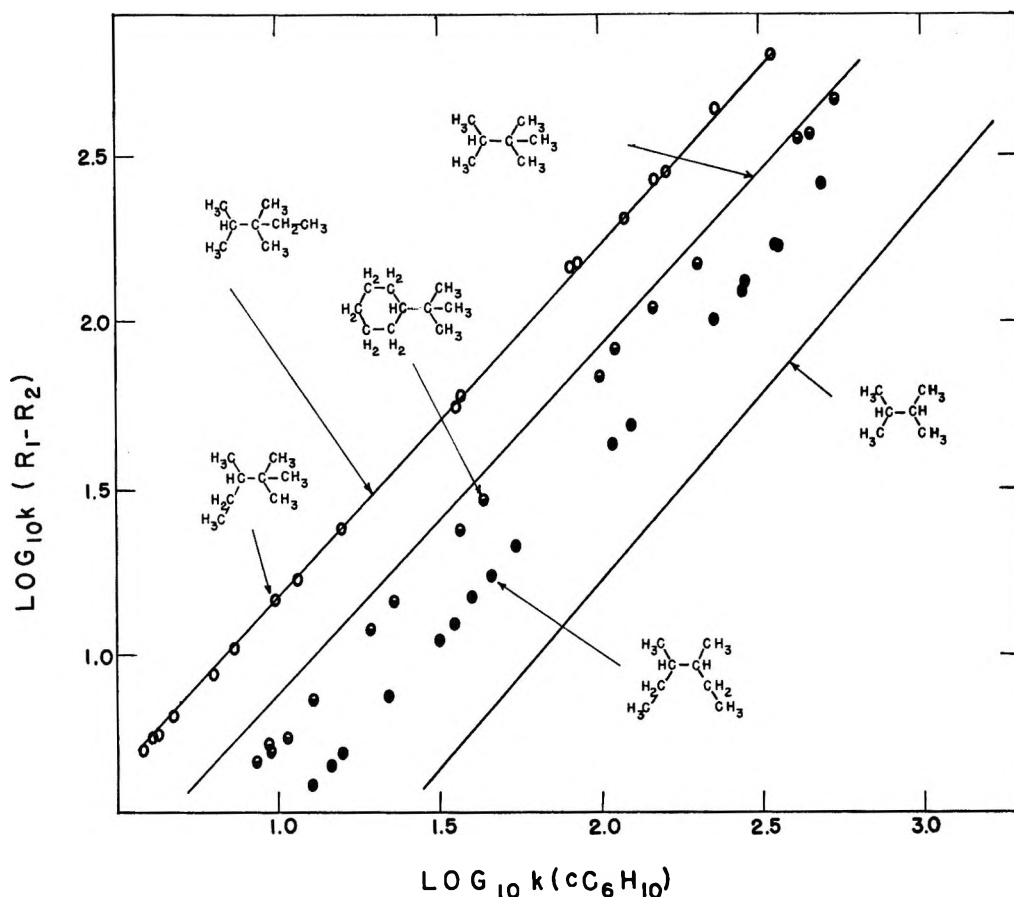


Figure 7. Summary of data on the effect of β -methylation. Comparative rate studies of decomposition of various alkanes with cyclohexene decyclization.

communication and has subsequently been confirmed from flow,^{15a} static,^{15b,c,d} and chemical activation¹⁶ studies. This revision brings the activation energy in accord with $\Delta H_{f,300}(\text{CH}_3\cdot) = 142 \text{ kJ/mol}$.^{4,5}

There have not been any previous determinations of the rate constants or parameters for the processes listed in Table IV. They follow the general trends that have been noted in previous single-pulse shock tube studies. Thus, for the alkanes the preexponential factors per equivalent carbon-carbon bond cluster about $10^{16.2} \text{ sec}^{-1}$. All important variations in rate constants are due to changes in activation energies. This general trend also holds for all the alkene, alkyne, and benzyl compounds that have been studied. The absolute uncertainty in these calculated rate parameters has been given as $10^{\pm 0.6} \text{ sec}^{-1}$ in preexponential factor and 12 kJ in activation energy. But as noted earlier, the internal consistency should be better, perhaps of the order of $10^{\pm 0.3} \text{ sec}^{-1}$ and 6 kJ, respectively. Past experiences have shown the rate constants to be accurate to at least a factor of 1.5.

(c) *Effects of β -Methylation.* The results on the effects of β -methylation on rates of decomposition of alkanes are summarized in Figure 7. Also included are the data for the "comparison" compounds (no β -methylation) and 2,2,3-trimethylpentane which have

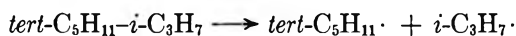
been deduced from a previous investigation. It can be seen that, as before, the effect of one β -methyl group in these highly branched systems is to increase bond cleavage rate by a factor of 2. For two β -methyl groups the appropriate ratio is 2.4. This is fairly close to the factor of 3 given in an earlier communication. The latter has been deduced from various side reactions that occurred in the course of other alkane decompositions and may be subject to some uncertainty. Or, more likely, this may reflect the differences in the molecules being studied. Indeed, an examination of the data on Table IV suggests a relationship between the importance of β -methylation with the extent of α -methylation. Thus, the calculated rate of scission of the most highly substituted C-C bond in 3,3,4-trimethylhexane is a factor of 4 higher than the experimentally determined number for an analogous process in 2,2,3-trimethylbutane, while calculated rates of

(15) (a) J. E. Taylor, D. A. Hutchings, and K. J. Frech, *J. Amer. Chem. Soc.*, **91**, 2215 (1969); (b) M. P. Halstead, R. Martin, D. A. Leathard, R. M. Marshall, and J. H. Purnell, *Proc. Roy. Soc., Ser. A*, **310**, 525 (1969); (c) J. Engel, A. Combe, M. Letort, and M. Niclause, *C. R. Acad. Sci.*, **244**, 453 (1957); (d) F. Baronnet, M. Dzierzynski, G. M. Côme, R. Martin, and M. Niclause, *Int. J. Chem. Kinet.*, **3**, 197 (1971).

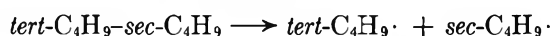
(16) R. L. Johnson, W. L. Hase, and J. W. Simons, *J. Chem. Phys.*, **52**, 3911 (1970).

cleavage per equivalent C-C bond for isobutane and isopentane are almost equal. However, the calculated numbers are subject to some uncertainties, thus these factors cannot be regarded as quantitative. Finally, it is clear that with the introduction of cyclization other factors become important. Thus, *tert*-butylcyclohexane, although it does possess 2- β -methylene groups, is, in fact, more stable than 2,2,3-trimethylbutane. In addition, from Table IV, it appears that this is also true for a variety of analogous systems.

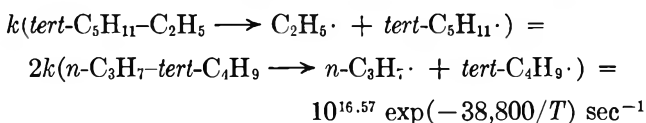
A most interesting observation is the exact equivalence in rate constants for the processes



and



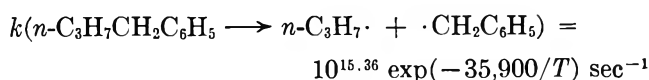
In other words, the effect of one added β -methyl group is the same regardless of whether it is on one or the other departing radical. In retrospect this is not surprising; nevertheless it has never been demonstrated before. In the present context this opens up the possibility that certain other rate constants may be estimated with high precision. Thus, from the earlier studies on 3,3-dimethylpentane decomposition



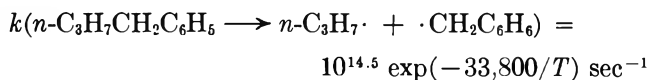
The factor of 2 accounts for the two equivalent C-C₂H₅ bonds available for cleavage in 3,3-dimethylpentane. This expression may be tested in two ways. First, from the activation energy of reaction and the usual assumptions (see above) one finds

$$\Delta H(\text{reaction}) = E(\text{activation energy}) = \\ 321 \text{ kJ} = (\Delta H_f^{n\text{-C}_3\text{H}_7\cdot})_{1100} + \\ (\Delta H_f^{\textit{tert}\text{-C}_4\text{H}_9\cdot})_{1100} - (\Delta H_f^{\text{C}_7\text{H}_{16}})_{1100}$$

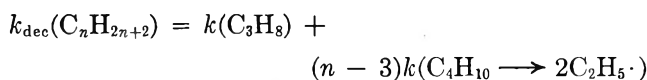
From $(\Delta H_f^{\text{C}_7\text{H}_{16}})_{1100} = -244^{13}$ and $(\Delta H_f^{\textit{tert}\text{-C}_4\text{H}_9\cdot})_{1100} = 11.7$ this leads to $(\Delta H_f^{n\text{-C}_3\text{H}_7\cdot})_{1100} = 65.1$ kJ/mol. Assuming the heat capacity of *n*-propyl radicals is intermediate between that of propylene and propane gives $(\Delta H_f^{n\text{-C}_3\text{H}_7\cdot})_{300} = 88$ kJ/mol (21.2 kcal/mol). This can be compared with $(\Delta H_f^{n\text{-C}_3\text{H}_7\cdot})_{300} = 94.5 \pm 7.5$ kJ/mol from the iodination study of Knox and Musgrove.¹⁷ From the pyrolysis of *n*-butylbenzene Esteban, Kerr, and Trotman-Dickenson find $(\Delta H_f^{n\text{-C}_3\text{H}_7\cdot}) = 79$ kJ/mol. Second, from the earlier studies of isobutylbenzene and 2,3-dimethylbutane decomposition and the present result the rate parameters for the thermal decomposition of *n*-butylbenzene can be found to be



This may be compared with the directly measured number



of Esteban, Kerr, and Trotman-Dickenson¹⁸ using their aniline carrier technique. The large variation in rate parameters is not unexpected since flow experiments are notorious in this regard.¹⁹ However, the agreement in rate constants is impressive. They are $k_{940}(\text{exptl}) = 0.08 \text{ sec}^{-1}$ and $k_{940}(\text{calcd}) = 0.06 \text{ sec}^{-1}$, where 940°K is the reaction temperature for the flow experiments. In view of the importance of *n*-propyl radicals as a cracking product in the pyrolysis of hydrocarbons, rate expressions for the decomposition of a variety of compounds that yield this radical are summarized in Table VI. It is interesting to note that in these cases, where α -methylation is at a minimum, the effect of β -methylation is as noted earlier, small. Thus, per C-C bond, rate constants for *n*-butane² (into ethyl radicals), *n*-pentane (into ethyl and *n*-propyl radicals), and *n*-hexane (into *n*-propyl radicals) are, within experimental error, equal to each other. This suggests that for a normal alkane the rate expression for decomposition can be written as



(d) *Constancy of A Factors for Alkane Decomposition.*

The present investigation offers confirmation of the earlier observation that the frequency factor for the cleavage of a particular carbon-carbon bond in an alkane is within the uncertainty limits ($10^{\pm 3}$ sec) constant. In order to emphasize this point, all the shock tube data on alkane decomposition are summarized in Table VII. Furthermore, all the calculated data on alkane decomposition given in this and earlier reports are all in conformity with these experimental results. Finally, mention should be made of a recent review on ethane decomposition by Back.²⁰ She recommends $k(\text{C}_2\text{H}_6 \longrightarrow 2\text{CH}_3\cdot) = 3 \times 10^{16} \exp(-44,300/T) \text{ sec}^{-1}$. Here again the preexponential factor is in the specified range.

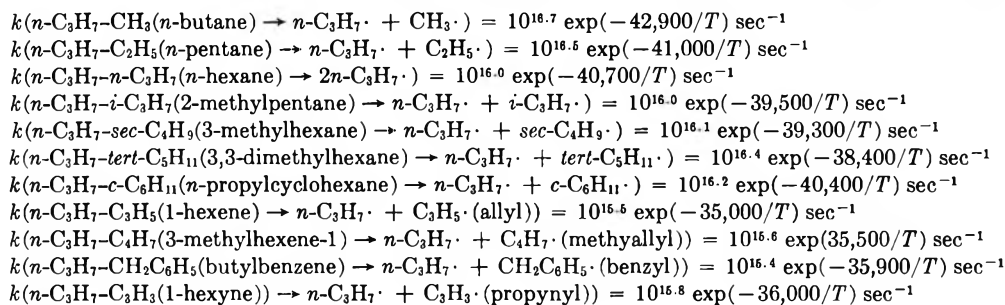
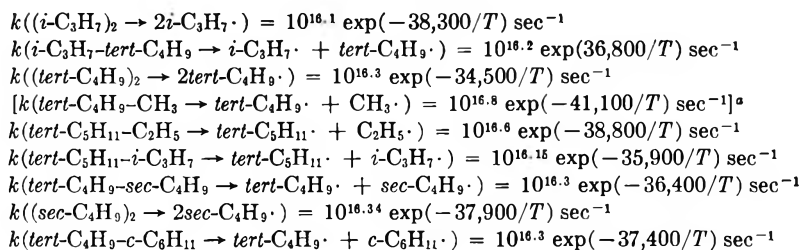
The essential equality of Arrhenius *A* factors for the cleavage of any particular C-C bond in alkanes sets important constraints on the nature of possible transition states. This should be the subject of further theoretical explorations. In addition, there is the pros-

⁽¹⁷⁾ J. H. Knox and R. G. Musgrove, *Trans. Faraday Soc.*, **63**, 2201 (1967).

⁽¹⁸⁾ G. L. Esteban, J. A. Kerr, and A. L. Trotman-Dickenson, *J. Chem. Soc.*, 3873 (1963).

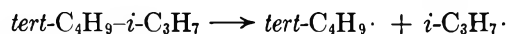
⁽¹⁹⁾ S. W. Benson, *J. Chem. Educ.*, **42**, 502 (1965).

⁽²⁰⁾ M. Back, in "The Mechanism of Pyrolysis, Oxidation, and Burning," Institute for Materials Research, National Bureau of Standards, Gaithersburg, Md (1970).

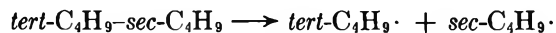
Table VI: Rate Expressions for the Thermal Decomposition of Hydrocarbons Involving the Formation of *n*-Propyl Radicals**Table VII:** Summary of Experimental Results on Alkane Decomposition

^a These are revised values. The activation energy is now compatible with the enthalpy of reaction.

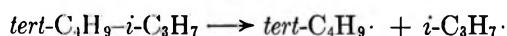
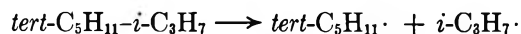
pect of determining certain differences in heats of formation or bond energies with unprecedented accuracy. The basic premise is that for pairs of reactions such as



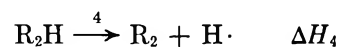
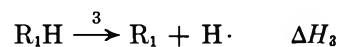
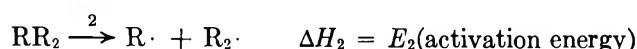
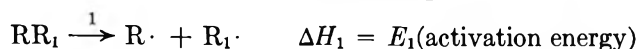
and



or



the preexponential factors must be exactly equal. This seems to be justified in view of the minimal changes of this number (within error limits they are constant) even with gross variations in structure. In the present case, the only change is that of β -methylation. Since the relative rates are known to within $\pm 10\%$ this leads to an uncertainty of ± 1 kJ. Differences in the heats of formation cannot be determined to this accuracy, since the relative heats of formation of the larger alkanes are themselves, uncertain to this extent.²¹ Nevertheless, ± 2 kJ error limit is still better than anything currently available. It is sufficient, for example, to make a meaningful test of the usual assumption regarding the equivalence of all types of tertiary, secondary, or primary carbon-hydrogen bonds. The processes in question are the following



where R refers to an arbitrary radical, the subscripts refers to species with or without β -methylation and the desired quantity is $\Delta H_{34} = \Delta H_3 - \Delta H_4$. The relevant relations are

$$\Delta H_{34} = \Delta H_f^{R_1\cdot} - \Delta H_f^{R_2\cdot} - (\Delta H_f^{R_1H} + \Delta H_f^{R_2H})$$

where

$$\Delta H_f^{R_1} - \Delta H_f^{R_2} - (\Delta H_f^{RR_1} - \Delta H_f^{RR_2}) =$$

$$E_1 - E_2 = E_{12}$$

With the data at hand, it is possible to consider the following pairs of radicals: *tert*-amyl and *tert*-butyl, *sec*-butyl and isopropyl, and *n*-propyl and ethyl. The compounds of interest are 2,3,3-trimethylpentane, 2,2,3-trimethylpentane, 2,2,3-trimethylbutane, 2,2-dimethylpentane, and 2,2-dimethylbutane. For the relative heats of formation, the results are

$$\Delta H_f^{tert\text{-C}_5\text{H}_{11}\cdot} - \Delta H_f^{tert\text{-C}_4\text{H}_9\cdot} = -18.7$$

$$\Delta H_f^{sec\text{-C}_4\text{H}_9\cdot} - \Delta H_f^{i\text{-C}_3\text{H}_7\cdot} = -22.9$$

$$\Delta H_f^{n\text{-C}_3\text{H}_7\cdot} - \Delta H_f^{C_2\text{H}_5\cdot} = -24.1$$

where in the first two cases $\Delta E_{12} = -6$ kJ (from a factor of 2 in rate constants) and in the third case $\Delta E_{12} = -2.6$ kJ (from a factor of 30% difference in rate

(21) D. Wagman, personal communication.

constants). Note that the latter number has been determined from the estimated and calculated values for the rate of decomposition of 2,2-dimethylpentane and 2,2-dimethylbutane, respectively, and thus may have somewhat larger uncertainties than for the others. This in turn leads to

$$\Delta H_{34}(\text{tert-C}_5\text{H}_{11}, \text{tert-C}_4\text{H}_9) = 5.4 \pm 2 \text{ kJ/mol}$$

$$\Delta H_{34}(\text{sec-C}_4\text{H}_9, \text{i-C}_3\text{H}_7) = 3.5 \pm 2 \text{ kJ/mol}$$

$$\Delta H_{34}(n\text{-C}_3\text{H}_7, \text{C}_2\text{H}_5) = -1.5 \pm 5 \text{ kJ/mol}$$

The interesting point here is that for the branched systems the effect of β -substitution on C-H bond strengths seems to be exactly opposite to that for C-C bonds. Normal C-H bonds do appear to be invariant. This is the same situation with respect to C-C bonds. Furthermore, incremental data of this sort provide a basis for the empirical prediction of the heats of formation of arbitrary alkyl radicals. Coupling this with the earlier observations regarding the essential constancy of preexponential factors for alkane decomposition suggests that the initial cracking pattern of any alkane can now be predicted with a great deal of confidence.

(e) *Absolute Magnitude of A Factors for Alkane Decomposition.* In all of the comparative rate single-pulse shock tube studies on alkanes the A factors have always been a factor of 10 to 1000 smaller than expected. The "expected" value being the expression derived from the experimental or estimated combination rate, the thermal properties of the substances in question and the familiar relation $k(\text{forward})/k(\text{reverse}) = K(\text{equilibrium})$. Since the activation energies have, in general, turned out to be compatible with established heats of formation of the appropriate radicals, this enormous discrepancy is reflected directly in the rate constant. It has therefore been necessary to check the experimental data in considerable detail. This has included experiments with different internal standards, with bond-breaking reactions whose preexponential factors have been fairly well accepted (unsaturated hydrocarbons), investigations on the possibility of induced and/or chain decomposition and calculations on the possibility of energy transfer effects.¹⁴ They have confirmed the correctness of the single-pulse shock tube results.

Furthermore, during the course of this investigation, Johnson, Hase, and Simons¹⁶ published the results of an investigation on the decomposition of chemically activated isobutane and neopentane. They present nine sets of Arrhenius parameters which are compatible with their results on isobutane and a similar number for neopentane. Depending on the thermal values, the range of A factors are from $10^{15.8}$ to $10^{16.9} \text{ sec}^{-1}$ for the former and $10^{16.1}$ to $10^{17.3} \text{ sec}^{-1}$ for the latter. Within this range of A factors all available results can be accommodated although the authors favor the higher values.²² An alternative approach is

to derive from their rate expressions the actual rate constants and observe how these compare with the published values. Thus, actual experimental quantities are being tested. They are less subject to uncertainties (not much more than a factor of 2) than the A factors which are usually used in making comparisons between chemical activation and thermal rate data. The results may be found in Table VIII. The temperatures are those used by Johnson, Hase, and Simons¹⁶ in computing their rate expressions. With respect to isobutane, they impose a particularly severe test on the shock tube number, since it involves an extrapolation of 9 orders of magnitude. For neopentane the static measurements must be extrapolated by 6 orders of magnitude. An examination of Table VIII demonstrates, as noted earlier,¹⁴ very satisfactory agreement between all thermal measurements on neopentane.¹⁵ It is therefore reassuring to find the new chemical activation data encompassing all of these numbers. Furthermore, it is clear that the calculated numbers of Frey and Walsh²³ (in the manner described above) are in disagreement with every possible experimental value. For isobutane the chemical activation results are at least a factor of 10 lower than the static²⁴ and calculated²³ results and a considerably larger factor for the flow²⁵ experiment. There is thus no possibility of explaining away such discrepancies on the basis of small experimental errors. On the other hand, the chemical activation results once more straddle the shock tube numbers.

Mention should also be made of two additional pieces of information which support the low values of A factors for alkane decomposition. First, Spokes²⁶ has reported on experiments with hexamethylethane using the Very Low Pressure Pyrolysis technique. This is a thermal activation technique with energy transfer being affected by collision with the wall. He interprets his results as compatible with the shock tube data. Second, Whitten and Rabinovitch²⁷ have reexamined their data on chemically activated n -butane decomposition and found these previously published rate constants to be a factor of 10 too high. Since they have interpreted their earlier results as compatible with the value ($10^{17.2} \text{ sec}^{-1}$) calculated from recombination rates, the new information destroys this agreement and suggests that $10^{16.2} \text{ sec}^{-1}$ will be a more ap-

(22) This is in agreement with our revised numbers (W. Tsang, *Int. J. Chem. Kinet.*, **1**, 245 (1969)). Unfortunately, Johnson, *et al.*, made their comparisons on the basis of an earlier report, thus leading to the conclusion that A factors from shock tube and chemical activation studies may be in some disagreement.

(23) H. M. Frey and R. Walsh, *Chem. Rev.*, **69**, 103 (1969).

(24) R. S. Konar, R. M. Marshall, and J. H. Purnell, *Trans. Faraday Soc.*, **64**, 401 (1968).

(25) C. T. Brooks, *ibid.*, **62**, 935 (1966).

(26) N. Spokes, personal communication.

(27) G. L. Whitten and B. S. Rabinovitch, *J. Phys. Chem.*, **73**, 4433 (1969).

Table VIII: Comparison of Rate Constants for Isobutane and Neopentane Decomposition

Method	Isobutane (750°K)			Neopentane (1000°K)		
	Log A	E, kJ/mol	k, sec ⁻¹	Log A	E, kJ/mol	k, sec ⁻¹
Chemical activation ¹⁶	15.8-16.9	336-355	0.6-5.5 × 10 ⁻⁸	16.1-17.3	326-344	0.08-0.37
Shock tube ^{27a}	15.7	331	3.6 × 10 ⁻⁸	16.1	326.5	0.11
b	16.6	347	1.5 × 10 ⁻⁸	16.8	340	0.095
Flow ^{15a,c}	18.9	344	3900 × 10 ⁻⁸	16.6	336	0.1
Static ^{16b,e,d}	17.8	334	57 × 10 ⁻⁸	18.1	358	0.22
				17.4	347	0.18
				16.8	342	0.08
Calculation ^e	17.7	333	55 × 10 ⁻⁸	17.9	326	4.1

^a Original rate expression. ^b Revised values, activation energy, and A factors adjusted so that $\Delta H_{f,300}(\text{CH}_3\cdot) = 142$ kJ/mol. ^c C. T. Brooks, *Trans. Faraday Soc.*, **62**, 935 (1966). ^d R. S. Konar, *et al.*, *ibid.*, **64**, 401 (1968). ^e H. M. Frey and R. Walsh, *Chem. Rev.*, **69**, 103 (1969).

propriate A factor. This can be compared with a value of $10^{16.3}$ sec⁻¹, derived from the shock tube data¹ and published several years ago. Thus, all the non-equilibrium measurements are now compatible with the shock tube results.

With regard to equilibrium rate measurements, the good agreement between shock tube, static, and flow results on neopentane decomposition have been noted. It is interesting to note that Back²⁰ has demonstrated and Waage and Rabinovitch²⁸ confirmed that the static experiments for ethane decomposition are, in general, a factor of 6 smaller than that predicted from radical recombination rates. If $\Delta H_{f,300}(\text{CH}_3\cdot) = 142$ kJ/mol, this factor is directly reflected in the A factor. There is, in fact, almost no direct experimental support for the high preexponential factor for alkane decomposition. The flow and static determination which appear to offer support involve studies of extremely complex

processes from which it is difficult, if not impossible, to extract rate constants for the basic underlying process. It is probably not accidental that in the two cases where the static experiments also show the unexpected features first observed from shock tube studies are kinetically the two simplest hydrocarbon systems, neopentane and ethane. Both compounds possess one type of C-C and C-H bond. It should be noted that the instinctive distrust most kineticists have of measurements of initial alkane decomposition rates originate from a knowledge of the problems involved in making such determinations in static systems. The present series of studies suggest that the conditions which minimize such factors can be achieved in appropriate comparative rate single-pulse shock tube experiments.

(28) E. V. Waage and B. S. Rabinovitch, *Int. J. Chem. Kinet.*, **3**, 105 (1971).

Electron Spin Resonance Study of the $\text{SO}_2\cdot^-$ Formation in the Thermal Decomposition of Sodium Dithionite, Sodium and Potassium Metabisulfite, and Sodium Hydrogen Sulfite¹

by Edward G. Janzen

Department of Chemistry, University of Georgia, Athens, Georgia 30601 (Received May 24, 1971)

Publication costs assisted by the U. S. Air Force Office of Scientific Research

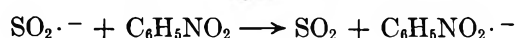
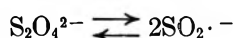
The thermal decomposition of sodium dithionite ($\text{Na}_2\text{S}_2\text{O}_4$), sodium and potassium bisulfite ($\text{Na}_2\text{S}_2\text{O}_5$, $\text{K}_2\text{S}_2\text{O}_5$), and sodium hydrogen sulfite (NaHSO_3) gives sulfur dioxide radical anion ($\text{SO}_2\cdot^-$) as an esr detectable transient reaction product. The $\text{SO}_2\cdot^-$ present in commercial sodium dithionite samples decays rapidly to a lower "steady state" level at 180–220°. The $\text{SO}_2\cdot^-$ radical is detected in sodium and potassium bisulfite as a reaction product which first increases and then decreases in amount as a function of time at temperatures between 200 and 230° for $\text{Na}_2\text{S}_2\text{O}_5$ and 238 and 280° for $\text{K}_2\text{S}_2\text{O}_5$. Similar results are found in heating sodium hydrogen sulfite except that the amount of $\text{SO}_2\cdot^-$ detected is less. It is concluded that those compounds which evolve SO_2 upon heating may all give detectable amounts of $\text{SO}_2\cdot^-$ as an intermediate reaction product.

Introduction

The electron spin resonance (esr) spectra of a large number of inorganic radicals and radical ions have been reported. These radicals are usually obtained by γ - or X-irradiation of suitable crystalline materials. From these studies g values and hyperfine coupling constants are available. Atkins and Symons have collected and reviewed these data.²

Since dithionites and dithionates can be considered as dimers of the $\text{SO}_2\cdot^-$ and $\text{SO}_3\cdot^-$ radicals, respectively, it seemed likely that these radicals might be detectable reaction intermediates in the thermal decomposition of such salts. This discovery of $\text{SO}_2\cdot^-$ radicals in the thermal decomposition of sodium dithionite ($\text{Na}_2\text{S}_2\text{O}_4$), sodium, potassium, and zinc metabisulfite ($\text{Na}_2\text{S}_2\text{O}_5$, $\text{K}_2\text{S}_2\text{O}_5$, ZnS_2O_5), and sodium hydrogen sulfite (NaHSO_3) is reported here.

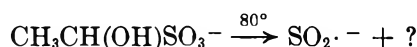
The discovery of an exceptionally long S–S bond in an X-ray study of sodium dithionite prompted Dunitz³ to suggest that the well-known reducing reactions of sodium dithionite might proceed *via* the $\text{SO}_2\cdot^-$ radical ion. The detection of an esr signal attributed to $\text{SO}_2\cdot^-$ in solid sodium dithionite was reported about the same time.⁴ Symons⁵ and coworkers subsequently obtained esr spectra of $\text{SO}_2\cdot^-$ in the irradiation of sodium metabisulfite; the g value was 2.0061. A basic solution of sodium dithionite was found to contain detectable amounts of $\text{SO}_2\cdot^-$ in equilibrium with the dimer.⁶ The g value obtained was 2.0057. This radical has also been detected during the reduction of nitrobenzene with sodium dithionite in aqueous acetone.⁷



Acidified solutions of sodium formaldehyde sulfoxylate gave $\text{SO}_2\cdot^-$ radicals.⁸ We have found that thermal



decomposition of sodium hydrogen sulfite addition products of aldehydes and ketones gives $\text{SO}_2\cdot^-$ at temperatures up to 80°.^{1b}



Sulfur trioxide radical anion, $\text{SO}_3\cdot^-$, is also known⁹ but, as will be shown in this study, this radical appears not to be as stable as $\text{SO}_2\cdot^-$.

Experimental Section

The salts studied were used as obtained commercially: sodium dithionite ($\text{Na}_2\text{S}_2\text{O}_4$) was Baker puri-

(1) (a) "ESR Studies of Thermal Decomposition Mechanisms. II." Research sponsored by AFOSR-(SRC)-OAR, U. S. Air Force Grant No. 1069-66. (b) Part I, see E. G. Janzen and C. M. DuBose, Jr., *Tetrahedron Lett.*, 2521 (1965).

(2) P. W. Atkins and M. C. R. Symons, "The Structure of Inorganic Radicals," Elsevier, Amsterdam, 1967.

(3) J. D. Dunitz, *J. Amer. Chem. Soc.*, **78**, 878 (1956).

(4) W. G. Hodgson, A. Neaves, and C. A. Parker, *Nature (London)*, **178**, 489 (1956).

(5) M. C. R. Symons *Advan. Chem. Ser.*, No. **36**, 76 (1962); P. W. Atkins, A. Horsfield, and M. C. R. Symons, *J. Chem. Soc.*, 5220 (1964); H. C. Clark, A. Horsfield, and M. C. R. Symons, *ibid.*, 7 (1961), and ref 2, p 146.

(6) R. G. Rinker, T. P. Gordon, D. M. Mason, and W. H. Corcoran, *J. Phys. Chem.*, **63**, 302 (1959); see also K. P. Dinse and K. Moebius, *Z. Naturforsch. A*, **23**, 695 (1968).

(7) P. L. Kolker and W. A. Waters, *Proc. Chem. Soc. London*, 55 (1963); *J. Chem. Soc.*, 1136 (1964).

(8) R. G. Rinker, T. P. Gordon, and W. Corcoran, *Inorg. Chem.*, **3**, 1467 (1964).

(9) G. W. Chantry, A. Horsfield, J. A. Morton, and D. H. Whiffen, *Mol. Phys.*, **5**, 233 (1962); ref 2, p 172.

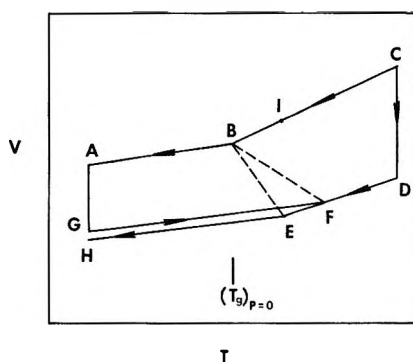


Figure 1. Diagram of cycles to measure T_g as a function of pressure P .

fied grade chemical; sodium metabisulfite ($\text{Na}_2\text{S}_2\text{O}_5$) and sodium hydrogen sulfite (NaHSO_3) were Baker analyzed reagent grade chemicals.

A Varian V-4502 epr spectrometer with the Varian variable temperature accessory was used to heat the samples inside the cavity. Cylindrical Varian thin-wall quartz sample cells open at the top were used to permit escape of the SO_2 produced. Samples under vacuum gave essentially the same results except that serious difficulty was experienced with "bumping" of the powder and rising of portions of the sample during heating apparently due to the escape of SO_2 from the particles.

The temperature was measured directly above the sample by a thermocouple during the experiment or in the sample cell in the cavity after the experiment. In experiments involving the measurements of peak heights immediately after the start of heating, a dual channel recorder was used to monitor the temperature and the esr signal simultaneously. The time lag in attaining the desired temperature as dialed on the regulator is shown in Figure 1.

The g values were obtained by the use of a dual cavity and a stable radical (diphenylpicrylhydrazyl) as a crystalline powder. γ -Radiolysis was performed with a Gammacell ^{60}Co source for 15 min per sample.

Results

Sodium Dithionite. A sample of Baker purified grade sodium dithionite give a strong esr signal at room temperature. The signal is slightly asymmetric (Figure 2). An evacuated sample gave the same signal at the same intensity as a sample open to air. The g value was found to be 2.0055 ± 0.00004 . γ -Irradiation had no effect on the signal or g value. Based on previous work,¹⁻⁸ it is safe to assign the signal to sulfur dioxide radical anion, $\text{SO}_2\cdot^-$. The g values previously reported for $\text{SO}_2\cdot^-$ are 2.0057 in water, 2.005 ± 0.002 in $\text{Na}_2\text{S}_2\text{O}_4$, and 2.0061 in $\text{Na}_2\text{S}_2\text{O}_5$. The amount of $\text{SO}_2\cdot^-$ in the commercial sample of $\text{Na}_2\text{S}_2\text{O}_4$ was calculated from a comparison of the esr signal with the signal obtained from a known amount of paramagnetic

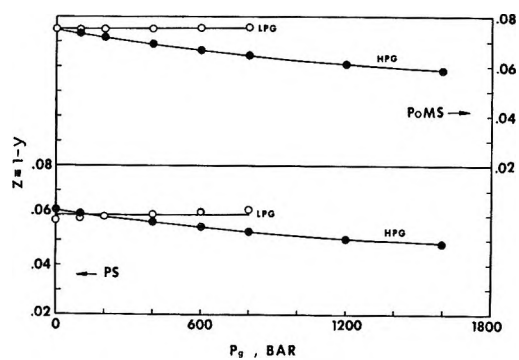


Figure 2. Ordering parameter Z identified with vacancy fraction $(1 - \gamma)$ of the Simha-Somcynsky theory as a function of transition pressure P_g for low and high pressure glasses.

carbon sample in a dual cavity and found to be 0.01 mol %.

The line width of the $\text{SO}_2\cdot^-$ signal in sodium dithionite is 9.2 G at room temperature (Figures 1 and 2) but decreases with increase in temperature. A simultaneous increase in apparent g value is observed. This change in line width and g value was found to be reversible. The narrowing and loss of asymmetry of the $\text{SO}_2\cdot^-$ signal with simultaneous change in g value as the temperature is increased can be attributed to an increase in freedom of motion for the $\text{SO}_2\cdot^-$ radical with a concomitant decrease in g value anisotropy.

A rather abrupt change in line width and g value is observed in the temperature range 160–200°. Presumably at this temperature and above considerably more freedom of motion is allowed for $\text{SO}_2\cdot^-$ (Figure 3).

The $\text{SO}_2\cdot^-$ signal in sodium dithionite decays at temperatures above 160° at a rate which increases with increase in temperature (Figure 4). After heating the sample for approximately 30 min a fairly constant signal intensity is observed as a function of time. The relative amounts of $\text{SO}_2\cdot^-$ present after heating for longer periods increase with increase in temperature (Figure 4). The initial decay of the $\text{SO}_2\cdot^-$ signal is too rapid to follow at temperatures above 200°. Irradiation in a ^{60}Co source for 15 min gives a sample with slightly diminished $\text{SO}_2\cdot^-$ signal intensity which produces essentially the same decomposition curve at elevated temperatures as an unirradiated sample.

As stated earlier, the $\text{SO}_2\cdot^-$ signal line width narrows with increase in temperature with the most abrupt change occurring between 160 and 200°. The line width and apparent g value is shown as a function of temperature in Figure 3, which also gives the initial rate of decay of the $\text{SO}_2\cdot^-$ as a function of temperature (taken from Figure 4). It is clear that the fastest initial rate of decay of the $\text{SO}_2\cdot^-$ signal occurs slightly above the temperature where the line width has narrowed to a minimum. This result implies that the decomposition reaction of $\text{SO}_2\cdot^-$ is faster when the

ERRATA

The figures published on pages 158–160 of this issue of *The Journal of Physical Chemistry* in the paper by Edward G. Janzen titled “Electron Spin Resonance Study of the $\text{SO}_2\cdot^-$ Formation in the Thermal Decomposition of Sodium Dithionite, Sodium and Potassium Metabisulfites, and Sodium Hydrogen Sulfite” are incorrect. The correct figures for Dr. Janzen’s paper are printed below.

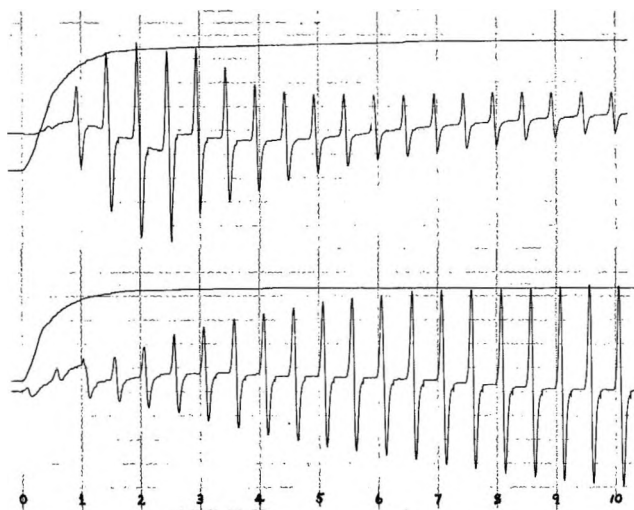


Figure 1. Repeat esr trace obtained in heating sodium hydrogen sulfite (NaHSO_3) as a function of time at 200° (lower) and 227° (upper); continuous curve is a temperature record as a function of time (in minutes).

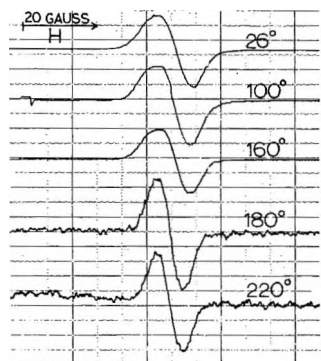


Figure 2. ESR signal of $\text{SO}_2\cdot^-$ in sodium dithionite at different temperatures.

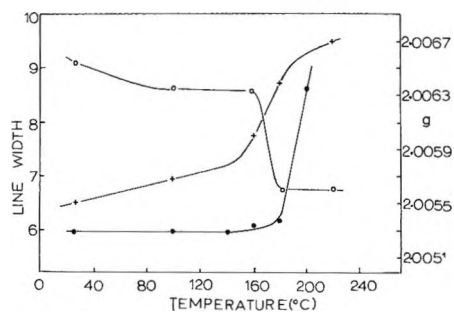


Figure 3. Plot of line width in gauss, $\circ-\circ-$; g value, $-X-X-$ and initial rate of decay of $\text{SO}_2\cdot^-$ signal, $\bullet-\bullet-$ in sodium dithionite as a function of temperature.

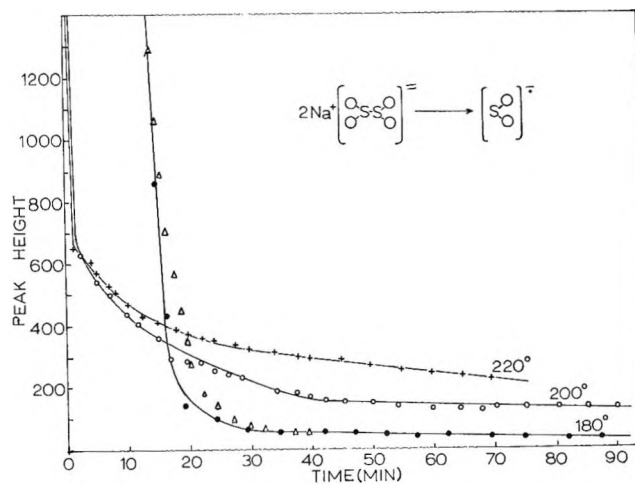


Figure 4. Plot of esr signal peak height of $\text{SO}_2\cdot^-$ in sodium dithionite as a function of time at different temperatures (°C).

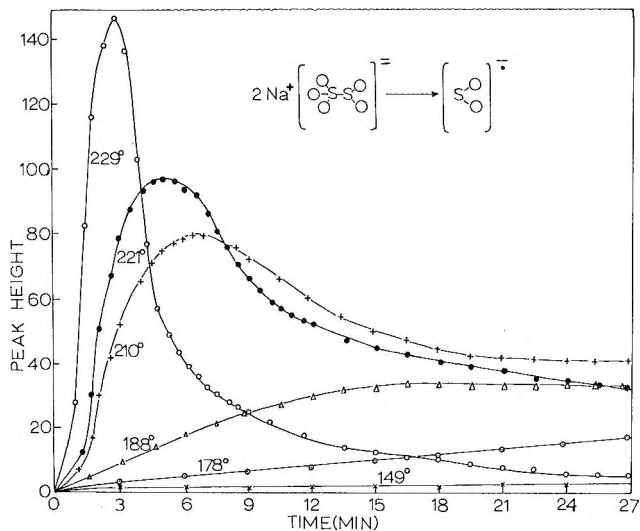


Figure 5. Plot of esr signal peak height of $\text{SO}_2\cdot^-$ in sodium metabisulfite ($\text{NaO}_2\text{SSO}_3\text{Na}$) as a function of time at different temperatures.

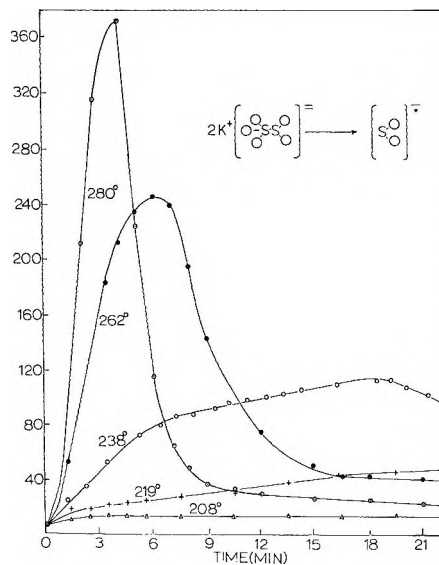


Figure 7. Plot of esr signal peak height of $\text{SO}_2\cdot^-$ in potassium metabisulfite ($\text{KO}_2\text{SSO}_3\text{K}$) as a function of time at different temperatures.

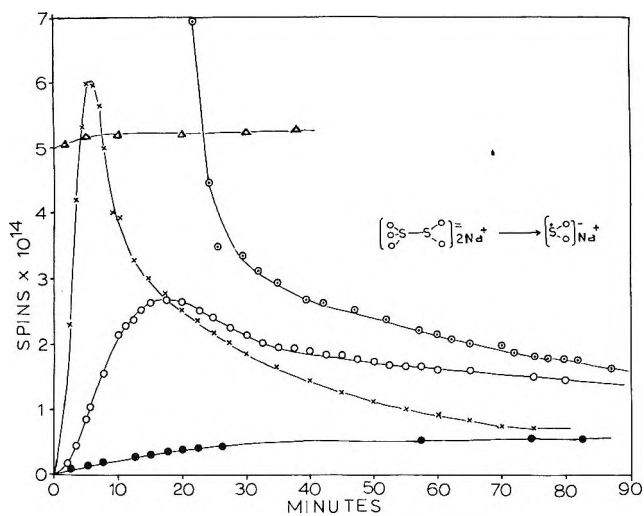


Figure 6. Calibrated plot of esr signal peak height of $\text{SO}_2\cdot^-$ in sodium metabisulfite ($\text{NaO}_2\text{SSO}_3\text{Na}$), $\bullet-\bullet-$ at 180° , $-O-O-$ at 200° , and $-X-X-$ at 220° ; similar plot of $\text{SO}_2\cdot^-$ in sodium metabisulfite at 180° after γ -radiolysis at room temperature, $-\Delta-\Delta-$, similar plot of $\text{SO}_2\cdot^-$ in sodium dithionite at 180° , $-O-O-$ as in Figure 4.

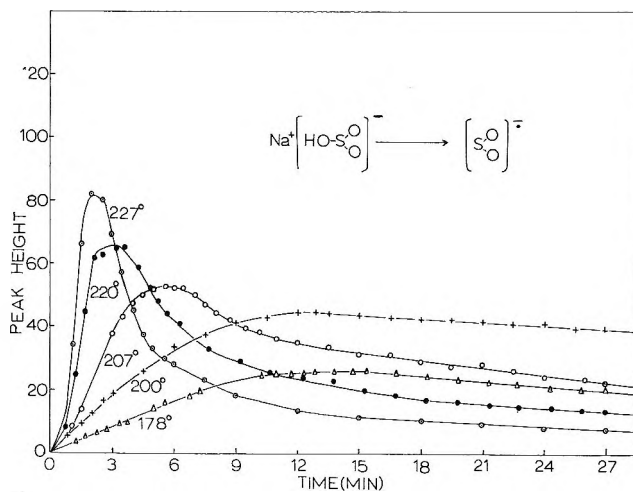


Figure 8. Plot of esr signal peak height of $\text{SO}_2\cdot^-$ in sodium hydrogen sulfite (HOSO_2Na) as a function of time at different temperatures.

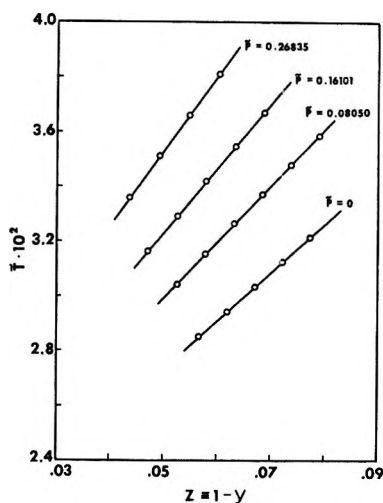


Figure 3. Reduced temperature \bar{T} as a function of ordering parameter $Z \equiv 1 - y$ at a series of pressures in the region of the glass transition, eq 6 and 7.

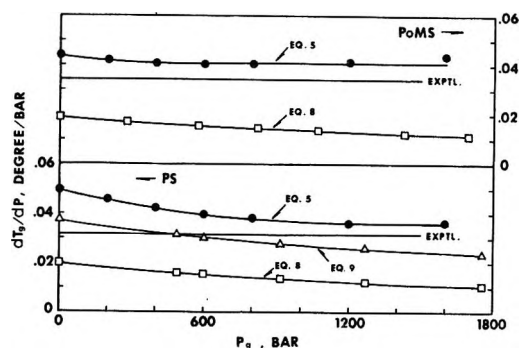


Figure 4. Comparison of various expressions (see text) for the pressure coefficient of T_g of high pressure glasses.

radical is free to rotate in the lattice. ZnS_2O_4 gave the $\text{SO}_2\cdot^-$ signal at room temperature which continually increased in intensity to a strong signal at 278° .

Sodium and Potassium Metabisulfite: $\text{NaO}_2\text{SSO}_3\text{Na}$ and $\text{KO}_2\text{SSO}_3\text{K}$. Commercial samples of sodium metabisulfite gave no signals at room temperature. Upon heating the only signal observed was due to $\text{SO}_2\cdot^-$ first detected at 150° . The signal has the same g value and asymmetry at room temperature as found for $\text{SO}_2\cdot^-$ in sodium dithionite. Upon heating the asymmetry disappears reversibly as for $\text{SO}_2\cdot^-$ in dithionite, but signals obtained at temperatures above 150° do not disappear on cooling.

The intensity of the $\text{SO}_2\cdot^-$ signal increases with time at temperatures between 150 and 188° and after approximately 20 min levels off (Figure 5). At 200° and above the initial intensity of $\text{SO}_2\cdot^-$ increases rapidly and reaches a maximum at a time which decreases with an increase in temperature and finally decays at a rate which increases with increase in temperature. The strongest signal observed was at 220 – 229° . However, this intensity corresponds only to approximately 1/100 of the number of radicals found in commercial sodium

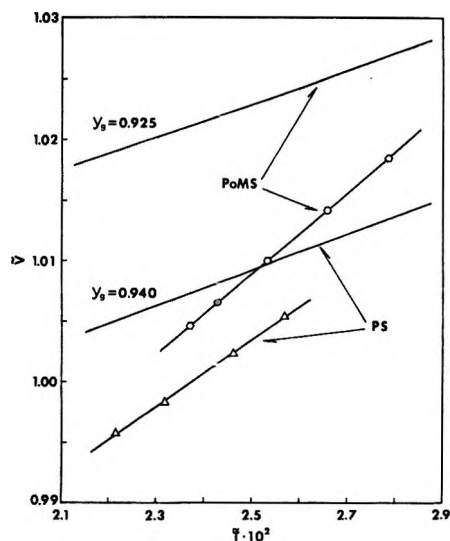


Figure 5. Reduced volume-temperature curve at atmospheric pressure. (Δ) polystyrene, (\circ) poly(e-methylstyrene). Other lines, theoretical, eq 6 with constant $y = y_g$.

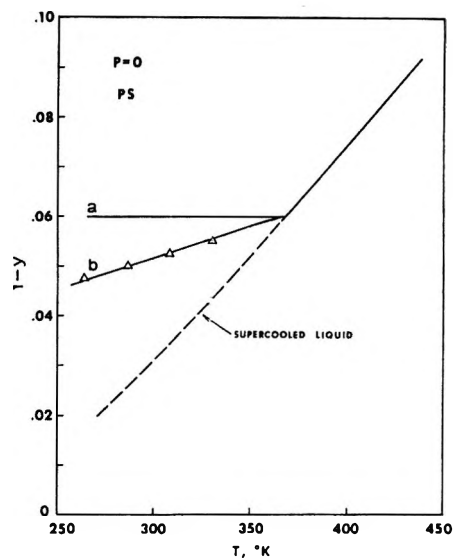


Figure 6. Variation of vacancy fraction $1 - y$ with temperature at atmospheric pressure for polystyrene glass. Dashed line, supercooled liquid, eq 6 and 7. Solid line a, assumption of constant $y = y_g$, b, from eq 6 and experimental volume-temperature data.

dithionite. A comparison is shown in Figure 6.

γ -Irradiation produces approximately the same number of radicals as the maximum number found at 220° . Heating this sample at 180° did not affect the signal intensity (Figure 6).

Since no evidence was obtained for the sulfur trioxide radical anion, $\text{SO}_3\cdot^-$, it was relevant to this problem to look into the threshold temperature for the detection of $\text{SO}_3\cdot^-$. To this end a sample of sodium dithionate, $\text{NaO}_3\text{SSO}_3\text{Na}$, was subjected to γ -radiation and a signal at $g = 2.0033$ due to $\text{SO}_3\cdot^-$ was obtained. The sample was heated under the same experimental conditions as sodium metabisulfite. At 100 – 120° the

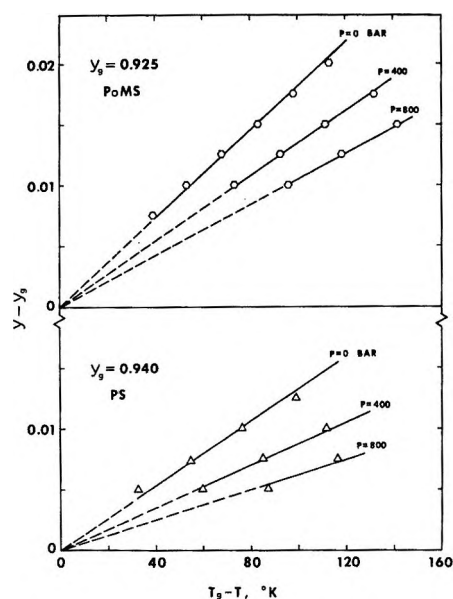


Figure 7. Difference in vacancy fraction $y - y_g = Z_g - Z$ as a function of temperature and pressure, derived from eq 6, pressure dependence of glass transition temperature and value of y at T_g .

$\text{SO}_3\cdot^-$ signal disappeared. It is apparent that $\text{SO}_3\cdot^-$ is not stable in sodium dithionate-dithionite salts at temperatures where thermal decomposition to produce $\text{SO}_2\cdot^-$ first begins. It is thus not too surprising that no signals were detected at any temperature in the thermal decomposition of sodium dithionate itself.

Thermal decomposition results with potassium metabisulfite were similar to those obtained from sodium metabisulfite (Figure 7) except that a $\text{SO}_2\cdot^-$ signal is detected at room temperature in commercial samples and that the temperatures required for reaching the maximum amount of $\text{SO}_2\cdot^-$ were higher ($\sim 240\text{--}280^\circ$).

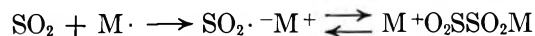
Sodium Hydrogen Sulfite: NaHSO_3 . In a continuation of the search for $\text{SO}_2\cdot^-$ radicals in the thermal decomposition of R-SO_2^- derivatives sodium bisulfite ($\text{HO-SO}_2\text{Na}$) was investigated. Commercial samples have a very weak signal at $g = 2.0057$ which shows essentially no change in intensity until $150\text{--}170^\circ$. Above 170° very similar plots of signal intensity as a function of time at temperatures up to 227° are obtained as found in the metabisulfite cases (Figure 8) except that the signal is always weaker. The maximum amount of $\text{SO}_2\cdot^-$ detected was found at 227° after 2 min, but this amount was about half the maximum amount found in sodium metabisulfite at approximately the same temperature.

γ -Radiolysis of sodium sulfite gave a signal at $g = 2.0038$ assigned to the $\text{SO}_3\cdot^-$ radical. No radicals were detected in heating sodium thiosulfate or sodium dithionate.

Discussion

It is not too surprising that $\text{SO}_2\cdot^-$ exists in detect-

able amounts in commercial dithionites since the general method of preparation involves precipitation of the product of a sodium or zinc reduction of SO_2 ¹⁰



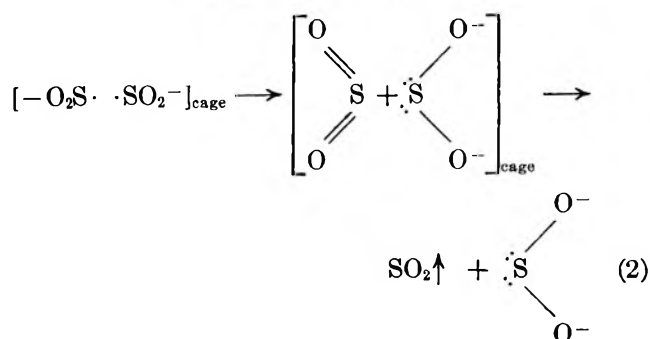
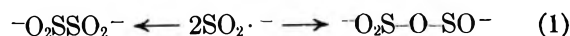
The thermal decomposition of sodium dithionite is known to give sulfur dioxide, sodium thiosulfate, and sodium sulfite¹¹



At 200° $\Delta H = -20.8$ kcal/mol.¹¹ Other minor products are sulfate and sulfur.¹²

The $\text{SO}_2\cdot^-$ signal intensity in the sodium dithionite thermal decomposition should be viewed in two parts: (1) the rapid decomposition of the $\text{SO}_2\cdot^-$ in the starting material; (2) the relatively slow "steady-state" decay of radicals produced in the thermal decomposition reaction. Since the starting concentration of $\text{SO}_2\cdot^-$ in $\text{Na}_2\text{S}_2\text{O}_4$ is 0.01 mol %, the reaction of $\text{SO}_2\cdot^-$ to non-radical products must be with the host molecules. What this reaction could be is not clear, except that SO_2 is probably produced.

The second part of the decomposition of $\text{SO}_2\cdot^-$ has the appearance of a steady-state reaction wherein the rate of production of $\text{SO}_2\cdot^-$ slightly exceeds the rate of the consumption of the radical. The most obvious reaction produces two $\text{SO}_2\cdot^-$ radicals by cleavage of dithionite. These two radicals would be confined to the "cage" of the lattice molecules. At higher temperatures the greater mobility of the radicals would permit (1) dimerization, or (2) electron transfer disproportionation to occur



There is support for the intermediacy of SO_2^{2-} in aqueous solutions. Thus, Co^{2+} induces a quantitative conversion of sodium dithionite to CoSO_2 and sulfurous acid ($\text{H}_2\text{O} + \text{SO}_2$)¹³ $\text{Na}_2\text{S}_2\text{O}_4 + \text{Co}^{2+} + \text{H}_2\text{O} \rightarrow \text{CoSO}_2 + \text{NaSO}_3 + 2\text{H}^+$. However, Na_2SO_2 is not stable in

(10) R. C. Brasted, "Comprehensive Inorganic Chemistry," Vol. 8, Van Nostrand, Princeton, N. J., 1961.

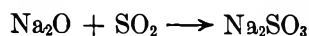
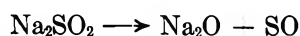
(11) P. J. Durrant and B. Durrant, "Introduction to Advanced Inorganic Chemistry," Longmans, Green and Co., 1962, p 840.

(12) O. Deines and G. Elstner, *Z. Anorg. Allg. Chem.*, **191**, 340 (1930).

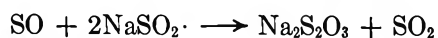
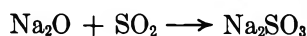
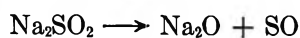
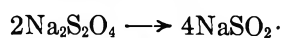
(13) R. Scholder and G. Denk, *ibid.*, **222**, 17, 48 (1935).

water and rapidly goes to thiosulfate¹³ ($2\text{Na}_2\text{SO}_2 + \text{H}_2\text{O} \rightarrow \text{Na}_2\text{S}_2\text{O}_3 + 2\text{NaOH}$). It is further of interest to speculate on the mechanism of $\text{Na}_2\text{S}_2\text{O}_3$ and Na_2SO_3 production. The sulfur-oxygen dimer could give Na_2SO_3 and SO directly ($\text{O}_2\text{S}-\text{O}-\text{SO}^- \rightarrow \text{SO}_3^{2-} + \text{SO}$). SO is a triplet molecule¹⁴ like oxygen and might combine with $\text{SO}_2\cdot^-$ to give a precursor to thiosulfate ($\text{O}_2\text{S}\cdot\text{SO}\cdot \rightarrow \text{O}_2\text{S}-\text{S}\cdot\text{O}\cdot \xrightarrow[\text{SO}_3^{2-}]{+e} \text{S}_2\text{O}_3^{2-}$).

The decomposition of Na_2SO_2 could also give SO for thiosulfate production

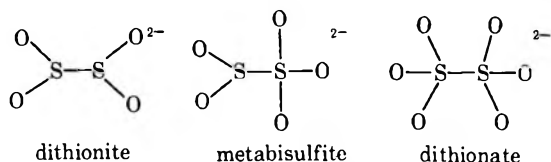


This overall mechanism fits the stoichiometry found for the thermal decomposition of sodium dithionite¹¹



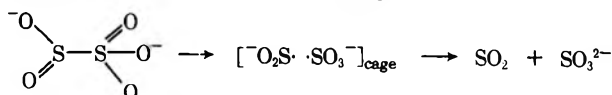
It is reasonable to question whether the esr signal is due to two radicals in close proximity or due to isolated $\text{SO}_2\cdot^-$ radicals. At this time we have no evidence that "caged" radicals contribute to the spectrum although it would be of interest to look for such species in samples rapidly quenched to low temperatures.

The structure of sodium metabisulfite (or pyrosulfite) is similar to that of dithionite in that a sulfur-sulfur bond connects the sulfur oxide parts¹⁵



The dithionate also has a similar structure.¹⁶

The $\text{SO}_2\cdot^-$ radical producing reaction in the thermal decomposition of sodium and potassium metabisulfite must be sulfur-sulfur bond cleavage

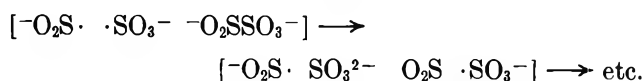


Simple electron transfer disproportionation would give SO_2 and Na_2SO_3 . These are in fact the products formed under nitrogen in the thermal decomposition between 100 and 400°C¹⁷

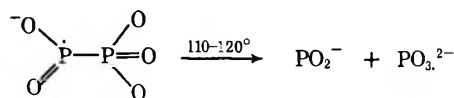


However, since the $\text{SO}_3\cdot^-$ is not observed the above reaction cannot account solely for the observation of the esr of $\text{SO}_2\cdot^-$. If the only mechanism of decay of

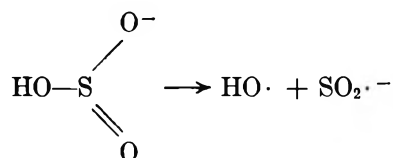
$\text{SO}_3\cdot^-$ radical was electron transfer from $\text{SO}_2\cdot^-$, either both or no radicals should be detected. A possibility here as in the case of the dithionite is radical transmission through the lattice which would in effect isolate the radicals from each other, *e.g.*



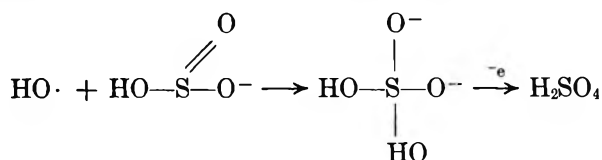
It is of interest to note that radical cleavage which is formally similar to the above has been reported by Morton¹⁸ although at somewhat lower temperatures.



The detection of $\text{SO}_2\cdot^-$ in the thermal decomposition of NaHSO_3 is perhaps the most surprising. Formally it would appear that a hydroxy radical should be the other radical produced

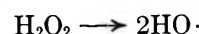


This radical would be expected to react with NaHSO_3 to give the precursor to sulfate ion, a product which is obtained, in addition to water, sulfur, thiosulfate, and SO_2 , in the thermal decomposition of NaHSO_3 ¹⁹



The latter has ample precedence in the addition reaction of hydroxy radicals to sulfoxides.²⁰

It is noteworthy that the temperature for the former reaction is lower than for latter as shown.²¹



In summary, this work shows that systems which produce sulfur dioxide as a thermal decomposition re-

(14) J. M. Daniels and P. B. Dorain, *J. Chem. Phys.*, **45**, 26 (1966); A. Carrington and D. H. Levy, *J. Phys. Chem.*, **71**, 2 (1967).

(15) I. Lindquist and M. Mörtzell, *Acta Crystallogr.*, **10**, 406 (1957).

(16) E. Stanley, *ibid.*, **9**, 897 (1956).

(17) F. Foerster and G. Hamprecht, *Z. Anorg. Allg. Chem.*, **158**, 277 (1926).

(18) J. R. Morton, *Mol. Phys.*, **6**, 193 (1963).

(19) J. S. Muspratt, *Chemist*, **4**, 433 (1843).

(20) W. T. Dixon, R. O. C. Norman, and A. L. Buley, *J. Chem. Soc.*, 3625 (1964); C. Lagercrantz and S. Forshult, *Acta Chem. Scand.*, **23**, 811 (1969).

(21) Y. M. Gershenzon, A. Dement'ev, and A. B. Nalbandyan, *Dokl. Akad. Nauk SSSR*, **180**, 1147 (1968).

action product develop readily detectable amounts of $\text{SO}_2 \cdot^-$ during the course of the reaction. Mechanisms

based on reaction products can accommodate this radical as an intermediate in the reaction.

Transfer Diffusion. III. Kinetics and Mechanism of the Triiodide-Iodide Exchange Reaction

by I. Ruff,* V. J. Friedrich, and K. Csillag

Institute of Inorganic and Analytical Chemistry, L. Eötvös University, Budapest, Hungary (Received July 5, 1971)

Publication costs borne completely by The Journal of Physical Chemistry

The I_2 transfer in the exchange reaction of iodide with triiodide ion has been studied by the transfer diffusion method. The product of the rate constant and the square of the reactant distance in the activated complex ($k\delta^2$) has been measured. The geometry of the activated complex was supposed to be a linear arrangement of the four iodine atoms with an interatomic distance of 2.90 Å which value corresponds to the available crystallographic data. The second-order rate constant calculated from the value of $k\delta^2$ with the former assumption is about $2.3 \times 10^9 \text{ M}^{-1} \text{ sec}^{-1}$ in good agreement with the value of $(2.4 \pm 0.4) \times 10^9$ determined by nmr line broadening. Taking into account the nonspherical symmetry of the triiodide ion in the collision with iodide, the observed rate constant seems to be identical with the diffusion limit.

1. Introduction

In previous papers,¹⁻⁴ the effect of transfer diffusion has been applied to study reaction rates near the diffusion limit. The theoretical basis of the method has been given in the first part of this series,³ and its applicability has been demonstrated by the kinetic investigation of the ferrocene-ferricinium electron exchange reaction.⁴ According to this, transfer diffusion seems to give reliable information also about the geometry of the activated complex as a directly measurable parameter. No other methods with such an advantageous property have been known so far.

The effect of transfer diffusion appears in the increase of the diffusion coefficient because the exchange reaction results in a displacement of the mass centers of the reactants in every successful collision; *i.e.*, they gain the path length of the distance between the mass centers of the reactants in the activated complex.

An elementary step of this accelerating effect on the migration of the species is shown schematically in Figure 1 for the iodide-triiodide exchange. It is seen that iodide is displaced by the distance δ_A , while the mass center of the triiodide ion jumps the distance δ_{AX} . It can be shown that the flux of the transferring particle X (I_2 in the present case) is

$$\left(\frac{dn_{\text{I}_2}}{dt}\right)_s = -\left[D_{\text{I}_3} + \frac{k\delta_{\text{I}_3}^2\pi}{4} \times \left(c_{\text{I},s} - c_{\text{I}_3,s} \frac{\delta_{\text{I}} \text{grad}_s c_{\text{I}}}{\delta_{\text{I}_3} \text{grad}_s c_{\text{I}_3}}\right)\right] \text{grad}_s c_{\text{I}_3} \quad (1)$$

where the flux is defined for the moles of I_2 crossing the unit area of a surface s along which the concentration of the reactants is constant, D_{I_3} is the diffusion coefficient of the triiodide ions, k is the second-order rate constant of the exchange reaction ($\text{I}^- + \text{I}_3^- \rightleftharpoons \text{I}_3^- + \text{I}^-$), the δ 's are the corresponding displacement of the mass centers, while $c_{\text{I},s}$ and $c_{\text{I}_3,s}$ are the concentration of the iodide and triiodide ions along the surface in question, respectively. The increase in the diffusion rate is related to the second term in the brackets in eq 1. It has been shown³ that this term exceeds the errors in the determination of D_{I_3} , if the rate constant is equal to the diffusion limit or approaches this value at least up to about one or two orders of magnitude. This lower limit in the determination of the rate constant coincides with the upper limit of the isotope exchange and nmr line broadening techniques.

2. Experimental Section

Materials. All chemicals were of analytical grade purchased from the Reanal Co.

Apparatus. Triiodide diffusion was measured in the photographic apparatus described elsewhere.⁴ Iodide diffusion was determined in a modified Oeholm cylinder.¹

(1) I. Ruff and I. Korösi-Ódor, *Inorg. Chem.*, **9**, 186 (1970).

(2) I. Ruff, *Electrochim. Acta*, **15**, 1959 (1970).

(3) I. Ruff and V. J. Friedrich, *J. Phys. Chem.*, **75**, 3297 (1971).

(4) I. Ruff, V. J. Friedrich, K. Demeter, and K. Csillag, *ibid.*, **75**, 3303 (1971).

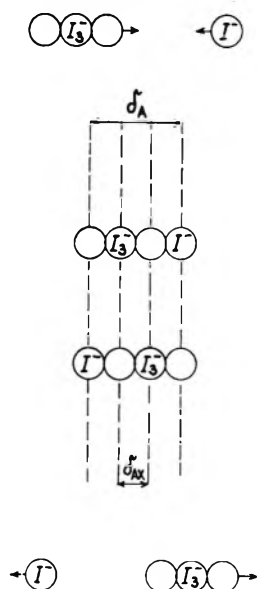


Figure 1.

The ionic strength of the solution was adjusted to 5 M by KBr . The initial concentrations in the photographic measurements were 0.01 M KI_3 , 0.1–5 M KI , and 4.9–0 M KBr in the lower solution, while in the upper one an additional amount of 0.01 M KBr was added instead of KI_3 . The iodide concentration was always constant all along the tube which permitted a simplification of the correlation in eq 1. When measuring the diffusion of iodide, the lower solution contained 3.5–5.0 M KI and 1.5–0 M KI_3 . The composition of the upper solutions ranged between 2.5 and 5.0 M KBr and 1.5 and 0 M KI_3 , and the excess iodide was always twice as much as the triiodide concentration (except the case of no triiodide present). Here the concentration of the triiodide was kept constant all along the tube.

Concentration distribution was determined either by photographic method using a Zeiss microphotometer or by iodometric titrations of the fractions obtained by slowly draining the solution from the Oehlm column. In this latter case every tenth drop was used which was supposed to correspond to a given height in the column. The concentration distribution curves were, then, evaluated by the curve-fitting method described earlier.^{1,4}

3. Results and Discussion

Since one reactant was macroscopically immobile and only one reactant could diffuse, eq 1 becomes much simpler

$$\left(\frac{dn_{I_3}}{dt}\right)_x = -\left(D_{I_3} + \frac{k\delta^2\pi}{4}c_I\right)\frac{dc_{I_3}}{dx} \quad (2)$$

where a transformation has been made for linear diffusion with respect to the axis x , and δ denotes the displacement of the mass center of the triiodide ions due to the exchange reaction δ_{I_3} in eq 1. It is seen that the term in the brackets at the right-hand side became in-

dependent on the position coordinate; *i.e.*, a normal concentration distribution should be observed with a constant apparent diffusion coefficient D_{I_3}'

$$D_{I_3}' = D_{I_3} + \frac{k\delta^2\pi}{4}c_I \quad (3)$$

This equation involves a linear relationship between the apparent diffusion coefficient and the concentration of the nondiffusing species. The slope of this straight line gives information about the value of $k\delta^2$ which can be compared to that calculated from the crystallographic and nmr data.

For the flux of the iodide ions, an equation similar to eq 1 can be formulated, but with exchanged subscripts. The data of the experiments in which iodide is the diffusing particle and the concentration gradient of the triiodide ions is zero can be evaluated according to the equation

$$D_{I'} = D_I + \frac{9k\delta^2}{4}c_{I_3} \quad (4)$$

where $D_{I'}$ and D_I are the apparent and real diffusion coefficients of the iodide ions, respectively, and the factor of 9 arises from inserting the correlation $\delta_I = 3\delta_{I_3} = 3\delta$ assuming a linear arrangement for the activated complex. This assumption is supported by the smallest possible coulombic repulsion between the two negative charges of the activated complex, though its correctness is to be proved by the experiments.

As it is seen in Figure 2, the apparent diffusion coefficients of triiodide show a linear increase with increasing concentration of iodide at all the three temperatures investigated. This increase which is about 100% in the whole concentration range appreciably exceeds the errors.

The slopes of the straight lines measured by triiodide diffusion result in $(2.1 \pm 0.4) \times 10^9$, $(2.4 \pm 0.1) \times 10^9$, and $(2.3 \pm 0.5) \times 10^9 M^{-1} \text{sec}^{-1}$ for the second-order rate constant at 15, 25, and 35°, respectively, using the crystallographic interatomic distance of 2.90 Å. These values are in excellent agreement with the nmr measurements which gave $(2.4 \pm 0.4) \times 10^9 M^{-1} \text{sec}^{-1}$ at 27°.^{5,6}

The intercepts correspond to the true diffusion coefficient of the triiodide ion. This value is $(8.6 \pm 1.0) \times 10^{-6} \text{cm}^2 \text{sec}^{-1}$ independently of the temperature. To test the reliability of the photographic method, the diffusion coefficient of the triiodide ions was determined also under the same conditions as in ref 7 in which a value of $11.3 \times 10^{-6} \text{cm}^2 \text{sec}^{-1}$ in 0.1 M KI has been

(5) "Tables of Interatomic Distances," The Chemical Society, London, 1960.

(6) O. E. Myers, Symposium on Exchange Reactions, Brookhaven, 1965; E. E. Genser, U. S. Atomic Energy Commission, UCRL-9846 (1962).

(7) J. D. Newson and A. C. Riddiford, *J. Electrochem. Acta*, **108**, 695 (1961).

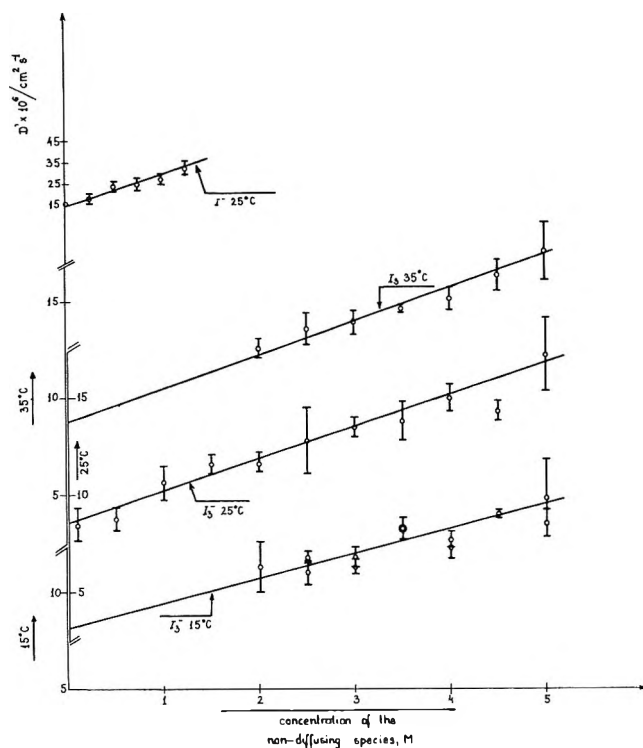


Figure 2.

reported. This coulometric datum could be satisfactorily reproduced in the photographic equipment: $(10.4 \pm 1.0) \times 10^{-6} \text{ cm}^2 \text{ sec}^{-1}$.

To exclude the possibility that the increase in the diffusion coefficient is due to some other effect of the change in the composition of the rather concentrated electrolyte solution, the viscosity was also measured as the function of the Br^-/I^- ratio in 5 M total ionic strength. The results in Table I show that the small decrease in the viscosity cannot be responsible for the twofold increase in the diffusion coefficient.

Table I: Viscosity of 5 M K (I, Br) Solutions at 25°

$[\text{I}^-]$, M	$[\text{Br}^-]$, M	η , cP
1	4	1.089
2	3	1.074
3	2	1.068
4	1	1.057

Iodide diffusion was studied in a much narrower concentration range than that in the former measurements, since a certain amount of iodide is required for keeping the iodine-triiodide equilibrium to be shifted towards practically complete triiodide formation and, thus, the difference in iodide concentration between the two solutions of the diffusion system rapidly decreases with increasing triiodide content. The apparent diffusion coefficients of iodide are plotted in the upper part of Fig-

ure 2. The expected ninefold increase in the slope of this straight line has been really found which can be seen from the parallelism of the line with those of the triiodide diffusion taking into account the ninefold shortage of the scale on the ordinate. With respect to the errors, the slope is 8.3 ± 0.8 times that of the triiodide plot at 25°. This confirms the assumption that the activated complex has a linear arrangement for the four iodine atoms involved. It should be emphasized that none of the common kinetic methods is suitable to give such information about the geometry of the activated complex.

The viscosity of the solutions used for this latter series of the measurements is shown in Table II. It can be seen that there is an appreciable increase in the viscosity with increasing triiodide content which would somewhat enhance the slope, but its effect is by all means less than the experimental errors in the apparent diffusion coefficients of iodide ions.

Table II: Viscosity of 5 M K (I, I_3) and K (I, I_3 , Br) Solutions at 25°

$[\text{I}^-]$, M	$[\text{I}_3^-]$, M	$[\text{Br}^-]$, M	η , cP
4.75	0.25	0.00	1.093
0.50	0.25	4.25	1.090
4.50	0.50	0.00	1.133
1.00	0.50	3.50	1.187
4.00	1.00	0.00	1.277
2.00	1.00	2.00	1.311
3.75	1.25	0.00	1.343
2.50	1.25	1.25	1.361

The temperature dependence of the rate constant determined by the transfer diffusion method is less than about 2 kcal/mol. This is in agreement with some simple theoretical calculations on the coulombic repulsion energy that can be estimated to be less than 1 kcal/mol. On the other hand, the diffusion limit can be calculated³ to be $5.5 \times 10^9 \text{ M}^{-1} \text{ sec}^{-1}$, if spherically symmetrical reactants are considered. This value is also independent of temperature, since the diffusion coefficient of neither the iodide nor the triiodide ions depends on it within the experimental errors. Considering, however, that the collision probability is not spherically symmetrical with respect to the shape of the triiodide ion and the activated complex, the difference between the diffusion limit and the observed rate constant can be attributed to the fact that the only efficient approach of an iodide to a triiodide is that to one of the ends of the triiodide ion within an angle of about 45° on the either side of the I_3^- axis. This would lower the diffusion limit by a factor of about $1/2$. In this way, the reaction under discussion can be regarded as a diffusion-controlled one, since an energy of activation less

than 1 kcal/mol means no restriction in comparison to RT , while the spacial requirement for the collision explains the slower rate. Thus the energy of activation observed in the nmr measurements to be 4 ± 1 kcal/mol⁶ can arise from the different conditions, *i.e.*, from the temperature dependence of the diffusion coefficient of the reactants in the more dilute solutions which results in an enhancement of the diffusion limit itself.

Hence, it seems that not the reaction, but the translational movement of the reactants—when approaching each other—needs some energy of activation, if any.

It can be concluded from the results discussed above that transfer diffusion is suitable for gaining information about significant details in the mechanism of very fast exchange reactions and can be successfully applied in their kinetic study.

The Photochemistry of Benzene in Oxygenated Aqueous Solution in the $^1B_{2u}$ First Excited Singlet State

by Menahem Luria and Gabriel Stein*

Department of Physical Chemistry, Hebrew University, Jerusalem, Israel (Received March 15, 1971)

Publication costs assisted by Israel Academy of Sciences

The photochemistry of benzene in water, by excitation at 2288, 2537, and 2652 Å into different vibrational levels of the first excited singlet state ($^1B_{2u}$), gives in the presence of O_2 at neutral pH only one major stable product. The kinetics and mechanism of its formation was investigated using continuous illumination and also flash photolysis techniques. The quantum yield of the product is steady with increasing quantum energy; the fluorescence yield decreases. A mechanism is proposed which involves formation of a labile energetic isomer of the ground state singlet from a nonstationary energy-rich state of the excited singlet before the fluorescent level is reached, and in competition with intersystem crossing. This labile isomer adds O_2 . The primary photooxide rearranges to give the final product.

Introduction

The pathways of reaction—radiative and nonradiative—of excited molecules are modified by introducing the molecule into a solvent. Even if the solvent does not participate chemically in the reactions, it provides a route to partial energy loss by the excited solute, which otherwise could occur only by a radiative pathway. Therefore in solution specific states, still energy rich, may be readily reached.

Under suitable conditions, water is such a chemically inert solvent for benzene. Comparison with the absorption spectrum of benzene in the gas phase indicates that the ground and excited state the solute molecule is little perturbed in water, less so than, *e.g.*, in cyclohexane. Chemical product formation permits one to follow interactions resulting from the excited state resulting on light absorption, before thermal equilibrium is established.

We studied the photoreactions of benzene in the presence of oxygen in aqueous solution, under conditions where oxygen did not interact with the ground or primary excited state of benzene, and served only to fix

by chemical reaction an intermediate in competition with a pathway to radiationless deactivation.

The photochemistry of benzene has been investigated, especially in the vapor phase, but also in the liquid phase and in solution. Little has been published on the photooxidation of benzene in these systems.

The photochemistry in the vapor phase has been thoroughly studied in all regions of the uv spectrum. In the far-uv (1165–1470 Å), the photoproducts are hydrogen and various hydrocarbons from C_2H_2 to $C_6H_5C_6H_7$.^{1,2} In the range 1600–2000 Å an isomer of benzene was obtained which is probably fulvene^{3,4} rather than benzvalene,^{5,6} as previously proposed. It has also been shown that photochemistry at 1849 Å

- (1) R. Hentz and S. J. Rzed, *J. Phys. Chem.*, **71**, 4096 (1967).
- (2) W. M. Jackson, J. L. Faris, and B. Donn, *ibid.*, **71**, 3346 (1967).
- (3) L. Kaplan and K. E. Wilzbach, *J. Amer. Chem. Soc.*, **89**, 1030 (1967).
- (4) H. R. Ward and J. S. Wishnok, *ibid.*, **90**, 5353 (1968).
- (5) K. Shindo and S. Lipsky, *J. Chem. Phys.*, **45**, 2292 (1966).
- (6) J. K. Foote, M. H. Mallon, and J. N. Pitts, Jr., *J. Amer. Chem. Soc.*, **88**, 3698 (1966).

breaks the benzene ring and gives rise to 1,3-hexadien-5-yne.⁷ Irradiation at 2537 Å of benzene vapor also gives a rearrangement of the benzene ring, contrary to earlier ideas.⁸ This is illustrated by the change of 1,3,5-*d*₃-benzene to 1,2,4-*d*₃-benzene⁹ and by the production of benzvalene at a low yield.¹⁰

In the liquid phase and in hydrocarbon solution benzvalene has been identified after irradiation at 2537 Å.¹¹ Benzvalene, Dewar-benzene, and fulvene were identified after irradiation in liquid phase below 2000 Å.⁴

Oxidation of benzene in the gas phase by atomic oxygen gives phenol.¹² Photooxidation in liquid benzene gives mucondialdehyde and polyenic dialdehydes.¹³ In the presence of O₂, C₆H₆ in the vapor phase at 2537 Å gives a number of simple hydrocarbons, and carbon oxygen compounds, such as acetylene, 1,3-butadiene, acrolein carbon suboxide, and others.¹⁴ Earlier work showed that the product of photooxidation of benzene in water is similar to, but not identical with, mucondialdehyde.¹⁵ More recently, it was shown that the product of photooxidation of benzene in water on irradiation at 2537 Å is an isomer of mucondialdehyde, 2-formyl-4*H*-pyrane,^{16,17} or a cyclopentadienyl isomer.¹⁷

We report our results on the kinetics of this reaction and attempt to derive a mechanism to account for these. We shall correlate our results with previous ones, summed up above, to connect spectroscopy and photochemistry.

Experimental Section

For irradiation at 2288 Å we used a 25-W Philips cadmium lamp. Under the conditions employed the only line observed of significant intensity in the region of 2200–2800 Å was at 2288 Å.

The light sources used for 2537-Å irradiation were low-pressure mercury resonance lamps made by Thermal Syndicate Ltd. Of the two types used, one was a small flat spiral, and the other a large spiral cylinder. The former was used for the irradiation of 5 ml of solution in a 1-cm path length Spectrosil cell. A filter containing 1 *M* KCl with an optical path length of 1 cm was placed between the light source and the solution. The second lamp was used for the irradiation of 250 ml of solution in a quartz cell which was inserted within the spiral of the lamp. The cell was double-walled, and the space between the walls was filled with 2 *M* KCl solution which acted as a filter with an optical path length of 0.5 cm. The KCl filters eliminate light from the 1849-Å line of the lamp.

The quantum yield at ~265 nm was obtained from experiments using a 100-W Hanovia medium pressure mercury lamp, Type SH. This lamp has a number of lines around 265 nm. These and the line at 2537 Å are the only ones of the lamp's output absorbed by our solutions. From the known intensities in the separate lines we calculated the effect due to 2537-Å light and

hence the quantum yield at ~265 nm. The uranyl oxalate actinometer was used, taking¹⁸ $\phi_{2288} = 0.55$; $\phi_{2537} = 0.60$; $\phi_{2652} = 0.60$. The light intensities of the lamp were about 6×10^{-6} einstein l.⁻¹ sec⁻¹ at 2288 Å for the cadmium lamp, 2×10^{-6} einstein l.⁻¹ sec⁻¹ for the small spiral, 5×10^{-6} einstein l.⁻¹ sec⁻¹ for the large spiral at 2537 Å, and 2×10^{-6} einstein l.⁻¹ sec⁻¹ for the medium pressure mercury lamp at ~265 nm. Light intensities were accurately determined for every series of experiments. Spectra were measured in the visible and uv range using Cary 14 and Perkin-Elmer 450 spectrophotometers and in the ir region, a Perkin-Elmer ir spectrophotometer; pH measurements were carried out with a Metrohm-pH meter, the flash photolysis experiments with the apparatus described by Ottolenghi and Rabani,¹⁹ and fluorescence measurements with a Turner spectrofluorimeter Model 210.

Chemicals and Solutions. Benzene Fluka Puriss. (99.93%) thiophen-free was used without further purification. A further distillation did not affect the results. The water used was triple distilled. All other reagents, oxygen, xenon, HClO₄, KOH, CH₂Cl₂, and dinitrophenylhydrazine (DNP), were of analytical grade.

The irradiated solutions contained about 1.2×10^{-2} *M* benzene in water. The solution used in the flash photolysis experiments contained about 4×10^{-3} *M* benzene. In the fluorescence experiments the solution used was around 3×10^{-4} *M*. Concentrations of benzene in water were determined using the method of Marketos.²⁰ After adding the benzene, the solutions were stirred for 2 hr to dissolve the benzene and to allow saturation of air. During the irradiation the solutions were mixed with a Teflon-coated magnetic stirrer.

The oxygen concentration in the solution was 2.2×10^{-4} *M* (calculated from the atmospheric pressure taken as 696 ± 3 mm and by Henry's constant for oxygen). In the experiments on the dependence of quan-

(7) L. Kaplan and K. E. Wilzbach, *J. Amer. Chem. Soc.*, **90**, 5646 (1968).

(8) J. N. Pitts, Jr., J. K. Foote, and J. K. S. Wan, *Photochem. Photobiol.*, **4**, 323 (1965).

(9) L. Kaplan and K. E. Wilzbach, *J. Amer. Chem. Soc.*, **90**, 1116 (1968).

(10) L. Kaplan and K. E. Wilzbach, *ibid.*, **90**, 3291 (1968).

(11) L. Kaplan and K. E. Wilzbach, *ibid.*, **89**, 1031 (1967).

(12) E. Grovenstein and A. J. Mosher, *ibid.*, **92**, 3812 (1970).

(13) K. Wei, J. C. Mani, and J. N. Pitts, Jr., *ibid.*, **89**, 4225 (1967).

(14) A. Morikawa and D. J. Cvetanovic, *J. Chem. Phys.*, **52**, 3237 (1970).

(15) I. Loeff and G. Stein, *Nature*, **184**, 901 (1959); *J. Chem. Soc.*, 2623 (1963).

(16) E. Farenhorst, *Tetrahedron Lett.*, 4835 (1968).

(17) M. Luria and G. Stein, *Chem. Commun.*, 1650 (1970).

(18) E. Bowen, "Chemical Aspect of Light," 2nd ed, Oxford University Press, London, 1949, p 283.

(19) M. Ottolenghi and J. Rabani, *J. Phys. Chem.*, **72**, 593 (1968).

(20) D. G. Marketos, *Anal. Chem.*, **41**, 195 (1969).

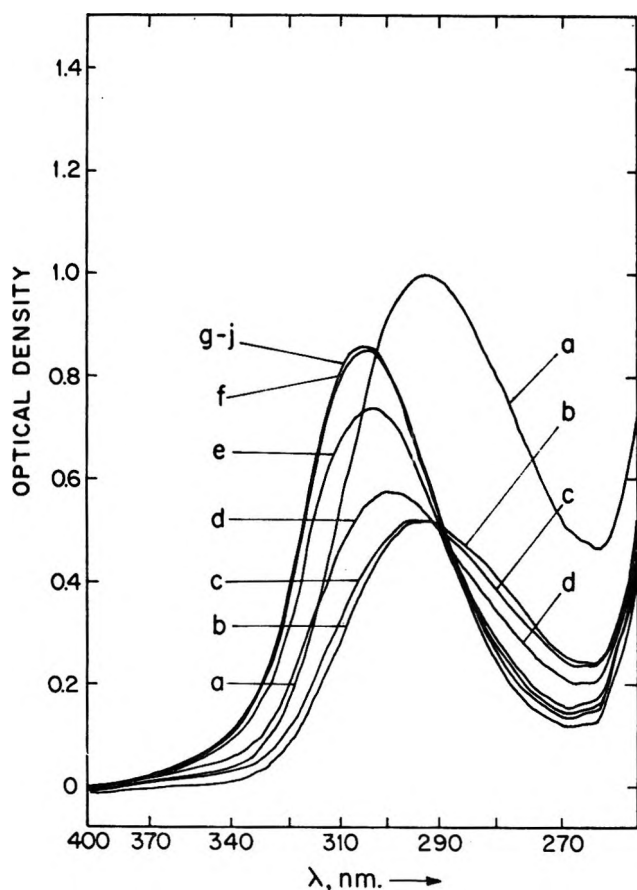


Figure 1. Absorption spectrum of the photoproduct in aerated solution; dose 9.2×10^{-6} einstein $l^{-1} \text{ sec}^{-1}$: curve a, the solution irradiated at 2537 Å; curves b-j, 50% of the irradiated solution with 50% KOH solution added at different concentrations.

tum yield on oxygen concentration and in the experiments done under vacuum, the solutions were evacuated using freeze-thaw cycles to a pressure of less than 10^{-4} mm; then oxygen was introduced at the appropriate concentration. The initial pH of the solutions was 6.5. The experiments were carried out at room temperature, $23 \pm 2^\circ$, except for those in which the temperature effect was investigated.

Results

Continuous Illumination. In short irradiations at doses of 10^{-3} einstein l^{-1} or less, one major photochemical product appears only with maximum absorbance at 294 nm. Figure 1 shows the absorption spectrum obtained in neutral solution. Figure 2 shows that the relationship between dose and product concentration is linear. This product has been identified^{16,17} as 2-formyl-4*H*-pyran or its cyclopentadienyl isomer.¹⁷ Addition of alkali to the solution resulted in a shift of the maximum absorbance to 308 nm. Reacidifying brought the maximum absorbance back to the original. Another product band was found around 220 nm.

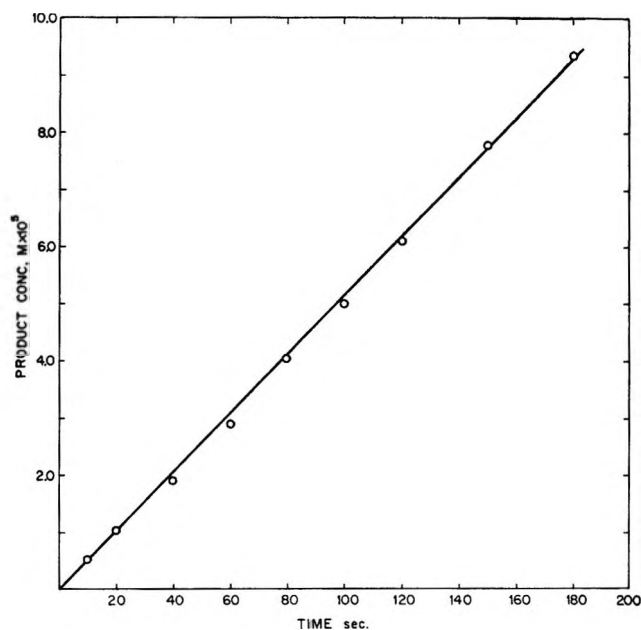
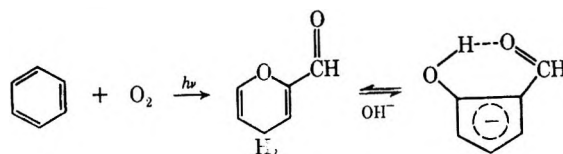


Figure 2. Photoproduct yield as function of irradiation time at a constant dose rate of 8.2×10^{-6} einstein $l^{-1} \text{ sec}^{-1}$.

The major photochemical product only appeared in the presence of O_2 . The dependence of quantum yield on oxygen concentration shows an increase to a limiting value with increase of oxygen concentration.

The major photochemical product only appeared in O_2 -containing solutions around neutral pH. At pH values greater than 10 or lower than 4, the product did not appear. On the other hand, in basic or acidic O_2 -containing solutions and in evacuated solutions some absorbance around 220 nm still appeared, indicating the formation of some other product, albeit with apparently low quantum yield. In previous work¹⁶ the product in the absence of O_2 or in its presence, but in acid or alkaline solutions, was thought to be due to the addition of H_2O to benzene. We have not investigated this product further in the present work.

The major photooxidation product can be extracted into polar solvents from acid and neutral solutions but not from basic solutions. The photooxidation product was stable. There is no change in the absorption spectrum on extracting the product into dichloromethane, evaporation of most of the solvent, re-extracting into a basic aqueous solutions and reacidifying. Making use of these properties we established¹⁷ the structure of the product, in agreement with the proposal of Farenhorst,¹⁶ as 2-formyl-4*H*-pyran or its cyclopentadienyl isomer¹⁷ so that the overall photochemical process is



To determine the quantum yield, we note that after 180 sec of irradiation at a dose rate of 9.2×10^{-6} einstein $l^{-1} \text{ sec}^{-1}$, the resulting product had an optical density of 1.0 at 294 nm (Figure 1a). Nine portions of 5 ml each were taken from the irradiated solution, and to each of these a solution of $4 \times 10^{-4} M$ KOH was added from 0 to 5 ml; finally water was added to make the solutions up to 10 ml. The resulting spectra are shown in Figure 1, curves b-j.

It can be seen that the curves pass through a common isosbestic point, in going from the acidic to basic form of the product. Figure 3 shows the relationship

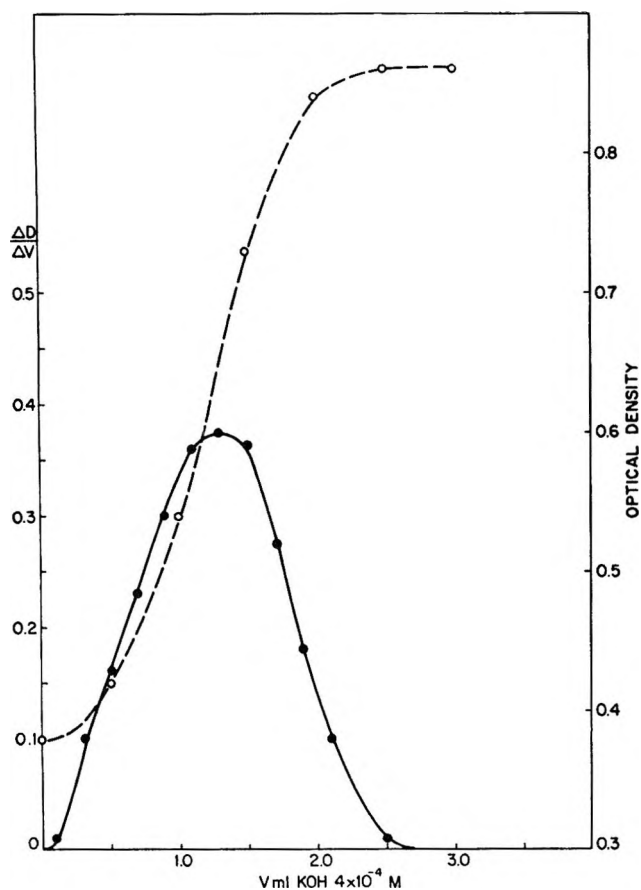


Figure 3. Titration curves of the photoproduct. The right-hand scale and broken line denote the optical density as a function of milliliters of KOH added. The left-hand scale and continuous line show the change of the optical density per unit volume as a function of the volume of the base added.

between optical density at 308 nm and the amount of added alkali. The equivalent point was determined by plotting $\Delta V/\Delta(\text{OD})$ against added volume. The equivalent volume of the base was 1.3 ml. Hence the product concentration was $1.04 \times 10^{-4} M$, and the extinction coefficient at 294 nm was calculated as $9630 M^{-1} \text{ cm}^{-1}$. From the relationships of the absorbances at 294 nm in the acid form, and 308 nm in the basic form, the extinction coefficient was found to be $15,640 M^{-1} \text{ cm}^{-1}$ at 308 nm. The light intensity and resul-

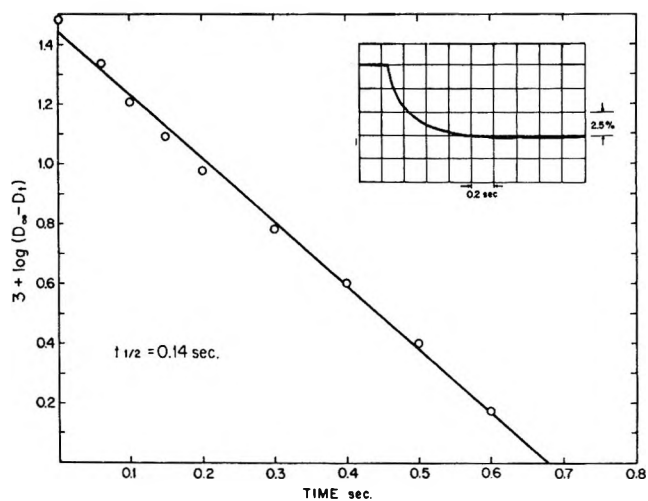


Figure 4. First-order formation of the photoproduct at 294 nm. Insert: oscilloscope trace of absorption.

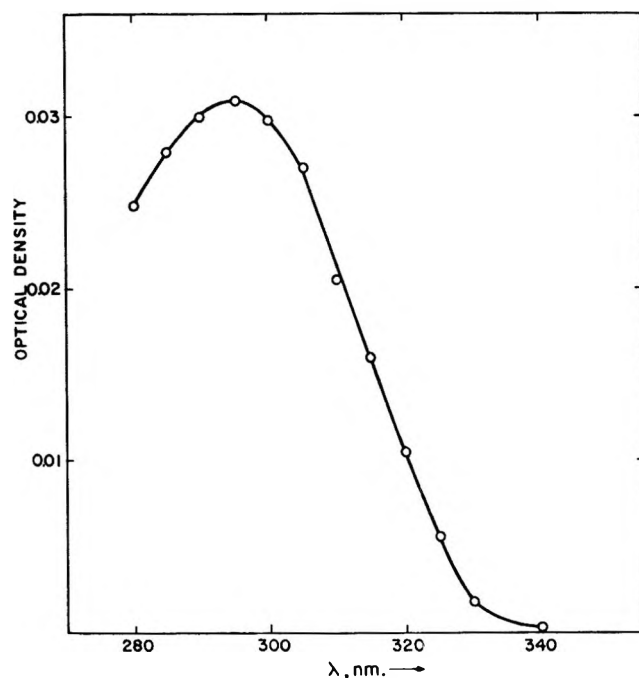


Figure 5. Absorption spectrum of the photoproduct 0.4 sec after irradiation by flash.

tant product concentration gave the quantum yield $\phi = 0.065$ in aerated solution. We also obtained $\phi_{\text{max}} = 0.095$ in solutions saturated with O_2 at 1 atm.

The pK_a of the photoproduct was found from the pH measurement. The pH of the solution which gave curve d (Figure 1) was 7.45 and in curve e was 7.9. Therefore, the pH at the equivalent point which is equal to the pK_a is approximately 7.7.

Flash Photolysis of Aerated Solutions. For these experiments, a 5 Torr oxygen lamp was used. To cut off radiation below 220 nm, a 9-54 Corning filter was employed. Using 20- μsec half-life flashes, transient spectra of intermediates could not be observed. The formation of the final product could be followed. This

product appeared in a first-order reaction (Figure 4). From the plot of $3 + \log(D_\infty - D_t)$ vs. t , the rate constant of the formation is 5 sec^{-1} . Figure 5 shows the spectrum after 0.4 sec. It is similar to the absorption spectrum of the final product. When solutions free of O_2 were flashed, the absorption at 292 nm did not appear.

Irradiations at 2288 Å and $\sim 265 \text{ nm}$. The product obtained at the above wavelengths was identical with that obtained by irradiation at 2537 Å. However, the quantum yield has a different value. At 2288 Å the yield was 0.085 in aerated solution, and 0.11 in solutions saturated with O_2 at 1 atm. At 265 nm the quantum yield was calculated from the relative intensity of the spectral lines and a value of 0.08 estimated in aerated solutions.

Temperature Effect. In the range of $5\text{--}65^\circ$, at 2537 Å, no effect was observed on the quantum yield of photooxidation within our experimental accuracy.

Some experiments were carried out in the presence of xenon at a concentration of $\sim 5 \times 10^{-3} M$. Its presence had no effect on photochemistry or fluorescence.

Discussion

Figure 6 shows the absorption spectrum of benzene ($7 \times 10^{-3} M$) in H_2O . In agreement with Mantione and Daudey,²¹ who calculate the interaction energy between the solute molecule and a complete shell of surrounding solvent molecules and find it smallest in the case of benzene with water as the solvent, we find the spectrum less affected by water than, *e.g.*, by cyclohexane. Thus, for the ${}^1\text{B}_{2u}$ first excited singlet electronic state with the $\text{A}_1^\circ (1\nu_2 + 1\nu_{18})$ vibrational component in the excited state, the peak is at $39,534 \text{ cm}^{-1}$ in the gas phase, $39,385 \text{ cm}^{-1}$ in water (2539 Å), and $39,245 \text{ cm}^{-1}$ in cyclohexane.

At the concentration of benzene employed, interaction between benzene molecules in the ground or excited state does not occur.

Absorption of light at ~ 265 , 254, or 229 nm brings benzene into the ${}^1\text{B}_{2u}$ first excited singlet state, with increasing vibrational energies. Comparison between the dependence of photochemical and fluorescence yields on some variables enables one to deduce the reactions of the primary excited state, *i.e.*, the one resulting directly on light absorption.

We are engaged in a study of fluorescence spectrum, yield, and decay time of benzene in aqueous solution. We plan to publish our detailed results separately. Here we give our relevant results briefly.

The decay time of fluorescence was found to be 2.2 nsec at a benzene concentration of $\sim 10^{-2} M$. Fluorescence yield or lifetime were not affected by changing of O_2 pressure between zero and 1 atm, or varying pH over the range of 1–13. The fluorescence yield was measured as a function of exciting wavelength over

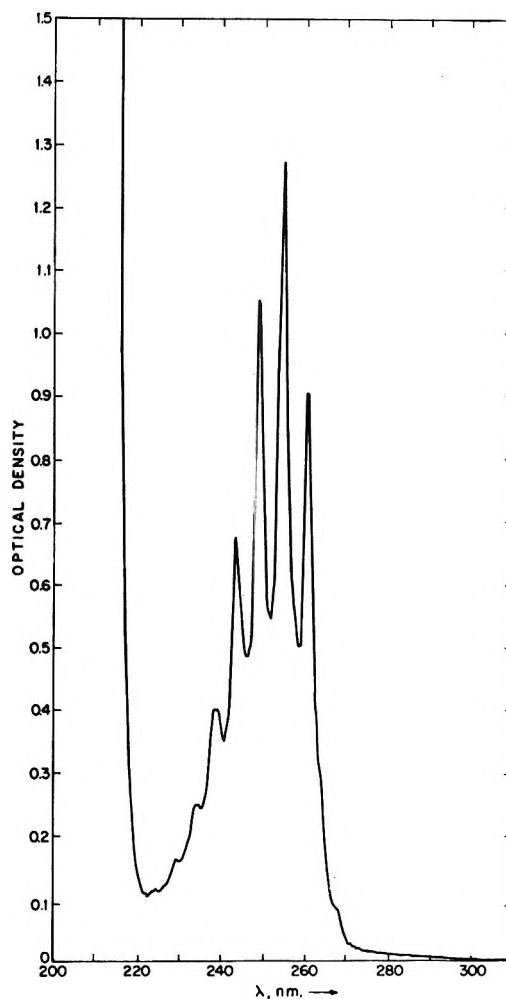


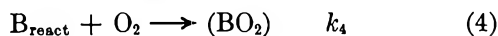
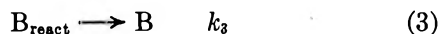
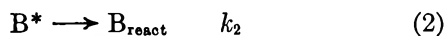
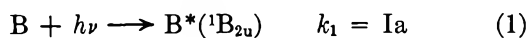
Figure 6. Absorption spectrum of benzene in water; $\epsilon_{254} \approx 180$.

the region of 2665–2250 Å. It was found to be almost constant between 2665 and 2450 Å, and was observed to decrease below 2400 Å.

By contrast, quantum yield of our product is steady with increasing quantum energy between 265 and 229 nm and is strongly affected by O_2 pressure and pH. We conclude that it is not the fluorescent state itself, *i.e.*, the lowest vibrational level of ${}^1\text{B}_{2u}$ which reacts with O_2 . This is also to be expected from the short lifetime which makes dynamic quenching by O_2 impossible. At the benzene and O_2 concentration employed static quenching through interaction existing in the ground state is not likely to be of importance, and there is no evidence for it in the spectrum, *e.g.*, in the neighborhood of the $\text{S}_0 \rightarrow \text{T}_1$ absorption.

From the dependence on O_2 concentration, and assuming that the reactive benzene intermediate adds O_2 at the diffusion-controlled rate, we calculate the lifetime of the benzene intermediate which reacts with O_2 , according to the scheme

(21) M. J. Mantione and J. P. Daudey, *Chem. Phys. Lett.*, **6**, 93 (1970).



Here, reaction 1 represents excitation to a specific vibrational level of the $^1B_{2u}$ electronic state.

k_6 represents all decay pathways, radiative and non-radiative, of B^* other than reaction 2. It includes (Figure 7) radiationless decay from the nonstationary energy-rich vibrational level to the ground state or to the relatively long-lived quasistationary fluorescent level, followed by processes a and b—fluorescence, and intersystem crossing from the $^1B_{2u}$ state (in solution probably mainly from the zero vibrational level) to T_1 .

The fact that with increasing $[O_2]$ we reach a limiting yield of our product, steady with the quantum energy of the exciting wavelength but independent of temperature, is consistent with the assumption that under these conditions all B_{react} yields (BO_2) , and (BO_2) quantitatively yields the final product, so that the limiting yield at high $[O_2]$ corresponds to the yield of B_{react} .

The quantum yield is

$$\Phi = k_2 k_4 [O_2] / (k_2 + k_6)(k_4 [O_2] + k_3) \quad (7)$$

At high $[O_2]$, $k_4 [O_2] \gg k_3$, therefore at 2537 Å

$$\Phi_{\text{max}} = k_2 / (k_2 + k_6) = 0.095 \quad (8)$$

Hence at 2537 Å $k_6 \simeq 9k_2$.

In view of the constancy of Φ with increasing wavelength the main competition appears to be with radiationless decay directly to the ground state or, at higher wavelengths, to some extent to the fluorescent lowest vibrational level of $^1B_{2u}$. The rate constant k_6 is probably of the order of 10^{12} sec^{-1} .

At any concentration of O_2

$$\Phi_{\text{max}} / \Phi = (k_4 [O_2] + k_3) / k_4 [O_2] = (k_3 / k_4 [O_2]) + 1 \quad (9)$$

Plotting $(\Phi_{\text{max}} / \Phi) - 1$ against $1/[O_2]$ (Figure 8), the straight line gave the slope $k_3/k_4 = 1.5 \times 10^{-4} M$. Assuming that reaction 4 is diffusion controlled with $k_4 \simeq 10^{-10} M^{-1} \text{ sec}^{-1}$, $k_3 \simeq 1.5 \times 10^6 \text{ sec}^{-1}$. Thus $\tau_{1/2} \sim 5 \times 10^{-7} \text{ sec}$, of B_{react} , the intermediate reacting with O_2 . This intermediate is not likely to be the triplet state, T. Available information indicates^{22,23} that the formation of T decreases with decreasing λ similar to the dependence of the fluorescent state. The reactivity with O_2 now observed does not resemble the effect of O_2 on S_1 or T_1 .¹⁴ Our reactive intermediate is more likely to be an energetic isomer of ground state benzene, for example, benzvalene, or the precursor which yields benzvalene under some conditions.²⁴

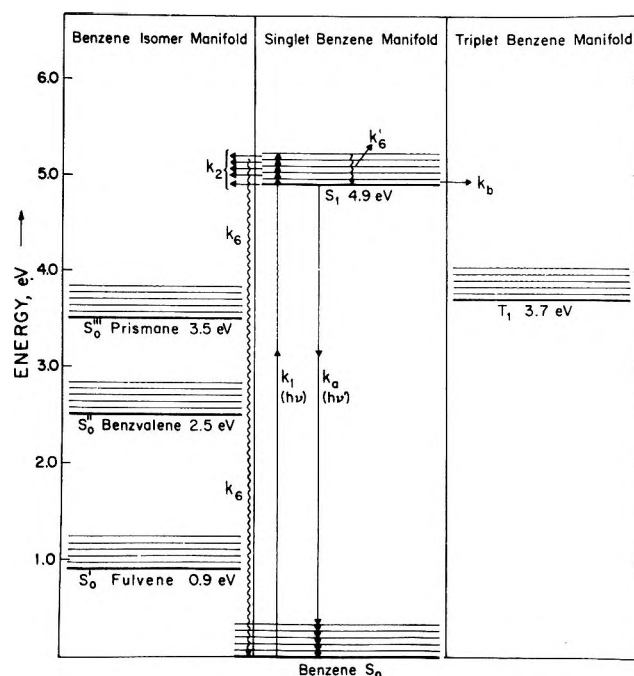


Figure 7. Schematic representation of states involved in radiative and radiationless transitions in the benzene system. Energy scale above the S_0 state is for the zero vibrational level. Vibrational levels are not drawn to scale.

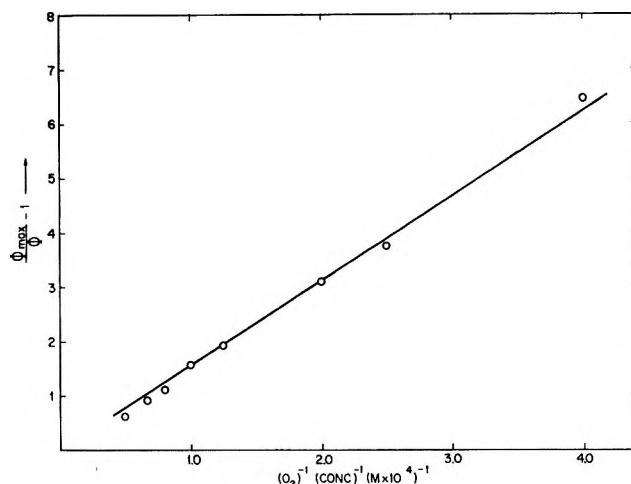


Figure 8. The determination of k_3 by plotting $(\Phi_{\text{max}}/\Phi) - 1$ against the reciprocal of the oxygen concentration.

We thus envisage a reaction in which the primarily formed $^1B_{2u}$ species may convert in the course of vibration to a highly energy-rich isomer of the ground state. Losing energy to the solvent, it will cascade down the energy levels, there being a finite probability of some of the molecules becoming trapped in metastable

(22) W. A. Noyes, Jr., and D. H. Harter, *J. Chem. Phys.*, **46**, 674 (1967).

(23) R. B. Cundall and W. Tippett, *Trans. Faraday Soc.*, **66**, 350 (1970).

(24) D. Bryce-Smith and H. C. Longuet-Higgins, *Chem. Commun.*, 593 (1966); D. Bryce-Smith, *Pure Appl. Chem.*, **16**, 56 (1968).

states, prismane being the most energy rich of these²⁵ (Figure 7).

Some of the species thus formed become a sufficiently long-lived metastable form to react with O₂.

Our work relates to the recent interest in processes resulting on exciting benzene to single vibronic levels in the vapor phase.²⁶ As mentioned, from the point of view of the spectroscopic process, the situation in aqueous solution is particularly close to the vapor phase, more so than in cyclohexane. The fluorescence yield on excitation at 2537 Å in aqueous solution is, however, only²⁷ ~0.006 compared with ~0.07 in cyclohexane²⁸ and ~0.25 in the gas phase.²⁶ For the ¹B_{2u} → ³B_{1u} transition, all vibronic levels, including the lowest²⁶ lie in the statistical limit²⁹ in the gas phase. Our results are consistent with the assumption that the role of the water solvent, which appears to affect little the electronic wave functions of the ground or first excited singlet state of benzene, lies in facilitating the pathway to chemical relaxation and metastable isomer formation, in competition with processes which lead to the zero vibrational ¹B_{2u} or to the ³B_{1u}. The sum of fluorescence (F) and triplet formation (T) is less than unity in benzene solutions. The pathway now described may contribute to the difference 1 - (F + T).

After submitting our manuscript, our attention was drawn to two recent communications by Kaplan, Wendling, and Wilzbach³⁰ on the nature of the product of photooxidation of aqueous benzene. They identify the product as cyclopentadienecarboxaldehyde. The conditions under which they obtain their product in water free of O₂ and the rate of formation of their product is sufficiently different from ours to leave open the possibility of a different mechanism and product in their case. This possibility remains to be clarified.

Acknowledgment. We thank Dr. Kaplan for communicating his results before publication. This research was supported by a grant from the Israel Academy of Sciences.

(25) N. Colin-Baird and M. J. S. Dewar, *J. Amer. Chem. Soc.*, **91**, 352 (1969).

(26) B. K. Selinger and W. R. Ware, *J. Chem. Phys.*, **53**, 3160 (1970); C. S. Parmenter and M. W. Schuyler, *Chem. Phys. Lett.*, **6**, 339 (1970); R. R. Ware, B. K. Selinger, C. S. Parmenter, and M. W. Schuyler, *ibid.*, **6**, 342 (1970).

(27) M. Luria and G. Stein, to be published.

(28) I. B. Berlman, "Handbook of Fluorescence Spectra of Aromatic Molecules," Academic Press, New York, N. Y., 1965, p 42.

(29) G. W. Robinson, *J. Chem. Phys.*, **47**, 1967 (1967).

(30) L. Kaplan, L. A. Wendling, and K. E. Wilzbach, submitted for publication.

Chlorophyll-Poly(vinylpyridine) Complexes. IV. Transfer of Energy to a Complex of Pyrochlorophyll with DTNB¹

by G. R. Seely

Charles F. Kettering Research Laboratory, Yellow Springs, Ohio 45387 (Received June 15, 1971)

Publication costs assisted by C. F. Kettering Research Laboratory

Pyrochlorophyll and 5,5'-dithiobis(2-nitrobenzoic acid) (DTNB) form a complex which is stable when both components are bound to poly(4-vinylpyridine) in nitromethane. The complex is characterized by displacement of the pyrochlorophyll absorption band in the red 50 Å to longer wavelengths, and by a fluorescence quantum yield of about 0.009. These properties of the complex are more pronounced than might have been expected from the properties of associations of pyrochlorophyll with the simpler molecules *o*-nitrobenzoic acid (*o*-NBA) and 2,2'-dithiodibenzoic acid (DTBA). The complex serves to trap and quench singlet excited state energy from neighboring uncomplexed pyrochlorophyll molecules; to this extent it is analogous to the reaction center of a photosynthetic unit. Although fluorescence quenching may proceed at least partly through an electron transfer reaction, no net photochemical reduction of complexed DTNB could be detected. The rate of nonradiative energy transfer among pyrochlorophylls was calculated over a range of pigment densities on the polymer. Although the rates so calculated extend into the hundreds per excited state lifetime, the efficacy of trapping by the complex is in practice limited by the presence of pairs or higher aggregates of pyrochlorophyll which also quench fluorescence.

Introduction

Complexes between chlorophyll or its derivatives and poly(4-vinylpyridine) in nitromethane constitute a useful model system with which to study energy transfer at controlled, variable pigment densities which approach those in the natural photosynthetic unit.²⁻⁴ We now describe the introduction of a simple trap for energy into the system and calculate the rate of nonradiative energy transfer to it for various pigment concentrations. As in previous work, we used pyrochlorophyll in place of chlorophyll because of its greater stability.

Most of the chlorophyll in a photosynthetic unit is "antenna chlorophyll," the function of which is to collect light energy and transfer it to a small amount of "reaction center chlorophyll," where the electronic energy of excitation is converted into chemical or electrochemical form.⁵ Furthermore, there appear to be at least two kinds of photosynthetic units in green plants, each with its own reaction center: System 1 (CO₂ reduction), with a specialized reaction center chlorophyll called P700,⁶ and System 2 (O₂ evolution), with a less well characterized reaction center chlorophyll absorbing at 682 nm.⁷

In both systems, the reaction center chlorophyll absorbs at longer wavelengths than the antenna chlorophyll. In both systems, the reaction center chlorophyll is associated with an oxidant, sometimes designated "Z" for System 1 and "Q" for System 2, the chemical nature of which is unknown. Energy conversion is initiated by transfer of an electron from the chlorophyll to the oxidant, according to the evidence of

absorption spectral and fluorescence yield changes in the light. The absorption of light by the reaction center chlorophyll at slightly longer wavelengths than by the antenna chlorophyll, although probably not an essential characteristic of the trap,⁸ does tend to increase the rate of energy transfer to it. It is not known whether the displaced absorption of reaction center chlorophyll is a direct consequence of its association with the oxidant.

There are several ways of attaching molecules to poly(vinylpyridine) which may interact with chlorophyll in its ground or excited state. Perhaps the simplest way, and the way chosen here, is reaction of a carboxylic acid function with a pyridine group of the polymer. The pyridinium carboxylate ion pair so formed should be stable in nitromethane. It was expected that the fortuitous proximity of pyrochlorophyll to an oxidant attached in such a way to the polymer would create a trap for energy by electron transfer.

Aromatic nitro compounds quench fluorescence and react by electron transfer with singlet and triplet ex-

(1) Contribution No. 448.

(2) G. R. Seely, *J. Phys. Chem.*, **71**, 2091 (1967).

(3) G. R. Seely, *ibid.*, **74**, 219 (1970).

(4) G. R. Seely, *ibid.*, **75**, 1667 (1971).

(5) R. K. Clayton in "The Chlorophylls," L. P. Vernon and G. R. Seely, Ed., Academic Press, New York, N. Y., 1966, Chapter 19.

(6) B. Kok and G. Hoch in "Light and Life," W. D. McElroy and B. Glass, Ed., Johns Hopkins Press, Baltimore, Md., 1961, pp 397-423.

(7) G. Döring, G. Renger, J. Vater, and H. T. Witt, *Z. Naturforsch. B*, **24**, 1139 (1969); Govindjee, G. Döring, and R. Govindjee, *Biochim. Biophys. Acta*, **205**, 303 (1970).

(8) Reference 5, p 623.

cited pyrochlorophyll.^{9,10} Nitrobenzoic acid derivatives would therefore be suitable for investigation as trapping agents. One of those tested was 5,5'-dithio-bis(2-nitrobenzoic acid), also known as DTNB and Ellman's reagent for the determination of sulfhydryl groups of proteins.¹¹ This compound promised certain advantages. As an *o*-nitrobenzoic acid derivative it should be readily reduced by excited singlet or triplet pyrochlorophyll.^{9,10} As a dicarboxylic acid, it should be firmly attached to the polymer by two ion pairs. Finally, the product of this reduction, 2-nitro-5-mercaptobenzoic acid, forms a yellow thiophenolate anion in mildly basic aqueous solution, with a strong absorption band by which a photochemical reduction might be followed.

With this compound, we found not just a fortuitous proximity but a rather strong complex formation with pyrochlorophyll, and a strong quenching action on the fluorescence. A complex of DTNB and pyrochlorophyll, together with uncomplexed pyrochlorophyll surrounding it, constitute a small system which is analogous in some respects to a photosynthetic unit. The extent of the analogy, and the insight it provides into the working of the photosynthetic unit, are discussed.

Experimental Section

Materials. Preparation and purification of pyrochlorophyll, poly(4-vinylpyridine), nitromethane, and hydrazobenzene were performed as described in the preceding paper of this series⁴ and the references cited therein. Other reagents were obtained commercially and, with the exception of DTNB and DTBA, were used as received.

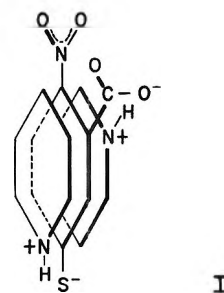
DTNB was recrystallized from acetic acid and dried over KOH under vacuum. The absorptivity of the 409-nm absorption band of the anionic form of its reduction product was determined by adding quantities of DTNB solution to an excess of ethyl mercaptan in 0.4% Na₂HPO₄. The absorbance followed Beer's law up to 2 cm⁻¹; the molar absorptivity so determined, 13840 M⁻¹ cm⁻¹, was slightly greater than the usually cited value of 13600 M⁻¹ cm⁻¹.¹¹ DTBA was recrystallized from acetic acid.

Procedure. Most experiments were made by adding increments of a solution of DTNB in nitromethane to a cuvette containing pyrochlorophyll and poly(vinylpyridine) in nitromethane. Spectra were taken on a Cary 14R spectrophotometer; fluorescence, excited by Cd 6438-Å radiation, was measured and corrected as described previously.^{3,10} From the spectrum, the position (λ) and half-width (δ) at half height of the pyrochlorophyll absorption band near 666 nm were determined as described previously.² The pyrochlorophyll concentration was *ca.* 2 × 10⁻⁵ M. Polymer pyridine and DTNB concentrations are expressed as multiples of the pyrochlorophyll concentration, (py)/(chl) and (DTNB)/(chl).

Calculation of energy transfer rates was performed by the Mark II Computer through the General Electric time-sharing service.

Results

Pyrochlorophyll sensitizes the photoreduction of DTNB by hydrazobenzene in nitromethane containing a small amount of pyridine. (In the absence of pyridine, DTNB reacts with pyrochlorophyll to form pyropheophytin.) A product of the reaction, which has an absorption band at 485 nm, was identified as the thiophenolate ion by extraction into water. The quantum yield for appearance of reduction product was about 0.029. The position of the absorption band and its low apparent absorptivity (*ca.* 2860 M⁻¹ cm⁻¹) suggest that the thiophenol is only partially ionized in nitromethane, and that the anion exists as an ion triplet with two pyridinium ions (I).



The situation is quite different when the pyridine is replaced by poly(4-vinylpyridine). When DTNB is added to a solution containing pyrochlorophyll and the polymer, the absorption band of pyrochlorophyll is displaced to the red, and the fluorescence of pyrochlorophyll is strongly quenched. Neither of these phenomena is observed in the presence of pyridine. On exposure to light, no photosensitized reduction of DTNB is observed.

These effects are best explained by assuming that pyrochlorophyll and DTNB form a complex, which is stable so long as both molecules are attached to the polymer. The complex quenches excited singlet state energy efficiently, without the performance of any net photochemistry.

A prominent feature of the pyrochlorophyll-poly(vinylpyridine) system is the self-quenching of fluorescence at high pigment densities. This concentration quenching is apparently dependent on energy transfer to interacting pairs and higher aggregates of pyrochlorophyll molecules which are only weakly fluorescent. We have examined the effects of DTNB in the range of (py)/(chl) ratios over which self-quenching varies from negligible to maximal. The results of these experiments are summarized in Table I.

(9) G. R. Seely, *J. Phys. Chem.*, **73**, 117 (1969).

(10) G. R. Seely, *ibid.*, **73**, 125 (1969).

(11) G. L. Ellman, *Arch. Biochem. Biophys.*, **82**, 70 (1959).

Table I: Position (λ) and Half-Width (δ) of Red Band, and Relative Measured Fluorescence Intensity (I_f), before and after a Series of Additions of DTNB to Pyrochlorophyll-Poly(vinylpyridine) Complexes, and Further Treatment as Indicated

(py)/(chl)	(DTNB)/(chl) (+ further treatment)	λ , Å	δ , Å	I_f^a	Remarks
358	0	6662	104	1000	reference fluorescence intensity
	2.55	6680	115	310	turbidity
	4.46	6693	123	285	increased turbidity
	(+ N ₂ H ₄ , 0.035 M)	6649	112	556	turbidity dissolved
189	0	6663	105	829	
	6.74	6700	122	69	
160	0	6665	104	674	
	6.41	6699	116	35	
	(+ N ₂ H ₄ , 0.017 M)	6645	band at 490 nm of reduced DTNB rises
145	0	6664	105	807	
	1.29	6687	120	199	turbidity noted
	6.44	6720	134	228	turbidity strong
119	0	6665	106	607	
	6.50	6707	120	27	
79	0	6667	109	407	
	6.47	6712	121	32	
	(+ C ₂ H ₅ SH, 0.1 M)	6676	122	44	band at 495 nm
40	0	6669	115	186	
	6.62	6713	126	31	
	(+ C ₃ H ₅ N ₂ H ₃ , $\sim 10^{-1}$ M)	6701	132	54	
19	0	6675	210	93	
	1.56	6701	129	34	min value of fluorescence
	6.24	6713	136	51	
	(+ HSCH ₂ CH ₂ , COOH, 0.02 M)	pyropheophytin formed
74	0	6665	110	442	6 × 10 ⁻³ M hydrazobenzene present
	6.05	6712	121	34	
	(+ C ₅ H ₅ N, 0.35 M)	6639	104	728	complex dissociated
89	0	6671	110	381	test of reversibility
	1.57	6688	118	64	
	1.57	6677	115	180	
178	0	6665	106	736	
136	(DTBA)/(chl) = 18.1	6686	106	268	2,2'-dithiodibenzoic acid
	0	6664	106	752	
	(<i>o</i> -NBA)/(chl) = 22.4	6660	113	187	<i>o</i> -nitrobenzoic acid
172	(+ C ₅ H ₅ N, 0.33 M)	6635	103	774	complex dissociated
	0	6667	107	589	
	(<i>p</i> -NBA)/(chl) = 24.6	6656	107	195	<i>p</i> -nitrobenzoic acid
161	0	6662	104	714	
	(BA)/(chl) = 22.4	6661	104	638	benzoic acid
171	0	6665	104	764	
	(LA)/(chl) = 21.1	6662	106	658	lipoic acid

^a Approximate fluorescences not corrected for concentration changes, etc., relative to 1000 for uncomplexed pyrochlorophyll in sparse aggregate.

Addition of DTNB to a solution of pyrochlorophyll and poly(vinylpyridine) in fixed ratio displaces the absorption band of pyrochlorophyll from about 6662 to 6712 Å and broadens the half-width of the band from about 105 to 122 Å. The initial position and half-width of the band vary somewhat with the initial extent of aggregation of pyrochlorophyll.²

In Figure 1, fluorescence quantum yields are plotted against (DTNB)/(chl) for the experiments for which reasonably complete data were available. The qualitative effects of treatments on the fluorescence are also noted in Table I. Because of energy transfer, the

quenching of fluorescence is more nearly complete at small values of (DTNB)/(chl) than the spectral changes. The limiting yield of fluorescence at high (DTNB)/(chl) appears to be independent of the initial extent of self-quenching by interacting pyrochlorophyll pairs.

We sought to determine whether the nitro groups of DTNB, the disulfide group, or both were responsible for the strength of the complex with pyrochlorophyll, and for its spectral and fluorescence quenching properties, by experiments with *o*- and *p*-nitrobenzoic acid (*o*- and *p*-NBA) and the commercially available disul-

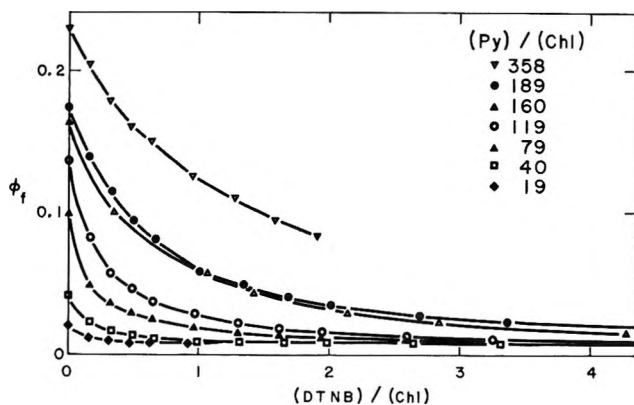


Figure 1. Fluorescence quantum yields ϕ_f upon addition of DTNB to solutions of poly(4-vinylpyridine) and pyrochlorophyll at ratios designated. Concentration of pyrochlorophyll $ca. 2 \times 10^{-6} M$ in nitromethane.

fide, 2,2'-dithiodibenzoic acid (DTBA), in place of DTNB. The effects of DTBA, *o*-NBA, and DTNB on the position of the absorption band are shown in Figure 2; the effects on the fluorescence yield are shown in Figure 3. Results are also summarized in Table I.

o-NBA produced at most a small blue shift of the absorption band and a gradual broadening. *p*-NBA produced a somewhat larger blue shift but no broadening. DTBA produced no broadening but was responsible for a distinct red shift of the band. All three compounds quenched fluorescence, but not nearly so strongly as DTNB. However, the quenching obtained even with these compounds was well in excess of that which would have been obtained had the quenchers been free in solution and not bound to the polymer.¹⁰ Addition of benzoic acid or lipoic acid had no effect on the spectrum or on the fluorescence intensity (Table I).

The effects of DTNB are much greater than can be ascribed to the sum of the effects of the disulfide group and the nitro group separately. The red shift appears at least partially due to the presence of the disulfide group, and it is possible that the shift would have been larger if the 3,3' isomer of DTBA had been used. But in general, the marked effects of DTNB would not have been anticipated from the effects of the simpler compounds.

The effects of other reagents upon the pyrochlorophyll-DTNB complex are also noted in Table I. The relatively strong bases pyridine and hydrazine dissociate pyrochlorophyll from the polymer and restore the fluorescence of quenched solutions. Phenylhydrazine may bind to pyrochlorophyll, but apparently does not disrupt the complex with DTNB, because fluorescence is not restored. Hydrazobenzene is too weak a base to affect the spectrum or the fluorescence.

Hydrazine, but not phenylhydrazine, reduces DTNB in the dark to the thiophenolate ion, the absorption band of which appears at 490 nm. Ethyl mercaptan also reduces DTNB, but the product apparently re-

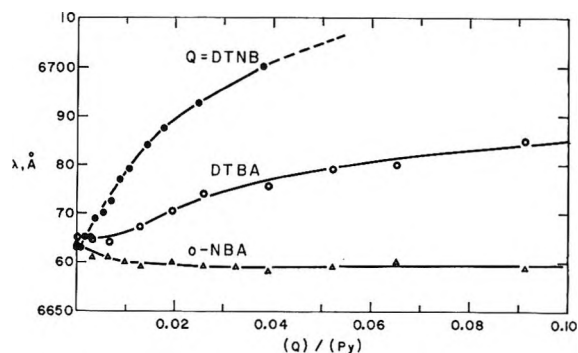


Figure 2. Comparison of band displacements λ induced by addition of DTNB, DTBA, and *o*-NBA to pyrochlorophyll-poly(vinylpyridine) aggregates at (py)/(chl) ratios designated in Figure 3.

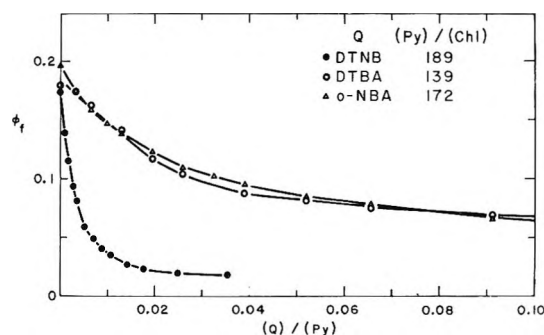


Figure 3. Comparison of effects of addition of DTNB, DTBA, and *o*-NBA on fluorescence quantum yield ϕ_f of pyrochlorophyll-poly(vinylpyridine) aggregates at (py)/(chl) ratios designated.

mains associated with pyrochlorophyll because the absorption band of the latter shifts only to 6676 Å and remains broad, and fluorescence is not restored. Under these conditions the band of the thiophenolate ion appears at 495 nm.

In an experiment to test the reversibility of the association of pyrochlorophyll, DTNB, and the polymer, addition of more polymer after addition of DTNB restored fluorescence to about the level expected if both pyrochlorophyll and DTNB had redistributed onto the newly added polymer.

Two of the runs were interrupted by the appearance of turbidity in the solution, which increased upon further addition of DTNB. With increasing turbidity, the pyrochlorophyll band moved steadily to the red and broadened. The fluorescence intensity remained nearly constant. The appearance of turbidity was not related in an evident way to the ratio (DTNB)/(chl), the humidity, or the water content of the solution. The cause of the turbidity has not been found, but because it is dissipated by hydrazine and pyridine, it is natural to suspect that the presence of an acidic impurity led to the formation of a polymeric salt. Data from turbid solutions were excluded from further treatment.

Discussion

It is evident from the foregoing that DTNB and pyrochlorophyll form on the polymer a complex of unexpected stability. The complex acts as a quenching center and thus as a trap for the singlet excited state energy of uncomplexed pyrochlorophyll. It would therefore be analogous to the reaction center of a photosynthetic unit, except for the fact that no net photochemistry is observed. Since photochemistry is observed in the nonpolymeric system (*i.e.*, with pyridine), it is a reasonable conjecture that quenching in the polymeric system is due to an electron-transfer reaction, but that back transfer is so fast in the complex that no net photochemistry is possible.

From the spectral and fluorescence data, we may now calculate the efficiency of trapping excited singlet state energy in systems containing DTNB. The calculations are made over a range of (py)/(chl) ratios, and the results are extrapolated to pigment densities similar to those in the photosynthetic unit.

First, it is necessary to estimate the fraction of pyrochlorophyll complexed with DTNB from changes in the position and half-width of the absorption band near 666 nm. The strength of the complex is expressed by an association constant K . The rate of nonradiative transfer of energy between pyrochlorophylls is then calculated from the fraction of pyrochlorophyll complexed and the fraction of fluorescence quenched, with the aid of a simple scheme for disposition of energy in the system.

Calculation of K . The fraction f_Q of pyrochlorophyll complexed with DTNB is calculated from eq 1¹²

$$f_Q = \frac{1}{1 + \frac{\epsilon_2 (\lambda_2 - \lambda) \delta_1^2}{\epsilon_1 (\lambda - \lambda_1) \delta_2^2}} \quad (1)$$

in which λ_1 , ϵ_1 , and δ_1 are the position, absorptivity, and half-width of the absorption band of uncomplexed pyrochlorophyll, and λ_2 , ϵ_2 , and δ_2 are those of the pyrochlorophyll-DTNB complex. With the approximation that $\epsilon_2/\epsilon_1 = \delta_1/\delta_2$,¹³ eq 1 simplifies to eq 2.

$$f_Q = \frac{1}{1 + \frac{(\lambda_2 - \lambda) \delta_1^3}{(\lambda - \lambda_1) \delta_2^3}} \quad (2)$$

The initial values, λ_1 and δ_1 , are noted in Table I. The value of λ_2 for complexed pyrochlorophyll was taken as 6713 Å, and the value of δ_2 as 122 Å, except for (py)/(chl) = 40 and 19, where 126 Å and 130 Å were used.

Values of f_Q calculated from eq 2 were plotted as in Figure 4 for the seven runs in which data were sufficiently complete. The values of f_Q used thenceforth were taken from smooth curves drawn through the points.

In order to calculate K consistently at high pigment densities it was necessary to take site attrition into

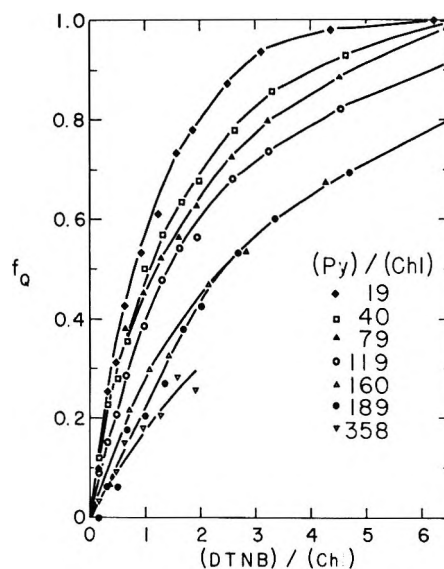


Figure 4. Fraction f_Q of pyrochlorophyll in complex with DTNB as function of (py)/(chl) and (DTNB)/(chl), calculated from absorption spectra by eq 2 of the text.

account, as was done in previous calculations of the extent of chlorophyll aggregation on the polymer.² In a polymeric system containing P pyridine units, C pyrochlorophyll units, and D DTNB units, each pyrochlorophyll physically blocks approximately 6 pyridine units. It is further assumed that each DTNB requires 2 pyridine units for binding to the polymer, but when complexed with pyrochlorophyll, it is bound to 2 of the 6 pyridine units already blocked by the pyrochlorophyll. If the number of pyrochlorophyll-DTNB complexes is C_Q , the number of unoccupied sites available for DTNB is $(1/2)(P - 6C - 2D + 2C_Q)$. If the number of free pyrochlorophyll molecules, bound to the polymer but available for complexing with DTNB, is C_1 , the association constant is expressed by eq 3.

$$K = \frac{C_Q(P - 6C - 2D + 2C_Q)}{2(D - C_Q)C_1} \quad (3)$$

Division throughout by C gives eq 4, in which $f_1 = C_1/C$

$$K = \frac{f_Q(P/2C - 3 - D/C + f_Q)}{(D/C - f_Q)f_1} \quad (4)$$

$P/C \equiv (\text{py})/(\text{chl})$, and $D/C \equiv (\text{DTNB})/(\text{chl})$.

We have pointed out that pyrochlorophyll is associated to some extent into interacting pairs and higher aggregates on the polymer. Values of K calculated from eq 4 without regard to pyrochlorophyll aggregation (*i.e.*, with $f_1 = 1 - f_Q$) appeared abnormally low for (py)/(chl) = 40 and 19, where the amount of aggregation was large. This suggested the physically plausible assumption that aggregated pyrochlorophyll

(12) G. R. Seely, *Spectrochim. Acta*, 21, 1847 (1965).

(13) G. R. Seely and R. G. Jensen, *ibid.*, 21, 1835 (1965).

is unavailable or less readily available for complexing with DTNB. Somewhat more consistent values of K could be obtained if the fraction of pyrochlorophyll aggregated, f_x , was estimated, and K was calculated on the assumption that $f_1 = 1 - f_Q - f_x$.

Aggregation of pyrochlorophyll was previously treated² by an adaptation of the one-dimensional Ising model of Reiss.¹⁴ Here, the fraction of pyrochlorophyll f_1 associated neither with another pyrochlorophyll nor with DTNB is calculated from eq 5-7, drawn from ref 2 but modified to exclude that part of the pyrochlorophyll complexed with DTNB.

$$f_1 = (1 - f_Q)A\mu(1/n - 2 + A) \quad (5)$$

$$A = 1 + \frac{\mu - \sqrt{\mu^2 + 4\mu(1 - \mu)n(1 - n)}}{2(1 - \mu)n} \quad (6)$$

$$n = (1 - f_Q)/(P/6C - f_Q) \quad (7)$$

In these formulas, μ is a function of the free energy of interaction of pyrochlorophyll pairs, A is an "activity" function, and n is the fraction of available sites occupied by pyrochlorophyll not complexed with DTNB. Because of extensive cancelation of terms, eq 6 is difficult to use when n is small. In practice we used an expanded form of it, eq 8, valid when n is not too large.

$$A = n[1 + (1 - n)^2(1 - \mu) \times (1 - 2n(1 - n)(1 - \mu)/\mu)/\mu] \quad (8)$$

In our previous estimation of f_x and μ from spectral changes in the absence of DTNB,² the data for pyrochlorophyll at high pigment densities were best accounted for by the value $\mu = e^{-2}$. In the present work, f_x and μ before addition of DTNB were estimated from fluorescence data as explained further on. The value $\mu = e^{+0.5}$ provided the best fit for data for which (py)/(chl) > 100, and was applied uniformly in all runs to calculate f_1 and f_x in the presence of DTNB. The correction to K is a small one except when (py)/(chl) = 40 and 19. In these cases the subsequent calculation of energy transfer rates must be regarded as very approximate because the detailed state of the system is not clearly defined.

Values of K were calculated at intervals throughout the ranges of available data and are listed in Table II for $f_Q = 0.25, 0.5,$ and 0.75 . The values tabulated show some spread but no consistent trends with either f_Q or (py)/(chl), except that the values for (py)/(chl) = 40 and 19 are still somewhat lower than the others. Over one-half the values are within the range $K = 46 \pm 10$. If values for (py)/(chl) = 40 and 19 are omitted, two-thirds of the remaining values lie within the range $K = 55 \pm 10$. A value of K in the neighborhood of 50 corresponds to a Gibbs energy of association of only about 2.35 kcal/mol. This value represents the net effect of attraction of the two molecules

Table II: Values of the Equilibrium Constant K for Formation of a Complex between Pyrochlorophyll and DTNB on Poly(vinylpyridine) at $f_Q = 0.25, 0.5,$ and 0.75 .

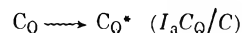
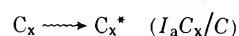
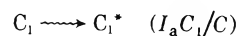
K Calculated by Eq 4 with $\mu = e^{0.5}$ and Values of (DTNB)/(chl) from Curves of Figure 4

(py)/ (chl)	K		
	$f_Q = 0.25$	0.5	0.75
358	56
189	36.5	46	58
160	40	40	47
117	64	62	61.5
79	76	55	52
40	45	33.5	30
19	36	25	21

and any weakening of the binding of either to the polymer.

Calculation of Energy Transfer. We now calculate the average number of nonradiative transfers of energy that follow absorption of light by pyrochlorophyll, from the quenching efficiency of the pyrochlorophyll-DTNB complex. This is done with the aid of a kinetic scheme in which certain simplifications are introduced from the outset. The processes considered and their rates are the following, in which $C_1, C_x, C_Q,$ and C now represent the concentrations of uncomplexed pyrochlorophyll, aggregated pyrochlorophyll, pyrochlorophyll complexed with DTNB, and total pyrochlorophyll.

Excitation



I_a is the rate of light absorption, in einsteins sec^{-1} . It is assumed that the absorptivities of the three species of pyrochlorophyll are equal at the exciting wavelength, 6438 Å. This assumption is reasonable because 6438 Å lies near a minimum in the absorption spectrum of the bound pigment, where absorptivity changes slowly with wavelength.

Nonradiative Transfer

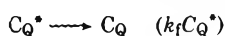
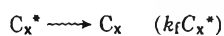
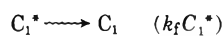


The rate of transfer in the system is assumed to be governed by a quantity T (sec^{-1}), which depends on the pigment density, *i.e.*, (py)/(chl), but not on the identities of the donor and the acceptor. Because of

(14) H. Reiss, *J. Chem. Phys.*, **40**, 1783 (1964).

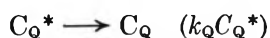
the short lifetime of the quenching species, back transfer from C_X to C_1 and from C_Q to C_1 or C_X would be relatively unimportant and is neglected.

Fluorescence



Since the integrated absorption intensity of the pyrochlorophyll band is changed very little by complexing, the rate constants for radiative loss of energy are taken to be the same.

Internal Conversion



However, alternative paths of energy dissipation depend very much on the state of complexing of pyrochlorophyll. Under these constants are subsumed, for the sake of brevity, all nonradiative paths for dissipation of energy, including possible triplet-state and electron-transfer intermediates.

When equations for the above processes are solved to find the steady state concentrations of C_1^* , C_X^* , and C_Q^* , and these are inserted into the expression for fluorescence yield (ϕ), $\phi = k_f(C_1^* + C_X^* + C_Q^*)/I_a$, the result is eq 9.

$$\phi = \frac{k_f}{(1 + \tau_1 T(1 - f_1))} \left\{ f_1 \tau_1 + \frac{f_X \tau_X (1 + \tau_1 T)}{(1 + \tau_X f_Q T)} + \frac{(f_Q \tau_Q (1 + \tau_1 T)(1 + \tau_X T(1 - f_1)))}{(1 + \tau_X f_Q T)} \right\} \quad (9)$$

In this equation, the excited state lifetimes, $\tau_1 = 1/(k_f + k_i)$, $\tau_X = 1/(k_f + k_X)$, and $\tau_Q = 1/(k_f + k_Q)$, have been introduced.

Equation 9 can be rearranged into the form of eq 10.

$$1 + \tau_1 T = \frac{f_1(\phi_0/\phi - 1)}{(1 - f_1) - F(X, Q, T)(\phi_0/\phi)} \quad (10)$$

In eq 10, $\phi_0 = k_f \tau_1$, and $F(X, Q, T)$ contains those terms pertaining to fluorescence of species C_X and C_Q (eq 11).

$F(X, Q, T) =$

$$\frac{f_X(\tau_X/\tau_1) + f_Q(\tau_Q/\tau_1)(1 + \tau_X T(1 - f_1))}{1 + \tau_X f_Q T} \quad (11)$$

Whereas T is the average number of transfers an excitation will undergo per second, $\tau_1 T$ is the number of transfers during the lifetime of an excited state of uncomplexed pyrochlorophyll. The latter quantity is therefore more directly related to the size of the "photosynthetic unit" in the present model system,

and hence is of greater interest in the present context. The ratios τ_X/τ_1 and τ_Q/τ_1 are given by the limiting values of ϕ/ϕ_0 at high pigment density without DTNB, and at high DTNB concentration, respectively. From previous experience the best value for τ_X/τ_1 is 0.0868, and from the present work $\tau_Q/\tau_1 = 0.0395$.

As explained before, the fraction of pyrochlorophyll complexed with DTNB (f_Q) was calculated from the spectrum by eq 2, and the fractions of monomeric and aggregated pyrochlorophyll (f_1 and f_X) by eq 5, 7, and 8, with $\mu = e^{+0.5}$. The value of μ was estimated on the assumption that interacting pyrochlorophyll pairs are as efficacious traps for singlet excited state energy as pyrochlorophyll-DTNB complexes. The fraction of pyrochlorophyll aggregated initially in an experiment was estimated from the increase in quenching upon addition of DTNB to the solution. The calculation is simple, however, only so long as $F(X, Q, T)$ in eq 10 is small enough to be neglected.

When DTNB is absent, and $F(X, Q, T) \approx 0$, the fluorescence yield ϕ_X is related to f_X by eq 12, which follows from eq 10. When DTNB is added, the ex-

$$\frac{\phi_0}{\phi_X} - 1 = \frac{f_X(1 + \tau_1 T)}{1 - f_X} \quad (12)$$

pression for the quantum yield ϕ becomes

$$\frac{\phi_0}{\phi} - 1 = \frac{(f_X' + f_Q)(1 + \tau_1 T)}{(1 - f_X' - f_Q)} \quad (13)$$

With the further approximation that the aggregated pyrochlorophyll fraction $f_X' = f_X(1 - f_Q)$, eq 13 reduces to eq 14.

$$\frac{\phi_0}{\phi} - 1 = \frac{(1 + \tau_1 T) \left\{ \frac{f_X}{(1 - f_Q)} + f_Q \right\}}{(1 - f_Q)} \quad (14)$$

The initially aggregated fraction f_X is determined from the intercept on the abscissa axis of a plot of $\phi_0/\phi - 1$ against $f_Q/(1 - f_Q)$, or by some equivalent procedure.

If the extent of aggregation is not small and $F(X, Q, T)$ is not negligible, eq 13 no longer holds, and the unknown $(1 + \tau_1 T)$ cannot be factored out as in eq 14. The estimate of μ was therefore based on data for which $(py)/(chl) > 100$. The value obtained from these data, $e^{+0.5}$, indicates a slightly less favorable energy for aggregation than was obtained before (e^{-2}).² However, the latter value was estimated from data at high pyrochlorophyll densities. It is quite conceivable that the interaction energy depends somewhat upon the pigment density, and indeed Figure 11 of ref 2 allows this interpretation.

The general validity of the foregoing assumptions and analysis is proved by the constancy of the value of $\tau_1 T$, calculated by eq 10, throughout each run. In Figure 5, where $\tau_1 T$ is plotted against f_Q , $\tau_1 T$ is seen to be approximately constant as long as fluorescence is less than 90% quenched. (For $(py)/(chl) = 19$,

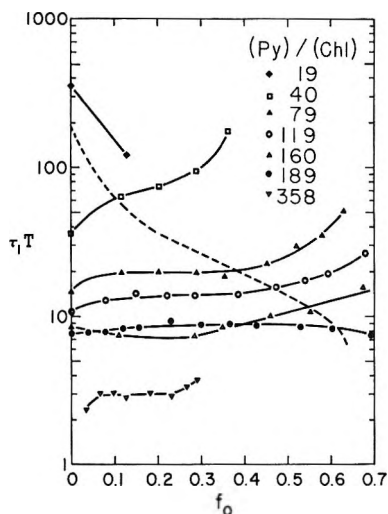


Figure 5. Number of nonradiative energy transfers $\tau_1 T$ between pyrochlorophylls per lifetime of uncomplexed excited singlet state, plotted as a function of the fraction of pyrochlorophyll complexed. Dashed line delineates region below which fluorescence is less than 90% quenched.

the calculation procedure evidently failed, for $\tau_1 T$ became negative or oscillatory after the first two points. These only are therefore shown, and are to be considered indicative of the order of magnitude only.)

Values of $\tau_1 T$ taken from the flat parts of the curves of Figure 5 below the 90% quenched line are plotted logarithmically against $(py)/(chl)$ in Figure 6. For $(py)/(chl) = 19$, both points of Figure 5 are plotted. The points are correlated quite well by a power law, eq 15.

$$\tau_1 T = 7400[(chl)/(py)]^{1.325} \quad (15)$$

The straight line of Figure 6 permits extrapolation of the number of transfers to chlorophyll densities typical of the photosynthetic unit. According to the data of Thomas, *et al.*, the distance between centers of neighboring chlorophyll molecules in plastid lamellae is 16–18 Å.¹⁵ This average distance corresponds on the polymer to a ratio of $(py)/(chl) \cong 7$. At that concentration, $\tau_1 T$ extrapolates to 560 transfer per lifetime.

Energy transfer in photosynthetic units has been reviewed several times in recent years.^{5,16,17} Theoretical treatments of energy transfer in the photosynthetic unit are usually based on a random walk model or its analog in the form of a diffusion equation.^{18–20} Attempts to determine the number of transfers experimentally have depended upon the postulation of certain relationships between fluorescence yield and trapping efficiency.²¹ These relationships, admittedly tenuous, are further complicated by the presence of two photosynthetic unit systems in green plants.²²

Teale, employing *m*-dinitrobenzene as a quencher in an experiment conceptually similar to that described here, derived a value of 275 for the quantity we call

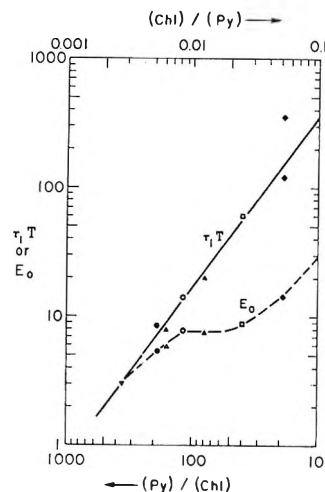


Figure 6. Number of nonradiative transfers $\tau_1 T$ and efficacy of trapping E_0 (see eq 17 of text) as functions of $(py)/(chl)$ (lower abscissa scale) or $(chl)/(py)$ (upper scale).

$\tau_1 T$.²³ Duysens has estimated that a value of 1200 or more is possible.¹⁶ Our extrapolated value from Figure 6 is clearly in the same range as these estimates. Since a photosynthetic unit, at least of System I, is believed to contain 200–400 chlorophylls per reaction center, these values would appear to be none too large.

Theoretical calculations of trapping rates have been made for both 2- and 3-dimensional arrays of chlorophyll.^{19,20} Because of the random coil configuration of the polymer, the present results are for an essentially 3-dimensional random distribution of pyrochlorophyll.³

A measure (E) of the efficacy of trapping may be defined as the fraction of absorbed light quanta transferred to pyrochlorophyll–DTNB complexes divided by the fraction of pyrochlorophyll so complexed.

$$E = \frac{TC_1 * f_Q + TC_x * f_Q}{I_a f_Q} \quad (16)$$

This may also be regarded as the average size of the model “photosynthetic unit,” or the average number of pyrochlorophylls serviced by one trap. At low DTNB concentration, E approaches a limiting value E_0 .

(15) J. B. Thomas, K. Minnaert, and P. F. Elbers, *Acta Bot. Neer.*, **5**, 315 (1955).

(16) L. N. M. Duysens, *Progr. Biophys. Mol. Biol.*, **14**, 1 (1964).

(17) G. Hoch and R. S. Knox, in “Photophysiology,” Vol. 3, A. C. Giese, Ed., Academic Press, New York, N. Y., 1968, Chapter 7.

(18) G. W. Robinson in “Energy Conversion by the Photosynthetic Apparatus,” Brookhaven Symposia in Biology, No. 19, 1967, pp 16–48.

(19) Z. Bay and R. M. Pearlstein, *Proc. Nat. Acad. Sci. U. S.*, **50**, 1071 (1963); R. M. Pearlstein in “Energy Conversion by the Photosynthetic Apparatus,” Brookhaven Symposia in Biology, No. 19, 1967, pp 8–15.

(20) J. Lavorel, *J. Chem. Phys.*, **47**, 2235 (1967).

(21) R. K. Clayton, *J. Theor. Biol.*, **14**, 173 (1967).

(22) R. M. Pearlstein, *Proc. Nat. Acad. Sci. U. S.*, **52**, 824 (1964).

(23) F. W. J. Teale, *Biochim. Biophys. Acta*, **42**, 69 (1960).

$$E_0 = \frac{\tau_1 T f_1 (1 + 0.0868 \tau_1 T f_x)}{1 + \tau_1 T f_x} + 0.0868 \tau_1 T f_x \quad (17)$$

Values of E_0 are plotted below those of $\tau_1 T$ in Figure 6. For (py)/(chl) = 19, the extrapolated value $\tau_1 T = 150$ was used.

The effect of association of pyrochlorophyll on E_0 is readily seen. Instead of increasing coincidentally with $\tau_1 T$, the curve for E_0 reaches a plateau value of about 8, then increases again as pyrochlorophyll becomes predominantly associated. The plateau value represents a limitation imposed by competition with trapping by aggregated pyrochlorophyll molecules. Increased efficacy at high pyrochlorophyll densities corresponds to transfer of energy through the short-lived states of aggregated pyrochlorophylls to the even shorter lived pyrochlorophyll-DTNB traps. (In these calculations, back transfer from pyrochlorophyll-DTNB to associated pyrochlorophyll was neglected; inclusion of it would appreciably reduce the efficacy of trapping at high pyrochlorophyll density.)

In 1964 Duysens remarked that here was little evidence for chlorophyll dimer formation in the chloro-

plast, and that one of the functions of the lamellar structures might be to keep the molecules of chlorophyll apart.¹⁶ The cogency of that remark is well illustrated in our model systems, where it is evident from Figure 6 that "photosynthetic units" 10 times the size of the calculated ones could have been attained if the self-quenching of pyrochlorophyll could have been avoided.

Reaction center chlorophyll generally absorbs at longer wavelengths than antenna chlorophyll. Whether this plays a necessary role in the transference of energy to the trap, or is only an epiphenomenal consequence of the special environment surrounding reaction center chlorophyll, is unknown. DTNB certainly is not a natural constituent of the chloroplast, but its association in a complex with pyrochlorophyll indicates how an electron accepting natural constituent could exist in a complex with chlorophyll that is stabilized by attachment of both to the lamellar substrate.

Acknowledgments. This work was supported in part by National Science Foundation Grant No. GB-7893. The able technical assistance of T. H. Meyer is appreciated.

The Photolysis of Hydroxylamine in Aqueous Solution

by D. Behar, D. Shapira, and A. Treinin*

Department of Physical Chemistry, Hebrew University, Jerusalem, Israel (Received August 18, 1971)

Publication costs borne completely by The Journal of Physical Chemistry

The photolysis of NH_2OH in aqueous solution at 2139 Å can be closely represented by the overall reaction $3\text{NH}_2\text{OH} \rightarrow \text{NH}_3 + \text{N}_2 + 3\text{H}_2\text{O}$, with some H_2 also produced. Flash photolysis and pulse radiolysis of hydroxylamine solutions have proved that NHOH is an intermediate in the photolysis, and the properties of this radical were investigated. The effect of ethanol on the yields of NHOH and the final products strongly suggest that the major primary process is $\text{NH}_2\text{OH} \xrightarrow{h\nu} \text{NH}_2 + \text{OH}$. A minor parallel process leads to the production of H_2 . The photolysis of NH_2OH^+ was also investigated. At pH ~2 the major nitrogen-containing products are NH_3 and N_2O . This change is related to transformation of the hydroxylamino radical to its acidic form ($\text{p}K = 4.0 \pm 0.1$). Additional information is presented on the reactions of hydroxylamine with OH, H, and e_{aq}^- . The rate constants derived: $k(e_{\text{aq}}^- + \text{NH}_2\text{OH}) = 6.6 \times 10^8 \text{ M}^{-1} \text{ sec}^{-1}$, $k(e_{\text{aq}}^- + \text{NH}_2\text{OH}^+) = 1.0 \times 10^{10} \text{ M}^{-1} \text{ sec}^{-1}$.

The direct photolysis and Hg-photosensitized decomposition of NH_2OH has been studied in the gas phase.^{1,2} According to Betts and Back² the direct photolysis involves two primary processes yielding $\text{NH}_2 + \text{OH}$ (40%) and $\text{NH}_2\text{O} + \text{H}$ (60%), respectively, whereas the Hg-photosensitized decomposition proceeds primarily by the first process. The radicals NH_2 , OH, and H were considered subsequently to attack

NH_2OH yielding NH_3 , H_2O , and H_2 , respectively, as final products and the intermediate NHOH, the annihilation processes of NHOH and NH_2O being the source of N_2 and N_2O , respectively.² Some of these re-

(1) R. N. Smith and P. A. Leighton, *J. Amer. Chem. Soc.*, **66**, 172 (1944).

(2) J. Betts and R. A. Back, *Can. J. Chem.*, **43**, 2678 (1965).

actions were postulated for the radiation chemistry of hydroxylamine in aqueous solution³ and some information on NHOH has been recently obtained from pulse radiolysis experiments.⁴

Here we present the first results on the photochemistry of hydroxylamine in aqueous solution. Both steady and flash techniques were employed for this purpose. Additional information on the formation and properties of NHOH were also derived from pulse radiolysis of aqueous hydroxylamine.

Experimental Section

A. Steady Photolysis. Solutions of hydroxylamine were irradiated at $23 \pm 1^\circ$ with a 25-W Philips zinc lamp No. 93106; the light was filtered by 0.5-cm layer of water. Only the strong 2139-Å and weak 2062- and 2025-Å lines were absorbed by the solutions. Cutting off the weak lines with a KCl solution, we could show that about 96% of the photolysis was due to the 2139-Å line. The optical path of the irradiation cell was 3 cm, and it was attached to a 25-ml bulb, where the solution was degassed before irradiation.

Chemical actinometry was conducted with azide solution.⁵ An air-containing solution of 10^{-3} M NaN_3 at pH 7.7 (with a borate buffer) was irradiated under the same conditions and the azide depletion was determined, taking $\Phi_{-\text{N}_3^-} = 0.32 \pm 0.01$.

The degassing and analysis of products were conducted as described elsewhere.⁵ The gaseous products were also subjected to mass spectrometric and gas chromatographic analysis, using appropriate blanks.

B. Flash Photolysis and Pulse Radiolysis. The flash apparatus and experimental technique were described elsewhere.⁶ A linear accelerator operating at 5 MeV and 200 mA was used for pulse radiolysis. The pulse duration was varied in the range 0.2–1.5 μsec in order to change its dose. An optical path length of 12 cm was attained by passing the monitoring light three times through the irradiation cell. A modified Fricke dosimeter⁷ was used to determine radical yields.

To reduce stray light effects a 60-W deuterium lamp was the source of monitoring light and for detection we used a "solar blind" R166 photomultiplier, which does not respond to light above 320 nm. With the aid of two filters we measured the stray light coming from within and outside the absorption region of the transient. The first contribution was predominant and as an approximation its intensity was assumed to be reduced by one-half owing to absorption.

C. Materials and Solutions. Solutions of hydroxylamine were prepared from $(\text{NH}_2\text{OH})_2 \text{H}_2\text{SO}_4$ (UCB, analytical grade). In the photochemical experiments (steady and flash) the pH was adjusted in the range 1.0–6.7 by adding HClO_4 or NaOH ; pH 7.4 was attained by neutralizing the material with an equivalent amount of NaOH and adding a borate buffer. In the pulse radiolysis experiments, when studying reactions

of e_{aq}^- produced by 0.2- μsec pulses, self-buffering of the hydroxylamine system (in the pH range 5.4–6.7) and a borate buffer were employed. In other pulse experiments a phosphate buffer was used for the range above pH 4.0.

Ethanol was of spectroscopic grade, water was triply distilled, and all other materials were of analytical grade.

Results

A. Steady Photochemistry. Figure 1 shows the uv absorption of hydroxylamine at pH 6.9, where ca. 90% is in the basic form. The acidic form absorbs much less in this region. The band of NH_2OH in water appears to be blue shifted by ~ 7 kcal relative to the gas phase.² This energy is comparable to the solvation energy of gaseous NH_2OH ($\Delta H_{\text{sol}} = -11.5$ kcal⁸) and therefore similar to other related molecules the assignment of the band to $n \rightarrow \sigma^*$ transition seems plausible,⁹ with the nonbonding electrons of N being mainly in-

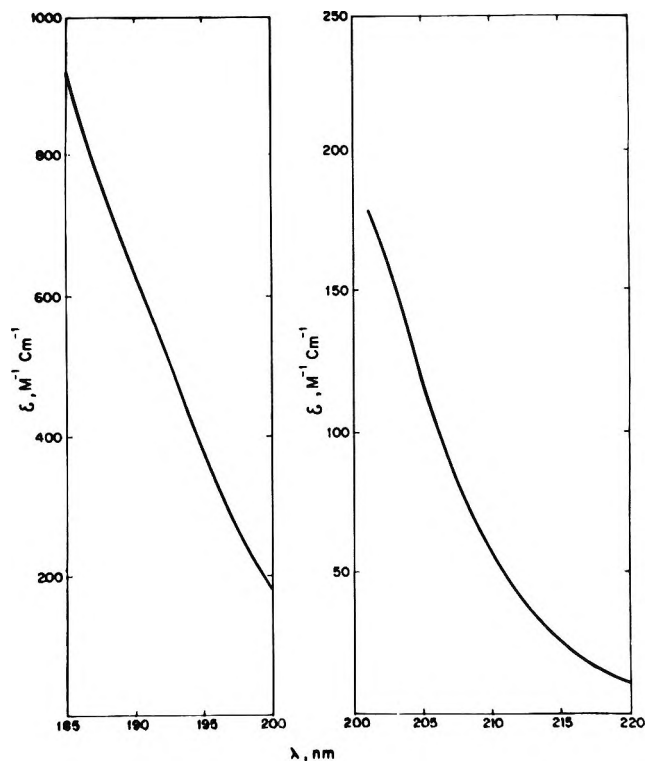


Figure 1. The electronic spectrum of NH_2OH in aqueous solution at pH 6.9.

- (3) M. Lefort and X. Tarrago, *J. Inorg. Nucl. Chem.*, **16**, 169 (1961).
- (4) M. Simic and A. Hayon, *J. Amer. Chem. Soc.*, in press.
- (5) I. Burak, D. Shapira, and A. Treinin, *J. Phys. Chem.*, **74**, 568 (1970).
- (6) D. Behar and G. Czapski, *Israel J. Chem.*, **6**, 43 (1968).
- (7) M. S. Matheson and L. M. Dorfman, "Pulse Radiolysis," MIT Press, Cambridge, Mass., 1969.
- (8) R. A. Back and J. Betts, *Can. J. Chem.*, **43**, 2157 (1965).
- (9) D. P. Stevenson, G. M. Coppinger, and J. W. Forbes, *J. Amer. Chem. Soc.*, **83**, 4350 (1961).

Table I: Yields of Photolysis in Air-Free Solutions of Hydroxylamine at 2139 Å

Solution		pH	Time, min	Yield, $10^{-6} M$					
$[NH_2OH], M$	$[Ethanol], M$			$[N_2]$	$[H_2]$	$[NH_3]$	$-\Delta[NH_2OH]^a$	$2[N_2] + [NH_3]$	$[N_2O]$
2×10^{-3}	...	7.4	72	14.5	1.6	17.0	47.2	46.0	...
2×10^{-3}	...	7.4	100	19.0	1.9	18.6	58.0	56.6	...
2×10^{-3}	...	7.4	107	21.3	2.3	20.5	64.0	63.1	...
2×10^{-3}	...	7.4	116	22.5	2.6	23.0	67.8	68.0	...
2×10^{-3}	...	7.4	120	22.2	2.8	23.0	70.3	67.4	...
2×10^{-3}	...	7.4	150	26.0	2.9	26.2	81.5	78.2	...
2×10^{-3}	...	7.4	150	30.0	3.1	27.0	85.2	87.0	...
2×10^{-3}	0.06	7.4	140	8.6	2.9	22.8	41.3	40.0	...
2×10^{-3}	0.43	7.4	140	5.4	3.3	23.0	34.3	33.8	...
2×10^{-3}	0.43	7.4	140	5.3	3.2	23.0	33.9	33.6	...
1.0	0.10	7.4	45	18.2	1.9				
1.0	...	7.4	45	17.7	1.9				
5×10^{-2}	...	4.3	180	13.4	0.6				2.4
5×10^{-2}	...	2.0	180	2.1	...	$\sim 30^b$			10.6

^a In presence of alcohol acetaldehyde is probably formed (from the alcohol radical) and reacts with NH_2OH to produce the oxime. However, under the conditions employed for the analysis (ref 5), all the oxime was hydrolyzed. ^b In presence of $5 \times 10^{-2} M$ hydroxylamine the determination of ammonia is not accurate;⁵ estimated limit of error, $\pm 15\%$.

involved. The large decrease of absorption on protonation is also in agreement with this assignment.

The photolysis of NH_2OH in aqueous solution (pH 7.4) leads to the formation of nearly equivalent amounts of N_2 and NH_3 , as major products, and a relatively small amount of H_2 . No N_2O could be detected: all the gas that could be condensed at liquid air temperature could also be condensed in a CO_2 -acetone trap.¹⁰

Working with $2 \times 10^{-3} M$ NH_2OH we measured the yields of products and depletion of NH_2OH ; the results are summarized in Table I and Figure 2. (The non-linear dependence on time of irradiation was due to change of light absorption. With initial absorbance below 0.25 the photolysis closely followed first-order kinetics.) The nitrogen balance (Table I, columns 8 and 9) also implies that no other nitrogen products are formed in considerable amounts. The following stoichiometric relations were found

$$[N_2] = [NH_3] = -(0.33 \pm 0.02) \times \Delta[NH_2OH]$$

$$[H_2] \simeq -(0.035 \pm 0.002) \times \Delta[NH_2OH]$$

The quantum yield of N_2 was measured under conditions of total absorption: $\phi_{N_2} = 0.25 \pm 0.02$, independent of the NH_2OH concentration up to 1 M.

In the presence of ethanol both ϕ_{N_2} and ϕ_{-NH_2OH} decrease but ϕ_{NH_3} and ϕ_{H_2} hardly change; N_2 and NH_3 still account for the nitrogen balance (Table I). The effect of alcohol increases with the ratio $[C_2H_5OH]/[NH_2OH]$; at ratios $\lesssim 0.1$ no effect of alcohol could be discerned.

In acidic solutions the photolysis reveals new features: there is a pronounced decrease in ϕ_{N_2} relative to ϕ_{NH_3} and N_2O is produced. These results were observed at pH values where almost all the hydroxylamine was in its acidic form; still a remarkable effect of pH

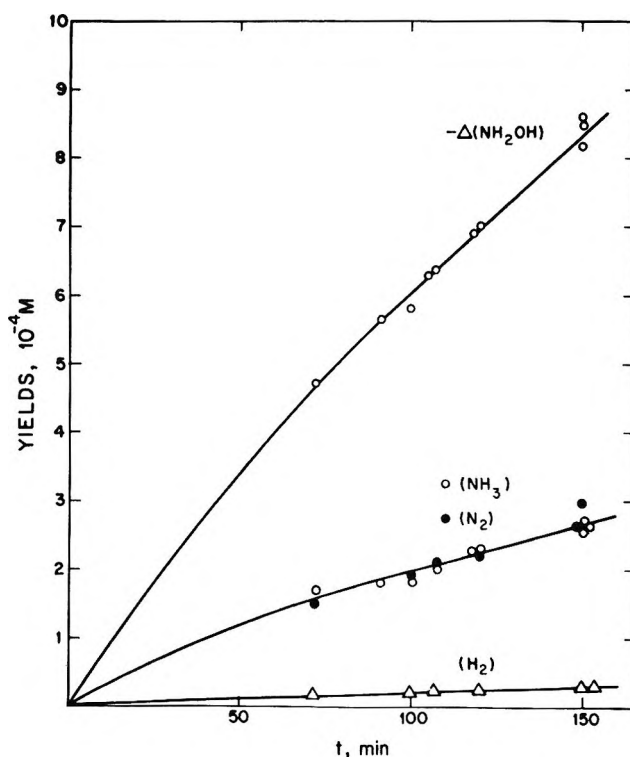


Figure 2. Yields of photolysis of degassed 2 mM NH_2OH solutions at pH 7.4, 23°.

was detected on lowering its value from 4.3 to 2.0 (Table I). At pH 2.0 NH_3 and N_2O are the major N-containing products, and no H_2 could be detected. Owing to the high concentration of hydroxylamine a large error was involved in determining the yield of NH_3

(10) Mass spectrometric analysis of the gaseous products showed traces of N_2O , the amount of which increased gradually on standing. This was probably due to thermal decomposition of NH_2OH , which was carried with the gas, inside the mass spectrometer.

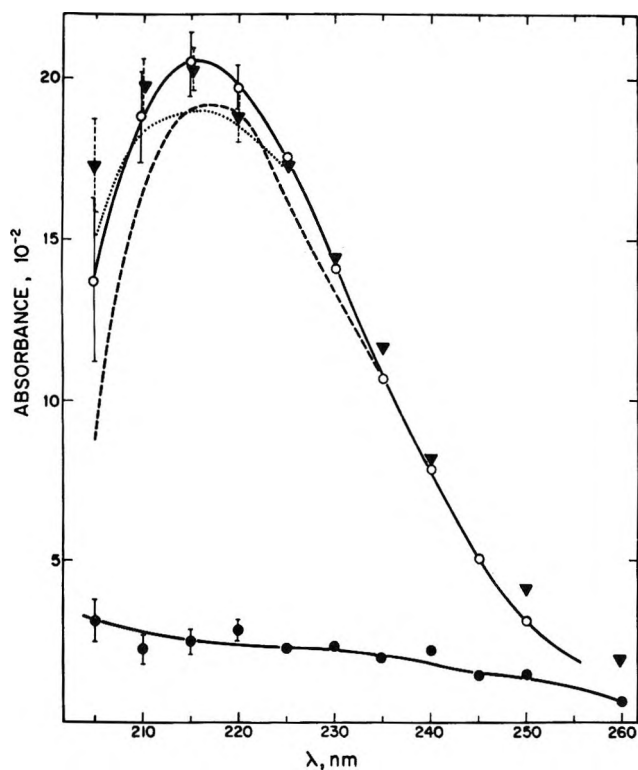


Figure 3. Transient spectra produced by pulse radiolysis and flash photolysis of hydroxylamine solutions, corrected for stray light (solid curves, the spectrum produced by flash was normalized): \circ , pulse radiolysis, 1 mM, N_2O (20 mM), pH 7.6 and 5.4, 0.75 msec after pulse (each point is the average of six measurements, three at each pH, with a scatter of $\pm 5\%$); \bullet , pulse radiolysis, 1 and 5 mM, N_2O (20 mM), pH 2.1, 1 msec after pulse; ∇ , flash photolysis, 10 (pH 5.4) and 2 mM (pH 7.3), N_2 , 0.75 msec after flash. Dashed and dotted curves represent the spectra without correction for the pulse and flash experiments, respectively. The limits of error for stray light are shown by lines, solid (pulse) and dashed (flash).

($\pm 15\%$), but it appeared to be the same at pH 4.0 and 2.0.

B. Flash Photolysis. The flash photolysis of N_2 -saturated solutions of hydroxylamine gives rise to a transient absorption below 300 nm. No other absorption was detected up to 740 nm. The same band was produced at pH 5.4 and 7.3, showing a well-defined peak with λ_{max} 216 ± 1 nm (Figure 3). (The figure shows the measured spectrum and that corrected for stray light effects. λ_{max} was determined by the method of midpoints.¹¹)

The decay rate of the 230-nm absorption was studied at pH 7.6 and was found to obey a second-order law with $2k/\epsilon_{230} = (1.0 \pm 0.3) \times 10^5$ cm sec⁻¹. At pH 5.5 the rate constant was somewhat lower but still within the limit of error (Table II).

Figure 4 (insert) shows the pH dependence of initial transient absorption (*i.e.*, absorption extrapolated to zero time) at 230 nm. The measurements were limited to pH ≤ 4.2 , where hydroxylamine is in effect totally in its acidic form and therefore its absorption should

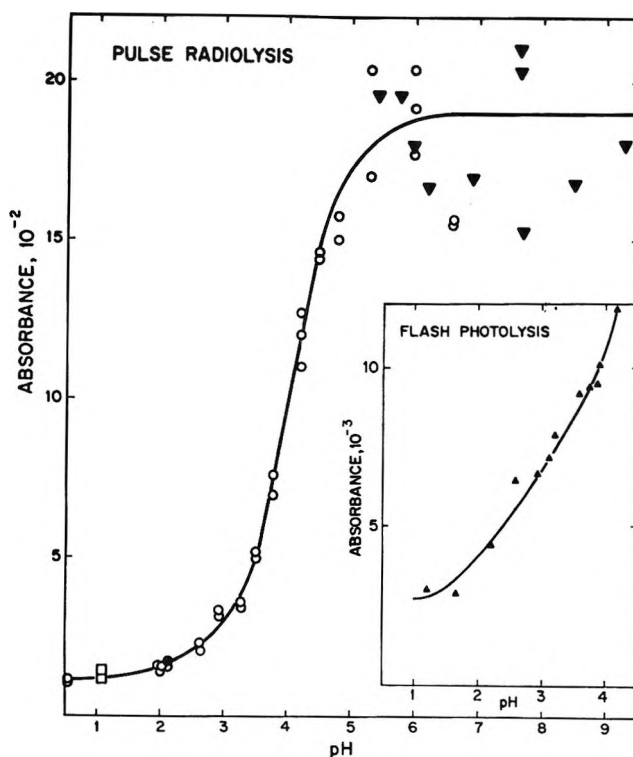


Figure 4. The pH dependence of initial transient absorption produced by pulse radiolysis and flash photolysis (insert) of hydroxylamine solutions. Pulse duration, 1.5 μ sec; \circ , pulse radiolysis, 5 mM, Ar; ∇ , pulse radiolysis, 10 mM, N_2O (20 mM); \square , pulse radiolysis, 1 mM, Ar; \bullet , pulse radiolysis, 1 and 5 mM, N_2O (20 mM); \blacktriangle , flash photolysis, 20 mM, N_2 .

Table II: Decay Kinetics of the Hydroxylamino Radical

$[NH_2OH]$, M	pH	Method	$2k/\epsilon_{230}$, cm sec ⁻¹
10^{-2}	7.3	Flash photolysis	$(1.0 \pm 0.3) \times 10^5$
2×10^{-3}	5.4	Flash photolysis	$(7.0 \pm 2.0) \times 10^4$
10^{-3}	7.6	Pulse radiolysis	$(1.0 \pm 0.3) \times 10^5$
10^{-3}	5.5	Pulse radiolysis	$(7.5 \pm 2.5) \times 10^4$

hardly vary with pH. Thus this figure might represent the pH variation of absorbance at constant yield of radicals. It shows a large change around pH 4 and levels off at pH $\lesssim 2$, where the absorption was too low for a kinetic study.

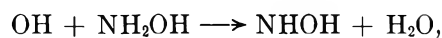
The effect of ethanol was studied on solutions of 2×10^{-3} M hydroxylamine, saturated with N_2 at pH 6.5. With 1.4×10^{-2} M ethanol the initial transient absorption (measured at 220 nm) was lowered but the decay kinetics hardly changed. Most of the absorption could be quenched on raising the alcohol concentration above 0.05 M, but a new transient spectrum emerged which was weak, smeared, and extending to longer wavelengths. This absorption, probably being due to

(11) G. Scheibe, *Ber.*, **58**, 586 (1925).

the ethanol radical,¹² could mask any residual absorption of the 216-nm transient.

C. Pulse Radiolysis. The pulse radiolysis of hydroxylamine solutions gives rise to a transient absorption which is identical with that produced by flash photolysis. This is illustrated in Figure 3, which records the spectrum obtained with N₂O-saturated solutions at pH 5.4 and 2.6, and in Table II where some kinetic data are summarized. The extinction coefficient $\epsilon_{230} = 1020 \pm 30 M^{-1} \text{ cm}^{-1}$ at pH 5.5 was determined by dosimetry ($\epsilon_{216} \sim 1500 M^{-1} \text{ cm}^{-1}$); this leads to $2k = (7.7 \pm 2.4) \times 10^7 M^{-1} \text{ sec}^{-1}$ for the rate constant of decay at pH 5.5. Somewhat different results have recently been reported by Simic and Hayon⁴ for the same transient: $\lambda_{\text{max}} 217 \text{ nm}$, $\epsilon_{\text{max}} = 2.5 \times 10^3 M^{-1} \text{ cm}^{-1}$, $2k/\epsilon_{240} = (4.1 \pm 1.5) \times 10^5 \text{ cm sec}^{-1}$ and $2k = (4.5 \pm 2.0) \times 10^8 M^{-1} \text{ sec}^{-1}$. They also found some deviations from second-order kinetics, which we could not verify. The difference in pH cannot explain this discrepancy (see Table II and Figure 4), the reason for which is not clear.

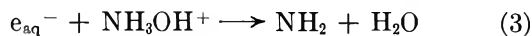
In agreement with recent work,⁴ we assign this transient absorption to the radical NHOH, produced by reaction 1



$$k_1 = 9.5 \times 10^9 M^{-1} \text{ sec}^{-1} \quad (1)$$

or by the slower reaction of OH with NH₃OH⁺. We could verify that the radical is neutral by not observing any distinct ionic effect on adding 0.1 M Na₂SO₄ to 10⁻³ M hydroxylamine at pH 7.2.

The pulse radiolysis of 5.6 × 10⁻³ M solutions of hydroxylamine at pH 5.5 produced the same amount of transient irrespective of whether they were saturated with N₂O (2 × 10⁻² M) or N₂. Under these conditions about three-fourths of the solvated electrons are scavenged by N₂O to produce OH radicals ($k(e_{\text{aq}}^- + \text{N}_2\text{O})^{13} = 5.6 \times 10^9 M^{-1} \text{ sec}^{-1}$; for the rate constant of e_{aq}^- with hydroxylamine see below). This implies that by attacking NH₂OH, e_{aq}^- , and OH give rise to identical yields of NHOH. The following reactions can account for this result

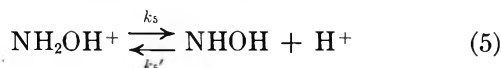


and similar reactions with the species involved being in their acidic forms. Experimental evidence has recently been provided for formation of the amino radical by reactions of e_{aq}^- with hydroxylamine.⁴

Figure 4 shows the pH dependence of the initial transient absorption at 230 nm. Most of the data were taken with 5 × 10⁻³ M hydroxylamine saturated with Ar, but other conditions were also employed to show that within the small dose variation, Figure 4 represents the change of absorption of a constant amount of hydroxylamino radicals (provided G_{OH} and $G_e + G_{\text{H}}$

are independent of pH in this pH region¹⁴). In addition to the foregoing conclusion about the equivalent effects of e_{aq}^- and OH (compare the Ar and N₂O experiments at pH >5) it could be shown that OH and H radicals attack NH₃OH⁺ to produce the same amount of the transient. Thus identical transient absorption were obtained with solutions of 10⁻³ M NH₃OH⁺ at pH 2.1 irrespective of whether they were saturated with Ar (when ~95% of e_{aq}^- are converted into H atoms) or with 2 × 10⁻² M N₂O (when 60 and 37% of e_{aq}^- are converted into H and OH radicals, respectively) (Figure 4).

Figure 4 is a typical titration curve, from which pK = 4.0 ± 0.1 could be derived for the equilibrium



in good agreement with recent results (pK = 4.2 ± 0.1⁴). Under the conditions employed the decay of radicals could hardly disturb the acid-base equilibrium. Assuming that $k_5' \sim 10^{10} M^{-1} \text{ sec}^{-1}$, i.e., $k_5 \sim 10^6 M^{-1} \text{ sec}^{-1}$, then under the conditions employed (concentration of radicals ≤ 2 × 10⁻⁵ M) the decay of NH₂OH⁺ was always much slower than reaction 5. As for the back-reaction, up to pH 5 the decay of NHOH was much slower than protonation. At higher pH values, reactions with other Lewis acids (NH₃OH⁺, H₂PO₄⁻, or water) should be considered, but their quantitative effect is not known. A high pH sensitivity of the absorbance was observed at pH ≥ 5.5 (Figure 4), which might reflect changes in rate of protonation of NHOH by the various Lewis acids. (The pK values of NH₃OH⁺ and H₂PO₄⁻ are 6.0 and 7.2, respectively.¹⁵)

The flash photolysis results (Figure 4, insert) show similar features but the titration curve is somewhat flatter. In this case considerable errors could be involved in measuring the low absorbance of the acidic form. The spectrum of this form obtained by pulse radiolysis is included in Figure 3.

The rate constants of reactions 2 and 3 were investigated by following the decay of the e_{aq}^- absorption at 600 nm in pulsed hydroxylamine solutions saturated with Ar (in presence of 1.3 × 10⁻² M isopropyl alcohol to scavenge the OH radicals). Figure 5 shows the dependence of the pseudo-first-order rate constant on the hydroxylamine concentration at three pH values. No further change was observed on raising the pH from 7.7 to 8.2 (Figure 5). From these results we could derive $k_2 = 6.6 \times 10^8 M^{-1} \text{ sec}^{-1}$, $k_3 = 1.0 \times 10^{10} M^{-1} \text{ sec}^{-1}$, and pK = 5.8 for the dissociation constant of NH₃OH⁺. The pK is in good agreement with avail-

(12) M. Simic, P. Neta, and E. Hayon, *J. Phys. Chem.*, **73**, 3794 (1969).

(13) M. Anbar and P. Neta, *Int. J. Appl. Radiat. Isotopes*, **18**, 493 (1967).

(14) G. Czapski, *Advan. Chem. Ser.*, **No. 81**, 106 (1968).

(15) "Handbook of Chemistry and Physics," 51st ed, Chemical Rubber Publishing Co., Cleveland, Ohio, 1970-1971.

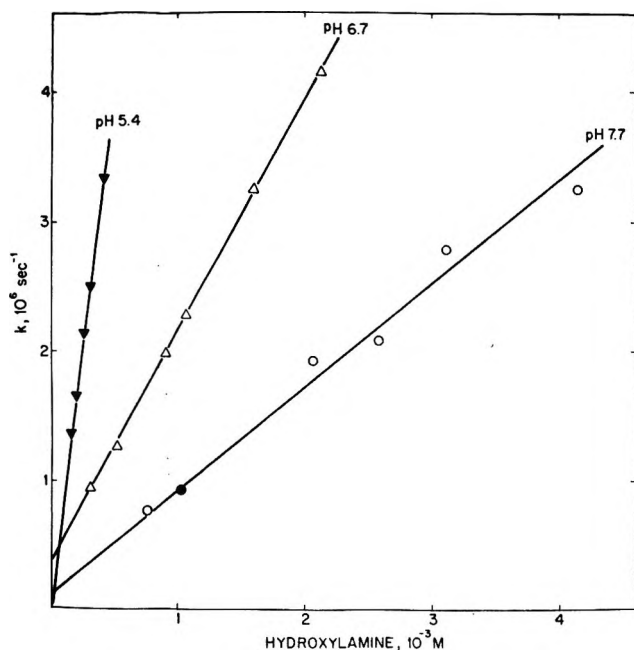


Figure 5. Pseudo-first-order plots for the reaction of e_{aq}^- with hydroxylamine at various pH values. (Full circle represents a measurement at pH 8.2.) The solutions were saturated with Ar and contained 13 mM isopropyl alcohol. Pulse duration: 0.2 μ sec.

able data.¹⁵ The values of k_2 and k_3 are much higher than the recorded value $k < 2 \times 10^7$ (at unspecified pH)¹³ but are close to that recently reported.⁴

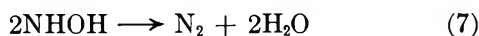
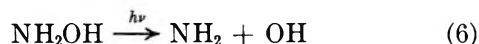
Discussion

A. *Photolysis of NH₂OH*. Most of the photochemical experiments were carried out at pH 7.4, where ca. 96% of the hydroxylamine is in its basic form. But even at pH 5.4, where some flash experiments were conducted, NH₂OH was the major light absorber.

The stoichiometry of photolysis of NH₂OH in aqueous solution is essentially identical with that of its Hg-photosensitized decomposition in the gas phase²



The following mechanism (I) accounts for these results



The flash photolysis experiments provide direct evidence for the generation of NHOH. However, a second mechanism (II) should also be considered



followed by reactions 4 and 7. Reaction 10 was introduced to account for the H₂ produced, with $k_9/k_{10} \sim 10$ (since $\phi_{\text{NH}_3}/\phi_{\text{H}_2} \sim 10$).

Mechanism II can be ruled out as the major one by considering the alcohol effect.

1. Mechanism II predicts that not more than 50% of the yields of NHOH and N₂ can be suppressed by a substance which can completely scavenge H atoms without reacting with NHOH. Our results indicate that ethanol behaves in this way since it affects neither the decay rate of NHOH (flash photolysis experiment) nor the yield of N₂ when NH₂OH is present in excess (Table I). But much more than 50% of NHOH and N₂ could be quenched by alcohol.

2. Under conditions where ethanol should effectively compete with NH₂OH for H atoms to produce H₂,¹⁶ it exerts no distinct effect on ϕ_{H_2} and ϕ_{NH_3} . This is in complete disagreement with mechanism II.

Mechanism I is in agreement with the major features of our results. On complete scavenging of NH₂ and OH by ethanol, NHOH and N₂ should not be produced, but the yield of NH₃ should not be affected by replacing reaction 4 by reaction 11.



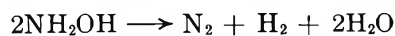
To account for the small and constant yield of H₂, a minor primary process should be considered as occurring in parallel to reaction 6. The possibility that H₂ results from some side reactions of the radicals (involved in mechanism I) can be ruled out, since in this case ϕ_{H_2} should decrease on adding ethanol.

A possible reaction that was already proposed for the gas photolysis² involves internal recombination



but NOH is expected¹⁷ to yield N₂O, which was not detected on photolyzing neutral solutions. Still reaction 12 cannot be discarded because under the condition employed some HNO could exist in solution as the dimer hyponitrous acid.

It is also possible that reaction 8 does take place to a small extent and that reaction 10 is much faster than 9. In this case, no change of ϕ_{H_2} is expected to occur when ethanol competes with NH₂OH on H atoms. The overall decomposition through this parallel mechanism is



The ratio $\phi_{\text{N}_2}/\phi_{\text{H}_2} = 9 \pm 1$ can be accounted for by assuming that 89 and 11% of NH₂OH undergo reactions 6 and 8, respectively. However, a picture like this requires that on adding ethanol not more than 89% of

(16) The rate constant for the reaction of H with ethanol is $2.5 \times 10^7 \text{ M}^{-1} \text{ sec}^{-1}$ [P. Neta, G. R. Holdren, and R. H. Schuler, *J. Phys. Chem.*, **75**, 449 (1971)]. That for NH₂OH is unknown but it is not likely to be considerably higher than 10⁹.

(17) O. P. Strausz and H. E. Gunning, *Trans. Faraday Soc.*, **60**, 347 (1964).

NHOH should be quenched and that ϕ_{N_2} should not fall below $0.5\phi_{H_2}$. We were unable to check these predictions because (a) the spectrum of the alcohol radical could mask any residual absorption of NHOH; (b) the ratio $[C_2H_5OH]/[NH_2OH]$ had to be below ~ 200 , so that with sufficient light absorbed by NH_2OH the absorption by alcohol was relatively small. Therefore no limiting value of ϕ_{N_2} could be measured.

According to the proposed mechanism ϕ_{N_2} equals the total quantum yield of primary dissociation. The excited state of NH_2OH involved is dissociative,² and since $\phi_{N_2} = 0.25$ irrespective of $[NH_2OH]$ up to 1 M, an efficient primary recombination should occur.

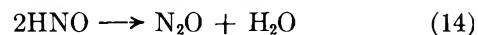
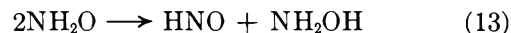
The direct photodissociation of NH_2OH to $NH_2O + H$, which is a major process in the gas phase,² does not appear to take place in solution. We have no explanation for this and for the close resemblance between the direct photolysis in solution and Hg-photosensitized decomposition in the gas phase.

B. The Photolysis of NH_3OH^+ . Below pH 4.5 almost all the light was absorbed by NH_3OH^+ , and the photolysis displayed new features. They do not necessarily reflect a change in nature of the primary processes, but they must involve some modification of the secondary reactions. Thus no change in the nature of light absorbing molecules is produced on lowering the pH from 4.3 to 2.0, but the photochemistry is considerably affected (Table I). NHOH is the only radical involved which has its pK within ± 1 in this region. (The pK of NH_2 is 6.7 ± 0.24). Therefore we believe that this pH effect reflects different chemical properties of the basic and acidic forms of the hydroxylamino radical.

Simic and Hayon⁴ presented evidence that the basic form is indeed NHOH, but since there is esr evidence for the structure NH_2O in acidic solutions¹⁸ and in solid $NH_2OH \cdot HCl$,¹⁹ the acidic form was considered⁴ to exist in some equilibrium with NH_2O .

In several works dealing with the photolysis of gaseous hydroxylamine² and its electrolysis in solutions,²⁰ NHOH and NH_2O were assumed to yield N_2 and N_2O , respectively, on their annihilation. If this assumption is correct, then the present work supports the view that NHOH is transformed to NH_2O (or NH_3O^+) in acidic

solutions. At pH $\lesssim 2.0$, when almost all the hydroxylamino radical is in acidic form, reaction 7 is probably replaced by reactions 13 and 14²



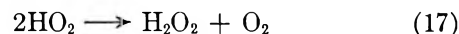
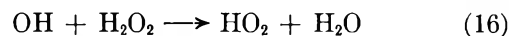
and the stoichiometry of photolysis is now



Considering the low accuracy of our results concerning this pH region (Table I), they are not in discord with the proposed mechanism. In addition, the quenching of ϕ_{H_2} suggests that the minor primary reaction leading to H_2 formation (possibly reaction 8 or 12) does not occur with NH_3OH^+ .

C. Analogies with the Photolysis of H_2O_2 . NH_2OH and H_2O_2 are isoelectronic and bear some resemblance. The dissociation energies NH_2-OH and $HO-OH$ are relatively low (61 and 51 kcal/mol, respectively⁸), and therefore it is reasonable to expect the rupture of these bonds as the primary processes.

The mechanism proposed for the photolysis of H_2O_2 in aqueous solution is²¹



Reaction 16 is analogous to reactions 1 and 4, and the radical HO_2 is isoelectronic with NHOH. The spectrum of HO_2 (λ_{max} 230 nm, ϵ_{max} $1.2 \times 10^3 M^{-1} cm^{-1}$) resembles that of NHOH and it decays even more slowly than NHOH.²²

(18) (a) C. J. W. Gutch and W. A. Waters, *J. Chem. Soc.*, 751 (1965); (b) J. Q. Adams, S. W. Nicksic, and J. R. Thomas, *J. Chem. Phys.*, **45**, 654 (1965).

(19) H. Ohigashi and Y. Kurita, *J. Phys. Soc. Jap.*, **24**, 654 (1968).

(20) (a) A. D. Goolsby and D. T. Sawyer, *J. Electroanal. Chem.*, **19**, 405 (1968); (b) G. R. Rao and L. Meites, *J. Phys. Chem.*, **70**, 3620 (1966).

(21) C. H. Bamford and R. P. Wayne in "Photochemistry and Reaction Kinetics," Cambridge University Press, New York, N. Y., 1967, p 33.

(22) D. Behar, G. Czapski, J. Rabani, L. M. Dorfman, and H. A. Schwarz, *J. Phys. Chem.*, **74**, 3209 (1970).

Electronegativity Effects in T-for-CH₂X Substitutions for Recoil

Tritium Reactions with *n*-Propyl Fluoride¹

by Thomas Smail, Bartyra Arezzo, and F. S. Rowland*

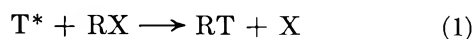
Department of Chemistry, University of California, Irvine, California 92664 (Received August 16, 1971)

Publication costs assisted by the Division of Research, U. S. Atomic Energy Commission

The relative yields for the substitution of energetic T atoms for heavy substituents has been compared in the *n*-C₃H₇F system. Formation of CH₂TF is only 0.80 (+0.05, -0.15) as likely as of CH₃CH₂T, after correction for secondary decomposition of both products. The lower yield for CH₂TF is attributed to an electron-withdrawal effect of the F atom, thereby hindering successful formation of the new C-T bond. Rotational inertia effects should be negligible in such a comparison because of the near-equivalence of F and CH₃ in such inertial properties.

Introduction

Numerous studies have established that energetic recoil tritium atoms are able to substitute not only for H atoms in reactant molecules, but also for heavier groups, as in (1), with apparently very little qualitative limitation on the chemical identity of the replaced group, X.^{2,3} Systematic studies of the replacement by T of



Cl in CH_{4-n}Cl_n and of F in CH_{4-n}F_n have shown that the absolute percentage yields of these T-for-X reactions fall off sharply in gas phase experiments with increasing values of the subscript *n*.^{4,5} Subsequent competitive experiments in both gas and liquid phases, while demonstrating that these gas phase yields are seriously depleted by secondary decomposition (factors of 2-3),⁶⁻⁹ have confirmed the general decrease in absolute primary yield with increase in *n*. This steady variation in the yields for T-for-Cl and T-for-F substitution reactions served as one basis for the "rotational inertia" hypothesis, in which the heavier substituent groups are postulated to prevent formation of a bonding orbital between the tritium atom and the residual R group because of their much greater inertial resistance to rotation.³⁻⁵

A second hypothesis concerning the effects of additional Cl or F substituents on reaction 1 is based on the increased electronegativity of these substituents. Such electronegative groups have been postulated to withdraw sufficient electron density during the critical phase of the atom-molecule collision to decrease the probability of bond formation between R and T.^{2,6,9,10} The yields of T-for-H reactions with halomethanes and hydrocarbons have been shown to decrease steadily with increasingly electronegative substituents (as monitored, for example, by proton nmr shifts) from a value of 1.00 for CH₄ to 0.56 for CHF₃.^{9,10} A qualitatively similar

effect is quite plausible with tritium atom substitutions for heavier substituents such as Cl or F.¹¹ Since the predictions for polyhalomethanes of an electronegativity effect are qualitatively in the same direction as a rotational inertia effect, no separate evaluation of the former can be made from the previous experimental data.

The experiments reported here have been intended to measure the magnitude of the possible electronegativity effect in the substitution reaction 1, in the absence of any important rotational inertia contribution, by measurement of the yields of CH₂TX and CH₂TY from a molecule XCH₂CH₂Y, in which X and Y are similar in mass but different in electronegativity. Our target molecule has been CH₃CH₂CH₂F, from which the products CH₂TF and CH₃CH₂T have been sought, as in (2) and (3). Since the rotational inertia hypothesis has broadly divided atoms and groups into light (H or D) and heavy (F, Cl, CH₃, etc.) substituents, the physical inertial effects of F and CH₃ should essentially cancel one another, leaving the electronegativity factor of F

(1) This research was supported by AEC Contract No. AT-(04-3)-34, Agreement No. 126, and by an International Atomic Energy Agency Fellowship (B. A.).

(2) F. Schmidt-Bleek and F. S. Rowland, *Angew. Chem., Int. Ed.*, **3**, 769 (1964).

(3) R. Wolfgang, *Progr. React. Kinet.*, **3**, 97 (1965).

(4) R. A. Odum and R. Wolfgang, *J. Amer. Chem. Soc.*, **83**, 4668 (1961).

(5) R. A. Odum and R. Wolfgang, *ibid.*, **85**, 1050 (1963).

(6) Y.-N. Tang, E. K. C. Lee, and F. S. Rowland, *ibid.*, **86**, 1280 (1964).

(7) Y.-N. Tang and F. S. Rowland, *ibid.*, **87**, 3304 (1965).

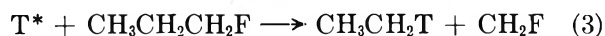
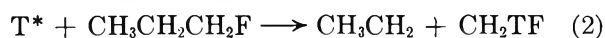
(8) Y.-N. Tang and F. S. Rowland, *ibid.*, **90**, 574 (1968).

(9) Y.-N. Tang, E. K. C. Lee, E. Tachikawa, and F. S. Rowland, *J. Phys. Chem.*, **75**, 1290 (1971).

(10) F. S. Rowland, E. K. C. Lee, and Y.-N. Tang, *ibid.*, **73**, 4024 (1969).

(11) Evidence for inductive effects of electronegative substituents at both C-H and Si-C bonds has also been presented through experiments with (CH₃)₃Si-F. S. E. Daniel and Y.-N. Tang, *ibid.*, **75**, 301 (1971).

vs. CH₃ as the chief variable remaining to affect the relative primary yields of CH₂TF and C₂H₅T.



Secondary Unimolecular Decay of Primary Products. Experiments to test the influence of electronegativity in the absence of possible rotational inertia effects were first planned and carried out several years ago, using a series of CH₃CH₂CH₂X molecules in the gas phase. These experiments invariably showed much more C₂H₅T than CH₂TX from CH₃CH₂CH₂X for a series of substituents, X, suggesting that electronegativity effects might well be present.^{2,12} At the same time, however, recoil tritium experiments with cyclobutane had conclusively established that the substitution of T-for-H in *c*-C₄H₈ left highly excited *c*-C₄H₇T* molecules, about 40% of which underwent secondary decomposition (to C₂H₃T + C₂H₄) at 1 atm pressure.¹³ Since further experiments with CH₃Cl and CH₂Cl₂ showed extensive decomposition in these systems, especially of CH₂TCl* formed by T-for Cl in CH₂Cl₂,^{7,8} it was felt that deductions from observed yield trends in experiments at 1 atm pressure were questionable until further information was available about the extent of secondary decomposition following such substitution reactions.

Subsequent experiments on the substitution of T-for-CH₃ in 1,3-dimethylcyclobutane,¹⁴ and T-for-H in CH₃NC,¹⁵ as well as T-for-H and T-for-F in fluoromethanes,¹⁶ have amply confirmed our reservations about the possibility of significant depletion of a primary absolute yield by secondary reaction: only about 2% of the methylcyclobutane-*t* molecules formed by T-for-CH₃ in 1,3-dimethylcyclobutane, and less than 0.3% of CH₂TNC following T-for-H in CH₃NC, fail to undergo secondary reaction in gas phase experiments. Satisfactory estimates of secondary decomposition are favored by experiments in high density systems, for which the collisional stabilization rates are greatly enhanced over the 1 atm gas phase values. In our systems, these collision rates have been attained with liquid phase experiments.

Bond Strength Effects in Alkyl Replacement Reactions. The rotational inertial and electronegativity hypotheses are not mutually exclusive, nor do they cover all possible parameters affecting such reactions. Root has demonstrated a correlation of gas phase yields with the bond strengths of the newly formed bonds, *e.g.*, R-T in (1).¹⁷ These relative yield measurements have also not included any corrections for secondary decomposition of the T-for-X products, and are thus subject to perturbation if one molecule of a pair under comparison has a markedly less energetic path for decomposition than the other.

Experimental Section

These experiments were performed by standard

techniques that have been applied in numerous other investigations,^{2,6-10,13-16} and involve formation of energetic tritium atoms by the nuclear reactions ³He(n,p)T and ⁶Li(n,α)T in the gas and liquid phases, respectively. The samples were analyzed by our standard radiogas chromatographic procedures¹⁸ using several different columns (dimethylsulfolane, di-*n*-butyl phthalate, propylene carbonate on alumina, and tritoyl phosphate) to assure that no undiscovered overlapping radioactive peaks were present in the analytical schemes employed.

Results

The most important radioactive products for the purposes of this experiment were the two competitors, CH₂TF and CH₃CH₂T, which possessed essentially equal inertial qualities. The observed yields of these two products under a variety of experimental conditions are summarized in Table I, as measured *vs.* the yield of HT measured in the same system. While the yield of HT is reasonably constant, the comparisons of the three listed gas samples are characteristic of the reproducibility of these measurements versus the HT standard.

The uniformly higher values in the liquid phase illustrate that appreciable decomposition occurs for both CH₂TF* and CH₃CH₂T* in the gas phase, and suggest that decomposition in the liquid phase may not be negligible. Measurements of the expected decomposition products were also carried out in the Br₂-scavenged liquid samples, *e.g.*, CHTFBr (0.49) *vs.* CH₂TF (1.58) and CH₂TBr (2.19) *vs.* CH₃CH₂T (2.05).

Secondary Reactions of Excited Products. Although evidence exists for smaller yields of decomposition by alternate, higher energy paths, the major observed mode of molecular decomposition or isomerization following recoil tritium substitution reactions has been in each system the same path as that found in pyrolysis or chemical activation experiments. Consequently, the chief mode of decomposition of C₂H₅T* is expected to be the C-C split into two radicals, with an activation energy of 88 kcal/mol, with a lesser contribution from C-H split, with an activation energy of 98 kcal/mol.^{19,20}

The least endothermic route for decomposition of CH₂TF* is the split into CHT and HF, which is about 78 kcal/mol endothermic.²¹ However, while the de-

(12) The ratio of C₂H₅T/CH₂TF was given as 1.7 in the gas phase in ref 3.

(13) E. K. C. Lee and F. S. Rowland, *J. Amer. Chem. Soc.*, **85**, 897 (1963).

(14) C. T. Ting and F. S. Rowland, *J. Phys. Chem.*, **74**, 445 (1970).

(15) C. T. Ting and F. S. Rowland, *ibid.*, **72**, 763 (1968).

(16) Y.-N. Tang and F. S. Rowland, *J. Amer. Chem. Soc.*, **89**, 6420 (1967).

(17) J. W. Root, *J. Phys. Chem.*, **73**, 3174 (1969).

(18) J. K. Lee, E. K. C. Lee, B. Musgrave, Y.-N. Tang, J. W. Root, and F. S. Rowland, *Anal. Chem.*, **34**, 903 (1962).

(19) S. W. Benson, *J. Chem. Educ.*, **42**, 517 (1965).

(20) D. M. Golden and S. W. Benson, *Chem. Rev.*, **69**, 125 (1969).

(21) The isotopic alternate, into CH₂ + TF, would also be expected with almost identical endothermicity.

Table I: Yields of CH₂TF and CH₃CH₂T from Recoil Tritium Reaction with CH₃CH₂CH₂F (Yields Relative to HT = 100)

Product	Experimental conditions				
	<i>n</i> -PrF Torr			Liquid phase	
	296	576	874	5.9% Br ₂	7.4% Br ₂
	O ₂ Torr				
	40	50	86		
CH ₂ TF	0.88	0.86	0.96	1.58	1.79
CH ₃ CH ₂ T	1.17	1.11	1.21	2.05	2.08
CH ₂ TF/CH ₃ CH ₂ T	0.75 ± 0.02	0.79 ± 0.02	0.77 ± 0.02	0.77 ± 0.02	0.86 ± 0.02

composition of C₂H₅F into C₂H₄ plus HF is endothermic by only 9 kcal/mol,²² the activation energy is 59 kcal/mol for this pyrolytic decomposition.¹⁹ No evidence has yet appeared to indicate that the pyrolysis of CH₃F proceeds through HF elimination as the primary step, and preliminary searches for HF elimination from excited CH₂TF* failed to disclose any evidence for CHT under conditions for which ample yields of CTF are found from the decomposition of CHTF.²³ Consequently, we assume that the primary mode of CH₂TF* decomposition is by C-H bond break with an activation energy of 103 kcal/mol. The expected CHTF radical has been detected through its reaction with Br₂ to form CHTFBr.

Unfortunately, while the measured yield of CHTFBr serves as a reasonable measure of the decomposition of CH₂TF*, the yield of CH₂TBr can include CH₂T radicals formed by processes other than the decomposition of CH₃CH₂T*. Among the other direct substitution products from energetic T reactions with *n*-C₃H₇F are *n*-C₃H₇T, CH₃T, *n*-C₃H₆TF, and CH₂TCH₂F; CH₂T should also be the prime labeled product from the secondary decomposition of both CH₃T* and *n*-C₃H₇T*. The total yield of CH₂T scavenged as CH₂TBr is large enough to correspond to appreciable decomposition from more than one path. However, no precise assignments of decomposition product yields can be made that would permit a completely unambiguous comparison of yields of [CH₂TF + CHTFBr] vs. [C₂H₅T and its CH₂T decomposition product]. The decompositions of both the labeled parent and of CH₂TCH₂F should proceed chiefly by HF (or TF) elimination with the respective formation of propylene-*t* and C₂H₃T;²² both products are found in measurable yield.

Relative Primary Yields of CH₂TF and CH₃CH₂T. The liquid phase measurements of the yields of CH₂TF (and correction for the isotopic alternate CH₂TF* → CH₂F + T) indicate a summed yield essentially equal to that of CH₃CH₂T without its decomposition product. Considering the 30–35% decomposition of CH₂TF* by a route with an activation energy of 103 kcal/mol, the contribution of CH₃CH₂T* decomposition to the measured CH₂TBr yield by an 88 kcal/mol path can be safely assumed to be at least 25%. On the other hand, the 40% decomposition of CHT <math>\begin{matrix} \text{CH}_2 \\ \text{CH}_2 \end{matrix}> \text{CHCH}_3^* (acti-

vation energy = 62 kcal/mol) formed by T-for-CH₃ in liquid 1,3-dimethylcyclobutane suggests that CH₃CH₂T* decomposition is probably not greatly in excess of 35–40%. We conclude that the measured ratio of 0.81 ± 0.04 for the yields of CH₂TF/CH₃CH₂T as measured in the liquid phase is not an unreasonable approximation to the ratio of primary yields, although probably slightly high; we estimate this ratio of yields prior to decomposition to be 0.80 (+0.05, -0.15).

Electronegativity Effect on T-for-X Reaction. The estimated 20 (+15, -5)% lower primary yield for CH₂TF than for CH₃CH₂T is consistent with an electronegative substituent effect involving greater electron withdrawal by F than CH₃ during the determining phase of the T-for-X substitution reaction. The corresponding reduction in yields for T-for-H reactions with CH₃F vs. C₂H₆ has been measured in separate binary solutions of each in liquid CH₃Cl, and is also about 20% within wide limits of error:⁹ CH₂TF (71 ± 2) vs. C₂H₅T (91 ± 5). These experiments thus furnish evidence that the yields of the substitution reactions for heavy groups are influenced by the electronegativity of adjacent substituents, with a quantitative effect roughly comparable to that found for T/H substitution.

A trend toward higher yields with the formation of strong C-T bonds¹ would favor a higher yield for CH₂TF (C-H = 103 kcal/mol) than for C₂H₅T (C-H = 98 kcal/mol),¹⁹ in opposition to the experimental observations. If such a bond-strength factor is also operative in our experiments, then the assessment of the importance of the electronegative substituents must be increased by an equivalent counterbalancing factor.

Since these experiments were deliberately designed to minimize any "rotational inertia" factors in the comparisons of yields, no information has been gained here concerning either the presence or quantitative estimation of the importance of this factor for T-for-X substitutions. Separately designed experiments, also involving appropriate corrections for secondary decomposition, will be required for attempts at quantitative estimation of the relative and combined importance of electronegativity and inertial effects in the replacement of heavy groups by energetic tritium atoms.

(22) A. MacColl, *Chem. Rev.*, **69**, 33 (1969).(23) E. K. C. Lee and F. S. Rowland, *J. Amer. Chem. Soc.*, **85**, 2907 (1963).

Temperature Dependence of the Reaction Yields from Recoil Tritium

Reactions. II. Tritium Atom Addition to 1-Butene and *cis*-2-Butene¹

by Richard Kushner and F. S. Rowland

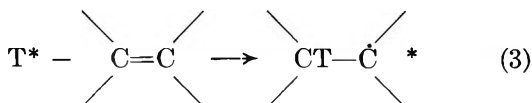
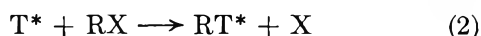
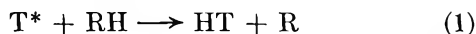
Department of Chemistry, University of California, Irvine, California (Received August 9, 1971)

Publication costs assisted by the Division of Research, U. S. Atomic Energy Commission

Energetic recoil tritium atoms react with 1-butene and *cis*-2-butene to form $\text{CH}_3\text{CH}_2\dot{\text{C}}\text{HCH}_2\text{T}^*$ and $\text{CH}_3\text{CHT}-\dot{\text{C}}\text{HCH}_3^*$ radicals, respectively. The yields of the corresponding secondary decomposition products, $\text{CH}_2\text{T}-\text{CH}=\text{CH}_2$ and $\text{CH}_3\text{CH}=\text{CHT}$, are higher when formed at 125° than at 24° over the pressure range from 50–1000 Torr. This temperature dependence of yields is consistent with an increase in excitation energy corresponding to the increased internal energy of the butene molecules at the higher temperature. Decomposition rate constants most sensitive to these pressures ($\sim 10^9$ – 10^{10} sec⁻¹) correspond to initial kinetic energies of tritium from about 10–40 kcal/mol; the median energy at which double-bond addition occurs is about 10 kcal/mol or less. The addition reaction of energetic tritium atoms with substrate olefins is apparently unaffected by the temperature of the substrate; the observable temperature effects are satisfactorily explained as the effects of substrate molecule temperature upon the secondary decomposition processes following the primary interaction. No temperature dependence was found for the hot products of energetic tritium atom reaction with CH_4 : HT, CH_3T , and CH_2T (measured as CH_2TBr).

Introduction

Tritium atoms with excess kinetic energy react with a variety of molecules by several reaction paths which can collectively be described as "hot atom" reactions, as shown in (1) to (3).²⁻⁴ Since both the ab-



straction reaction (1) and the addition reaction (3) are often characteristic of thermal systems as well, several techniques have been used to distinguish "hot" from "thermal" reactions, including sensitivity to competition with molecular species capable of scavenging thermal atoms and radicals. Among these identifying characteristics of hot atom reactions has been the essential absence of temperature effects on reaction yields.⁵ Since these changes in energy content of the partner molecule caused no observable effect upon the product yields, the strong inference was drawn that the reacting atom was supplying so much energy that the partner's energy content represented an essentially negligible contribution to the overall energy utilized in the process of chemical change.^{2,3} One early study of T atom reactions with CH_4 at 22° and 200° failed to disclose any difference in reaction yields (of HT and CH_3T),⁶ while experiments with acetone in condensed phases at -78 and -196° also showed no significant yield variations.⁷ A change in product distribution was observed for $\text{T}^* + \text{cis}$ -2-butene between -78°

(liquid) and -196° (solid), but could not be unambiguously assigned either to crystal-liquid or internal energy differences.⁸ A much smaller change was observed in the liquid range from 20° to -78°, and was further complicated by the absence of a suitable scavenger for thermalized radicals.⁸ Product differences have also been observed for other reactions in which temperature changes were always accompanied by phase changes.⁹

In summary, a few searches for variations in reaction yields of recoil tritium reactions with temperature were carried out with negative results a number of years ago, and no additional temperature dependence studies were

(1) This research formed part of the material submitted in partial fulfillment of the requirements for the Ph.D. degree by R. Kushner. This research was supported by A.E.C. Contract No. AT-(04-3)-34, Agreement No. 126. Fellowship support for R. Kushner from N.A.S.A. is gratefully acknowledged.

(2) F. Schmidt-Bleek and F. S. Rowland, *Angew. Chem., Int. Ed. Engl.*, **3**, 769 (1964).

(3) R. Wolfgang, *Progr. React. Kinet.*, **3**, 97 (1965).

(4) F. S. Rowland, "Molecular Beams and Reaction Kinetics," Academic Press, New York, N. Y., 1970, pp 108–138.

(5) In principle, one might prefer to measure temperature effects on rates of hot chemical reactions in such studies, but the usual hot atom experiment does not involve any knowledge of the time required for an energetic atom to react. The normal measurement is instead the distribution of atoms among the various possible products without any reference to the elapsed time between formation and reaction.

(6) M. A. El-Sayed, P. Estrup, and R. Wolfgang, *J. Phys. Chem.*, **62**, 1356 (1958).

(7) W. J. Hoff and F. S. Rowland, *J. Amer. Chem. Soc.*, **79**, 4867 (1957).

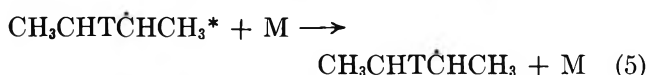
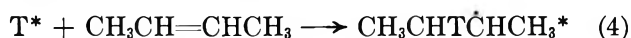
(8) E. K. C. Lee and F. S. Rowland, *J. Inorg. Nucl. Chem.*, **25**, 133 (1963).

(9) B. G. Dzantiev and A. P. Schvedchikov, "Chemical Effects of Nuclear Transformations," Vol. 1, International Atomic Energy Agency, Vienna, 1965, p 87.

conducted for many years, although a large number of experiments investigating a great variety of other possible parameters have been performed. Temperature effects have therefore been dismissed as generally insignificant in magnitude, as well as relatively unimportant in overall considerations,^{2,3} and the term "hot atom reaction" consequently may carry some connotations of complete independence of the energy restraints of ordinary chemical reactions.

Since the experimental and theoretical bases of recoil tritium reactions are now much better understood, and experimental reproducibility is also greatly improved, we have again initiated studies of the possible temperature effects on reactions (1) to (3). Our preliminary observations of measurable temperature effects upon the yields of addition-decomposition reactions with butene substrates have been reported;¹⁰ we now present the full details of these experiments. In addition, we have again looked for any temperature dependence of yields from reactions (1) and (2) with methane.

The chief reaction sequence for the addition of energetic tritium atoms to olefins is illustrated in (4) to (6) with 2-butene,²⁻⁴ in which it is clear that greater energy in the excited *sec*-butyl radicals (for example, from increased internal energy of CH₃CH=CHCH₃ at a higher temperature) can change the yield ratio for (5) *vs.* (6),



leading to a measurable temperature effect. Since changes in this yield ratio also vary as the pressure of *M* is varied, the magnitudes of temperature effects have been sought over a substantial pressure range in these experiments.

The addition of T* to CH₃CH₂CH=CH₂ can lead to the formation of CH₃CH₂CH₂T*, whose decomposition by (7) is closely analogous to (6) except for the position of the tritium label in the product propylene-*t*. Nonterminal addition to 1-butene can also lead to the formation of CH₂=CHT, as in (8). Both (7) and (8) are, of course, subject to a potentially pressure-dependent competition with the corresponding collisional stabilization reactions.



The direct substitution of T for CH₃ in 1-butene can also lead to the formation of CH₂TCH=CH₂. However, experiments with CH₃CH₂CH=CD₂ have shown that the yield of this reaction is both (a) small relative to that from CH₃CH₂CH₂T* decomposition, and (b) essentially pressure independent.^{11,12} Accordingly, the yield differences found in our current experiments have been assumed not to involve this direct reaction.

Experimental Section

Sample Preparation. These measurements of temperature effects have been complementary to our study of pressure effects on the reactions of T* with 1-butene and *cis*-2-butene,¹² with energetic tritium atoms formed by the nuclear reaction ³He(n,p)T.²⁻⁴ Techniques of sample preparation have been described in substantial detail earlier,^{2,3,13,14} and do not differ in any significant factors for the present experiments.¹⁴ Normally, three or four nearly identical samples were prepared as a group in order to have duplicate samples for irradiation at each of two temperatures.

Sample Analysis. The radio gas chromatographic analytical procedures for the butene analysis have been described in an earlier paper.¹² The analysis of the products from T* reaction with CH₄ were carried out on a 74-ft column of propylene carbonate on alumina.

Energy Content vs. Temperature. Between 24° and 125°, the internal energies at constant volume of methane, *cis*-2-butene, and 1-butene increase by 0.72, 1.99, and 2.25 kcal/mol, respectively.¹⁵

Irradiations. Most irradiations were carried out in the dry exposure room of the Mark F TRIGA reactor of the Northrop Space Laboratories in Hawthorne, Calif. This facility provides ample space for samples and auxiliary equipment, but with considerable variation in neutron flux for different locations within the room. The warm samples were thermostated in a simple oil bath at 125 ± 5° (maintained with a hot plate), and were held at this temperature during the exposure of the entire assembly to a nominal neutron flux of about 1 × 10¹² n/(cm² sec) for 1 hr. The neutron geometry of the several samples in each oil bath was very irregular, with the result that the actual neutron flux within a sample was known only semi-quantitatively. A general equivalence of neutron exposure for both room temperature and 125° samples was obtained by irradiating the former while immersed in an identical oil bath (unheated, 24 ± 1°). The temperature in the room was maintained during reactor operation by forced air draft. The uncertainty in neutron flux prevented any measurements of absolute yields at 125°; absolute yields for the butene systems have been determined at room temperature in other experiments.^{12,16}

The combined effects of varying distance from the reactor core and neutron absorption in the oil baths (and

(10) R. Kushner and F. S. Rowland, *J. Amer. Chem. Soc.*, **91**, 1539 (1969).

(11) E. K. C. Lee and F. S. Rowland, *J. Phys. Chem.*, **74**, 439 (1970).

(12) R. Kushner and F. S. Rowland, *ibid.*, **75**, 3771 (1971).

(13) J. W. Root, Ph.D. Thesis, University of Kansas, 1964; E. Tachikawa, Ph.D. Thesis, University of California, Irvine, Calif., 1967.

(14) R. Kushner, Ph.D. Thesis, University of California, Irvine, Calif., 1969.

(15) K. A. Kobe and E. G. Long, *Petrol. Refiner*, **28**, 125 (1949).

(16) A. H. Rosenberg and R. Wolfgang, *J. Chem. Phys.*, **41**, 2159 (1964).

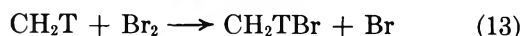
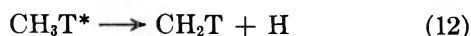
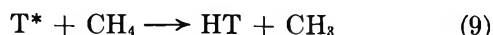
neighboring samples) substantially reduced the actual neutron flux within the samples below that indicated as the nominal flux, while total observed activities varied by as much as a factor of 5 between otherwise duplicate samples. A few samples which apparently received the nominal neutron flux were discarded because of too extensive ($\geq 1\%$) macroscopic radiation damage. Otherwise, the variations in activity level produced no systematic alteration in product distributions.

As is usual in our recoil tritium experiments, the sample bulbs were made from Pyrex 1720 glass, which is essentially impermeable to diffusion by small molecules, even at elevated temperatures. Thus, exposure to a temperature of 125° for a period of hours is not expected to permit backdiffusion out of the bulb walls of the energetic tritium atoms which have recoiled into it. In this way, the normal procedures of radio gas chromatographic analysis measure, as intended, only those tritium atoms whose high initial recoil energy does not carry them out of the gas phase before complete dissipation of this excess kinetic energy.

As a further check on the possible effects of elevated temperatures, several samples were irradiated at 24° and then subsequently heated to 125° for 3 hr after the irradiation. The postirradiation heat treatment had no apparent effect on the samples, giving results indistinguishable from samples irradiated at 24° and handled in the normal fashion.

Results and Discussion

Temperature Effects with Gaseous Methane. Several essentially identical samples of Br_2 -scavenged CH_4 ($\text{CH}_4/\text{Br}_2 = 10$) were filled simultaneously at each of three different pressures and were then irradiated in two groups—one at 24° and one at 125° . The relative yields of the three tritiated products formed by reactions 9–13 were measured for each sample, and are



plotted *vs.* the filling pressure of methane in Figure 1. The upper plot shows the slight dependence of the ratio of CH_2TBr to $\Sigma (\text{CH}_3\text{T} + \text{CH}_2\text{TBr})$ noted earlier,¹⁷ consistent with that expected for the competition between decomposition (12) and collisional stabilization (11).^{18,19} However, no significant difference was observed between experimental yield ratios found with samples irradiated at 24° and those at 125° .

The lower plot of Figure 1 shows the relative yield of HT by abstraction versus the total substitution yield. Again, no consistent difference was observed between experiments at 24° and 125° . The approximate 2%

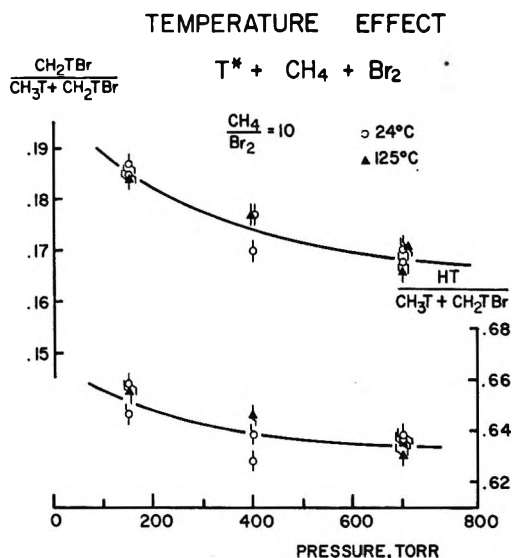


Figure 1. Temperature and pressure variations in relative yields of recoil tritium reactions with Br_2 -scavenged methane. Mole ratio; (CH_4/Br_2) = 10:1. Key: \circ , irradiated at 24° ; \blacktriangle , irradiated at 125° . Upper graph: ratio of CH_2TBr yield to sum of $\text{CH}_3\text{T} + \text{CH}_2\text{TBr}$ yields. Lower graph: Ratio of HT yield to sum of $\text{CH}_3\text{T} + \text{CH}_2\text{TBr}$ yields.

increase in HT yield with lowering pressure was not investigated in detail, since it was not affected by the variations in temperature.

The sum of CH_3T plus its decomposition product CH_2TBr , used as the denominator in Figure 1, is not a complete sum of the initial primary yield, since the alternate isotopic decomposition pathway to $\text{CH}_3 + \text{T}$ would leave no surviving C–T bond as evidence of the original reaction. The H/T isotope effect is not known (it is probably ≥ 1.73), but the ratio of $\text{CH}_3/\text{CH}_2\text{T}$ from CH_3T^* is certainly less than the statistical ratio of 1:3—corresponding to ≤ 0.06 in the units of Figure 1. If the statistical ratio is used as a crude estimate, the “missing” CH_3 yield would be about 0.062 at 150 Torr and 0.056 at 700 Torr, or a deviation of only 0.006 over this pressure range. Thus, although the “observed” CH_3T and CH_2TBr products are not a complete sum, no significant error is introduced by using their sum as the denominator in Figure 1. The increase in HT yield for low pressure *vs.* high pressure is about 4 times as large as the calculated statistical upper limit to the pressure deviation from omission of ($\text{CH}_3 + \text{T}$) reactions; the primary source of the HT pressure dependence must lie elsewhere.

Minor contributions of HT may arise from “wall” reactions, or possibly from the decomposition of CH_3T^*

(17) D. Seewald and R. Wolfgang, *J. Chem. Phys.*, **47**, 143 (1967).

(18) Y.-N. Tang and F. S. Rowland, *J. Phys. Chem.*, **72**, 707 (1968).

(19) The possibility that some CH_2T might be formed by a single-step primary process has been discussed in ref 4, 17, and 18. Whether this process is negligible or measurable is immaterial to the present study, since such highly energetic processes would be expected to be especially insensitive to temperature effects.

by loss of HT (and H₂) in small yield. The loss of HT certainly occurs from excited higher hydrocarbons, and it could readily be a minor source of HT in CH₄,^{20,21} perhaps sufficient to account for the 2% increase at lower pressures.

Variation in Collision Density with Temperature. Ideal gas samples filled at 24° will have 34% higher pressure after heating to 125° and will therefore undergo 16% more collisions per unit time because of this increase in average velocity. Since the secondary decomposition of CH₃T* competes with deexcitation by collision with the other molecules of the medium, a more appropriate comparison for the ratios of Figure 1 is probably that shown in Figure 2 in which the 125° data have been displaced by a factor of 1.16 in order to compare samples with equal collision frequencies during the period of irradiation.²² No significant temperature effect is shown by this comparison either, confirming the earlier observations for CH₄.⁶

Estimated Temperature Effects upon Residual Excitation Energies in Methane. The T-for-H substitution reaction in methane is believed to provide a broad distribution of excitation energies for the product molecules, but very little information can be deduced about the distribution for excited CH₃T* from the scant observed pressure dependence. One crude distribution consistent with the experimental observations was postulated to have CH₃T* molecules with equal probabilities for all energies from 0 to 132 kcal/mol.¹⁸ If the effect of temperature on such substitutions were postulated to be a simple increase in average excitation energy of the product molecules by an amount equal to the increase in internal energy of the target prior to the addition reaction, then the average excitation energy of the CH₃T* molecules would be raised by 0.72 kcal/mol—the increase in internal energy for CH₄ between 24° and 125° at constant volume. An upward shift by 0.7 kcal/mol of the (hypothetical) 0–132 kcal/mol equal probability distribution would increase the expected percentage decomposition of CH₃T* by only about 0.5%. The predicted shift in yield ratios with temperature for this (hypothetical) 0.7 kcal/mol increase in energy is illustrated by the dotted line in Figure 2 and is too small to be confirmed or negated by experiments with our present precision.

This flat distribution is very probably not a good simulation of the actual distribution of excitation energies of CH₃T*, since excitation energies below 50 kcal/mol seem quite unlikely in view of their absence in similar experiments concerning the reactions of recoil tritium atoms with methyl isocyanide.^{23,24} However, calculation of the anticipated temperature dependence of other hypothetical distributions of CH₃T* energies ultimately depends only upon those molecules with excitation energies in the 100–110 kcal/mol range for these pressures and temperatures. Molecules with energies <100 kcal/mol have too little excitation en-

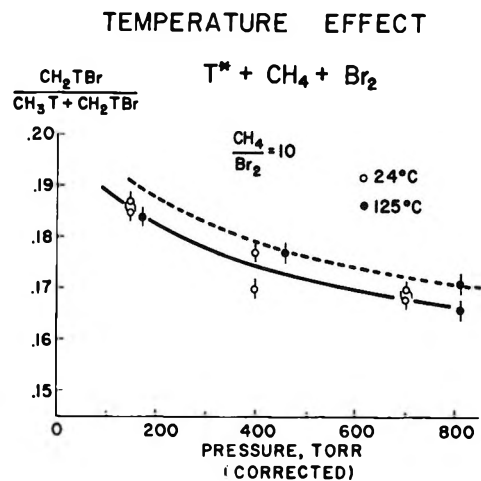


Figure 2. Temperature and collision density variations in relative yields of recoil tritium reactions with Br₂-scavenged methane. Mole ratio: (CH₄:Br₂) = 10:1.

ergy to decompose at all under these conditions, while those with energies >110 kcal/mol undergo complete decomposition even at the highest pressures involved in these experiments. Consequently, all postulated distributions consistent with the observed pressure dependence will give an essentially identical prediction of a very small temperature effect upon CH₃T* decomposition. The narrowness of the band of energies for which either pressure or temperature sensitivity might be detected is a strong contributing factor to the general insensitivity of the reaction yields with CH₄ to variations in these parameters.

The temperature effect on the abstraction of H from CH₄ is 0 ± 1% for the 101° increase from 24° to 125°. However, increases in HT yield have been observed with other alkanes over the same temperature range, and the absence of effect in CH₄ appears to be the less common observation.²⁵ The abstraction of H from CH₄ has an appreciably higher activation energy than that from all other alkanes, and the abstraction reaction is experimentally not observed from CH₄ by H atoms in thermal systems at 24°. The absence of temperature effect on abstraction of H from CH₄ by T* thus

(20) E. K. C. Lee, J. W. Root, and F. S. Rowland, "Chemical Effects of Nuclear Transformations," Vol. 1, International Atomic Energy Agency, Vienna, 1965, p 55.

(21) E. N. Avdonina, D. S. Urch, and G. K. Winter, *Radiochim. Acta*, **12**, 215 (1969).

(22) By correcting to equal collision frequencies, the assumption is implicitly made that the bath molecules remove equal amounts of energy per collision at both 24° and 125°. This assumption is probably not entirely correct, for more energetic molecules may not be quite as efficient sinks for excess energy as the less energetic molecules found at a lower temperature. For the stabilization of very highly excited radicals, however, this difference should be quite small.

(23) C. T. Ting and F. S. Rowland, *J. Phys. Chem.*, **72**, 763 (1968).

(24) C. T. Ting and F. S. Rowland, *ibid.*, **74**, 4080 (1970).

(25) R. Kushner, A. Hosaka, and F. S. Rowland, Abstracts, 158th Meeting of the American Chemical Society, New York, N. Y., Sept 1969.

Table I: Relative Yields from Recoil Tritium Reactions with Unscavenged 1-Butene at 24 and 125°

Irradiation temp, °C	24	125	24	125
	Composition (1-butene)			
³ He, Torr at 24°	10	10	19	19
Tritiated product	Relative yield (1-butene- <i>t</i> = 100)			
HT	132	144	167	199
CH ₃ T	9.2	10.7	10.7	20.0
CH ₂ =CHT	39.3	42.7	54.4	64.2
C ₂ H ₅ T	2.7	2.7	6.9	5.3
CH≡CT	2.0	1.4	2.9	4.4
C ₃ H ₇ T	0.4	0.2	2.5	1.4
Propylene- <i>t</i>	43.7	50.1	74.8	91.0
<i>n</i> -C ₄ H ₉ T	20.7	36.8	22.4	46.8
1-Butene- <i>t</i>	100	100	100	100
CH ₂ =C=CHT	1.1	1.0	n.d.	2.1
<i>trans</i> -2-C ₄ H ₇ T	7.0	5.9	9.1	15.2
<i>i</i> -C ₅ H ₁₁ T	3.8			
<i>cis</i> -2-C ₄ H ₇ T	4.1	3.2	5.4	5.2
<i>n</i> -C ₅ H ₁₁ T	2.2	n.d.	3.7	4.7
3,4-Di(Me)Hexane- <i>t</i> } + 3-(Me)Heptane- <i>t</i> }	16.0	17.0	19.7	19.3

Table II: Relative Yields from Recoil Tritium Reactions with Unscavenged *cis*-2-Butene at 24 and 125°

Irradiation temp, °C	24	125	24	125
	Composition (<i>cis</i> -2-butene)			
³ He, Torr at 24°	10	10	8	8
Tritiated products	Relative yield (Σ 2-butene- <i>t</i> = 100)			
HT	180	173	157	160
CH ₃ T	7.6	8.8	8.0	9.1
CH ₂ =CHT	5.3	5.3	4.0	4.6
C ₂ H ₅ T	1.9	0.8	1.0	1.0
CH≡CT	n.d. ^b	n.d. ^b	2.4	2.7
Propylene- <i>t</i> ^a	92.0	104	64.6	69.2
CH ₂ =C=CHT + MeAc- <i>t</i>	2.6	3.0	1.4	1.6
1-Butene- <i>t</i>	16.3	16.4	16.2	12.0
<i>n</i> -C ₄ H ₉ T	7.8	19.1	23.7	72.2
<i>trans</i> -2-C ₄ H ₇ T	13.8	17.4	14.1	26.3
<i>cis</i> -2-C ₄ H ₇ T	86.1	82.6	85.9	73.7
<i>i</i> -C ₅ H ₁₁ T	7.8	4.2	8.8	2.2
3,4-Dimethylhexane- <i>t</i> } + 3-Methylheptane- <i>t</i> }	6.4	6.8	14.5	5.8

^a Plus traces of C₃H₇T. ^b n.d. = not determined.

appears to be closely related to the relatively high threshold energy for such reactions.

The general lack of temperature effects on T* reactions with CH₄ provides some assurance that the overall chemical handling of hot atom processes and products can be carried out without difficulties at both 24 and 125°, and adds credence to the nonzero temperature effects described below for the reactions of T* with 1-butene and *cis*-2-butene.

Temperature Effects with Olefins. A comparison of the relative yields of all products from T* reactions with unscavenged olefins at 24 and 125° is shown in Tables I and II for 1-butene and *cis*-2-butene, respectively. While the general qualitative pattern of re-

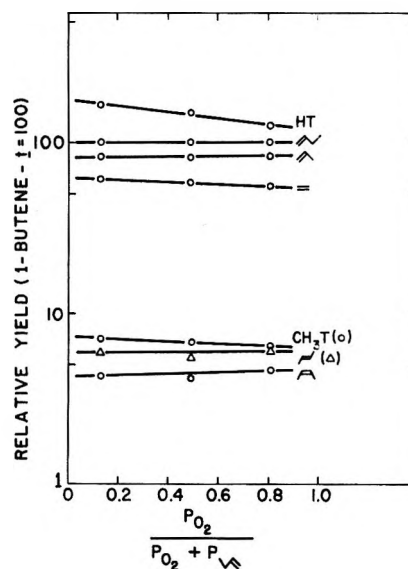


Figure 3. Relative product yields vs. O₂ mole fraction at 125° for recoil tritium reactions with 1-butene. (Yield of 1-C₄H₉T as standard = 100.)

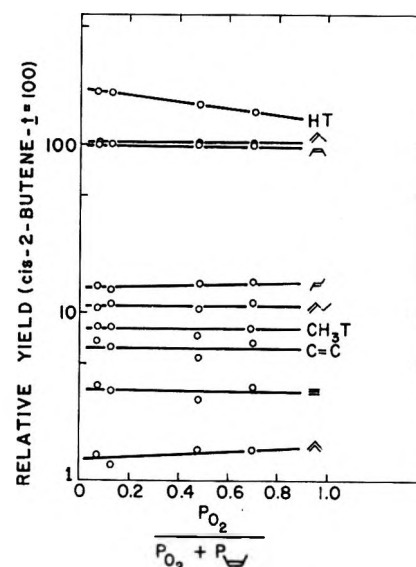


Figure 4. Relative product yields vs. O₂ mole fraction at 125° for recoil tritium reactions with *cis*-2-butene. (Yield of *cis*-2-C₄H₇T as standard = 100.)

sults is very similar at both temperatures, those molecules which involve an abstraction reaction as the final step (*e.g.*, HT, CH₃T, *n*-C₄H₉T) all show increased yields at the higher temperature, consistent with the increased likelihood for abstraction at 125°. The yields of propylene-*t* and ethylene-*t* from 1-butene are also higher—by different fractional increases—as is propylene-*t* from *cis*-2-butene. The *cis*-2-butene results were complicated by the 10–25% macroscopic *cis*-*trans* isomerization of 2-butene observed in the absence of scavenger at 125°. These results of Table II are consequently listed vs. the sum of the yields of *cis*- and *trans*-2-butene-*t* for these samples. Since these

preliminary runs indicated that the products arising from butyl-*t* radical decomposition were increasing at higher temperatures, extensive series of scavenged runs were made with both 1-butene and *cis*-2-butene. In view of the increasing problem of thermally-induced reactions between substrate (or products) and scavenger (e.g., H₂S) at 125° vs. room temperature, molecular oxygen was used as the scavenger in these series. The macroscopic mass peaks measured in these samples indicated that there were no unexpected chemical alterations in the 125° samples. As shown in Figures 3 and 4, the relative yields of all labeled products except HT are rather independent of the mole fraction of O₂ in the system at 125° and a total pressure of one atmosphere. The relative product yields also show a similar independence of O₂ mole fraction at 24°.¹²

A series of experiments were then carried out at both 24° and 125° with the olefin:O₂ ratio held constant at 10. The results are shown in Figures 5 and 6 for the ratio of propylene-*t* to labeled parent molecule, and demonstrate quite clearly that these ratios are temperature-dependent.²⁶ For convenience in comparison, the pressure readings (during sample filling at room temperature) for the 125° samples are displaced by 16% in order to permit comparison of samples with equal collision frequencies during irradiation. The analytical results of five experiments in which the samples were irradiated at 24° and then heated to 125° for 3 hr are included in Figure 5; these samples are experimentally indistinguishable from normally treated samples irradiated at 24°.

The only other labeled product whose relative yield is significant is that of CH₂=CHT from 1-butene. In this case, the difference in ratios for the two temperatures is about at the error limits for these ratio measurements, as shown in Figure 7, and there is no convincing evidence for a real difference in yield ratio with temperature.

The variations in propylene-*t*:butene-*t* yield ratios could indicate variations in either one or both of the absolute yields of the individual products. In the present situation, however, we have neither the precision control of the neutron flux nor the effective monitoring of all labeled products necessary for absolute comparisons. A separate comparison of propylene-*t* and ethylene-*t* yields vs. a different internal standard (HT) demonstrates that a consistent picture can be obtained by assigning the major changes in yield ratios as the consequence of a major change in the absolute yield of propylene-*t*.

Rates of Decomposition vs. Excitation Energy for Butyl Radicals. The butyl radical system has been the subject of both extensive experimentation and detailed RRKM calculations by Rabinovitch and his collaborators.²⁷⁻³⁴ Consequently, theoretical rate constants for decomposition are available over a wide range of excitation energies, and numerous experimental checks

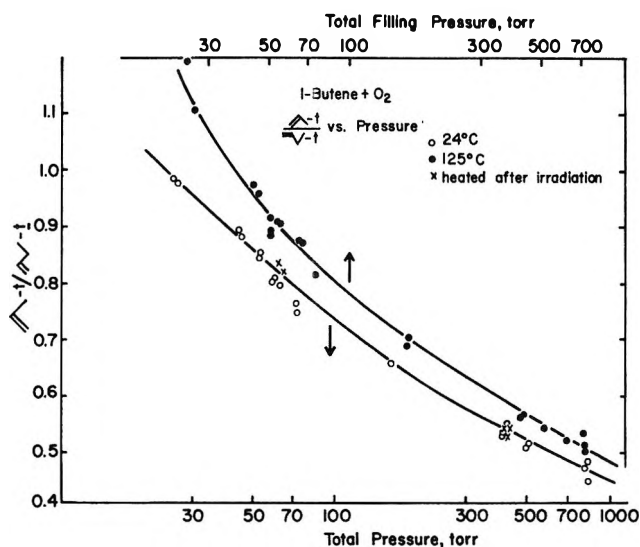


Figure 5. Ratio of experimental yields of CH₂TCH=CH₂/1-butene-*t* vs. collision density for recoil tritium reactions with 1-butene at 24° and 125°. Key: O, irradiated at 24°; X, irradiated at 24° plus post-irradiation heating at 125°; ●, irradiated at 125°. Samples are plotted vs. filling pressure at 24°. Samples irradiated at 125° have been displaced because of 16% higher collision density after heating from 24°.

have been made at the lower energies for various isotopic and isomeric combinations of hydrogen atoms with butane.

Estimates of reasonable magnitudes for temperature dependence of yields can be made from knowledge of excitation energies and the reaction rate constants corresponding to these excitation energies. For *sec*-C₄H₉ radicals formed by thermal H atom addition to *cis*-2-butene at 195°K, the average rate constant for CH₃ loss is about 0.75 × 10⁷ sec⁻¹, equivalent to 50% collisional stabilization at about 0.2 Torr of 2-butene.^{27,30} The additional internal energy present in the substrate at 300°K (about 2 kcal/mol) is sufficient to raise the decomposition rate constant to 1.6 × 10⁷ sec⁻¹. The additional 2.0 kcal/mol added to *cis*-2-butene in heating

(26) The same data are plotted in reference 10 vs. the gas density (i.e., the filling pressure for each sample), and again show a marked temperature difference—visually not quite as large, however, as that displayed by Figures 5 and 6. The actual pressure in the 125° samples at that temperature is of course 34% higher than the filling pressures listed on the figures.

(27) B. S. Rabinovitch and R. W. Diesen, *J. Chem. Phys.*, **30**, 735 (1959).

(28) R. E. Harrington, B. S. Rabinovitch, and R. W. Diesen, *ibid.*, **32**, 1245 (1960).

(29) R. E. Harrington, B. S. Rabinovitch, and M. R. Hoare, *ibid.*, **33**, 744 (1961).

(30) B. S. Rabinovitch, R. F. Kubin, and R. E. Harrington, *ibid.*, **38**, 405 (1963).

(31) G. H. Kohlmaier and B. S. Rabinovitch, *ibid.*, **38**, 1692 (1963).

(32) G. H. Kohlmaier and B. S. Rabinovitch, *ibid.*, **38**, 1709 (1963).

(33) D. W. Placzek, B. S. Rabinovitch, and F. J. Dorer, *ibid.*, **44**, 279 (1966).

(34) G. Z. Whitten and B. S. Rabinovitch, *ibid.*, **38**, 2466 (1963).

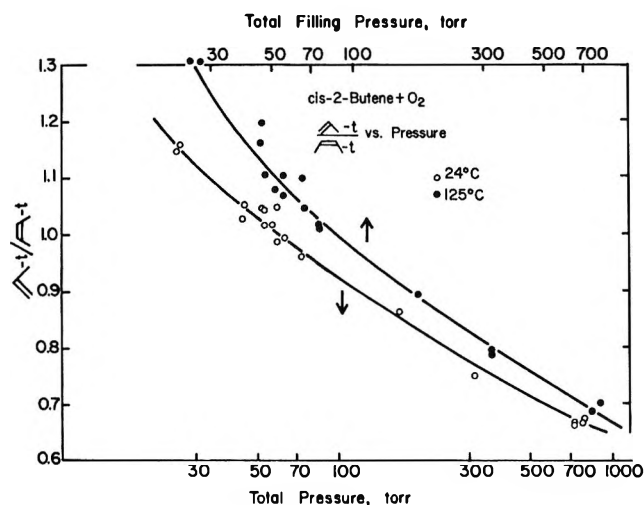


Figure 6. Ratio of experimental yields of $\text{CH}_3\text{CH}=\text{CHT}/\text{cis-2-butene-}t$ vs. collision density for recoil tritium reactions with *cis*-2-butene at 24° and 125°. Key: ○, irradiated at 24°; ●, irradiated at 125°. Samples are plotted vs. filling pressure at 24°. Samples irradiated at 125° have been displaced because of 16% greater collision density after heating from 24°.

it at constant volume from 24° to 125° should add an equal increment to the internal excitation energy of the $\text{CH}_3\text{CHT}\dot{\text{C}}\text{HCH}_3^*$ radical formed by T^* addition to *cis*-2-butene, with a corresponding increase in the rate of CH_3 loss.

The *sec*-butyl-*t* radicals formed by addition of 2.3 eV tritium atoms to butene have at least 100 kcal/mol excitation energy (kinetic energy, 54 kcal/mol; exothermicity, 46 kcal/mol), and an accompanying decomposition rate constant fast enough that >90% of the radicals undergo decomposition in one atmosphere of butene.^{10,12} Consequently, although a higher temperature can increase the internal energy of the substrate molecule and therefore the total excitation energy of the butyl-*t* radical, the temperature change can have little effect on the decomposition vs. stabilization of these 100 kcal/mol radicals, for almost all of them will decompose at this pressure regardless of substrate temperature. On the low end of the energy scale, the butyl radicals formed by low-energy addition (≤ 0.4 eV T^*) are almost entirely collisionally stabilized at 50 Torr or greater, and little temperature effect can be anticipated here, either. The observable temperature effects are thus limited essentially to those *sec*-butyl-*t* radicals formed by addition to butene of 0.4–2.0 eV tritium atoms.

Some typical results of these RRKM calculations are illustrated by the following data, using the "strong" collision assumption for stabilization: a *sec*-butyl-*t* radical from *cis*-2-butene excited by 70 kcal/mol (approximately 1 eV kinetic energy of tritium) will lose CH_3 with a rate constant $k = 4.1 \times 10^9 \text{ sec}^{-1}$, and undergo 21% decomposition at 760 Torr at 24°. Reduction of the pressure to 50 Torr at 24° increases the de-

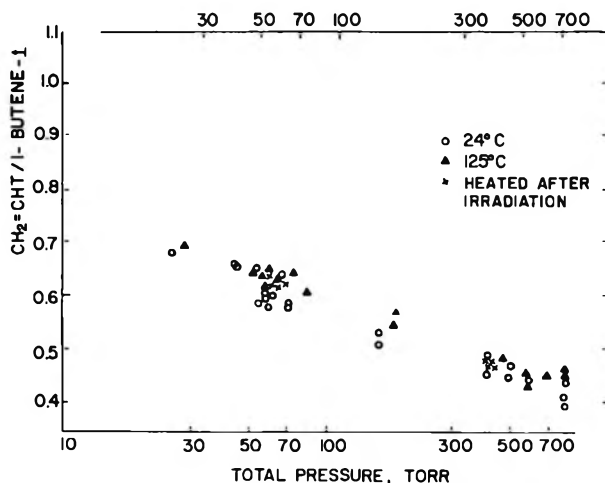


Figure 7. Ratio of experimental yields of $\text{CH}_2=\text{CHT}/1\text{-butene-}t$ vs. collision density for recoil tritium reactions with 1-butene at 24° and 125°. Key: ○, irradiated at 24°; ×, irradiated at 24° plus post-irradiation heating at 125°; ▲, irradiated at 125°. Samples are plotted vs. filling pressure at 24°. Samples irradiated at 125° have been displaced because of 16% greater collision density after heating from 24°.

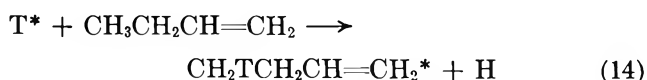
composition of this radical to 80%. With a sample filled to 760 Torr at 24° and then irradiated at 125°, the excitation energy of the corresponding radical is increased by 2.0 kcal/mol from the increased internal energy of the *cis*-2-butene to a total of 72 kcal/mol, and an increased decomposition rate constant of $5.6 \times 10^9 \text{ sec}^{-1}$. At 125°, the actual pressure in the sample bulb is now 1020 Torr, and collisions are 16% more frequent than in the same sample at 24°. Thus, although the rate of collisional deexcitation is 16% faster at 125°, the rate of decomposition is 37% faster and the per cent decomposition has increased from 21% to 24% (a 14% increase in the observed yield of propylene-*t*) over the 101° increase in temperature. In a sample correspondingly filled to 50 Torr at 24° and irradiated at 125°, the per cent decomposition will rise to 83% from the 80% found when irradiated at 24°.

Distributions of Excitation Energies of Butyl Radicals. The observations at 24° of an increase in propylene-*t* yield at low pressure (plus the complementary decrease in stabilized *sec*- $\text{C}_4\text{H}_8\text{T}$, measured as *n*- $\text{C}_4\text{H}_9\text{T}$ in the presence of H_2S) can be rationalized with a broad *sec*- $\text{C}_4\text{H}_8\text{T}^*$ excitation spectrum heavily weighted with low-energy (≤ 0.4 eV) tritium atom addition reactions.¹² The qualitative observation of a temperature dependence in propylene-*t* yield confirms the presence of *sec*-butyl-*t* radicals formed by tritium atom additions in the 0.4–2.5 eV range. The quantitative aspects of both the pressure and temperature dependence of propylene-*t* yields can be consistent only with certain kinds of postulated distributions of *sec*-butyl-*t* energies. The precise details of such distributions are somewhat mechanism dependent, most critically upon the assumptions made in regard to the magnitude of energy loss in "sta-

bilizing" collisions. Nevertheless, the plausible distributions of excitation energies have median initial tritium energies of 0.4–0.6 eV (10–14 kcal/mol), with a "tail" extending with decreasing probability to initial energies >2.5 eV. Some typical distributions have 50% below 0.4 eV, 20% above 3.5 eV, and the remainder distributed between.¹⁴ Median energies of 0.5 eV contrast strikingly with the 5 eV median energy estimated for the substitution of T for H³⁵ or T for D³⁶ in cyclobutane, and with other estimates in the 4–8 eV range for the median energy in other substitution reactions.^{2–4}

The "strong" collision assumption—used as the basis for the illustrative calculations above—is simply that one collision is enough to deexcite any *sec*-butyl-*t* radical, requiring that the radical lose sufficient excitation energy in its first collision with the bath molecules that no further decomposition is possible after that collision. The experiments of Rabinovitch, *et al.*, indicate that the average energy loss for *sec*-C₄H₉ radicals is 12–14 kcal/mol per collision with butene for excitation energies in the 50 kcal/mol range. With energy losses that large, the strong collision assumption is quite a good approximation for our experiments. In particular, while a 15 kcal/mol energy loss, *e.g.*, from 100 kcal/mol to 85, can leave a radical with enough excitation energy to undergo further decomposition reactions, the problem is largely an academic one at 760 Torr for only 9% of the radicals with 100 kcal/mol excitation energy ever make *any* collision before decomposition at this pressure. For the lower excitation energies, the loss of 15 kcal/mol energy in the first collision is almost always sufficient to ensure that decomposition after that collision will be negligible.

*Temperature Dependence of Butene-*t* Yields.* A direct estimate for possible temperature effects on the decomposition of labeled butene-*t* parent as formed by T for H reactions such as (14) is more difficult. However, the fractional decrease in yields measured for *c*-C₄H₇T*



and *c*-C₄D₇T* from T for H in *c*-C₄H₈ and T for D in *c*-C₄D₈, respectively, have been found to be about 0–2% over this same 24–125° temperature range, and are within the experimental error of no difference at all.³⁶ Inferences from hypothetical energy distributions fitted to the measured pressure dependences for the isotopic cyclobutanes suggest a fractional decrease in yield of about 0.02 between 24° and 125° for each of these cyclic molecules. Since the molecules are of comparable complexity, and the decomposition of 1-butene or *cis*-2-butene has a higher activation energy than the iso-

merization of cyclobutane, the temperature effects on butene-*t* decompositions should not be larger than those on cyclobutane-*t* isomerization.

The overall changes in the ratios of propylene-*t*:butene-*t* yields ratios for these olefins can thus be reasonably assigned as a fractional decrease of ≤0.02 in butene-*t* yield, while the major source of variation is the increased formation of propylene-*t* at higher temperatures through increased decomposition of *sec*-butyl-*t* radicals, as in (6) and (7).

Pressure Dependence of CH₂=CHT Yields. The decomposition of CH₃CH₂CHTCH₂* from 1-butene shows much less pressure dependence than for *sec*-butyl-*t* radicals from either butene substrate. Since this implies a smaller fraction of radicals in the pressure-sensitive range (*i.e.*, initial T energies 0.4–2.0 eV), a lesser temperature effect is also expected, and found—as shown in Figure 7. The stabilized *n*-C₄H₉T radical is measured in this system through the same final product, *n*-C₄H₉T, as that obtained from the stabilization of *sec*-butyl-*t* radical,³⁷ and no accurate measure of the total CH₃CH₂CHTCH₂ yield is feasible.

Absence of Temperature Effect upon the Primary Hot Atom Reaction. While the experimental evidence for observable temperature effects in these olefinic systems seems incontrovertible, our explanations have all been implicitly based upon a concept in which the initial primary hot atom reactions are essentially unaffected by the internal energy of the substrate molecule, and are therefore independent of temperature. The yield changes have all been attributed to secondary processes which determine the ultimate fate of the molecular fragment formed in the primary process. The effects of substrate internal energy (and temperature) are thus treated as small but measurable perturbations upon an overall pattern imposed by the mechanistic details of the primary interaction. The general success of this scheme supports this summary—the semiquantitative pattern of recoil tritium reactions with substrate molecules in the gas phase is practically independent of temperature. However, the final, experimentally observed product yields are also dependent upon the particular details of temperature and pressure insofar as collisional stabilization *vs.* secondary reaction of the excited primary products are concerned. When allowance is made for plausible effects upon secondary reactions, no residual temperature differences are left unexplained, suggesting that temperature effects on the hot processes themselves are indeed of minor importance.

(35) E. K. C. Lee and F. S. Rowland, *J. Amer. Chem. Soc.*, **85**, 897 (1963).

(36) A. Hosaka and F. S. Rowland, *J. Phys. Chem.*, **75**, 3781 (1971).

(37) We ignore here the positional isotopic difference between CH₃CH₂CHTCH₃ from *n*-butyl-*t* and CH₃CH₂CH₂CH₂T from *sec*-butyl-*t* in the 1-butene system.

Measurement of Excited Singlet Yields in γ Radiolysis of Benzene and Ketones.

The Radiation-Induced "Type II" Elimination of 4-Methyl-4-phenyl-2-pentanone

by Bizhan M. Zarnegar and David G. Whitten*¹

Department of Chemistry, University of North Carolina, Chapel Hill, North Carolina 27514 (Received May 3, 1971)

Publication costs assisted by the Department of Chemistry, University of North Carolina

A study of the radiolytic "type II" elimination of 4-methyl-4-phenyl-2-pentanone (MPP) is reported. The γ radiolysis of MPP in benzene solution or pure ketone leads to the type II process to yield α -methylstyrene and acetone as the only major decomposition pathway. Previous photochemical studies have shown that the type II process in MPP occurs exclusively from the excited singlet state of the ketone. Quenching studies with biacetyl indicate that all of the radiolytic type II process in benzene solution and possibly 60% in pure MPP arise from the MPP excited singlet. Kinetic analysis reveals that two processes lead to production of singlet MPP in dilute ($<0.1 M$) benzene solutions; one is energy transfer from the benzene lowest excited singlet. A value of $G^{1(B2u)} = 1.4$ is obtained from the concentration dependence of the reaction yield. The origin of the second source of MPP singlets in benzene is uncertain; one possibility is energy transfer from a higher singlet of benzene. The yield of excited singlet MPP in pure ketone is estimated to be $G = 5$, a value considerably higher than the singlet yield in liquid benzene.

Introduction

The role and yield of the lowest excited singlet and triplet in the radiation chemistry of benzene has received considerable attention recently.²⁻⁹ Various methods have been employed to separate and characterize the different species formed in irradiated benzene. Pulse radiolysis studies^{4,7,9} have shown the importance of excited state processes in irradiated benzene. Using nanosecond pulses, Cooper and Thomas⁵ studied the decay of benzene fluorescence and found it to be first order with $t_{1/2} = 18$ nsec. Using biphenyl as anion scavenger, they also found that the yield of ions, both negative and positive, was small ($G \sim 0.1$). Benzene fluorescence observed in a flowing target cell has been shown to be identical under either electron impact or ultraviolet excitation.¹⁰ Energy transfer studies have also demonstrated the formation of excited species in γ -irradiated benzene. Systems which have previously been well-characterized photochemically, such as 2-butene,⁸ stilbene,¹¹ butyrophenone,¹² and 3,5-cycloheptadienone,³ as well as other carbonyl compounds and hydrocarbons, have been shown to behave similarly under ultraviolet excitation and γ radiolysis in liquid benzene.

While the role of excited species in benzene radiation chemistry has been generally accepted, the absolute yields of the lowest excited singlet and triplet states of benzene have been the subject of some controversy as has been the mechanism of excited state production. Early estimates of the singlet yield $G_{(B^*1)}$ from benzene, which were usually based on estimates of luminescence yields of solutes in benzene, ranged from 0.5 to 8.5.^{13,14} More recently values for $G_{(B^*1)}$ have been determined using pulse radiolysis

techniques⁴⁻⁶ and energy transfer from the benzene singlet to solutes having photochemically reactive excited singlets.^{2,3} In two cases where the latter technique has been used, rather different $G_{(B^*1)}$ values were obtained (1.45³ and 3.4²) even though the reactions monitored in the solute acceptor were evidently exclusively excited singlet state processes. Similar discrepancies have been encountered in the use of energy transfer phenomena to measure the triplet yield in γ -irradiated benzene.^{2,4,11,15} At least part of the confusion regarding the relative importance of singlets and triplets in benzene radiolysis seems to

- (1) Alfred P. Sloan Foundation Fellow, 1970-1972.
- (2) G. S. Hammond, R. A. Caldwell, J. M. King, H. Kristinsson, and D. G. Whitten, *Photochem. Photobiol.*, **7**, 695 (1968).
- (3) R. R. Hentz and L. M. Perkey, *J. Phys. Chem.*, **74**, 3047 (1970).
- (4) R. B. Cundall, G. B. Evans, P. A. Griffiths, and J. P. Keene, *ibid.*, **72**, 3871 (1968).
- (5) J. K. Thomas, *J. Chem. Phys.*, **51**, 770 (1969).
- (6) R. Cooper and J. K. Thomas, *ibid.*, **48**, 5097 (1968).
- (7) E. J. Land and A. J. Swallow, *Trans. Faraday Soc.*, **64**, 1247 (1968).
- (8) R. B. Cundall and P. A. Griffiths, *ibid.*, **61**, 1968 (1965).
- (9) F. S. Dainton, G. A. Salmon, T. Morrow, and G. F. Thompson, *Chem. Commun.*, 326 (1968).
- (10) M. L. West and L. L. Nichols, *J. Phys. Chem.*, **74**, 2404 (1970).
- (11) R. A. Caldwell, D. G. Whitten, and G. S. Hammond, *J. Amer. Chem. Soc.*, **88**, 2659 (1966).
- (12) J. N. Pitts, Jr., D. R. Burley, J. C. Mani, and A. D. Broadbent, *ibid.*, **90**, 5902 (1968).
- (13) (a) W. van Dusen, Jr., and W. M. Hamill, *ibid.*, **84**, 3648 (1962); (b) D. B. Peterson, T. Arakawa, D. A. G. Walmsley, and M. Burton, *J. Phys. Chem.*, **69**, 2880 (1965); (c) V. A. Krongauz and I. N. Vasil'ev, *Kinet. Katal.*, **4**, 67 (1963); I. N. Vasil'ev and V. A. Krongauz, *ibid.*, **4**, 204 (1963).
- (14) P. Skarstad, R. Ma, and S. Lipsky, *Mol. Cryst.*, **4**, 3 (1968).
- (15) R. R. Hentz and H. G. Altmiller, *J. Phys. Chem.*, **74**, 2646 (1970).

have its source in the rather unfortunate choice (in retrospect) of stilbene and related olefins as acceptor solutes.^{2,3,11,15,16} It is now well established that these olefins undergo comparable isomerization processes from both excited singlets and triplets¹⁷ (as well as from radical ions in certain cases¹⁸) such that the use of stilbene, which can accept either singlet or triplet excitation from the appropriate excited state of benzene, to measure specifically the triplet yield in benzene is hazardous.^{19,20}

In the present paper we report an investigation of the radiolytic "type II" cleavage of 4-methyl-4-phenyl-2-pentanone (MPP). The photochemistry of this β -phenyl ketone has been previously investigated;²¹ although singlets and triplets are both formed in direct photolysis of MPP, it has been found that only the singlet state is reactive in the type II photoelimination. By a careful kinetic study of the radiolytic type II reaction of MPP in benzene we have been able to show that at least two precursors can generate the excited singlet of MPP in dilute benzene solutions. We obtain a value, $G_{(B^*1)} = 1.4$, in excellent agreement with the values recently obtained by 3,5-cycloheptadienone cleavage³ and terphenyl and biacetyl luminescence studies.^{4,14} Interestingly, studies of the radiolysis of pure MPP suggest that production of the lowest excited singlet in the ketone is considerably more efficient than is production of the lowest ($^1B_{2u}$) excited singlet in benzene.

Experimental Section

Materials. 4-Methyl-4-phenyl-2-pentanone was prepared by the procedure of Hoffman²² and purified (>99.9% by vpc) by preparation, purification, and decomposition of the semicarbazone. Zone-refined benzene (James Hinton and Columbia-Hinton, stated purity 99.99%) was used for the radiolysis experiments. Biacetyl (Aldrich) was distilled before use.

Preparation and Irradiation of Samples. Samples for radiolysis were degassed by three freeze-pump-thaw cycles and sealed in 13-mm diameter Pyrex ampoules. A ^{137}Cs source was used for the radiolysis studies. The γ radiation absorbed dose rate was $ca. 1.1 \times 10^{19}$ eV/(cm³ hr) corrected for the electron density of benzene and MPP. The water-cooled irradiation cavity temperature was $28 \pm 2^\circ$. The Fricke dosimeter ($G = 15.5$) was used to calibrate the source. Irradiations were carried out to very low conversions; both disappearance of MPP (in dilute solutions) and appearance of α -methylstyrene were used to follow the reaction. Analyses were by vpc; an internal standard was added after irradiation, and measurement of relative peak areas gave the amount of product after irradiation when the appropriate detector response correction was made.

Results

γ Radiolysis of benzene solutions of MPP led to the

"type II" elimination to yield α -methylstyrene (MS) and acetone (eq 1) as the only detectable reaction of the ketone on short-term irradiation.

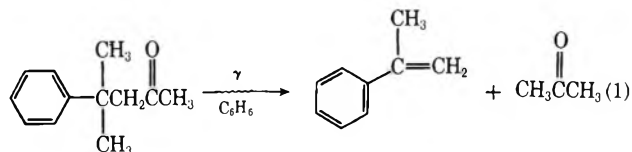


Table I lists values of G_{MS} at various MPP concentrations. Because a dose effect was noticed, probably due to the radiation sensitivity of α -methylstyrene, relatively low doses were used. The average absorbed dose was 6×10^{19} eV/cc of benzene. For doses in this range no dose effect was observed. Figure 1 shows the concentration dependence of G_{MS} .

Table I: Type II Elimination of γ -Irradiated Benzene Solutions of 4-Methyl-4-phenyl-2-pentanone as a Function of Ketone Concentration

[MPP], <i>M</i>	G_{MS}	Precision, %
0.005	0.011	7.1
0.006	0.012	1.2
0.008	0.0147	2.3
0.010	0.015	...
0.020	0.022	2.6
0.040	0.0295	1.1
0.050	0.031	0.6
0.060	0.035	0.5
0.080	0.039	0.7
0.100	0.040	2.2

To determine whether the radiolytic reaction of MPP in benzene was originating from excited singlet states of MPP, studies were made on quenching of the radiolytic type II process by biacetyl. Biacetyl has previously been found to quench excited singlet states of several ketones and hydrocarbons at diffusion-controlled rates.^{23,24} In studies of the photochemistry of MPP it was found that biacetyl quenched the type

(16) R. R. Hentz, D. B. Peterson, S. B. Srivastava, H. F. Barzynski, and M. Burton, *J. Phys. Chem.*, **70**, 2362 (1966).

(17) J. Saltiel and E. D. Megarity, *J. Amer. Chem. Soc.*, **91**, 1265 (1969), and references therein.

(18) R. Chang and C. S. Johnson, Jr., *J. Chem. Phys.*, **46**, 2314 (1967).

(19) Analysis of the effect of azulene on the stilbene radiostationary state in γ -irradiated benzene solutions indicates considerable isomerization occurs *via* nontriplet paths even at concentrations as low as 0.005 *M* stilbene.²⁰

(20) B. M. Zarnegar, unpublished results.

(21) D. G. Whitten and W. E. Punch, *Mol. Photochem.*, **2**, 77 (1970).

(22) A. Hoffman, *J. Amer. Chem. Soc.*, **51**, 2542 (1929).

(23) J. T. Dubois and B. Stevens in "Luminescence of Organic and Inorganic Materials," M. P. Kallman and G. M. Spruch, Ed., Wiley, New York, N. Y., 1962, p 115; J. T. Dubois and J. W. van Loben Sels, *J. Chem. Phys.*, **45**, 1522 (1966).

(24) N. C. Yang and S. P. Elliott, *J. Amer. Chem. Soc.*, **90**, 4194 (1968).

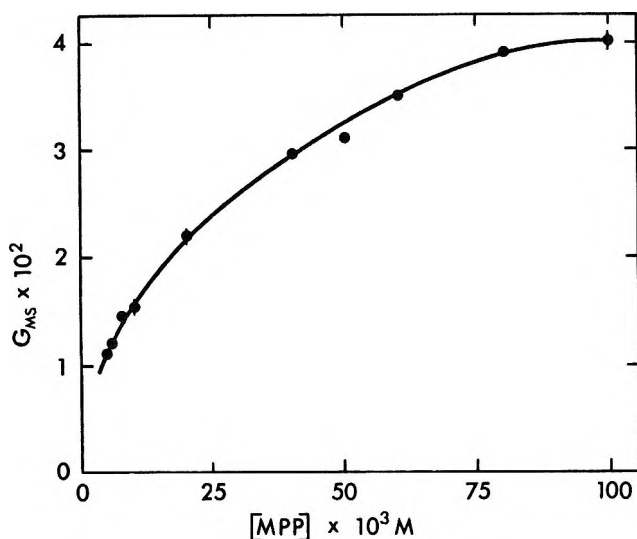


Figure 1. Plot of G_{MS} vs. MPP concentration for γ -irradiated 0.1 M solutions of MPP in benzene.

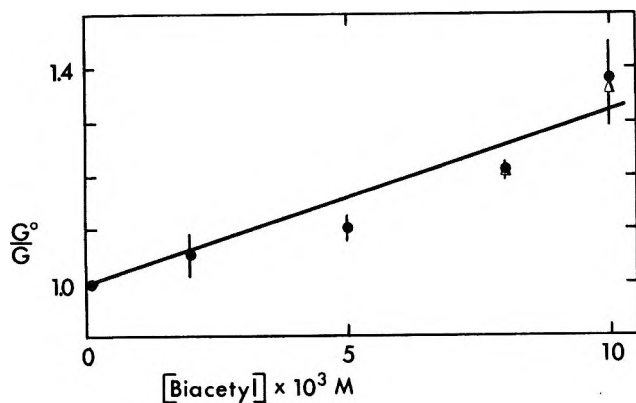


Figure 2. Plot of G_{MS}^0/G_{MS} vs. biacetyl concentration for γ -irradiated 0.1 M solutions of MPP in benzene: ●, experimental points; Δ, experimental points corrected for $[Bi]^2$ terms.

II process such that a linear Stern-Volmer plot of ϕ_{II}^0/ϕ_{II} vs. $[biacetyl]$ gave a slope of $23 M^{-1}$.²¹ Since it has been reported¹⁵ that solute concentrations $<0.1 M$ have little effect on those processes that determine the ultimate yields of the lowest excited states in benzene, it was expected that analysis of biacetyl slopes in the radiolytic type II processes of MPP might demonstrate singlet participation in the radiolysis. The results of the biacetyl quenching experiments with 0.1 M MPP are listed in Table II. Figure 2 gives a "Stern-Volmer" plot of G^0/G vs. $[biacetyl]$. Competition between biacetyl and MPP limits the utility of a similar study at lower MPP concentrations (*vide infra*).

The "type II" process was also found to be the only detectable reaction of MPP in pure ketone solution and in benzene-ketone mixtures where considerable energy is deposited directly in the ketone. The effect of biacetyl on G_{MS} was investigated in pure MPP; as data in Table III and Figure 3 indicate, approxi-

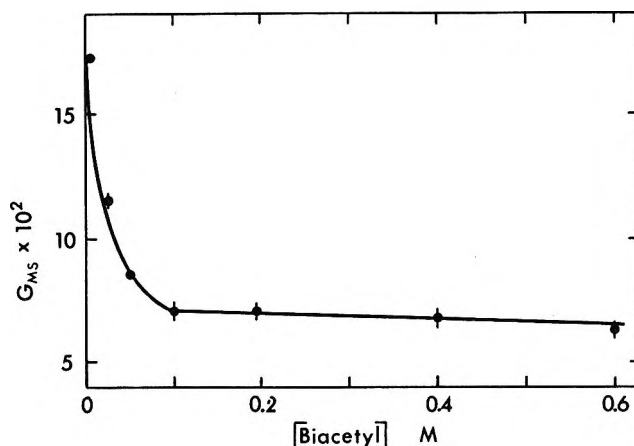


Figure 3. Plot of G_{MS} vs. biacetyl concentration for γ -irradiated 5.5 M (neat) MPP solutions.

Table II: Biacetyl Quenching of the Type II Process of 0.1 M 4-Methyl-4-phenyl-2-pentanone in Benzene

[Biacetyl], M	G_{MS}	Precision, %
0.000	0.040	2.2
0.002	0.038	3.9
0.005	0.036	3.0
0.008	0.033	1.2
0.010	0.029	4.8

mately 60% of the reaction was quenched by biacetyl. The remaining 40% of the reaction is not quenched by biacetyl and must arise from a different precursor than the ketone excited singlet.

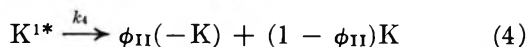
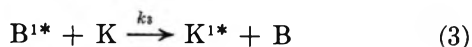
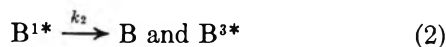
Table III: Biacetyl Quenching of the Type II Process of Neat 4-Methyl-4-phenyl-2-pentanone

[Biacetyl], M	G_{MS}^a	Precision, %
0.00	0.172	0.1
0.025	0.115	2.6
0.05	0.085	1.9
0.10	0.071	4.0
0.20	0.071	4.2
0.40	0.068	1.1
0.60	0.063	5.2

^a Average unquenchable yield from several runs is $G_{MS} = 0.068$.

Discussion

Radiolysis in Benzene Solutions. Previous studies have shown that the photochemical type II process in MPP occurs exclusively from the excited singlet. Assuming the lowest excited singlet of MPP is responsible for the radiolytic type II process in benzene (*vide infra*) we can write the following scheme



where B = benzene and K = MPP. The product yield, G_{MS} , should be related to the yield of MPP excited singlets, $G_{K^{1*}}$, by

$$G_{K^{1*}} = G_{MS}/\phi_{II} \quad (5)$$

where $\phi_{II} = 0.02$, the quantum efficiency for the photochemical type II process for MPP. From eq 1-5 the relationships

$$G_{K^{1*}} = G_{B^{1*}} \left(\frac{k_3[K]}{k_2 + k_3[K]} \right) \quad (6)$$

$$\frac{1}{G_{K^{1*}}} = \frac{1}{G_{B^{1*}}} \left(1 + \frac{k_2}{k_3[K]} \right) \quad (7)$$

can be written which predict a linear relationship between $1/G_{K^{1*}}$ and $1/[K]$ whose intercept should equal $1/G_{B^{1*}}$ and whose slope to intercept ratio should equal $1/k_3\tau_s$, where τ_s is the singlet lifetime of benzene. Figure 4 is a plot of $1/G_{K^{1*}}$ vs. $1/[K]$. The plot is not a

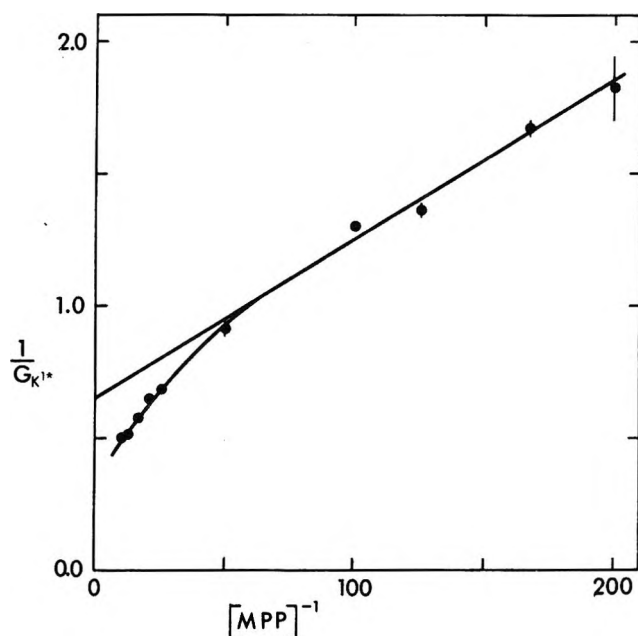
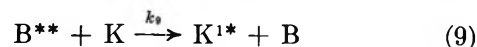
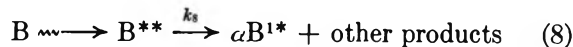


Figure 4. Plot of $1/G_{K^{1*}}$ vs. $[MPP]^{-1}$ for γ -irradiated benzene solutions.

simple straight line; while the low concentration data yield a fairly good plot there is a marked negative deviation at higher concentrations (low $1/[MPP]$ values.) The results suggest that more than one process is producing excited singlets of MPP and the scavenging of the second precursor is more important at high MPP concentrations. A modified kinetic scheme incorporating activation by B^{**} , a species preceding the benzene excited singlet, is given by eq 1-4 plus eq 8 and 9.



(α denotes the fraction of B^{**} that decays to B^{1*} in the absence of quenching such that k_8 is the rate constant for all processes deactivating B^{**} in the absence of quencher and αk_8 is the rate constant for forming B^{1*} .) If benzene singlets are formed by two separate processes eq 1 and 8,²⁵ the total yield of the lowest singlet, $G_{B^{1*}}$, becomes

$$G_{B^{1*}} = G_{B^{1*}} + \alpha G_{B^{**}} \quad (10)$$

From eq 1-10 an expression for the product yield can be derived

$$G_{MS} = G_{B^{1*}} \cdot \phi_{II} \left(\frac{k_3[K]}{k_2 + k_3[K]} \right) + \quad (I)$$

$$G_{B^{**}} \cdot \phi_{II} \left(\frac{k_9[K]}{k_8 + k_9[K]} \right) + \quad (II)$$

$$\alpha G_{B^{**}} \cdot \phi_{II} \left(\frac{k_8}{k_8 - k_9[K]} \right) \left(\frac{k_3[K]}{k_2 + k_3[K]} \right) \quad (11)$$

(III)

Analysis of this relationship at high ketone concentrations is complicated; however, at low ketone concentrations $k_9[K]$ should be sufficiently small to render term II negligible and simplify term III to

$$\alpha G_{B^{**}} \cdot \phi_{II} \frac{k_3[K]}{k_2 + k_3[K]}$$

The linear portion at low concentrations for the reciprocal plot in Figure 4 should have intercept

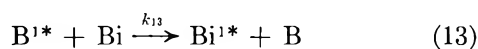
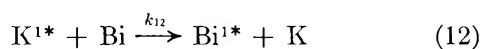
$$\text{intercept} = \frac{1}{G_{B^{1*}} + \alpha G_{B^{**}}}$$

the reciprocal of the total yield of the lowest excited singlet of benzene,²⁵ and an intercept-to-slope ratio of $k_3\tau_s$. This intercept $1/G_{K^{1*}} = 0.714 \pm 0.07$ (least squares) yields $G(^1B_{2u}) = 1.4$. This value is in excellent agreement with the value of 1.45 obtained by Hentz and Perkey³ in the radiolytic cleavage of 3,5-cycloheptadienone. This value also compares well with the values of 1.62 obtained using naphthalene,⁶ 1.43 using biacetyl,⁴ and 1.55 using terphenyl¹⁴ as benzene singlet quenchers. If we assume a lifetime of 27 nsec for benzene,⁶ a value, $k_3 = 5 \times 10^9$ l. mol⁻¹ sec⁻¹, is obtained for quenching of the benzene singlet by MPP.

(25) If benzene singlets were formed by only one process (i.e., all formed via eq 8 or eq 1), the kinetic treatment for the low concentration data would still give the limiting value for the $^1B_{2u}$ state. In principle, analysis of the high concentration data should permit a determination of whether direct production of the $^1B_{2u}$ state is important, but scatter of the results renders this impossible.

The negative deviation of the plot in Figure 4 obtained at high MPP concentrations suggests production of MPP excited singlets *via* a different precursor than the lowest singlet of benzene. The highest value of G_{K1^*} is 2.0 for 0.1 M MPP; the intercept for the high concentration region corresponds to $G_{K1^*}^{max} \simeq 3.3$. Both of these values are substantially higher than the value obtained from the low concentration intercept. Interestingly, the latter value compares closely with the value obtained by Hammond, *et al.*,² in experiments using tetramethyloxetanone as a singlet scavenger.

Analysis of the biacetyl quenching data (Table II and Figure 2) indicates that MPP excited singlets are the precursors of the radiolytic type II elimination. In direct photolysis of MPP biacetyl quenches only excited singlets of MPP (eq 12)



while in the radiolytic experiments biacetyl can also quench benzene singlets (eq 13).²⁶ The photochemical "Stern-Volmer" plot yields a value of $23 M^{-1}$ for k_{12}/k_4 . A comparable treatment for the radiolytic type II process from eq 11-13 yields the relationship

$$\frac{G_{MS}^c}{G_{MS}} = \left[1 + \frac{k_{12}[Bi]}{k_4} \right] \times \left[\frac{A + B(k_3[K]/k')}{A + B(k_3[K]/(k' + k_{13}[Bi]))} \right] \quad (14)$$

where $A = G_{B^{**}}(k_9[K]/(k_8 + k_9[K]))$, $B = G_{B1^*} + \alpha G_{B^{**}}(k_8/(k_8 + k_9[K]))$, $k' = k_2 + k_3[K]$, and $k'' = k_8 + k_9[K]$. An equivalent relationship is

$$\frac{G_{MS}^o}{G_{MS}} = \left[1 + \frac{k_{12}[Bi]}{k_4} \right] \times \left[\frac{C(k' + k_{13}[Bi])}{k'(C + G_{B^{**}}k_9k_{13}[Bi])} \right] \quad (15)$$

where $C = G_{B1^*}k''k_3 + G_{B^{**}}k'k_9 + \alpha G_{B^{**}}k_8k_3$. It can be seen that the first term in eq 14 and 15 is identical with the photochemical Stern-Volmer relationship. From eq 14 it can be seen that the limiting values of the remainder are unity where $A \gg B$ and $(1 + (k_{13}/k')[Bi])$ where $B \gg A$. It is difficult to precisely evaluate A and B (since $G_{B^{**}}$, G_{B1^*} and α are unknown); however, in the equivalent eq 15 it can be shown that Ck' is much larger than $k'G_{B^{**}}k_9k_{13}[Bi]$ at $[Bi] < 0.01 M$ and $[K] = 0.1 M$ such that the latter term in the denominator can be neglected. Accordingly eq 15 can be rewritten (at high $[K]$)

$$\frac{G_{MS}^o}{G_{MS}} = \left[1 + \frac{k_{12}[Bi]}{k_4} \right] \left[1 + \frac{k_{13}[Bi]}{k'} \right] \quad (16)$$

Equation 16 predicts a plot of G^o/G curved concave upwards at higher $[Bi]$; at lower $[Bi]$ the plot should

give a straight line with a limiting slope of $k_{12}/k_4 + k_{13}/k'$. The latter term, k_{13}/k' , can be approximately evaluated as $9.3 M^{-1}$ using $k_{13} = 5 \times 10^9 M^{-1} \text{sec}^{-1}$ ²³ and $k' = 5.4 \times 10^8 \text{sec}^{-1}$. Subtraction of k_{13}/k' from the measured slope of $33 M^{-1}$ (least squares, correlation coefficient 0.97) yields a value of $24 M^{-1}$ for k_{12}/k_4 in good agreement with the photochemical value.

The cause of the increased efficiency of production of singlet ketone at higher ketone concentration is uncertain. As suggested in the kinetic scheme, singlet ketone could be produced by interaction of MPP with a short-lived product of benzene radiolysis, possibly an ion or, perhaps more likely, an upper excited state of benzene. Chemistry from upper excited singlet states of benzene has been observed in previous studies;²⁷ however, the lifetime of this state appears to be too short to permit energy transfer at solute concentrations where the present phenomena are observed. Cooper and Thomas⁶ have attributed differences in the yields of solute triplets produced with anthracene and naphthalene to singlet energy transfer to the solute from a higher benzene singlet which does not decay to the ${}^1B_{2u}$ state; evidently the benzene state responsible has a $t_{1/2}$ of *ca.* 3 nsec and can activate anthracene at low concentrations (0.01-0.001 M).⁶ The role of upper excited singlets of benzene has also been invoked to account for discrepancies in the count of singlet states of benzene obtained with different solutes in recent work by Cundall, *et al.*⁴ Results obtained in the present study provide no evidence as to what the additional short-lived precursor of the solute singlet is; however, they do provide clear evidence that solute excited singlets can be produced in the radiolysis of benzene solutions by means other than energy transfer from the ${}^1B_{2u}$ state.

Radiolysis in Pure Ketone. As previously mentioned, radiolysis of pure MPP leads to the "type II" products by what are evidently two distinct pathways. The portion quenched by biacetyl could be ascribed to singlet MPP; however, a "Stern-Volmer" plot of the "quenchable" portion of the reaction *vs.* $[biacetyl]$ does not yield a straight line and the limiting slope is much higher than the photochemical value. If the quenchable type II process represents reaction due to singlet MPP, comparison of G_{MS} with ϕ_{II} indicates $G_{K1^*} = 5$ in pure MPP, a value considerably higher than the $G = 1.4-1.6$ for production of the ${}^1B_{2u}$ state in benzene. The portion of the reaction not quenchable by biacetyl must involve precursors other than the lowest singlet and triplet of the ketone. One attractive possibility for this reaction is the positive ion of MPP since it has

(26) Presumably biacetyl could also quench B^{**} ; however, inspection of the data in Figure 4 suggests that quenching of B^{**} at comparable concentrations (0.01 M) by MPP is unimportant such that quenching of B^{**} by low concentrations of biacetyl can probably be ignored.

(27) J. K. Foote, M. H. Mallon, and J. N. Pitts, Jr., *J. Amer. Chem. Soc.*, **88**, 3698 (1966); C. I. Braun, S. Kato, and S. Lipsky, *J. Chem. Phys.*, **39**, 1645 (1963); K. Shindo and S. Lipsky, *ibid.*, **45**, 2292 (1966).

previously been shown that MPP undergoes the analogous "McLafferty rearrangement" in the gas phase.²⁸ It is reasonable that biacetyl would not effectively scavenge positive ions of MPP, since the ionization potential of biacetyl (9.25–10.22 eV)²⁹ is higher than that of MPP (<9.2 eV).²⁸

Acknowledgment. We are grateful for support of this work by the University of North Carolina Mate-

rials Research Center in conjunction with the Advanced Projects Research Agency (Contract No. SD-100).

(28) M. M. Bursley, D. G. Whitten, M. T. McCall, W. E. Punch, M. K. Hoffman, and S. A. Benzra, *Org. Mass. Spectrom.*, **4**, 157 (1970).

(29) "Ionization Potentials, Appearance Potentials, and Heats of Formation of Gaseous Positive Ions," NSRDS-NBS 26, U. S. Government Printing Office, Washington, D. C., 1969, p 136.

Pulse Radiolysis of Sodium Metaphosphate Glasses

by Aaron Barkatt,¹ Michael Ottolenghi, and Joseph Rabani*

*Department of Physical Chemistry, The Hebrew University, Jerusalem, Israel
(Received June 1, 1971)*

Publication costs borne completely by The Journal of Physical Chemistry

The effects of ionizing radiation on sodium metaphosphate glasses are investigated using pulse radiolysis techniques. In pure glasses the transient absorbance changes can be described by the consecutive exponential decays of three fractions exhibiting absorption maxima at 6900 Å (fraction I, $\tau_{1/2} = 3.2 \mu\text{sec}$), 5600 Å (fraction II, $\tau_{1/2} = 0.29 \text{ msec}$), and 5200 Å (fraction III, $\tau_{1/2} = 6.3 \text{ msec}$). After all decays a residual permanent absorption at 5000 Å (fraction IV) is left. The effects of doping the glass with various metal cations are analyzed. Characteristic electron scavengers (*e.g.*, Ag^+ , Cd^{2+} , Pb^{2+}) are found to inhibit the formation of fraction I while hole scavengers (Ce^{3+} , Ag^+) prevent the formation of the other fractions. The effects are analyzed and attributed to reactions between the ions and the precursors of fraction I and fractions II–IV, the precursors being identified as very mobile electron-excess (e^-) and electron-deficiency (h^+) centers, respectively. Accordingly, the decaying fraction I is tentatively attributed to solvated electrons (e_1^-) while fractions II–IV are assigned to various electron deficiency (hole) centers (h_{II}^+ , h_{III}^+ , h_{IV}^+). In Ag^+ -doped glasses the very fast primary processes $\text{Ag}^+ + e^- \rightarrow \text{Ag}^0$ and $\text{Ag}^+ + h^+ \rightarrow \text{Ag}^{2+}$ are followed by slower reactions attributed to $\text{Ag}^0 + \text{Ag}^+ \rightarrow \text{Ag}_2^+$ and $h_{IV}^+ + \text{Ag}^+ \rightarrow \text{Ag}^{2+}$. The feasibility of a third process $\text{Ag}_2^+ + \text{Ag}^+ \rightarrow \text{Ag}^{2+} + \text{Ag}_2$ is considered.

Introduction

Extensive work has been carried out dealing with the effects of ionizing radiation on phosphate glasses, either pure or doped with positive ions.^{2–10} In sodium metaphosphate glasses, a permanent optical absorption peaking around 5000 Å is induced by radiation and has been attributed to "positive holes."⁵ A second absorption observed in the uv range was assumed to be due to electrons attached to polyphosphate groups^{5,6} or to free radicals obtained by bond cleavage.^{6–8} The effects of doping the glasses with metal cations, *e.g.*, with salts of Ce^{3+} , Mn^{2+} , Pb^{2+} , Cd^{2+} , were investigated and interpreted in terms of reactions of the corresponding ions with electron deficiency or electron excess centers.^{2–6,9} Thus, ions such as Cd^{2+} , Ag^+ , and Tl^+ are reduced to Cd^+ , Ag^0 , and Tl^0 , respectively, while Ce^{3+} , Ag^+ , and Tl^+ are oxidized to Ce^{4+} , Ag^{2+} , and Tl^{2+} . ESR work provided evidence for the existence of several types of stable electron deficiencies and electron excess centers.^{2–8,10}

A recent application of the pulse radiolysis method to sodium metaphosphate glasses¹¹ led to the detection

- (1) In partial fulfillment of the requirements for a Ph.D. degree.
- (2)(a) For a review see: A. Treinin in "Radical Ions," E. T. Kaiser and L. Kevan, Ed., Interscience, New York, N. Y., 1968, p 525; (b) R. F. Tucker, 6th International Congress on Glass (Technical Papers), Washington, D. C., 1962.
- (3) J. W. H. Schreurs and R. F. Tucker, "Physics of Non-Crystalline Solids," (Proceedings of the International Conference, Delft, Netherlands, 1964), North-Holland Publishing Co., Amsterdam, 1964, p 616.
- (4) J. S. Stroud, J. W. H. Schreurs, and R. F. Tucker, 7th International Congress on Glass, Brussels, 1965, Chapter 42.
- (5) T. Feldmann, A. Treinin, and V. Volterra, *J. Chem. Phys.*, **42**, 3366 (1965).
- (6) T. Feldmann and A. Treinin, *ibid.*, **47**, 2754 (1967).
- (6a) A. Treinin and E. Stern, private communication.
- (7) M. Miura, A. Hasegawa, and T. Fukui, *Bull. Chem. Soc. Jap.*, **39**, 1432 (1966).
- (8) M. Miura and A. Hasegawa, *ibid.*, **40**, 2553 (1967).
- (9) J. H. Schulman, R. J. Ginther, C. C. Klick, R. S. Alger, and R. A. Levy, *J. Appl. Phys.*, **22**, 1479 (1951).
- (10) Y. Nakai, *Bull. Chem. Soc. Jap.*, **38**, 1308 (1965).
- (11) J. Rabani and M. Ottolenghi, *Israel J. Chem.*, **7**, 606 (1969).

of transient absorbance changes around 5800 \AA , exhibiting a decay in the $\sim 10^{-7} < t < \sim 10^{-2}$ sec time range. However, no attempt was made to identify the nature of the species responsible for the new absorptions. The complex kinetic decay was tentatively attributed to nonhomogeneous (spur or cage) effects.

In the present work we have extended our preliminary investigation to longer wavelengths as well as to a broader temperature range, improving also the time resolution of the detection system. The effect of doping the glass with various cations, especially Ag^+ , was systematically investigated. It will be shown that the data shed new light on the fundamental processes induced by ionizing radiation in metaphosphate glasses.

Experimental Section

Preparation of Glasses. Either disks (~ 2.0 mm thick and ~ 22 mm in diameter), or nearly cylindrical rods (~ 17.5 mm long and ~ 5 mm in diameter) were used. $\text{NaH}_2\text{PO}_4 \cdot \text{H}_2\text{O}$ (Mallinckrodt, analytical grade) was heated in platinum crucibles at 700° for 2 hr and occasionally stirred with a platinum rod. The disks were prepared from the melt as described before.¹¹ Rods were prepared by casting into stainless steel forms. The planar surfaces of the rods were polished using silicon carbide abrasive paper followed by aluminum oxide powder.

Pulse Irradiations. Disks were irradiated at a 45° angle between the disk surface and both electron and analyzing beam, the light beam and the electron beam being perpendicular.¹¹ Three passes were usually used when disks were employed. The rods were irradiated so that the electron beam was perpendicular to their long axis, while the analyzing light beam passed along the same axis (one pass). Due to the longer light path in the rods, higher optical densities were observed relatively to those measured in disks made of the same material. An electron beam of 3 Mev and 350 mA (disks) or 5 Mev and 200 mA (rods) was used. The accelerator and optical detection method have been described previously.¹¹ The pulse intensity was monitored by means of the inductance current obtained in a coil surrounding a ferrite ring, at the center of which the electron beam passed. Changes of up to 5% from one pulse to another were measured during 1 day.

A 100-W halogen-tungsten lamp was used for slow (>10 msec) measurements at wavelengths above 4000 \AA . A 150-W Xe lamp was employed for other measurements. Scattered light, checked by means of glass filters, was less than 5% at 2800 \AA , less than 1% at 3000 \AA and above, and 5–15% between 2800 and 2600 \AA . The amount of scattered light depended on the nature of the glass and increased considerably below 3000 \AA when absorbing products were formed and accumulated by repetitive pulsing. All transient absorbance changes were calculated after correcting for

the scattered light. Usually not more than three 1.5- μsec pulses, and never more than six pulses or their equivalents, were used on the same sample.

An RCA IP28 photomultiplier was used for measurements below 6500 \AA . R136 and R196 photomultipliers were used in the range 6500 – $10,000 \text{ \AA}$.

The temperature was $25 \pm 2^\circ$ unless otherwise stated.

Results

Pure Sodium Metaphosphate—Pulse Radiolysis. The transient absorbance changes following a 500-nsec electron pulse (time resolution 750 nsec) are shown in Figure 1. It can be seen that the fraction decaying in the time range between 0.75 and $10 \mu\text{sec}$ (which will be referred to as fraction I) has a peak around 6900 \AA . The fraction decaying in the time range between $20 \mu\text{sec}$ and 2.5 msec (fraction II) exhibits a peak around 5600 \AA , and the small fraction decaying in the range of 2.5–30 msec (fraction III) seems to have a peak around 5200 \AA . However, due to the small change of optical density associated with fraction III, the exact location of the peak at 5200 \AA is doubtful. We cannot therefore exclude the possibility that fraction II and fraction III possess identical spectra.

The spectrum observed 30 msec after the electron pulse is practically identical with the permanent spectrum obtained in X-ray-irradiated sodium metaphosphate (fraction IV). In this respect, we have con-

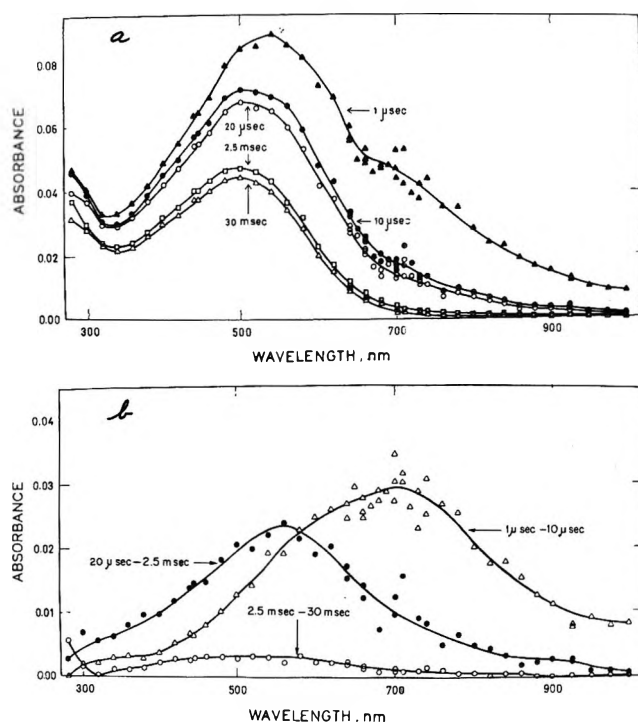


Figure 1. Spectra observed in pure sodium metaphosphate glass; light path, 1.75 cm; 0.5- μsec pulse ($t = 0$ is the beginning of the electron pulse): a, absorption spectra; b, difference spectra.

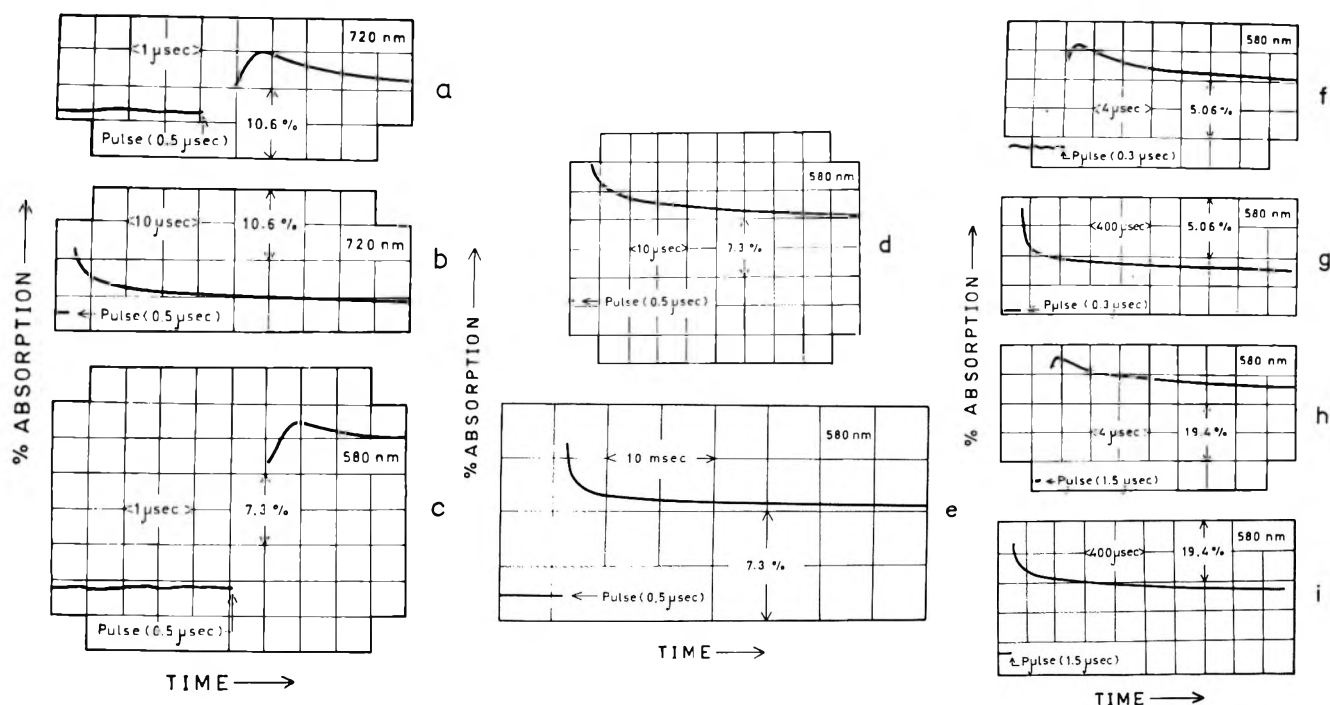


Figure 2. Oscilloscope traces in pure sodium metaphosphate.

firmed previous work which used steady state X-ray irradiation.⁵ (See also Figure 6.) We have not been able to detect any subsequent changes in absorbance between 30 msec and 25 hr.

In Figure 2, we present oscilloscope traces showing the time dependence of the optical density at 5800 and 7000 Å. The decay of the absorption is essentially a set of three distinct exponential decays. Thus, the optical density changes with time are in agreement with the equation

$$D_t/D_i = 1 + \alpha_I \exp(-k_1 t) + \alpha_{II} \exp(-k_2 t) + \alpha_{III} \exp(-k_3 t) \quad (I)$$

where D_t and D_i are the optical densities at time t and $t = 30$ msec (after the completion of all decays), respectively. α_I , α_{II} , α_{III} , k_1 , k_2 , and k_3 are constants, chosen so that the best agreement between the computed lines and the experimental results was obtained. It was found that α_I , α_{II} , and α_{III} are equal approximately to the ratios $(D_{0.75 \mu\text{sec}} - D_{15 \mu\text{sec}})/D_i$, $D_{15 \mu\text{sec}} - D_{2.5 \text{ msec}}/D_i$, and $D_{2.5 \text{ msec}} - D_t/D_i$, respectively. (The time intervals for which the absorbance values are reported fit the various stages of the decay process as determined from a visual observation.) This essentially means that the four fractions I, II, III, and IV are distinguishable both spectrally and kinetically. From computations of 40 traces, the average values $(2.2 \pm 0.4) \times 10^5$, $(2.4 \pm 0.7) \times 10^3$, and $(1.1 \pm 0.2) \times 10^2 \text{ sec}^{-1}$ were obtained for k_1 , k_2 , and k_3 , respectively. Equation I has been tested at various wavelengths in the 5800–7600-Å range. It was found that the numerical values of D_i , α_I , α_{II} , and α_{III} , but

not those of k_1 , are wavelength dependent. Changing the pulse intensity does not affect any of the parameters of eq I, with the exception of D_i , which is proportional to the pulse intensity. The results are demonstrated in Table I, in which both effects of wavelength and intensity are presented. The decay kinetics were found to be independent on whether the sample had been previously pulsed with up to at least 16 pulses.

The decay characteristics at, e.g., 5800 Å were precisely the same as those of the first pulse, up to at least 2 msec, indicating no interaction of the permanent irradiation products with either yields or kinetics corresponding to stages I–IV. This confirms our earlier findings.¹¹

Sodium Metaphosphate Doped with Ag_2SO_4 or AgNO_3 .
 1. *Kinetic effects.* Sodium metaphosphate glasses doped with AgNO_3 or Ag_2SO_4 were exposed to pulse irradiation. All phenomena, i.e., spectral changes and kinetic behavior, were found to be independent of the specific silver salt employed. When exposed to pulse irradiation, Ag^+ -doped glasses exhibit a strong emission in the uv with a lifetime of about 50 μsec. The emission interfered with relatively fast transient absorbance measurements below 3600 Å. Thus in each case, depending on the specific conditions of wavelength and sweep rate, appropriate corrections had to be introduced, accounting for the effect of the emission on the absorbance traces. No fast ($< \sim 40 \mu\text{sec}$) spectral measurements were carried out below 3600 Å where the correction exceeded $\sim 10\%$.

In Figure 3 we present the transient changes in absorbance observed upon pulsing an Ag^+ (added as Ag_2SO_4)-phosphate system. Some characteristic os-

Table I: Test of Eq I at Various Wavelengths and Pulse Intensities

Wavelength nm	Pulse intensity	$D^2 \mu\text{sec}$	D_t	α_I	α_{II}	α_{III}	$k_1 \times 10^{-5}$ sec ⁻¹	$k_2 \times 10^{-3}$ sec ⁻¹	$k_3 \times 10^{-2}$ sec ⁻¹
580 ^a	A	0.133	0.041	0.84	1.21	0.26		1.7	1.3
580	B		0.108		0.97	0.25		3.0	1.2
580	5C	0.193	0.077	0.90	0.71	0.25	2.7	2.8	
580 ^b	5C	0.167	0.056	1.07	1.09	0.25	3.0	2.8	
580	5C	0.196	0.079	0.79	0.77	0.19	2.5	2.6	1.4
580	C	0.041	0.014	0.77	0.99	0.32	2.2	2.3	1.2
580	D	0.103	0.036	1.20			2.8		
580	E	0.087					1.9		
580	E	0.087					2.4		
650	E	0.061					1.8		
700	E	0.033					2.3		
700	E	0.029					2.0		
710	E	0.034					1.6		
730	E	0.020					2.4		
740	E	0.041					2.5		
760	E	0.030					3.0		

^a Measurements made on glass disks (in all other cases, on glass rods). ^b Sixteenth pulse in a series of 16 pulses emitted at a rate of 100 pulses/sec.

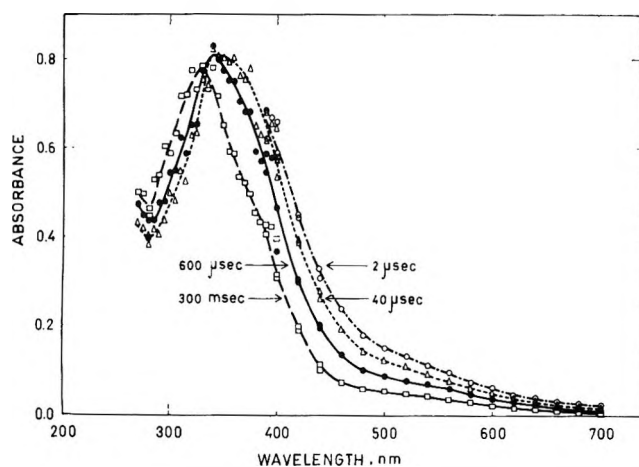


Figure 3. Absorption spectra in 0.117 *m* Ag⁺ (added as Ag₂SO₄); light path, 0.18 cm; 1.5-μsec pulse. The optical density was normalized to the light path and pulse intensity of Figure 1.

cilloscope traces, from which the spectra were derived, are shown in Figure 4. A detailed kinetic analysis of the data was carried out at 3650, 3150, and 2850 Å. Three processes, well separated in time, are observed. The time-dependent changes in absorbance can be represented by three pseudo-first-order reactions fitting the equation

$$D_t/D_a = 1 + \alpha_a \{1 - \exp[-k_a[\text{Ag}^+](t - t_a)]\} + \alpha_b \{1 - \exp[-k_b[\text{Ag}^+](t - t_a)]\} + \alpha_c \{1 - \exp[-k_c[\text{Ag}^+](t - t_a)]\} \quad (\text{II})$$

This equation is essentially analogous to eq I. However, in view of the very long decay times associated with the last process c, the final absorbance after the

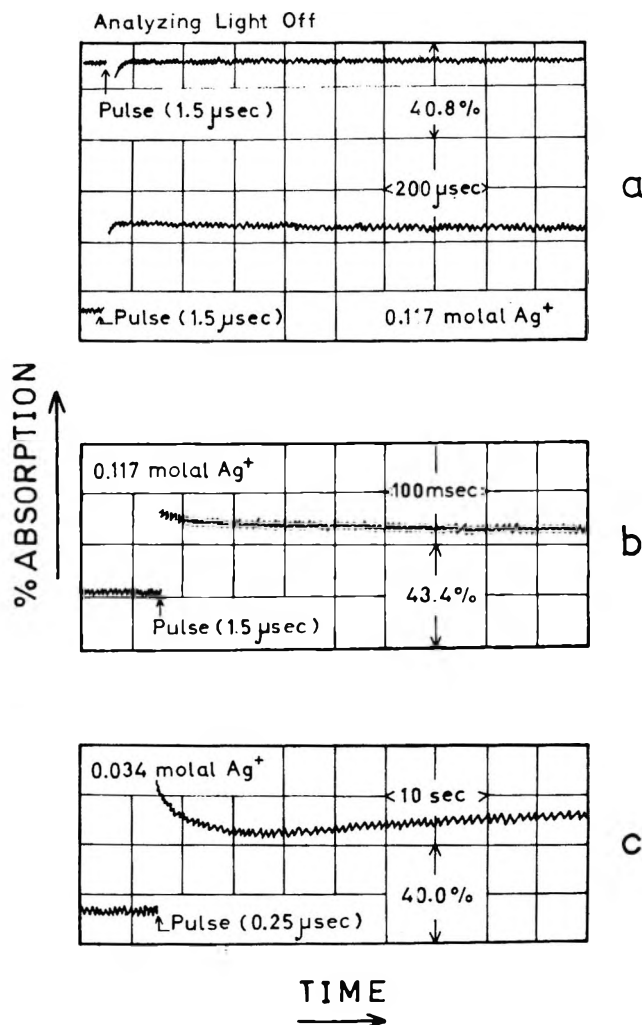


Figure 4. Oscilloscope traces at 365 nm obtained in 0.117 and 0.034 *m* Ag⁺ (added as Ag₂SO₄).

Table II: Test of Eq II at Various Wavelengths and Pulse Intensities

[Ag ⁺] <i>m</i>	Pulse intensity	λ = 365 nm			λ = 315 nm			λ = 285 nm		
		<i>D_a</i>	α	<i>k_{obsd}</i> / [Ag ⁺] <i>M</i> ⁻¹ sec ⁻¹	<i>D_a</i>	α	<i>k_{obsd}</i> / [Ag ⁺] <i>M</i> ⁻¹ sec ⁻¹	<i>D_a</i>	α	<i>k_{obsd}</i> / [Ag ⁺] <i>M</i> ⁻¹ sec ⁻¹
Stage a										
0.003	A	0.032	-0.07	5 × 10 ⁴	0.027	+0.13	5 × 10 ⁴	0.022	+0.10	4 × 10 ⁴
0.013	A	0.099	-0.06	6 × 10 ⁴	0.065	+0.12	3 × 10 ⁴			
0.039	A	0.128	-0.11	5 × 10 ⁴	0.103	+0.14	11 × 10 ⁴	0.064	+0.15	14 × 10 ⁴
0.277	A	0.073	-0.13	4 × 10 ⁴	0.075	+0.12	5 × 10 ⁴			
0.117	B	0.212	-0.08	3 × 10 ⁴	0.177	+0.11	7 × 10 ⁴	0.131	+0.05	4 × 10 ⁴
0.136	D	0.120	-0.13							
0.136	4D	0.335	-0.09							
0.977	D	0.111	-0.05							
0.977	4D	0.342	-0.06							
Stage b										
0.003	A	0.032	-0.23	1.7 × 10 ²						
0.003	5A	0.129	-0.25	1.7 × 10 ²						
0.013	A	0.099	-0.29	0.9 × 10 ²						
0.039	A	0.128	-0.21	0.8 × 10 ²						
0.039	5A	0.491	-0.22	0.7 × 10 ²						
0.277	A	0.073	-0.21	0.6 × 10 ²						
0.277	5A	0.446	-0.25	0.6 × 10 ²						
0.117	B	0.212	-0.24	0.6 × 10 ²	0.177	+0.23	0.9 × 10 ²	0.131	+0.21	0.7 × 10 ²
0.119	C	0.185	-0.28	1.0 × 10 ²						
0.136	D	0.120	-0.29	0.9 × 10 ²						
0.136	4D	0.335	-0.28	0.9 × 10 ²						
0.977	D	0.111	-0.18	1.4 × 10 ²						
0.977	4D	0.342	-0.19	1.4 × 10 ²						
Stage c										
0.039	A				0.103	+0.06	5	0.064	+0.08	6
0.039	5A					+0.06	6			
0.277	A	0.073	+0.02	5	0.075	+0.03	6			
0.277	5A	0.446	+0.02	4		+0.04	8			
0.136	D	0.120	+0.03							
0.034 ^a	E	0.314	+0.08	3	0.286	+0.02	3	0.221	+0.10	3

^a Under the same conditions a decay has been observed at 500 nm with a rate constant $k_{\text{obsd}}/[\text{Ab}^+] = 3 \text{ M}^{-1} \text{ sec}^{-1}$.

completion of all decays (D_i) is not easily determined in the present case. Thus, as reference we have chosen the time, t_a , by which the first stage (a) is essentially completed (five half-lives). The corresponding absorbance value is D_a . The values $k_a = (5 \pm 1) \times 10^4$, $k_b = 90 \pm 20$, and $k_c = 5 \pm 1 \text{ m}^{-1} \text{ sec}^{-1}$ were obtained independently of wavelength or pulse intensity. The relatively low accuracy in these values is due to the small absorbance changes associated with the corresponding processes. The latter are reflected by the values of α as shown in Table II. Both values and signs of α_a , α_b , and α_c are wavelength dependent. Explicitly, α_a is negative above 340 nm, representing a decay, and positive below this wavelength showing a matching growing-in in this lower wavelength region. α_b is negative above 330 nm and positive below this wavelength. α_c is positive in the uv and positive in the visible below 460 nm. As shown in Figure 5 and Table III, these last data represent a decay of a band around 500 nm with a matching growing-in of an ultra-

Table III: Rate Constants for the Decay of the Permanent Absorption (species h_{IV}^+) at 580 nm in the Presence of Ag⁺

[Ag ⁺] <i>m</i>	<i>k_{obsd}</i> sec ⁻¹	<i>k_{obsd}</i> /[Ag ⁺] <i>m</i> ⁻¹ sec ⁻¹
0.003	0.016	5.3
0.006	0.026	4.3
0.014	0.037	2.6
0.029	0.11	3.8
0.030	0.10	3.0
0.064	0.31	4.8
0.120	0.55	4.6

violet absorption. The detailed kinetic data are presented in Table II. All α values were found independent of pulse intensity. Attention should finally be paid to the relatively large scatter in the values of α as shown in Table II. It is not impossible that they actually exhibit a small dependence on [Ag⁺].

The final spectrum, obtained after the completion of

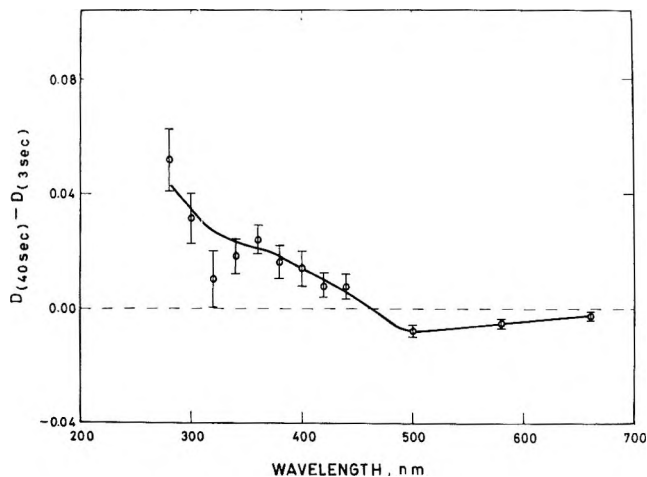


Figure 5. The difference spectrum $D^{40 \text{ sec}} = D^{3 \text{ sec}}$ in 0.034 m Ag^+ (added as Ag_2SO_4); light path, 1.75 cm; 0.25- μsec pulse. The optical density was normalized to the pulse intensity of Figure 1.

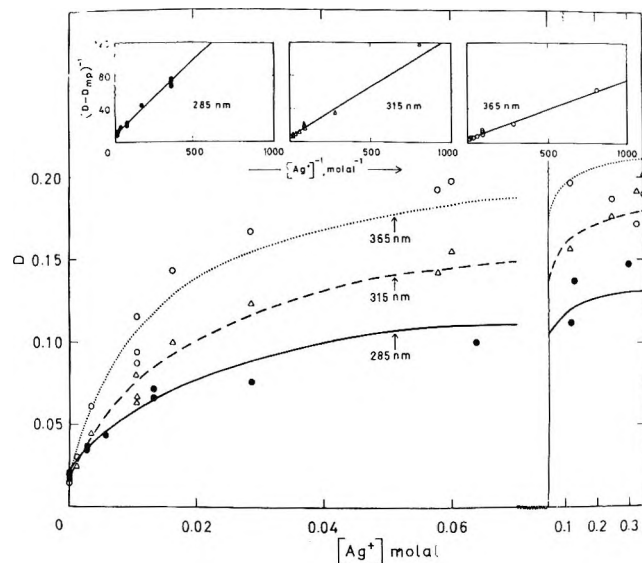


Figure 7. Analysis of the effects of Ag^+ in the uv according to eq III.

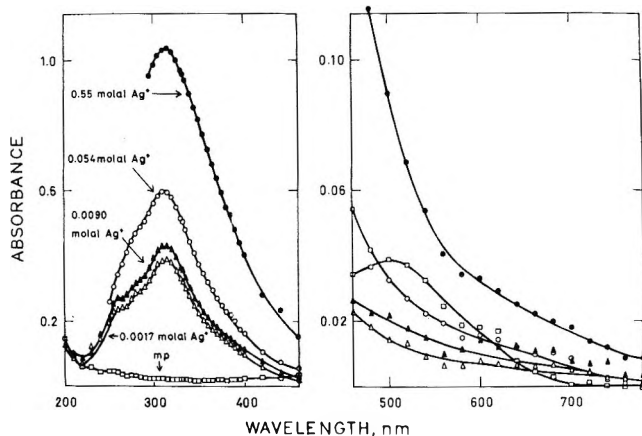


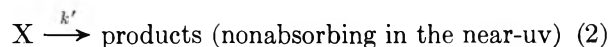
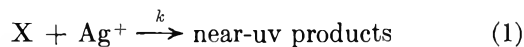
Figure 6. Absorption spectra in pure sodium metaphosphate and Ag^+ (added as Ag_2SO_4) doped glasses 25 hr after X-ray irradiation; light path, 0.18 cm; total dose, 4000 rads; dose rate, 2000 rads/min. The optical density was normalized to the light path and dose rate of Figure 1.

all transient phenomena, is best obtained by measurements carried out many hours after irradiation. The results recorded 25 hr after steady-state irradiation with X-rays are shown in Figure 6. They consist of an absorption peak at 3120 Å, and of a shoulder around 2600 Å.

As mentioned above, Ag^+ affects the stability of the permanent absorption at 5000 Å (fraction IV). However, Ag^+ does not exhibit any significant effect on the decay kinetics of fractions II and III in the visible range of the spectrum.

2. *Effects of $[\text{Ag}^+]$ on the Yields of Irradiation Products.* The effect of $[\text{Ag}^+]$ on the absorbance changes in the uv, measured 250 μsec after pulsing, is shown in Figure 7 for the three characteristic wavelengths, 2850, 3150, and 3650 Å. Attributing the rise in the absor-

ance change with $[\text{Ag}^+]$ to the simple competition scheme



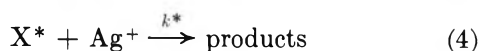
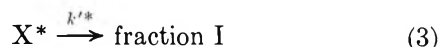
where X is a primary irradiation product, one expects the fulfillment of the equation

$$1/(D - D_{mp}) = 1/(D_p - D_{mp}) + \frac{K_I}{\{(D_p - D_{mp})[\text{Ag}^+]\}} \quad (\text{III})$$

where D is the optical density change measured at the respective Ag^+ concentration and D_{mp} is the initial change in absorbance observed at the same wavelength in the absence of Ag^+ . D_p is the maximum absorbance change (when D reaches a plateau) and $K_I = k'/k$. As shown in Figure 7 a plot of $1/(D - D_{mp})$ vs. $1/[\text{Ag}^+]$ does actually yield a straight line leading to the values: 0.020 ± 0.002 , 0.021 ± 0.002 , and 0.017 ± 0.002 m for K_I at 2850, 3150, and 3650 Å, respectively. From the slopes and intercepts of the same plots the value of D_p was derived and employed in the calculation of D as a function of $[\text{Ag}^+]$ according to eq III. The agreement between the computed curves and the experimental data confirms the simple kinetic scheme 1-2. It should be pointed out that due to the interfering emission, the above results have been obtained with absorbance measurements carried out 250 μsec after the pulse. Only at 3650 Å was it possible to obtain corresponding data at shorter time ranges (~ 10 μsec) which yielded an identical value for K_I . Measurements at 3150 and 2850 Å, 50 msec after pulsing, led again to the same results within $\sim 10\%$. We conclude that the value of K_I is essentially independent of wavelength in the uv range. The observation that K_I is the same for measurements made 250 μsec and those made

50 msec after pulsing is reasonable, noting that the process associated with stage a is essentially completed after 50 msec for all $[\text{Ag}^+]$ values, but practically no absorbance changes associated with stages b and c have taken place. Similar experiments at liquid nitrogen temperature yielded K_I values of (0.018 ± 0.005) , (0.014 ± 0.005) , and (0.024 ± 0.005) molal at 2850, 3150, and 3650 Å, respectively, in agreement with the results obtained at room temperature.

We turn now to a consideration of the effects of $[\text{Ag}^+]$ on the yields of the various fractions in the visible range. It has been mentioned above that Ag^+ has no effect on the decay kinetics of fraction I. However, Ag^+ was found to decrease markedly the yields of this fraction. Again a simple competition scheme such as



will be assumed, leading to the expression

$$1/D = \{[\text{Ag}^+]/K_I^*D_{mp}\} + 1/D_{mp} \quad (\text{IV})$$

where D_{mp} is the absorbance assigned to fraction I in pure metaphosphate. D is the absorbance due to the same fraction in the presence of Ag^+ , and $K_I^* = k^*/k^*$. A curve of D vs. $[\text{Ag}^+]$, computed by means of eq IV using $K_I^* = 0.018 \pm 0.004 m$, is compared in Figure 8 with the experimental points. It should be pointed out that within the limits of our experimental accuracy $K_I^* = K_I$.

A similar analysis was carried out for fraction II, which was also found to be suppressed by the addition of Ag^+ . Here, the value of the corresponding competition parameter, $K_{II}^* = 0.11 \pm 0.02 m$, is much larger than K_I^* (or K_I). The efficiency of Ag^+ in reducing the yields of fractions III and IV is of the same order of magnitude as that measured for fraction II (Table III). However, the accuracy of the experimental data in these cases does not allow a quantitative treatment as carried out for fractions I and II. This is due to the very small absorbance changes associated with fraction III and with the slow pseudo-first-order reaction (in $[\text{Ag}^+]$) undergone by fraction IV which prevents exact determination of its yields in the presence of Ag^+ .

Effects of Doping with Other Cations. 1. Pulse Radiolysis. The effects of various cations on the yields of fractions I to IV in the visible range, analyzed according to eq IV, are presented in Table IV. Excluding the previously described effect of Ag^+ on fraction IV, we have not observed any cation effect on the decay kinetics of the various fractions. It can be concluded that the amount of fraction I is strongly affected by Ag^+ , Cd^{2+} , and Pb^{2+} , and to a lower extent by Nd^{3+} . No effect of doping with Ce^{3+} is observed. The yield of fraction II is markedly influenced by Ce^{3+} and Ag^+ . Cd^{2+} and Pb^{2+} exhibit a smaller effect while Nd^{3+} has no effect on this fraction. The yield of the permanent

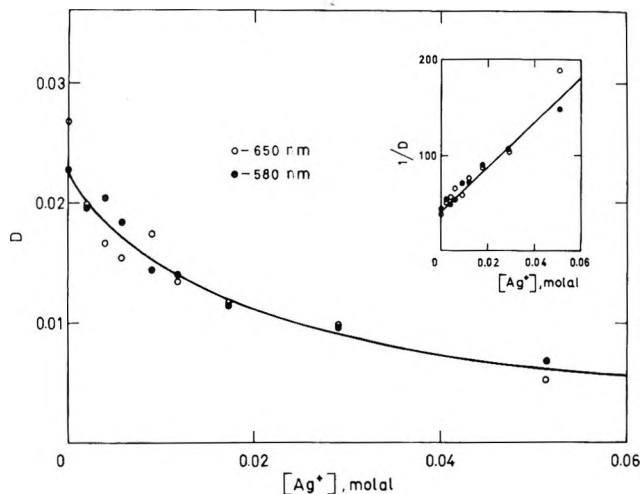


Figure 8. Analysis of the effects of Ag^+ in the visible range according to eq IV.

absorption (fraction IV) is reduced in the presence of Ag^+ or Ce^{3+} but not by Cd^{2+} or Pb^{2+} . In this respect, the general effects are in keeping with previous investigations using steady-state radiolysis.^{5,6}

Table IV: The Effect of Various Cations on the Decaying Fractions I and II and on the "Permanent" Absorption at 580 nm (Fraction IV)

Added cation	Compound	K_I^* M	K_{II}^* M	K_{IV}^* M	K_I M
Ag^+	Ag_2SO_4 , AgNO_3	0.018	0.11		0.019
Cd^{2+}	$3\text{CdSO}_4 \cdot 8\text{H}_2\text{O}$	0.024	>0.5	>0.5	0.028 ^a
Pb^{2+}	PbCO_3	0.026	0.15	>0.5	
Nd^{3+}	Nd_2O_3	0.089	>1		
Ce^{3+}	$\text{Ce}_2(\text{SO}_4)_3$	>1	0.11	0.08	

^a Calculated from the results included in Figure 5 of ref 11.

2. Steady-State X-Ray Irradiation. In Figure 9 we present absorption spectra following X-ray irradiation of metaphosphate glasses prepared with 0.38 m PbCO_3 in the presence and in the absence of 0.0017 m Ag^+ . The results show that the relatively small amount of Ag^+ (0.0017 m) has a large effect in increasing the uv absorption. Under the conditions of these experiments fraction I is totally eliminated by the action of Pb^{2+} present in a large excess (see Table IV for the relative efficiencies of Pb^{2+} and Ag^+ on this fraction). Since 0.0017 m Ag^+ is not sufficient to scavenge the precursors of fractions II, III, and IV, the effect of Ag^+ in increasing the uv absorption should be attributed to the slow reaction between Ag^+ and the permanent 5000-Å band (fraction IV).

Discussion

Stable and Transient Species in the Pure Phosphate Glass. We turn now to the identification of the various

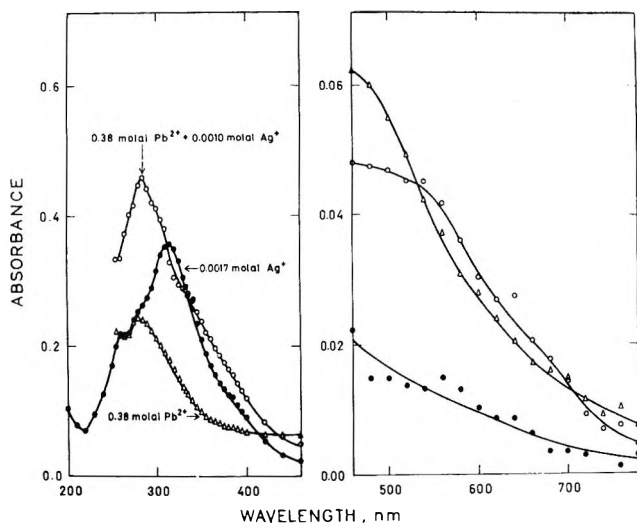
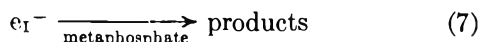
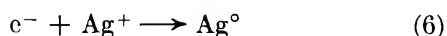


Figure 9. Absorption spectra in Pb^{2+} (added as PbCO_3) doped glasses in the presence and in the absence of Ag^+ ; light path, 0.18 cm; total dose, 4000 rads; dose rate, 2000 rads/min. The optical density was normalized to the light path and dose rate of Figure 1.

species observed in the pulse radiolysis of pure sodium metaphosphate.

Our experimental results indicate that the formation of fraction I, exhibiting the fast decay around 6900 Å, is inhibited by doping the glass with specific electron scavengers such as Ag^+ , Cd^{2+} , Pb^{2+} , and to some extent Nd^{3+} . The results can be interpreted in terms of a reaction such as (4) between the inhibitor and a precursor X^* of the species responsible for fraction I. This has been quantitatively demonstrated in the case of silver ions where the effect of $[\text{Ag}^+]$ on the yields of fraction I was analyzed according to reactions 3 and 4 (eq IV). As shown later in this work the initial absorbance changes in the uv are mainly due to the reduced Ag° form. Our observation that $K_I = K_I^*$ strongly suggests that the reaction of the precursor of fraction I with Ag^+ is responsible for the initial changes in absorbance in the uv. In other words, reaction 1 seems to be identical with (4) while (2) is identical with (3), implying of course the identity of X and X^* as well as that between k and k^* and between k' and k'^* . A similar analysis has been carried out in the case of Cd^{2+} , showing that the effect of $[\text{Cd}^{2+}]$ on fraction I ($K_I^* = 0.024 m$, see Table IV) is compared with the formation of an absorbance at 2900 Å due to Cd^+ , $K_I = 0.028 m$.¹¹ All these observations lead (*e.g.*, in the case of Ag^+) to the scheme



Explicitly, an extremely mobile electron species e^- can either react with an electron scavenger or decay expo-

entially to form fraction I denoted by e_1^- . A rough estimate of the high mobility of e^- can be derived from the comparison of the fast rate of its reaction with, *e.g.*, $\sim 0.1 m \text{ Ag}^+$ or Cd^+ (for which we have established the upper limit) $\tau_{1/2} < 5 \times 10^{-8} \text{ sec}$ with that of a presumably diffusion-controlled reaction such as $\text{Ag}^\circ + \text{Ag}^+ \rightarrow \text{Ag}_2^+$ which takes place in the millisecond range (see below). Thus the mobility of e^- is higher by a factor of at least 10^4 relative to that of species such as Ag^+ or Ag° . This argument is further supported by the observation that the limit $\tau_{1/2} < 5 \times 10^{-8} \text{ sec}$ for the trapping of e^- by Ag^+ is maintained even at 85°K.

The question arises as to the nature of e_1^- , exhibiting the 6900-Å band (fraction I). The fact that its precursor is a very mobile electron species and its unimolecular reaction with the medium both strongly suggest that we are observing a delocalized solvated electron, e_{sol}^- . In such a case reaction 5 is essentially a process of trapping by solvation. As to the product of reaction 7, we may suggest radicals resulting from electron capture. Such radicals have been suggested by Miura and Hasegawa to account for radiation-induced paramagnetic centers in polyphosphate glasses.^{7,8} Trapped electron species have been associated with the uv absorption around 2000 Å induced by irradiation in the pure phosphate glass.^{5,6} Unfortunately we have not been able to provide direct support favoring or contradicting this hypothesis. This is due to the fact that all additives employed to scavenge e^- form reducing species in the uv with an unknown contribution around 2000 Å. Also, we cannot tell at present if the 2000 Å species is formed from e_1^- via reaction 7.

Fractions II and III do not seem to represent species formed from electrons. The amount of fraction II is affected by Ag^+ and Pb^{2+} , but higher concentrations are needed (5–30-fold) relative to those required to suppress fraction I. Ce^{3+} , known as a positive hole scavenger,^{6,12} prevents the formation of fraction II but not of fraction I. The results concerning fraction III are not as quantitative, due to the small associated optical density changes. However, Ag^+ has a comparable effect on fractions II and III. These observations seem to suggest the assignment of these two fractions to positive centers, h_{II}^+ and h_{III}^+ . As in the case of the negative species e_1^- , the effects of cations on the yields of h_{II}^+ and h_{III}^+ can be interpreted in terms of reactions with a very mobile hole h^+ . Again the high mobility of h^+ is shown by its very fast reaction, $\tau_{1/2} < 10^{-7} \text{ sec}$, with, *e.g.*, Ce^{3+} .¹¹

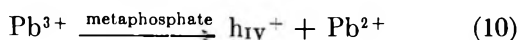
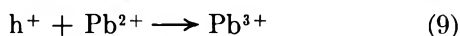
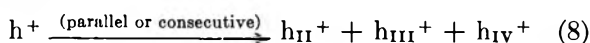
The yield of the permanent absorption (*i.e.*, fraction IV) is reduced by Ag^+ and Ce^{3+} but is practically unaffected by Cd^{2+} and Pb^{2+} . This supports the identification of Feldmann and Treinin,^{5,6} attributing it to a positive center, which we shall denote by h_{IV}^+ .

Two questions arise when attempting to formulate a

(12) J. S. Stroud, *J. Chem. Phys.*, **37**, 836 (1962).

reaction scheme for the various positive centers as was previously done for the negative ones. (a) Is h^+ a common precursor to h_{II}^+ , h_{III}^+ , and h_{IV}^+ ? (b) Is h_{II}^+ a precursor of h_{III}^+ or h_{IV}^+ , and h_{III}^+ of h_{IV}^+ ?

We have previously pointed out that within the limits of our experimental accuracy Ag^+ inhibits to the same extent the formation of all three centers h_{II}^+ , h_{III}^+ , and h_{IV}^+ . This is to be expected if all three species are formed from the same precursor h^+ . However, it is not possible to answer the second question, *i.e.*, to discriminate between a parallel formation of h_{II}^+ , h_{III}^+ , and h_{IV}^+ from h^+ , and a consecutive scheme, such as $h^+ \rightarrow h_{II}^+ \rightarrow h_{III}^+ \rightarrow h_{IV}^+$. These considerations are somewhat modified by the fact that Pb^{2+} was found to inhibit the formation of h_{II}^+ but not of h_{IV}^+ . This may imply that h_{II}^+ and h_{IV}^+ have different precursors (*e.g.*, excited states *vs.* mobile holes). Alternatively, one may still write down a scheme with h^+ as a common precursor

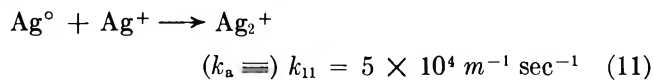


in which Pb^{2+} will inhibit the direct formation of all centers from h^+ but will yield h_{IV}^+ in a secondary stage.

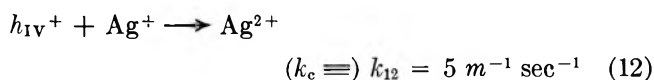
As discussed above, the transient kinetics in the pure metaphosphate glass can be accounted for by a set of three consecutive first-order processes. It is therefore unnecessary to invoke nonhomogeneous kinetic effects as was done previously in the absence of sufficient time resolution and sufficient spectral discrimination between the various decaying fractions.¹¹

Reaction Mechanism in the Ag^+ System. As previously discussed the primary effects of Ag^+ are attributed to the reaction with the mobile electron e^- , forming Ag^0 at the expense of fraction I. At higher $[Ag^+]$ an additional reaction with mobile holes presumably leads to Ag^{2+} , inhibiting the formation of fractions II, III, and IV. The very good agreement of our experimental results with eq III, yielding the same value of K_I at the three wavelengths 2850, 3150, and 3650 Å, means that the major fraction of the initial uv absorption in the presence of Ag^+ is exclusively due to Ag^0 . In view of the smaller efficiency of the reaction between h^+ and Ag^+ , Ag^{2+} is not supposed to contribute at relatively low Ag^+ values. One would expect however a considerable fraction ($\sim 50\%$) of the maximum obtainable Ag^{2+} amount to be present at high $[Ag^+]$, when the scavenging of e^- reaches a plateau (*i.e.*, when $D = D_p$). The fact that the fit with eq III at 2850 and 3150 Å is less satisfactory at high $[Ag^+]$ (see Figure 7) can be interpreted in terms of a small contribution (15–25%) of Ag^{2+} to the absorbance in this $[Ag^+]$ range. This is supported by Figure 5 and by the spectrum of Ag^{2+} obtained in aqueous solutions *via* the reaction of Ag^+ with OH radicals.¹³

We now turn to a discussion of the three kinetic stages, pseudo-first order in $[Ag^+]$, corresponding to fractions α_a , α_b , and α_c in eq II. There is little doubt that stage a should be attributed to the process



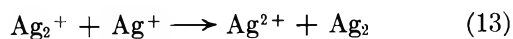
This has been suggested by Pukies, Roebke, and Henglein,¹³ on the basis of kinetic salt effects, to account for practically identical spectral changes in the pulse radiolysis of aqueous Ag^+ solutions. In water, reaction 11 is essentially a diffusion-controlled process ($k = 9 \times 10^9 \text{ M}^{-1} \text{ sec}^{-1}$ ¹³). Assuming that the same is true in the glass, then the value $k_{11} = 5 \times 10^4 \text{ M}^{-1} \text{ sec}^{-1}$ may serve as a measure of the rate of a diffusion-controlled reaction in sodium metaphosphate glasses. Stage c, involving a reaction between Ag^+ and the permanent 5000 Å positive product, can be written as



The decay of the 5000 Å absorbance due to h_{IV}^+ is in fact accompanied by the generation of a uv band (Figure 5) which closely resembles that of Ag^{2+} obtained in aqueous solutions.¹³ These arguments are further supported by the results of steady-state X-ray irradiation in the presence of Pb^{2+} (Figure 8). It can be seen that small amounts of Ag^+ cause a strong increase in the optical absorption observed in a Pb^{2+} -doped glass. Under the experimental conditions of Figure 7 neither fraction I nor fraction II is affected by Ag^+ . The precursors of these fractions react with Pb^{2+} only. Although no quantitative experimental data are available, it is reasonable to assume that fraction III was also unaffected by the small amount of Ag^+ ions present. We may thus conclude that the increase in the optical absorption upon addition of Ag^+ to Pb^{2+} -doped glasses (Figure 9) is solely due to Ag^{2+} , produced by reaction 12. Again a satisfactory agreement with the spectrum of Ag^{2+} both in water¹³ and in metaphosphate (Figure 5) is observed. From Table II it is evident that the uv absorption added by reaction 12 is small in comparison with the initial optical density change in the same region. This confirms our previous assumption that the contribution of Ag^{2+} to the initial absorbance changes at 2850 and 3150 Å is small even at relatively high $[Ag^+]$.

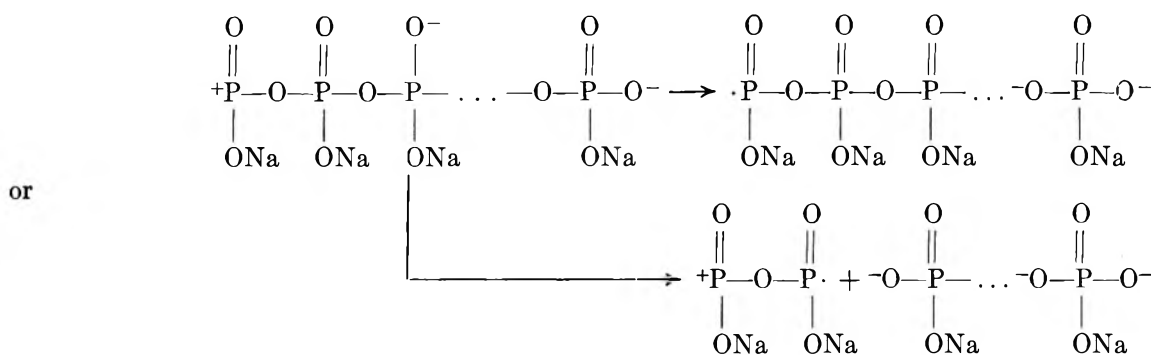
The analysis of the decay in the intermediate stage b met with some difficulties. Comparing the spectral changes associated with this decay with those observed in aqueous systems, one is tempted to adopt the mechanism of Pukies, *et al.*,¹³ attributing the second stage of the decay to the process

(13) J. Pukies, W. Roebke, and A. Henglein, *Ber. Bunsenges. Phys. Chem.*, **72**, 842 (1968).



meaning that Ag_2^+ will not be present as a permanent irradiation product in metaphosphate glasses. This appears to contradict the esr structure observed by Feldmann and Treinin,⁶ suggesting the species Ag_2^+ . One should also recall that the identification of Ag_2^+ by esr spectroscopy in irradiated ices seems quite unambiguous.¹⁴⁻¹⁶ Thus it is not unlikely that the reaction does not take place in the rigid systems. This is not surprising recalling that most of the complex kinetic patterns observed in aqueous solutions (attributed to processes such as $\text{Ag}_2 + \text{Ag}^+ \rightarrow \text{Ag}_3^+$, $\text{Ag}^{2+} + \text{Ag}^{2+} \rightarrow \text{Ag}^{3+} + \text{Ag}^+$ and $n\text{Ag}_3^+ \rightarrow \text{Ag}$ nuclei) do not take place in our rigid systems. Ruling out reaction 13 as a possible explanation to the decay stage b leads to difficulties when attempting to account for this decay in terms of only two primary silver products (*i.e.*, Ag^{2+} and Ag°). On the basis of the available experimental data we are unable at present to provide an alternative explanation to account for the absorption change in stage b.

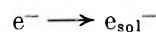
A Model for the Irradiation of Metaphosphates. The



effects of ionizing radiation on metaphosphate glasses are explainable in terms of the primary formation of very mobile electron (e^-) and positive hole (h^+) centers. Such species are probably the precursors of all other transient and permanent irradiation products observed by optical spectroscopy in either pure or doped glasses. Both reactions of e^- and of h^+ are several orders of magnitude faster than ordinary diffusion-controlled reactions in glasses. If the reaction $\text{Ag}^\circ + \text{Ag}^+ \rightarrow \text{Ag}_2^+$ is diffusion controlled (this is the situation in aqueous solutions¹³), then diffusion coefficients in the metaphosphate glasses are smaller by five or six orders of magnitude than in water.

The species e^- may be identified with "dry" electrons, namely, electrons ejected from a polyphosphate molecule which have not undergone a complete solvation process. These electrons have a very high mobility and may react efficiently with ions such as Ag^+ and Cd^{2+} to produce Ag° and Cd^+ , respectively. "Dry" electrons have previously been proposed in irradiated glasses, ices, and liquids.¹⁷⁻²² In the absence

of an appropriate scavenger, the first-order "solvation" of e^- takes place



We suggest that the "solvated electron" in this medium is an electron, shared between several >P=O groups. Such electrons are responsible for the optical absorption peaking at 6900 \AA , which decays away with $\tau_{1/2} \simeq 3 \mu\text{sec}$. The diffusion rate of such electrons may be of the same order of magnitude as the diffusion of most simple ions. (The diffusion coefficient of the hydrated electrons has been measured and found to be similar to that of OH^- ions²³). Therefore, the lifetime of $\tau_{1/2} = 3 \mu\text{sec}$ is too short for scavenger concentrations up to $0.3 m$ to compete for these electrons, as it is indeed found in our system. The decay of e_{sol}^- may be accounted for by a localization of the charge on an oxygen atom, from where it can travel quickly along the polymer chain and become stabilized at the end of the chain. Alternatively, localization of the charge, involving bond cleavage, may take place.^{6,24} (The second effect is known to occur in liquid water, where e_{aq}^- is localized on an OH group, with the simultaneous cleavage of the H-OH bond), *i.e.*

It is assumed that the radical products are stable and do not absorb in the visible.

The possibility of electrons traveling quickly along the metaphosphate polymer chains may explain the high mobility of h^+ . Assuming that h^+ is identical with

(14) L. Shields, *Trans. Faraday Soc.*, **62**, 1042 (1966).

(15) R. S. Eachus and M. C. R. Symons, *J. Chem. Soc. A*, 1329 (1970).

(16) B. L. Bales and L. Kevan, *J. Chem. Phys.*, **52**, 4644 (1970).

(17) T. Sawai and W. H. Hamill, *J. Phys. Chem.*, **73**, 2750 (1969).

(18) T. Sawai and W. H. Hamill, *ibid.*, **74**, 3914 (1970).

(19) R. K. Wolff, M. J. Bronskill, and J. W. Hunt, *J. Chem. Phys.*, **53**, 4211 (1970).

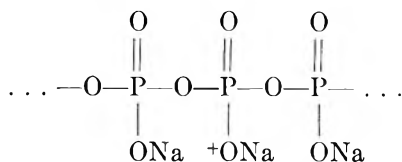
(20) H. B. Steen, *J. Phys. Chem.*, **74**, 4059 (1970).

(21) L. Kevan, *Progr. Solid State Chem.*, **2**, 304 (1965).

(22) L. Kevan in "Radiation Chemistry of Aqueous Systems," G. Stein, Ed., The Weizmann Science Press of Israel, Jerusalem, 1968, p 21.

(23) (a) K. H. Schmidt and W. L. Beck, *Science*, **151**, 70 (1966); (b) G. C. Barker, P. Fowles, and B. Stringer, *Trans. Faraday Soc.*, **66**, 1509 (1970).

(24) T. Feldmann and A. Treinin, *J. Phys. Chem.*, **72**, 3768 (1968).



then the positive hole may travel by a charge-transfer mechanism in which electrons are transferred to the positive center from adjacent $-\text{ONa}$ groups of the same chain or of adjacent chains. Again, the mobile positive hole may be stabilized either by localization at the negative end of a polymer chain or by bond cleavage. Several possibilities of stabilization are indicated by esr measurements.^{7,8} The optical absorption which is found in pure Na metaphosphate after 0.1 sec (h_{IV}^+) is similar to the spectra of H_2PO_4 and HPO_4^- reported in water.^{25,25} This supports the identification of fraction IV as due to stable "positive holes."

According to the above model the mobility of h^+ may be of the same order of magnitude as that of e_{sol}^- .

Unfortunately, this cannot be verified by our data which can only provide us with the decay rates of h^+ and e_{sol}^- . Such rates are affected not only by the mobility of the species considered, but also by the efficiency of their trapping by external scavengers or *via* bond cleavage or localization in the phosphate medium. The fact that h^+ is scavengeable by added metal cations but e_{sol}^- is not, may be rationalized in terms of the model, by the fact that e^- , the precursor of e_{sol}^- , is always more efficiently scavenged than e_{sol}^- . On the other hand, the capture of h^+ , being (like e^-) a primary product, will not be prevented by a faster scavenging of a precursor.

Acknowledgment. We wish to acknowledge the invaluable support of Mr. Y. Ogdan in maintaining and improving the system. We are indebted to Professor A. Treinin for very helpful comments.

(25) J. R. Huber and E. Hayon, *J. Phys. Chem.*, **72**, 3820 (1968).

(26) E. D. Black, and E. Hayon, *ibid.*, **74**, 3199 (1970).

Stereochemistry of the Silver-Catalyzed Epoxidation of Olefins

by W. F. Richey

Texas Basic Research Laboratory, The Dow Chemical Company, Freeport, Texas 77541 (Received May 6, 1971)

Publication costs assisted by The Dow Chemical Company

The stereochemistry of the epoxidation of the geometric isomers of 2-butene and dideuterioethylene on a silver catalyst was investigated along with the reactions of *trans*-2,3-epoxybutane on the surface of silver. *trans*-2-Butene produces an epoxide product which is 95% *trans* isomer. *cis*-2-Butene produces no epoxide product. Both *trans*- and *cis*-dideuterioethylenes give epoxide mixtures which retain about 70% of the original stereochemical configuration. The reaction of *trans*-2,3-epoxybutane on silver gives a mixture of 2-butenes in a *trans* to *cis* ratio of 70:30. These results are explained on the basis of the nature of the intermediate species produced when the epoxide molecule is adsorbed on the silver surface.

I. Introduction

In the past 25 years there have been numerous investigations of the silver-catalyzed epoxidation of olefins. These have included adsorption studies,¹⁻⁴ electron diffraction studies,^{5,6} electron work function measurements,⁷ rate studies,⁸⁻¹⁰ the effects of reaction variables,¹¹ and the effects of "promoters" and "moderators."¹¹⁻¹⁴ Several reaction mechanisms have been proposed on the basis of these results.

However, until this time there has been no effort made to determine the stereochemistry of this reaction. Such a study should yield a better understanding of the behavior of the olefin molecule as it interacts with oxygen on the silver surface to produce the epoxide. This

resulted in the investigation of the epoxidation of the *trans* and *cis* isomers of 2-butene and dideuterioethylene on a silver catalyst.

(1) G. H. Twigg, *Trans. Faraday Soc.*, **42**, 284 (1946).

(2) J. T. Kummer, *J. Phys. Chem.*, **60**, 666 (1956).

(3) A. W. Czanderna, *ibid.*, **68**, 2765 (1964).

(4) S. V. Gerei, K. M. Kholiyavenko, and M. Ya. Rubanik, *Ukr. Khim. Zh.*, **31**, 166 (1965).

(5) Yu. Ts. Vol and N. A. Shishakov, *Izv. Akad. Nauk SSSR, Otd. Khim. Nauk*, 586 (1962).

(6) Yu. Ts. Vol and N. A. Shishakov, *Izv. Akad. Nauk SSSR, Ser. Khim.*, **11**, 1920 (1963).

(7) L. A. Rudnitskii and N. V. Kul'kova, *Dokl. Akad. Nauk SSSR*, **162**, 617 (1965).

II. Experimental Section

A. *Apparatus.* The epoxidation of the olefins occurred in heated, flow-type reactors containing silver powder prepared by the reduction of silver oxide. In the experiments with the butenes, the feed gas consisted of either *trans*-2-butene or *cis*-2-butene mixed with oxygen in a ratio of 60:40. The initial experiments with the dideuterioethylenes involved the passing of an ethylene-oxygen mixture (volume ratio 80:20 at 1 atm) a single time through the reactor. The product was removed by bubbling the exit gas through a CCl₄ scrubber at 0°.

A circulating flow system was also utilized to oxidize dideuterioethylene. After the gas had passed through the reactor, it entered a trap containing 2-mm glass beads at -100°. Chromatographic analyses indicated the trap to be about 90% efficient for ethylene oxide at the concentrations produced under the reaction conditions.

The stereochemistry of the reaction of *trans*-2,3-epoxybutane on a silver catalyst was studied by using an all-glass static reactor with internal circulation, which was provided by a magnet-containing rotor in a side arm. The glass rotor was driven by an external magnet attached to a variable speed electric motor. The bottom part of this reactor was a cylinder 10 cm in length with Irtran 2 windows mounted on each end. This served as an infrared gas cell, and the entire system was placed into the sample chamber of a Perkin-Elmer 337 grating infrared spectrometer.

B. *Materials.* *trans*-2-Butene and *cis*-2-butene were Matheson CP grade and were used without further purification. *trans*-Ethylene-1,2-*d*₂ and *cis*-ethylene-1,2-*d*₂ were obtained from Merck Sharp and Dohme of Canada. Infrared analyses indicated that the isomers were at least 99% pure.

The *trans*-2,3-epoxybutane was separated from a mixture of *trans* and *cis* isomers obtained from K & K Laboratories. This was accomplished by means of a 10 ft × 0.25 in. Carbowax 20 M-TPA gas chromatographic column. The collected fraction was analyzed for impurities by GC-MS. The *cis*-2,3-epoxybutane content was measured to be less than 0.2 area %.

C. *Analysis.* The exit gas from the *trans*-2-butene reactor was passed through a trap at -75° designed to condense the *trans*-2-butene and the epoxide product. The olefin was removed from the condensate by distillation, and the remaining material was analyzed by infrared spectroscopy and gas chromatography.

Originally it was hoped to distinguish between the *cis* and *trans* isomers of dideuterioethylene oxide by nuclear magnetic resonance techniques. However, this did not prove to be feasible. Therefore the epoxide product was separated from the CCl₄ solution in which it was trapped and redissolved in CS₂. This solution was analyzed by infrared spectroscopy. The dideu-

terioethylene oxide condensed in the -100° trap was vaporized and analyzed in the gas phase by infrared spectroscopy.

The reaction of *trans*-2,3-epoxybutane on the silver catalyst was followed by analyzing the vapor inside the reactor by infrared spectroscopy. After reaction was complete, the vapor was analyzed by gas chromatography using a 10 ft × 3/16 in. Porapak R column at 110° to separate the *trans* and *cis* isomers of 2-butene. As in all the other chromatographic analyses, the peak areas were determined by means of an Infotronics Digital Readout System Model CRS-100.

III. Results

A. *Epoxidation of trans-2-Butene.* *trans*-2-Butene was mixed with oxygen and passed over the silver catalyst at 165-170°. Analysis of the exit gas showed that 25% of the butene which reacted produced epoxide; the rest was completely oxidized to CO₂. Over a period of several days the organic products were trapped in the manner described previously. The infrared spectrum of the material remaining in the flask after the butene had been distilled off showed the product to be about 95% *trans*-2,3-epoxybutane and less than 5% *cis*-2,3-epoxybutane with a trace of carbonyl species. Gas chromatographic analysis confirmed these data. Thus, for the epoxidation of *trans*-2-butene, the stereochemical configuration is preserved in the epoxide to an extent of better than 95%.

B. *Epoxidation of cis-2-Butene.* Epoxidation of *cis*-2-butene was examined at temperatures from 120 to 250°. No epoxide was ever detected; the sole products were carbon dioxide and water. For the same reaction conditions, *trans*-2,3-epoxybutane passed through the reactor when *trans*-2-butene was oxidized. Thus, if any *trans*-2,3-epoxybutane were formed in the oxidation of *cis*-2-butene, it should have been detected. This indicates that either *cis*-2-butene does not epoxidize under these conditions or that if any epoxide is formed, it is the *cis* isomer, which is strongly adsorbed and further oxidized.

That *cis*-2,3-epoxybutane is more readily adsorbed on the catalyst surface than is the *trans* isomer was demonstrated when a 20-μl slug of a *trans*-*cis* mixture was injected into a carrier gas before it entered a reactor filled with silver catalyst. The *trans* to *cis* ratio of the mixture before injection was determined to be 4.4:1.

(8) L. G. Nault, D. W. Bolme, and L. N. Johanson, *Ind. Eng. Chem., Process Des. Develop.*, **1**, 285 (1962).

(9) V. M. Belousov and M. Ya. Rubanik, *Kinet. Katal.*, **4**, 892 (1963).

(10) R. E. Kenson and M. Lapkin, *J. Phys. Chem.*, **74**, 1493 (1970).

(11) K. E. Murray, *Aust. J. Sci. Res.*, **3A**, 433 (1950).

(12) S. Hartwig and J. Bathory, *Z. Phys. Chem. (Frankfurt am Main)*, **55**, 208 (1967).

(13) E. Kh. Enikeev, O. V. Isaev, and L. Ya. Margolis, *Kinet. Katal.*, **1**, 431 (1960).

(14) R. G. Meisenheimer and J. N. Wilson, *J. Catal.*, **1**, 151 (1962).

Ten minutes after the injection, a chromatographic analysis of the exit gas showed that the trans-to-cis ratio was 9:1. After 35 min the ratio had dropped back to 4.9:1; and after 60 min all the epoxybutane had passed through the reactor. Thus, it is likely that *cis*-2-butene does form *cis*-2,3-epoxybutane, but the epoxide is adsorbed and further oxidized before it can leave the reactor.

C. *Epoxidation of trans-Dideuterioethylene and cis-Dideuterioethylene.* The CS₂ solutions of the epoxide products from the oxidation of the olefins were analyzed by means of infrared spectroscopy. The resulting spectra were compared with those of Spector.¹⁶ It was found that the principal difference between the spectrum of the *trans*-dideuterioethylene oxide and that of the *cis* isomer was the relative intensities of the bands at 945 and 935 cm⁻¹ and those at 875 and 835 cm⁻¹. However, because Spector used CCl₄ as a solvent, the intensities of the 835-cm⁻¹ absorption in his spectra were too distorted to be useful as a quantitative measure. Therefore, the relative intensities of the bands at 945 and 935 cm⁻¹ were used to determine the isomeric composition of the reaction products. On this basis it was determined that the epoxide product from the oxidation of *trans*-dideuterioethylene contained 68 ± 5% *trans*-dideuterioethylene oxide and 32 ± 5% *cis*-dideuterioethylene oxide. On the other hand, the epoxide product of the *cis*-dideuterioethylene oxidation contained 70 ± 5% *cis* isomer and 30 ± 5% *trans* isomer.

D. *Reactions of trans-2,3-Epoxybutane on a Silver Catalyst.* Twigg¹ and others have reported that when ethylene oxide is exposed to a silver catalyst in the absence of oxygen, ethylene is produced. Since this is ostensibly the reverse reaction to the formation of the epoxide, it is desirable to study the stereochemistry of this reaction as a part of the overall understanding of this catalytic system. For this purpose, *trans*-2,3-epoxybutane was chosen.

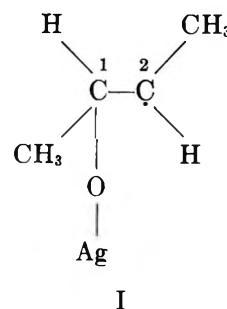
This epoxide was introduced into the static reactor which contained a silver powder freshly reduced from silver oxide with hydrogen. The initial pressure of epoxide vapor was 35 Torr, and the temperature in the reactor was 145°. After 200 min the infrared spectrum showed that the vapor in the reactor consisted solely of 2-butene, methyl ethyl ketone, and a small amount of CO₂. Chromatographic analysis showed that both the *trans* and *cis* isomers of 2-butene were produced with a *trans*-to-*cis* ratio of 70:30.

IV. Discussion

At first glance these results seem somewhat confusing. The *trans*-2-butene produces an epoxide product which is 95% *trans* isomer. The *cis*-2-butene produces no epoxide product. Both *trans*- and *cis*-dideuterioethylenes give epoxide mixtures which retain about 70% of the original stereochemical configuration. The re-

action of *trans*-2,3-epoxybutane on silver gives a mixture of 2-butenes (70% *trans*; 30% *cis*). Thus, any proposed mechanism must account for these diverse data.

The best approach to a consistent explanation of these observations involves the consideration of the intermediate species produced when the epoxide molecule is adsorbed on the silver surface. The reaction of *trans*-2,3-epoxybutane on silver in the absence of oxygen produces methyl ethyl ketone and a mixture of the *cis* and *trans* isomers of 2-butene. This indicates that upon adsorption, one of the carbon-oxygen bonds in the oxirane ring is broken to allow the oxygen to bond to the silver. The species I may then undergo bond



dissociation between the silver and oxygen with an accompanying hydrogen migration to produce methyl ethyl ketone, or the carbon-oxygen bond of I may break to form the olefin. Because free rotation is allowed about C₁ and C₂, the resulting olefin is a mixture of the *cis* and *trans* isomers. In the case of 2-butene, the *trans* isomer will predominate as the *cis* isomer is sterically hindered, the strain energy amounting to 1.00 kcal/mol.¹⁶ Another alternative is that the silver-oxygen bond may break to reform the oxirane ring. Even if before adsorption all of the epoxide molecules consist of a single isomer, the epoxide produced by reforming the oxirane ring will consist of a mixture of isomers as a result of free rotation about C₁ and C₂ during the molecule's residence time as species I.

The isomeric distribution observed for the epoxidation products of the dideuterioethylenes may be explained on the basis of the intermediate adsorbed species of ethylene oxide. In this case, the preliminary attachment produces a short-lived primary free radical. For this species desorption should be very rapid. On the other hand, the adsorption of 2,3-epoxybutane produces a secondary free radical. The greater stability of this species produces a longer residence time on the surface. Thus, the rate of desorption of the epoxybutane is not competitive with the rate of complete oxidation. This results in the lower yield of epoxide

(15) R. Spector, "A Study of the Mechanism of Polymerization of Ethylene and Propylene Oxides," Ph.D. Thesis, University of Pennsylvania, 1966.

(16) A. Almenningen, I. M. Anifinsen, and A. Haaland, *Acta Chem. Scand.*, **24**, 43 (1970).

product for the butene as compared to ethylene, but also ensures a high stereoselectivity in the epoxybutane.

The implication of the foregoing discussion is that the epoxidation reaction is concerted with a retention of olefin configuration. If both carbon-oxygen bonds of the oxirane ring were not formed simultaneously, then an open intermediate form, similar to that produced in the preliminary attachment of the epoxide to the surface, would be present during the reaction sequence. If such an intermediate existed, it is quite likely that a significant, and detectable, quantity of *trans*-2,3-epoxybutane would result from the oxidation of *cis*-2-butene. The *cis*-2,3-epoxybutane molecule is even more strained than is the *cis*-2-butene; thus if free rotation were allowed in an intermediate species, the more stable *trans*-epoxide would predominate over the *cis* isomer. However, as has been previously

stated, no *trans*-2,3-epoxybutane is detected as the product of the oxidation of *cis*-2-butene.

Finally, it must be concluded that the reaction which the epoxide undergoes to give the olefin is not the reverse of the epoxidation reaction. The oxygen species which results from the dissociation of the epoxide cannot be the same one which is responsible for the formation of the epoxide. The latter species may be an electrophilic peroxy oxygen as a concerted epoxidation reaction would be consistent with a mechanism similar to that proposed for the epoxidation of olefins by organic peracids.

Acknowledgments. I am pleased to acknowledge the assistance of Mr. J. E. Lentz in obtaining the infrared spectra and for many useful discussions. The infrared spectra of *trans*- and *cis*-dideuterioethylene oxide from Dr. Spector's thesis were generously provided by Dr. Charles C. Price of the University of Pennsylvania.

Temperature Dependence of the Kerr Constant of Water¹

by Yeong-jgi Chen² and William H. Orttung*

Department of Chemistry, University of California, Riverside, California 92502 (Received August 9, 1971)

Publication costs borne completely by The Journal of Physical Chemistry

The Kerr constant of liquid water was studied from 5 to 81° at a wavelength of 365 m μ . The data suggest a $1/T^2$ dependence at the high and low ends of the temperature range, with a broad inflection point of approximately zero slope near 35°. Less complete results were obtained for D₂O from 5 to 50°. Its Kerr constant is about 10% less than that of water at 25° and 365 m μ . The inflection point could not be predicted from calculations based on temperature-dependent angular correlation of neighboring molecules unless allowance was made for a variable optical anisotropy. It was shown that hyperpolarizability interaction with the strong electric field of neighboring dipoles could account for the temperature dependence of both the mean polarizability and the optical anisotropy. The effect of hydrogen bonding on the symmetry of the molecule was also considered as a factor in the temperature dependence and in the difference between H₂O and D₂O.

Introduction

The refractive index anisotropy of a sample subjected to an electric field was first observed in 1875 and is known as the electrooptic Kerr effect. In liquids, the effect depends on three factors: the optical and dielectric parameters of the individual molecules; the interactions between neighboring molecules; and the structure of the liquid. For many liquids, the molecular parameters may be evaluated from vapor data; the interactions are relatively weak, and the structure is conveniently chaotic. In liquid water, however, strong interactions perturb the molecular properties and induce considerable ice-like structure.

The optical anisotropy of the isolated water molecule can only be deduced from Kerr effect studies of water vapor; but in the liquid, the optical anisotropy must be small.³ As measured by the Kerr effect, the optical anisotropy of the water molecule is proportional to $\alpha_z - \frac{1}{2}(\alpha_x + \alpha_y)$, where α_i is a polarizability, x is perpendicular to the H-O-H plane, and z is the dipole

(1) This investigation was supported in part by Public Health Service Research Grant GM11683 from the Division of General Medical Sciences.

(2) Based on a thesis submitted by Yeong-jgi Chen in partial fulfillment of the requirements for the Ph.D. degree, June 1970.

(3) W. H. Orttung and J. A. Meyers, *J. Phys. Chem.*, **67**, 1905 (1963).

axis. The small observed anisotropy therefore implies that $\alpha_z \cong \frac{1}{2}(\alpha_x + \alpha_y)$, and not that $\alpha_x \cong \alpha_y \cong \alpha_z$. Molecular orbital calculations⁴ suggest that $\alpha_y > \alpha_z > \alpha_x$, as might also be predicted from the shape of the molecule.

The dielectric parameters of water in the solid, liquid, and vapor states have been extensively studied and analyzed,^{5,6} but not all of the mysteries of this phenomenon have been resolved.⁷ It is hoped that Kerr effect studies may lead to a better understanding of the problems of dielectric theory in its application to liquid water.

When the molecular properties are independent of temperature and interactions may be neglected, the Kerr constant will be expressible in the form, $A_0 + A_1/T + A_2/T^2$. The A_2 term is usually dominant if dipole orientation of optically anisotropic molecules occurs; but if the dipole moment or optical anisotropy is small, the contribution of molecular distortion, *i.e.*, field-induced anisotropy, to the A_0 and A_1 terms may be observed.⁸

If the molecular properties or interactions change with temperature, a more complex relationship will be observed. Buckingham and Raab⁹ developed a statistical mechanical theory that included temperature-dependent interactions between molecules. For water, they assumed a temperature-independent optical anisotropy and used the bendable hydrogen bond model of Pople¹⁰ to calculate an approximately $1/T^{1.8}$ dependence for the Kerr constant.

The results presented in the following sections show that the experimental temperature dependence is considerably more complex, and suggest that a temperature dependent molecular polarizability resulting from a changing environment may also have to be considered in a satisfactory interpretation. Both the results and interpretation have been considerably extended and improved since an early publication several years ago.¹¹

Experimental Section

A description of the general methods and procedures used to obtain the Kerr effect data has been published,³ and the apparatus has been described.¹² The method of pulse measurement was modified slightly by the substitution of a Tektronix Type W plug-in unit for the Type Z unit, and a Tektronix P6013 high voltage probe (1000:1) for the homemade divider used earlier. The voltage compensation feature of the Type W was not used. Measurement of the pulsed fields did not require absolute calibration since all data are reported as ratios to the water results at 25°. At the higher temperatures, it was necessary to substitute Dow-Corning Glass and Ceramic Cement for the Apiezon W that had been used to seal the windows to the cell at lower temperatures. The water and D₂O samples were slowly redistilled, the latter from 99.8% isotopic purity

Malinckrodt NMR-quality material. The specific conductances of the water and D₂O at 25° were generally about 2×10^{-6} and 3×10^{-6} ohm⁻¹ cm⁻¹, respectively.

The treatment of data followed earlier methods,³ except that analyzer rotations replaced neutral filter readings in determining I_0 . Corrections for residual birefringence were usually required. The residual effects were apparently caused by the frequent changes of cell temperature. Generally eight measurements were made with gradually increasing fields, and eight with decreasing fields, for each sample at a given temperature.

Results

Most of the data were taken at a wavelength of 365 m μ because of the greater light intensity and near-maximum Kerr constant at this wavelength.¹³ Some results were obtained at 436 m μ . All of the results are expressed as a ratio of the Kerr constant, B , to that of water at 25° and the same wavelength. B is defined in eq 2 below.

Water. Four series of experiments were carried out, all at 365 m μ . The temperature ranges covered were: (1) 5–54°; (2) 25–81°; (3) 25–79°; and (4) 25–50°. The data of the first series¹¹ have been recalculated for improved elimination of residual effects. The results are shown in Figure 1. The points shown for series 1–3 correspond to single experiments, each consisting of 8 to 16 measurements at different fields. The remaining points in the range 30–55° correspond to averages of many experiments, calculated by the following equation for each temperature

$$B = \frac{1}{n} \sum_{i=1}^n B_i w_i \quad (1)$$

where the weighting factors, w_i , were assigned values of $(1/\Delta B_i)^2 / \sum_{j=1}^n (1/\Delta B_j)^2$. The uncertainty, ΔB_i , for a given experiment was determined by a least-squares analysis of the δ'^2/E^2 vs. E^2 plot.³ The number of experiments at 30, 35, 40, 45, 50, and 55° was 3, 3, 5, 13, 8, and 5, respectively. The difficulty in achieving reproducibility in the range 30–55° may have been

(4) R. Moccia, *Theor. Chim. Acta*, **8**, 192 (1967).

(5) D. Eisenberg and W. Kauzmann, "The Structure and Properties of Water," Oxford University Press, New York, N. Y., 1969.

(6) N. H. Fletcher, "The Chemical Physics of Ice," Cambridge University Press, Cambridge, New York, N. Y., 1970.

(7) N. E. Hill, *Proc. Phys. Soc., London (Solid State Phys.)*, **3**, 238 (1970).

(8) A. D. Buckingham and J. A. Pople, *Proc. Phys. Soc., London, Sect. A*, **68**, 905 (1955).

(9) A. D. Buckingham and R. E. Raab, *J. Chem. Soc.*, 2341 (1957).

(10) J. A. Pople, *Proc. Roy. Soc., Ser. A*, **205**, 163 (1951).

(11) Y. Chen and W. H. Orttung, *J. Phys. Chem.*, **72**, 3069 (1968).

(12) W. H. Orttung, *ibid.*, **73**, 2908 (1969).

(13) J. Waibel, *Z. Naturforsch. A*, **21**, 186 (1966).

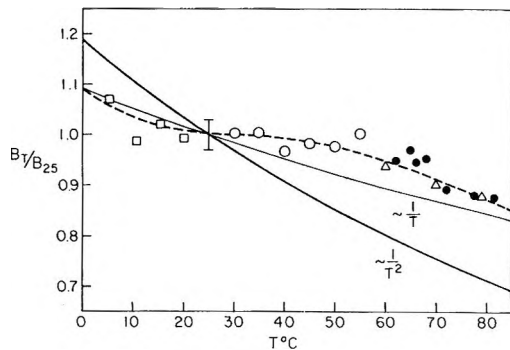


Figure 1. The temperature dependence of the Kerr constant of water at 365 μ : \square , first series; \bullet , second series; Δ , third series; \circ , weighted averages of the four series, as described in the text. The dashed line is suggested by the data and is compared with $1/T$ and $1/T^2$ curves.

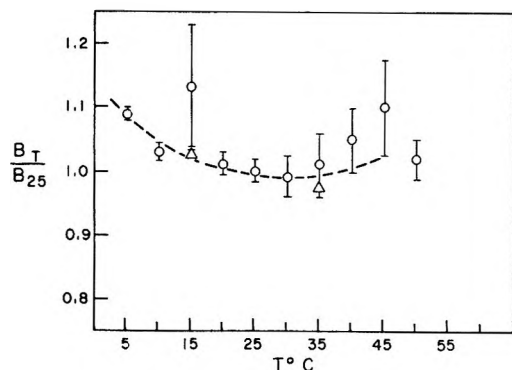


Figure 2. The temperature dependence of the Kerr constant of D_2O at 365 μ : \circ , first series; Δ , second series.

due to thermal strain caused by the window cement, which may not have been warm enough to relax quickly. In any case, reproducibility was more easily achieved above 55°. The 3% uncertainty shown in Figure 1 is suggested by the data and is consistent with anticipated uncertainties.

Deuterium Oxide. The conductance of D_2O increased too rapidly to allow experiments above 50°. Two series of experiments were carried out at 365 μ , and the results are shown in Figure 2. At 25° and 365 μ , the Kerr constant of D_2O was 90% \pm 4% that of H_2O . The results for one series of measurements at 436 μ are shown in Figure 3. The Kerr constant of D_2O increased from 436 to 365 μ , suggesting that its dispersion is not unlike that of water in this wavelength range.

Mixtures. The Kerr constant of a 50% H_2O -50% D_2O mixture (by volume) was approximately halfway between the Kerr constants of pure water and D_2O at 25° and 365 μ .

Interpretation

General Expressions. The Kerr constant is defined as

$$B = (n_{\parallel} - n_{\perp})/\lambda E^2 \quad (2)$$

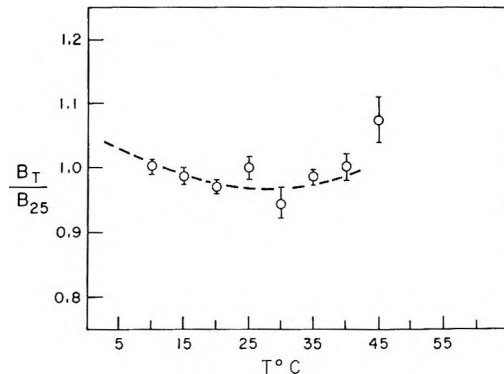


Figure 3. The temperature dependence of the Kerr constant of D_2O at 436 μ .

where n_{\parallel} and n_{\perp} are the refractive indices of the sample parallel and perpendicular to E , the average applied field in the medium in esu, at wavelength λ in air. For N interacting molecules per cm^3 , each having an optical polarizability tensor, $\pi_{\alpha\beta}$, the Kerr constant may be expressed in terms of the following molecular average

$$B = \frac{4\pi N}{\lambda E^2} \frac{(n^2 + 2)^2}{18n} \langle \pi_{\alpha\beta} (e_{\alpha}^{\parallel} e_{\beta}^{\parallel} - e_{\alpha}^{\perp} e_{\beta}^{\perp}) \rangle_E \quad (3)$$

where e_{α}^{\parallel} and e_{α}^{\perp} are unit vectors parallel and perpendicular to the applied field. (Summation over a Greek subscript is implied when it appears twice in a symbol or product of symbols.) The average is carried out at applied field strength, E . The factor, $(n^2 + 2)^2/6n$, in eq 3 is a consequence of assuming the validity at optical frequencies of the Lorentz internal field

$$F_i = \frac{n_i^2 + 2}{3} E_i \quad (4)$$

where i denotes parallel or perpendicular polarization.

If $\pi_{\alpha\beta}$ is written as an expansion in powers of the total field, F_{α} , at a molecule

$$\pi_{\alpha\beta} = \alpha_{\alpha\beta} + \beta_{\alpha\beta\gamma} F_{\gamma} + \frac{1}{2} \gamma_{\alpha\beta\gamma\delta} F_{\gamma} F_{\delta} + \dots \quad (5)$$

we obtain the definitions of the low field polarizability $\alpha_{\alpha\beta}$, and of the first and second hyperpolarizability tensors $\beta_{\alpha\beta\gamma}$ and $\gamma_{\alpha\beta\gamma\delta}$.⁸

The average of eq 3 was evaluated by Buckingham and Raab,⁹ who considered a sample in the shape of a sphere surrounded by vacuum. Using classical statistics, the average was expanded in powers of the uniform vacuum or "external" applied field, $E_0 = E(\epsilon + 2)/3$, where ϵ is the static dielectric constant of the sample. The first nonzero term, proportional to E_0^2 , led to a result of the form

$${}_m K \equiv \frac{6nV_m\lambda}{(n^2 + 2)^2(\epsilon + 2)^2} B = \frac{2\pi N_A}{27} \left[a_0 + \frac{a_1}{kT} + \frac{a_2}{(kT)^2} \right] \quad (6)$$

where V_m is the molar volume, N_A is Avogadro's number, and

$$a_2 = \frac{1}{15} \langle 3\pi_{\alpha\beta} M_\alpha M_\beta - \pi_{\alpha\alpha} M_\beta M_\beta \rangle_0 \quad (7)$$

in which M_α is the dipole moment of the spherical sample in a given configuration, and the average is carried out at zero applied field. Eq 7 contains $\pi_{\alpha\beta}$ rather than $\alpha_{\alpha\beta}$ (see eq 5) because $E_0 = 0$ does not imply $F_\alpha = 0$. Our analysis suggests that this consideration is of major importance in the temperature dependence of the Kerr effect in liquid water.

The result in eq 7 may be simplified if the traceless tensor, $\pi'_{\alpha\beta} = \pi_{\alpha\beta} - \delta_{\alpha\beta}\bar{\pi}$, is used¹⁴ where $\bar{\pi} = \pi_{\gamma\gamma}/3$ is the mean polarizability, and $\delta_{\alpha\beta} = 1$ if $\alpha = \beta$, or 0 if $\alpha \neq \beta$. Thus, eq 7 becomes

$$a_2 = 1/5 \langle \pi'_{\alpha\beta} M_\alpha M_\beta \rangle_0 \quad (8)$$

Simplifications for Water. The coefficients a_0 and a_1 of eq 6 depend directly on $\alpha_{\alpha\beta}$, $\beta_{\alpha\beta\gamma}$, and $\gamma_{\alpha\beta\gamma\delta}$. We need not discuss their explicit form because their contribution to the Kerr constant of liquid water is probably at least an order of magnitude smaller than that of a_2 . There are two reasons for this conclusion. First, the B vs. T plot of Figure 1 approaches a $1/T^2$ dependence at higher temperatures. Second, the data of Buckingham and Orr¹⁵ on CH_2F_2 suggest that the a_1 term is about 1/4 the a_2 term. If a similar ratio holds in water vapor, the dipole correlation effect in the liquid would decrease the ratio by a factor of about 1/2.5 to the order of 1/10.

The molecular axes, $(1,2,3) = (x,y,z)$, of the water molecule are taken according to the usual definition, with x perpendicular to the H-O-H plane, y parallel to the H-H line, and z along the H-O-H angle bisector to form a right-handed system. Since these axes are also principal axes of the polarizability tensor, with corresponding principal traceless polarizabilities denoted by π'_i , eq 8 may be written

$$5a_2 = \langle \pi'_1 M_1^2 + \pi'_2 M_2^2 + \pi'_3 M_3^2 \rangle_0 \quad (9)$$

which is algebraically equivalent to

$$5a_2 = 3/2 \langle \pi'_3 (M_3^2 - 1/3 M^2) \rangle_0 + 1/2 \langle (\pi'_1 - \pi'_2) (M_1^2 - M_2^2) \rangle_0 \quad (10)$$

where

$$M^2 = M_\alpha^2 = M_1^2 + M_2^2 + M_3^2$$

Temperature-Dependent Angular Correlation. Buckingham and Raab⁹ approximated $\pi_{\alpha\beta}$ by $\alpha_{\alpha\beta}$ and assumed that the second term of eq 10 was zero. Their expression for $5a_2$ then reduced to

$$5a_2 = 3/2 \alpha'_3 \langle M_3^2 - 1/3 M^2 \rangle_0 \quad (11)$$

because $\alpha'_{\alpha\beta}$ is independent of the configuration of neighboring molecules, according to eq 5. The aver-

age was worked out for the bendable hydrogen bond model of Pople,¹⁰ using the approach to dielectric theory proposed by Buckingham.¹⁶ The temperature dependence of B was found to be approximately $1/T^{1.8}$ (corresponding to $a_2 \simeq T^{0.2}$). A glance at Figure 1 shows that this result cannot explain the data.

We have also performed calculations of the type required by eq 10 (with $\pi'_{\alpha\beta}$ replaced by $\alpha'_{\alpha\beta}$) for rigid as well as for bendable hydrogen bonds.¹⁷ In both cases, the second term of eq 10 was found to be zero, verifying the assumption of Buckingham and Raab. The calculations considered first (and sometimes second) neighbors, and did not employ the dielectric theory of Buckingham.¹⁶ For bendable hydrogen bonds, the temperature dependence of B was always found to be greater than $1/T^2$, again in disagreement with the data. It was therefore decided to investigate the temperature dependence of π'_3 .

Temperature-Dependent Polarizability. Analyses of the refractive index of liquid water have suggested a decreasing mean molecular polarizability with increasing temperature.^{18,19} Orttung's calculation suggested a possible decrease in the mean polarizability, $\bar{\pi}$, of about 0.0018 \AA^3 between 0 and 50° , the value remaining constant at higher temperatures. Since $\pi'_3 = (\pi_3 - \bar{\pi}) = 0.013 \text{ \AA}^3$ at 25° ,³ it is clear that a small change in π'_3 , of the magnitude suggested by the change in $\bar{\pi}$ with temperature, could easily explain the results in Figure 1, in which $T^2 B$ increases about 35% from 0 to 60° .

A possible source of a temperature-dependent polarizability is the interaction of the first and second hyperpolarizabilities with the electrostatic field along the z axis of a molecule. This field arises mainly from the permanent dipoles of the neighboring molecules, and is strong enough in ice to increase the vapor dipole moment, $\mu_0 = 1.84 \text{ D}$, to $\mu = 2.60 \text{ D}$.²⁰ The ratio μ/μ_0 for the liquid was estimated for the bendable hydrogen bond model by Pople.¹⁰ Since $\mu = \mu_0 + \alpha_3 F$, Pople's result can be inverted to yield estimates of the field along the z axis as a function of temperature. The results, using $\mu_0 = 1.84$ debyes and $\alpha_3 = 1.59 \text{ \AA}^3$,²¹ are shown in Table I for the temperatures considered by Pople.

The distinct nonzero hyperpolarizabilities for a

(14) P. J. Flory and R. L. Jernigan, *J. Chem. Phys.*, **48**, 3823 (1968).

(15) A. D. Buckingham and B. J. Orr, *Trans. Faraday Soc.*, **65**, 673 (1969).

(16) A. D. Buckingham, *Proc. Roy. Soc., Ser. A*, **238**, 235 (1956).

(17) Y. Chen, "Temperature Dependence of the Kerr Constants of Water and Heavy Water," Ph.D. Dissertation, University of California, Riverside, June 1970.

(18) W. H. Orttung, *J. Phys. Chem.*, **67**, 503 (1963).

(19) E. Reissler and H. Eisenberg, *J. Chem. Phys.*, **43**, 3875 (1965).

(20) C. A. Coulson and D. Eisenberg, *Proc. Roy. Soc., Ser. A*, **291**, 245 (1966).

(21) N. E. Dorsey, "Properties of Ordinary Water-Substance," Reinhold, New York, N. Y., 1940.

molecule with C_{2v} symmetry are β_{113} , β_{223} , β_{333} ; γ_{1111} , γ_{2222} , γ_{3333} , γ_{1122} , γ_{2233} , and γ_{1133} .²² Since the hyperpolarizability tensors are symmetric to interchange of all subscripts, other nonzero coefficients have one of the values listed above. For tetrahedral symmetry, $\beta_{113} = \beta_{223} = \beta_{333}$; $\gamma_{1111} = \gamma_{2222} = \gamma_{3333}$; and $\gamma_{1122} = \gamma_{2233} = \gamma_{1133}$.²³

The mean polarizability of a water molecule subjected to a field, F_3 , is obtained from eq 5 as

$$\bar{\pi} = 1/3\alpha_{\alpha\alpha} + 1/3\beta_{\alpha\alpha 3}F_3 + 1/6\gamma_{\alpha\alpha 33}F_3^2 \quad (12)$$

Then since

$$\pi_{33} = \alpha_{33} + \beta_{333}F_3 + 1/2\gamma_{3333}F_3^2 \quad (13)$$

it follows that

$$\pi_{33} - \bar{\pi} = (\alpha_{33} - 1/3\alpha_{\alpha\alpha}) + (\beta_{333} - 1/3\beta_{\alpha\alpha 3})F_3 + 1/2(\gamma_{3333} - 1/3\gamma_{\alpha\alpha 33})F_3^2 \quad (14)$$

Eq 12 and 14 give the desired expressions for $\bar{\pi}$ and π'_{33} in terms of the first and second hyperpolarizabilities and the temperature-dependent field along the symmetry axis of the molecule.

To make numerical predictions, estimates of $\beta_{\alpha\beta\gamma}$ and $\gamma_{\alpha\beta\gamma\delta}$ are needed for the water molecule. No such data are yet available, but Buckingham and Orr¹⁵ have studied the Kerr effect of CH_2F_2 and similar molecules. The dipole moments and optical anisotropies of water and CH_2F_2 are very similar ($\mu_0 = 1.84$ vs. 1.97 D; $\pi'_{33} = 0.013$ vs. $\alpha'_{33} = -0.0135 \text{ \AA}^3$, respectively), so that it is not unreasonable to use the hyperpolarizabilities obtained for CH_2F_2 to calculate rough estimates for water. Buckingham and Orr reported $10^{30} \beta_{\alpha\alpha 3} = -0.18 \pm 0.04$ esu and $10^{36} \gamma_{\alpha\alpha\beta\beta} = 5.5$ esu.

$\gamma_{\alpha\alpha\beta\beta}$ cannot be used directly in eq 12 unless we make the approximation, $\gamma_{\alpha\alpha\beta\beta} = 3\gamma_{\alpha\alpha 33}$, which is valid

tions therefore provide a reasonable interpretation of the earlier calculations.

Eq 14 requires a knowledge of β_{333} and γ_{3333} that is not presently available. We are thus forced to calculate only limiting cases. The four cases considered in Table II are explained as follows: (1) and (2) set the γ term of eq 14 to zero, while (3) and (4) set the β term to zero; (1) assumes $\beta_{333} = 0$ and (2) assumes $\beta_{113} + \beta_{223} = 0$, while (3) assumes $\gamma_{3333} = 0$ and (4) assumes $\gamma_{1133} + \gamma_{2233} = 0$; (3) and (4) also assume $\gamma_{\alpha\alpha\beta\beta} = 3\gamma_{\alpha\alpha 33}$ as in the preceding paragraph. The four calculations are compared with the Kerr constant data in Table II. It is readily seen that cases (2) and (3) are capable of explaining the data. The range of values of α'_{33} obtained as a by-product of this calculation is also of interest.

The Effect of Hydrogen Bonding. Since the dielectric constants of H_2O and D_2O are almost the same (79.39 vs. 79.06) at 25°, the angular correlation and electric field arising from neighboring dipoles must be very similar in the two liquids. The 10% lower Kerr constant of D_2O relative to H_2O may therefore depend on an additional effect such as a difference in hydrogen bonding.

An increase of hydrogen bond strength would be expected to modify the C_{2v} symmetry of the water molecule toward a more tetrahedral structure in the liquid state. The increased symmetry could then account for a reduced optical anisotropy. Since it is generally thought that the D bond is stronger than the H bond, an effect of this type could explain the lower Kerr constant of D_2O . If this argument is valid, the same effect should also be of importance in the transition from vapor to liquid, or from high to low temperature in the liquid. Raising the temperature of the liquid should then change the molecular symmetry away from tetrahedral toward C_{2v} , thereby increasing the anisotropy.

Discussion

We may conclude from the foregoing considerations that hyperpolarizability interaction with the dipole field of neighboring molecules is capable of explaining the temperature dependence of the Kerr effect of liquid water. The same interaction also provides a very nice explanation of the temperature dependence of the mean polarizability. The direct effect of temperature-dependent angular correlations seems to be less important, but is not negligible, on the basis of relatively simple calculations. Improved calculations of this phenomenon would be desirable. The variation of hydrogen bond strength with temperature and isotopic substitu-

Table I: Temperature Dependence of the Local Field and the Mean Polarizability of Water

t , °C	μ/μ_0	$10^{-5}F_3$, esu	$10^2(\bar{\pi} - \bar{\alpha}), \text{ \AA}^3$	
			Hyper- polariz- ability effect	Data analysis ¹⁸
0	1.173	2.002	0.00	0.00
25	1.165	1.909	-0.05	-0.13
62	1.145	1.678	-0.17	-0.18
83	1.135	1.562	-0.21	...

^a Relative to $t = 0^\circ$.

for the case of tetrahedral symmetry. In this approximation the results for $\bar{\pi} - \bar{\alpha}$ from eq 12 are shown in Table I. The agreement with the earlier estimate¹⁸ of $\Delta\bar{\pi} = -0.0018 \text{ \AA}^3$ from 0 to 50°, and no further change from 50 to 60°, is very close. The present considera-

(22) A. D. Buckingham and B. J. Orr, *Quart. Rev. (London)*, **21**, 195 (1967).

(23) A. D. Buckingham, *Advan. Chem. Phys.*, **12**, 107 (1967).

(24) G. A. Vidulich, D. F. Evans, and R. L. Kay, *J. Phys. Chem.*, **71**, 656 (1967).

Table II: Temperature Dependence of the Optical Anisotropy of Water

Case	Assumptions ^a			$\pi'_3(t)/\pi'_3(t=0)$			
	β_{333}	γ_{333}	$10^{26}\alpha'_3$ ^c	$t = 0$	$t = 25$	$t = 62$	$t = 83$
1	0	$\frac{1}{3}\gamma_{\alpha\alpha 33}$	0.16	1.00	0.96	0.86	0.81
2	$\beta_{\alpha\alpha 3}$	$\frac{1}{3}\gamma_{\alpha\alpha 33}$	3.58	1.00	1.10	1.32	1.44
3	$\frac{1}{3}\beta_{\alpha\alpha 3}$	0	2.41	1.00	1.09	1.30	1.40
4	$\frac{1}{3}\beta_{\alpha\alpha 3}$	$\gamma_{\alpha\alpha 33}$	-0.92	1.00	0.85	0.53	0.37
Data ^b	1.00	1.09	1.30	1.34

^a The assumptions are described in the text. ^b Assuming that π'_3 is proportional to T^2B , the values are estimated from the dashed curve in Figure 1. ^c Assuming that $\pi'_3 = 0.013 \text{ \AA}^3$ at 25° .

tion must also be a factor in the temperature dependence, and quantum mechanical calculations of this effect would also be of interest.

The need to simultaneously unravel problems involving molecular parameters, interactions, and liquid structure suggests the desirability of investigations covering many types of phenomena. For example, an infrared band of intermolecular origin has been observed at 2100 cm^{-1} .²⁵ The intensity of this band de-

creases with increasing temperature and shows an inflection near 30° . The plot of intensity *vs.* temperature is remarkably similar to the plot of Kerr constant *vs.* temperature. Efforts to uncover possible common molecular origins in these and other observations might well lead to further important insights in the three difficult areas involved in this problem.

(25) C. Salama and D. A. I. Goring, *J. Phys. Chem.*, **70**, 3838 (1966).

The External Heavy Atom Effect on the Phosphorescence

Spectra of Some Halonaphthalenes

by Linda G. Thompson¹ and S. E. Webber*

Department of Chemistry, The University of Texas at Austin, Austin, Texas 78712 (Received August 9, 1971)

Publication costs assisted by the Robert A. Welch Foundation

Phosphorescence spectra are presented for 1- and 2-halonaphthalenes (halo = chloro, bromo, and iodo) in a series of matrices (ethanol and 1-propyl chloride, bromide, and iodide). The phosphorescence spectra of these molecules are found to be sensitive to external heavy atom perturbations, with 2-halonaphthalenes being more sensitive than 1-halonaphthalenes. It is suggested that the reason for this solvent effect is that the vibrationally induced portion of the $T_1 \rightarrow S_0$ transition intensity is not important in heavy atom solvents.

Introduction

It has been known since the early work of McClure² and Kasha³ that internal (*i.e.*, chemically bonded) or external heavy atoms have a striking effect on processes involving the triplet state of aromatic molecules. It is currently supposed that aromatic molecules possess this extreme sensitivity to heavy atoms as a consequence of their planarity, which symmetry reduces the magnitude of the spin-orbit coupling between singlet and triplet $\pi-\pi^*$ excited states.⁴ A number of reviews are available which discuss the so-called "heavy atom effect" in general.⁵⁻⁷

It is the purpose of this article to present some phosphorescence spectra of various 1- and 2-halonaphthalenes in various matrices (ethanol and 1-propyl chloride,

(1) Present address: Department of Chemistry, Memorial University, St. Johns, Newfoundland.

(2) D. S. McClure, *J. Chem. Phys.*, **17**, 905 (1949).

(3) M. Kasha, *ibid.*, **20**, 71 (1952).

(4) D. S. McClure, *ibid.*, **17**, 665 (1949).

(5) M. A. El-Sayed, *Accounts Chem. Res.*, **1**, 8 (1968).

(6) S. K. Lower and M. A. El-Sayed, *Chem. Rev.*, **66**, 199 (1966).

(7) S. P. McGlynn, T. Azumi, and M. Kinoshita, "Molecular Spectroscopy of the Triplet State," Prentice-Hall, Englewood Cliffs, N. J., 1969, Chapters 5-8.

bromide, and iodide) at 77°K. These spectra display a remarkable dependence on the degree of external spin-orbit coupling which is unique to the halonaphthalene series, as far as the present authors are aware. We may summarize our results as follows. (1) 2-Halonaphthalenes are more sensitive to external heavy atoms than 1-halonaphthalenes. (2) In all cases the phosphorescence spectrum of the halonaphthalene became more like that of naphthalene, indicating that the mixing scheme which gives rise to the phosphorescence in halonaphthalenes is simplified by the presence of an external heavy atom.⁸

Experimental Section

The experimental arrangement used to obtain the phosphorescence spectra was straightforward and has been described previously.⁹ Excitation was by means of a low pressure Hg lamp and a 100-Å band-pass, 3130-Å interference filter (Oriel Optics Corp.). No phosphorimeter was used as there was no scattered light or impurity fluorescence present. All spectra presented are uncorrected for photomultiplier response (EMI 9514 S). Typical slit widths on the McPherson Model 218 0.3-m monochromator were 1000 μ, which results in a 25-Å band pass.

Ethanol was freshly distilled from an ethanol-magnesium ethoxide mixture to ensure dryness. All propyl halides were passed through an activated alumina column before use, although propyl iodide was the only compound to show evidence of decomposition. No phosphorescence was detected from these solvents. Solvents were not outgassed before use as outgassing has not been found to affect phosphorescence spectra in solid matrices. The concentration of the naphthalenic species was approximately 10⁻³ M. The ethanol matrix was glassy but the propyl halides yielded white, opaque polycrystalline matrices. The present results are presented for pure solvent materials. Essentially the same effects are found when 1:1 ethanol-propyl halide glassy matrices are used. Apparently Eisenenthal¹⁰ has observed the same effect with even more dilute heavy atom solvents.

With the exception of 2-iodonaphthalene (Pfaltz and Bauer) all materials could be used without further purification (Eastman Organic Chemicals). The former material was passed through an alumina column and then recrystallized from ethanol. All phosphorescence spectra in ethanol agreed with those reported by Pavlopoulos and El-Sayed.¹¹

Results

In Figures 1 and 2 are presented the phosphorescence spectra of 1- and 2-chloronaphthalene, respectively. For 1-chloronaphthalene the phosphorescence spectra in ethanol and propyl chloride are essentially the same, with the latter spectrum being broadened slightly. The spectra in propyl bromide and propyl iodide are

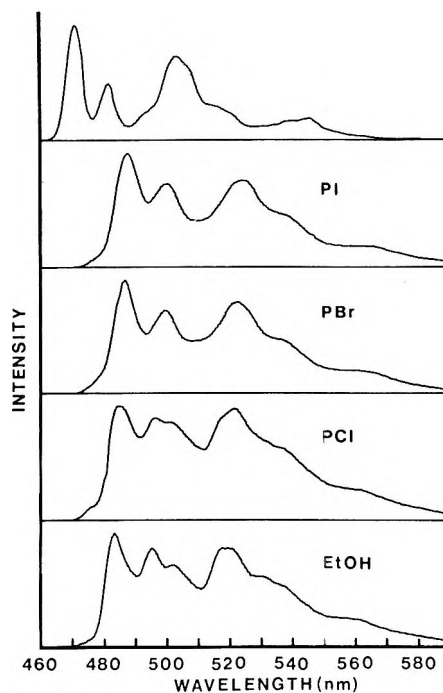


Figure 1. The phosphorescence spectrum of 1-chloronaphthalene in various matrices at 77°K. The following notation is used to denote the solvents: EtOH = ethanol, PX = 1-propyl halide where X = Cl, Br, I. The topmost spectrum in this and all succeeding figures is that of naphthalene in ethanol.

definitely perturbed and resemble the phosphorescence spectrum of naphthalene (upper spectrum). A similar but much more striking change occurs for 2-chloronaphthalene. For this molecule the presence of propyl chloride serves to perturb the spectrum. This observation is illustrative of the generally greater sensitivity to external heavy atoms of the 2-halonaphthalenes.

Similar sets of spectra are presented in Figures 3 and 4 for 1- and 2-bromonaphthalene. For the former molecule there is no significant perturbation except for the propyl iodide matrix while for the latter molecule a significant perturbation is present for the propyl bromide matrix. For the 2-bromonaphthalene case the matrices propyl chloride, bromide, and iodide form a clear progression of perturbative effects on the phosphorescence spectrum.

In Figure 5 we have combined the phosphorescence spectra for 1- and 2-iodonaphthalene. As expected, the perturbation on the phosphorescence spectrum is less important for these cases because the internal heavy atom effect is quite strong. In particular, the 1-iodonaphthalene spectrum is primarily broadened in going from an ethanol to propyl iodide matrix, although the

(8) In the notation of ref 5, our results demonstrate the external heavy atom enhancement of subspectrum I relative to subspectrum II.

(9) S. E. Webber, *J. Phys. Chem.*, **75**, 1921 (1971).

(10) K. B. Eisenenthal, *J. Chem. Phys.*, **45**, 1850 (1966).

(11) T. Pavlopoulos and M. A. El-Sayed, *ibid.*, **41**, 1082 (1964).

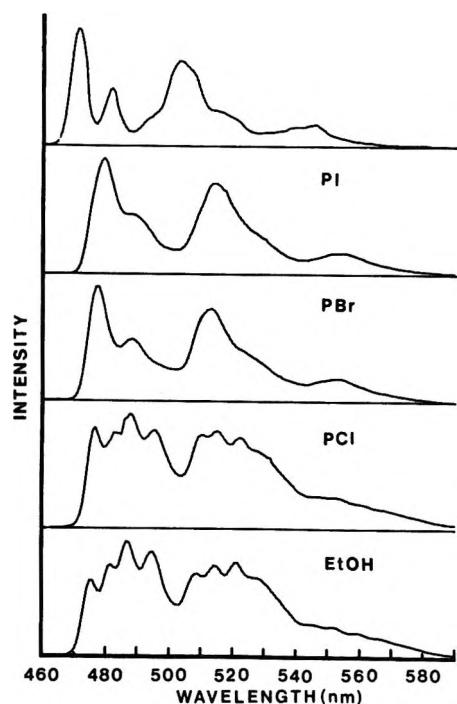


Figure 2. Phosphorescence spectra of 2-chloronaphthalene; see Figure 1 for notation.

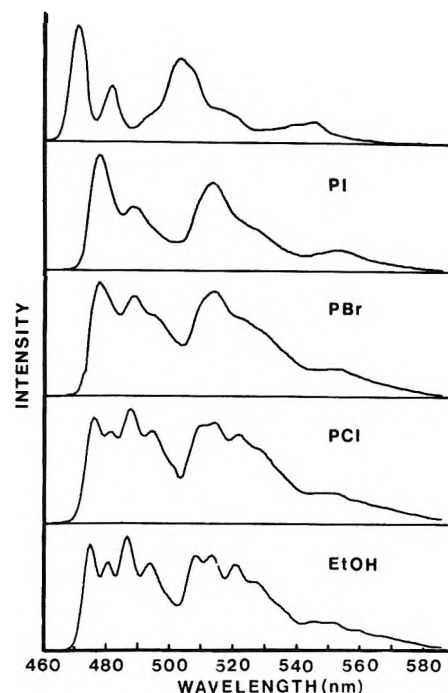


Figure 4. Phosphorescence spectra of 2-bromonaphthalene; see Figure 1 for notation.

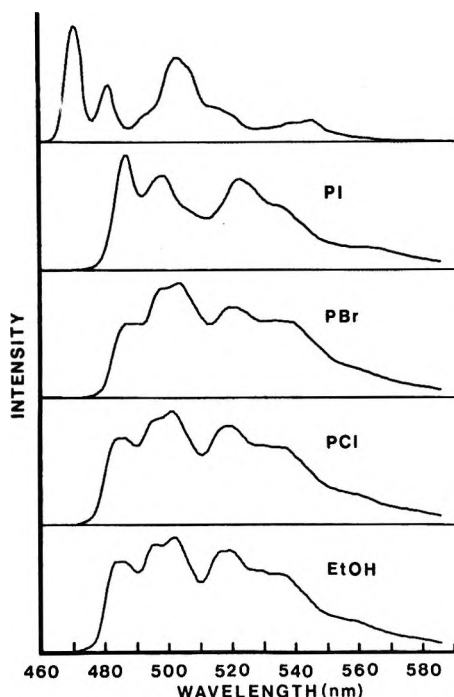


Figure 3. Phosphorescence spectra of 1-bromonaphthalene; see Figure 1 for notation.

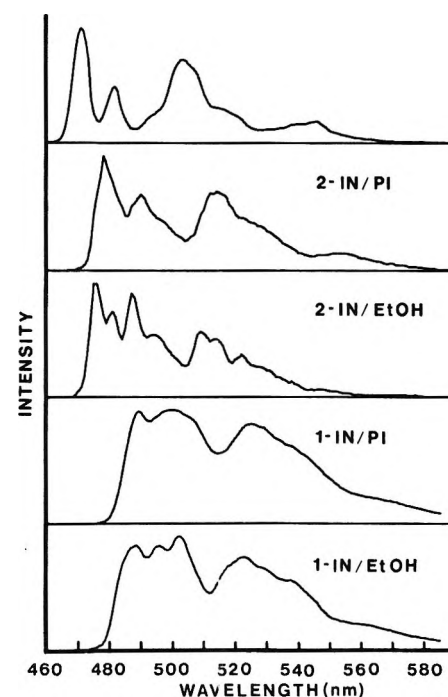


Figure 5. Phosphorescence spectra of 1-iodonaphthalene (1-IN) and 2-iodonaphthalene (2-IN). Other notation follows Figure 1.

O-O band is somewhat strengthened in the latter matrix. The 2-iodonaphthalene phosphorescence spectrum is more sensitive to a propyl iodide matrix than the 1-iodonaphthalene spectrum, consistent with the previously mentioned trend.¹²

An interesting empirical rule emerges from a study of these spectra. For 2-halonaphthalenes the external

heavy atom must be the same as (or exceed in atomic number) the internal heavy atom for an appreciable ef-

(12) The present results are in conflict with a part of the earlier work of S. P. McGlynn, M. J. Reynolds, G. W. Daigre, and N. D. Christodouleas, *J. Phys. Chem.*, **66**, 2499 (1962). These workers state that the phosphorescence spectrum of 1-iodonaphthalene is unchanged in cracked propyl halide glasses.

fect to be observed on the phosphorescence spectrum. For the 1-halonaphthalenes it is necessary for the atomic number of the external atom to exceed that of the internal atom for a spectral perturbation to occur. We are not aware of any reason why these different sensitivities should have been anticipated. The phosphorescent lifetimes of the 1- and 2-halonaphthalenes are similar for a given halogen substitution.^{2,12} This implies that the 1 or 2 positions are roughly equivalent as far as the efficiency of the internal heavy atom effect is concerned. If this were not the case one could argue that our observations reflect the relative magnitude of internal singlet-triplet coupling.¹³ Another possible explanation of the difference between 1- and 2-halonaphthalenes is that the latter steal intensity from the propyl halides triplet-singlet emission more efficiently than the former.^{14,15} We note that the triplet energy of the 2-halonaphthalenes is always higher than that of 1-halonaphthalene. Presumably the energy gap between the states described by ${}^3\psi(T_1 \times {}^1P_0)$ (triplet state of aromatic and ground state of "atomiclike" perturber) and ${}^3\psi(S_0 \times {}^3P_1)$ (ground state of aromatic and excited triplet of perturber) is less for the former molecule than for the latter. It follows from the so-called "exchange mechanism"^{14,16,17} that there will be a larger contribution of the perturber transition strength to the $T_1 \rightarrow S_0$ transition for the 2-halonaphthalenes than for the 1-halonaphthalenes.

We may note one further trend displayed by our spectra. The appearance of the phosphorescence spectra for all 1-halonaphthalenes in propyl iodide are quite similar to each other and likewise for the 2-halonaphthalenes. However, the phosphorescence spectra in propyl iodide for the 1- and 2-halonaphthalenes are dif-

ferent from each other. If our interpretation of the present results as intensity stealing from solvent transitions is correct, then the phosphorescence spectra in propyl iodide no longer reflect the vibronically induced transitions observed in the unperturbed halonaphthalenes.¹⁸ The similarity of the propyl iodide spectra reflects the similarity of the potential energy surfaces in the T_1 and S_0 electronic state for all naphthalenes substituted at a particular position but regardless of the halogen substituent. This observation should be of interest to theoreticians concerned with the effect of substituent groups on the energy levels of aromatic molecules.

Acknowledgments. We wish to acknowledge the generous support of this work by the Robert A. Welch Foundation. We have also benefited from NSF Grant GP-10021. We wish to thank Mrs. Rayna Kolb for her help in preparing the figures.

(13) The differences in the observed triplet lifetime for 1- or 2-halonaphthalenes do imply that the 1 position is slightly more efficient in spin-orbit coupling than the 2 position, *i.e.*, the lifetime of a 1-halonaphthalene is always shorter than that of a 2-halonaphthalene. The largest difference between positions is found for chloronaphthalenes ($\tau_p = 0.30$ and 0.47 sec for 1- and 2-chloronaphthalene, respectively).

(14) See ref 7, Chapter 8, section 6.

(15) Recent work by G. C. Giachino and D. R. Kearns, *J. Chem. Phys.*, **52**, 2964 (1970), has shown that the electronic states of the external heavy atom are mixed with those of the perturbed aromatic molecule.

(16) G. W. Robinson, *J. Mol. Spectrosc.*, **6**, 58 (1961).

(17) M. A. El-Sayed, *J. Chem. Phys.*, **47**, 2200 (1967).

(18) The presence of a vibronically induced pathway for $T_1 \rightarrow S_0$ in halonaphthalenes has been discussed in ref 5 and 11. For a discussion of halophenanthrenes see J. L. Ginsburg and L. Goodman, *J. Chem. Phys.*, **52**, 2369 (1970).

The Triplet States of Biphenylene

by F. Peradejordi,*

Centre de Mécanique Ondulatoire Appliquée, Paris, France

C. Tétreau, and D. Lavalette

Fondation Curie, Institut du Radium, Paris, France (Received July 30, 1971)

Publication costs borne completely by The Journal of Physical Chemistry

A theoretical study of the triplet-triplet spectrum of biphenylene has been performed employing the semi-empirical LCAO-SCF-MO theory with the inclusion of biexcited configurations. Ground and triplet state MO's have been computed considering various sets of parameters. The results agree with the lowest triplet state experimental observation and provide a plausible explanation for the failure to observe triplet-triplet absorption in this molecule.

Introduction

Biphenylene shows several unusual properties for an alternant hydrocarbon. Contrary to polyacenes, each two paired bonding and antibonding molecular orbitals in biphenylene have the same parity (u or g) with respect to an inversion through the molecular center of symmetry. As a result, the first transition (1L_a band) is symmetry forbidden.¹ Neither fluorescence nor phosphorescence emissions were detected in an EPA rigid glass.² This result, recently confirmed,³ allows setting an upper limit of 10^{-4} for the fluorescence and phosphorescence quantum yields in these conditions. A reported phosphorescence measurement in boric acid glass⁴ does not seem consistent with the location of the lowest triplet state observed by oxygen perturbation techniques.⁵ The oscillator strength of the first singlet-singlet ($S_1 \leftarrow S_0$) transition was estimated by Hochstrasser to be approximately 10^{-3} , in EPA at 90°K .⁶ Computed from this value, the radiative lifetime is of the order of 10^{-6} sec. Taking into account the quantum yield limit, this leads, for the first singlet excited state S_1 , to an actual lifetime lying in the subnanosecond region. The nature of the efficient deactivation processes occurring in biphenylene is still unknown. Attempts to obtain information from transient spectra were unsuccessful; no transient species of lifetime longer than 10 nsec could be detected in a laser photolysis experiment performed in rigid medium in the 400-600-nm region.³ The failure to observe an intense triplet-triplet ($T_n \leftarrow T_1$) absorption, if one was to be expected, could suggest an extremely small inter-system crossing yield since it is rather unlikely for the triplet state to have a lifetime shorter than 10^{-8} sec in a rigid solution.

To help clarify this situation we present here the results of a theoretical study on the $T_n \leftarrow T_1$ absorption spectra of the biphenylene molecule.

Theoretical Study

I. Method and Calculation Technique. It has been shown¹ that a satisfactory description of the uv spectrum of biphenylene can be attained in the framework of the semiempirical SCF-LCAO-MO theory. This approach required empirical core resonance integral values β_{C-C} that are different from the values generally assigned to polyacenes. Inclusion of biexcited electronic configurations has also proved to be essential. Therefore, the same procedure was followed in this work. Table I and Figure 1 indicate the values for the parameters used throughout the present calculation. All singly excited and 17 low energy biexcited configurations (with respect to the 1V_0 ground configuration) were considered. [The biexcited configurations taken into account are: V_{66}^{78} , V_{55}^{77} , V_{55}^{78} , V_{56}^{88} , V_{66}^{78} (3 cf.), V_{56}^{79} (3 cf.), V_{46}^{78} (3 cf.), V_{66}^{79} , V_{46}^{77} , V_{66}^{89} , and V_{46}^{77} .]

The configurations 3V_n associated with the triplet states T_n were constructed following two different procedures "S" and "T." In the "S" procedure, triplet configurations were built from SCF MO's obtained by minimizing the energy of the singlet ground 1V_0 configuration of biphenylene. In the "T" procedure, triplet configurations were built from SCF MO's obtained by minimizing the energy of the lowest triplet configuration 3V_1 .

As it was done in the study of the $S_n \leftarrow S_0$ spectrum,¹

(1) F. Peradejordi, R. Domingo, and J. I. Fernández-Alonso, *Int. J. Quant. Chem.*, **3**, 683 (1969).

(2) R. M. Hochstrasser and R. D. McAlpine, *J. Chem. Phys.*, **44**, 3325 (1966).

(3) D. Lavalette, unpublished results.

(4) I. H. Munro, T. D. S. Hamilton, J. P. Ray, and G. F. Moore, *Phys. Lett.*, **20**, 386 (1966).

(5) D. F. Evans, *Opt. Anregung Org. Syst.*, 586 (1966).

(6) R. M. Hochstrasser, *Can. J. Chem.*, **39**, 765 (1961).

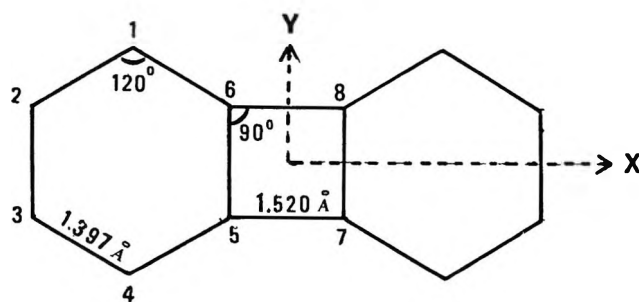


Figure 1. Geometric structural parameters.

Table I: Values of the Parameters Used in the Present Work (eV)^a

$\beta_{62} = -1.76$	$W_c = -11.22$
$\beta_{56} = -1.80$	$A_c = +0.62$
$\beta_{12} = -1.80$	$W'_c \left\{ \begin{array}{l} \text{Model A: } W'_1 = W'_6 = -11.22 \\ \text{Model B: } W'_1 = -11.22, W'_6 = -10.22 \end{array} \right.$
$\beta_{23} = -1.83$	
$\beta_{16} = -2.15$	

^a See text and ref 1.

the evaluation of the diagonal core matrix elements α_C was carried out using two different models "A" and "B." In model "A," all carbon atoms in the molecule were considered as being strictly equivalent. In the Pariser and Parr⁷ expression of the diagonal core matrix elements

$$\alpha_C = W_C - \sum_{C' \neq C} (C':CC) - \sum_H (H:CC) - \sum_{C' \neq C} (C'C'/CC)$$

where C letters denote carbon atoms and H letters denote hydrogen ones, the quantity

$$W_C' = W_C - \sum_{C' \neq C} (C':CC) - \sum_H (H:CC)$$

was assigned the same value $W_C' = -11.22$ eV for all the carbon centers. In model "B," in order to take into account environmental and σ core structural differences between secondary and tertiary biphenylene carbon atoms, the value $W_C' = -10.22$ eV was assigned to the four-membered ring carbon centers (see Table I and ref 1).

In every case, the two-center atomic coulombic integrals

$$(PP/QQ) = \int \chi_P(1)\chi_P(1) \frac{1}{r_{12}} \chi_Q(2)\chi_Q(2) d\tau_{12}$$

were computed following both the *Nishimoto-Mataga* ("M")⁸ and the *Pariser and Parr* ("P")⁹ approximations.

Several calculation procedures, S_{AM} , S_{BM} , and T_{AM} , S_{AP} , S_{BP} , and T_{AP} , obtained from different combinations of the preceding models and approximations, were used in this work. A critical comparison of the results is

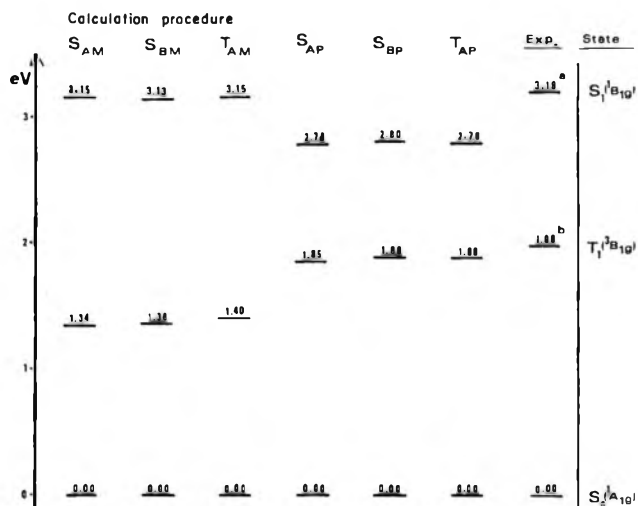


Figure 2. Relative location of the lowest triplet state of biphenylene: a, ref 6; b, ref 5.

made in order to assess the reliability of the theoretical predictions and their dependence from the specified factors.

II. Results and Discussion. A. The Lowest Triplet State. Figure 2 shows the type symmetry and the relative location of the lowest triplet state of biphenylene, obtained by the various calculation procedures. The results are compared with the experimental values.

The results from different procedures are mutually similar and in good agreement with experience. The location for the T_1 state is the same when determined from SCF MO's associated with the 1V_0 ground configuration as when obtained from SCF MO's associated with the 3V_1 lowest triplet configuration (compare, for instance, S_{AM} and T_{AM} results). The results obtained are not much different whether or not the structural differences between secondary and tertiary carbon atoms are taken into account (cf. S_{AM} and S_{BM} results). The theoretical interpretation does not change significantly with the method used in calculating the (PP/QQ) coulombic integrals (cf. S_{AM} and S_{AP} results). The utilization of Nishimoto-Mataga integrals gives an interval separation between S_1 and T_1 states greater than the experimental separation. The utilization of Pariser and Parr type integrals, on the contrary, leads to an interval separation smaller than the experimental one (the β_{C-C} values are always adjusted¹ to reproduce the experimental location of the S_1 state by means of Nishimoto-Mataga integrals).

The dominant configuration in the first triplet state is by far the first monoexcited one $\Rightarrow V_6^7$. This may be seen, for instance, in the results obtained by the T_{AM} procedure

(7) R. Pariser and R. G. Parr, *J. Chem. Phys.*, **21**, 466 (1953).(8) K. Nishimoto and N. Mataga, *Z. Phys. Chem. (Frankfurt am Main)*, **12**, 335 (1957).(9) R. Pariser and R. G. Parr, *J. Chem. Phys.*, **21**, 767 (1953).

$$\begin{aligned}
 T_1(B_{1g}) = & 0.844^3 V_6^7 - 0.315^3 V_4^9 + \\
 & 0.291^3 V_5^8 - 0.215^3 V_3^{10} - 0.186^3 V_2^{11} + \\
 & 0.129^3 V_1^{12} + 0.053^3 V_6^{11} - 0.053^3 V_2^7 + \\
 & 0.008^3 V_1^9 - 0.008^3 V_4^{12} + \dots
 \end{aligned}$$

Like the first singlet excited state S_1 , the triplet state T_1 has the same central symmetry parity g as the ground state S_0 . Fluorescence $S_1(^1B_{1g}) \rightarrow S_0(^1A_{1g})$ and phosphorescence $T_1(^3B_{1g}) \rightarrow S_0(^1A_{1g})$ are symmetry forbidden. This behavior is essentially different from that of benzenoid hydrocarbons belonging to the same symmetry point group D_{2h} as biphenylene. For these hydrocarbons both L_a transitions are allowed: $^1L_a(^1B_{2u}) \rightarrow S_0(^1A_{1g})$ and $^3L_a(^3B_{2u}) \rightarrow S_0(^1A_{1g})$. As pointed out by Hush and Rowlands,¹⁰ each two paired MO's in biphenylene have opposite symmetry properties when compared with the polyacenes.

This particular behavior of biphenylene is imposed by the presence of the central tetragonal ring as a consequence of the general formal rule that we may establish in the following terms. "Alternant hydrocarbons belonging to the D_{2h} symmetry group are of two different symmetry character types. *Type a*—Hydrocarbons *symmetrically starred* with respect to central molecular inversion (*cf.*, biphenylene). For these hydrocarbons, bonding and antibonding paired MO's have the same symmetry character, u or g . *Type b*—Hydrocarbons *asymmetrically starred* with respect to central molecular inversion (*cf.* acenes). For these hydrocarbons, bonding and antibonding paired MO's have opposite symmetry character, u and g ." This statement is easily proved. According to the Coulson and Rushbrooke theorem,¹¹ occupied and unoccupied MO's in alternant hydrocarbons occur in pairs, ψ_i and ψ_i' . The coefficients in an occupied MO ψ_i equal those in the paired unoccupied MO ψ_i' , apart from a factor -1 for all the atoms of one set, starred or unstarred. Now, in *asymmetrically starred* alternant hydrocarbons, carbon atoms symmetric with respect to the molecular center belong to different atomic sets, starred and unstarred (Figure 3). As a consequence, when passing from an occupied MO to its paired unoccupied one, the coefficients of symmetric carbon atoms *change* their sign parity. Then, for this type of hydrocarbons, each pair of MO's ψ_i and ψ_i' , have opposite symmetry characters u and g . This is the case for polyacenes. On the contrary, in *symmetrically starred* hydrocarbons, carbon atoms symmetric with respect to the molecular center belong to the same atomic set, starred or unstarred (Figure 3). Then, by the same principle, the coefficients of symmetric carbon atoms *keep* their sign parity when passing from ψ_i to ψ_i' and, as a consequence, paired MO's have the same symmetry character u or g . This is the case for biphenylene.

B. The Triplet-Triplet $T_n \leftarrow T_1$ Spectrum of Biphenylene. Table II summarizes the $T_n \leftarrow T_1$ excitation en-

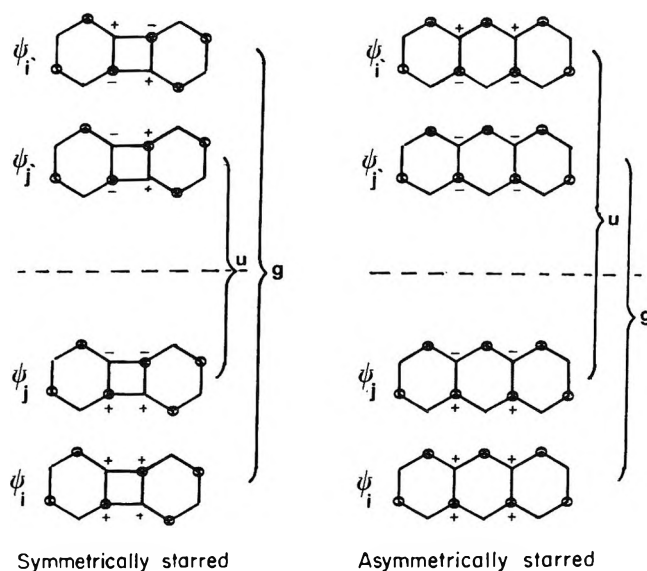


Figure 3. D_{2h} alternant hydrocarbons symmetrically and asymmetrically starred with respect to inversion. Comparison of MO symmetry properties. The signs are those of the AO coefficients in the LCAO MO development.

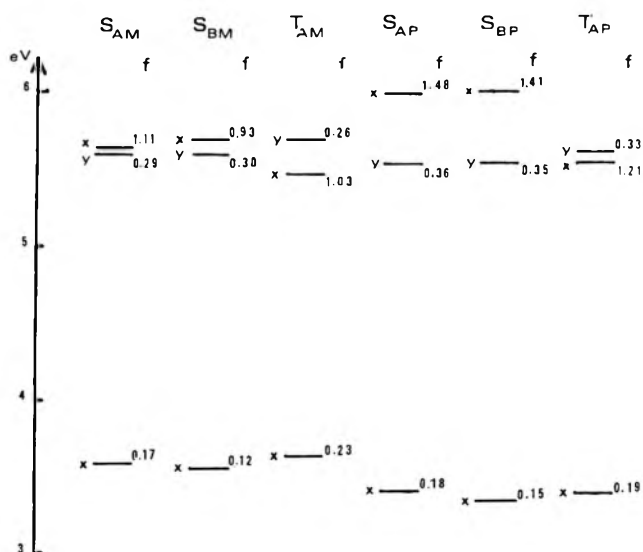


Figure 4. $T_n \leftarrow T_1$ spectrum of biphenylene, predicted by the various calculation procedures.

ergies and oscillator strengths obtained by the various calculation procedures. In Figure 4, the transitions with an oscillator strength larger than 0.1 are represented.

The predicted spectrum characteristics are as follows. In the *visible region*, the calculated oscillator strengths are smaller than 0.0005 for any triplet-triplet transition. The theory does not predict any observable transition in this spectral range. In the *uv region*, three transitions with an oscillator strength larger than

(10) N. S. Hush and J. R. Rowlands, *Mol. Phys.*, **6**, 317 (1963).

(11) C. A. Coulson and G. S. Rushbrooke, *Proc. Cambridge Phil. Soc.*, **36**, 193 (1940).

Table II: Calculated $T_n \leftarrow T_1$ Excitation Energies (eV) and Oscillator Strengths (f)

State	Sign ^a	Calculation procedure											
		S _{AM}		S _{BM}		T _{AM}		S _{AP}		S _{BP}		T _{AP}	
		eV	f	eV	f	eV	f	eV	f	eV	f	eV	f
B _{2u}	-	5.64	1.11	5.68	0.93	5.46	1.03	5.98	1.48	6.05	1.41	5.53	1.21
B _{3u}	-	5.59	0.29	5.59	0.30	5.68	0.26	5.53	0.36	5.53	0.35	5.62	0.33
B _{2u}	+	5.37	0.00	5.35	0.00	5.52	0.00	5.64	0.00	5.59	0.00	5.70	0.00
B _{1g}	+	5.31	0.00	5.30	0.00	5.55	0.00	5.55	0.00	5.54	0.00	5.80	0.00
B _{1g}	+	5.19	0.00	5.15	0.00	5.41	0.00	5.44	0.00	5.39	0.00	5.73	0.00
B _{3u}	-	5.08	0.04	5.03	0.03	5.01	0.07	4.99	0.03	4.96	0.02	4.99	0.07
A _{1g}	+	5.08	0.00	5.07	0.00	5.20	0.00	5.11	0.00	5.10	0.00	5.30	0.00
B _{2u}	-	4.87	0.04	4.85	0.04	4.89	0.00	5.00	0.02	4.98	0.03	5.15	0.00
B _{1g}	-	4.50	0.00	4.54	0.00	4.61	0.00	4.55	0.00	4.62	0.00	4.75	0.00
B _{2u}	+	4.48	0.00	4.46	0.07	4.33	0.00	4.75	0.00	4.75	0.10	4.36	0.00
A _{1g}	-	4.37	0.00	4.32	0.00	4.49	0.00	4.23	0.00	4.19	0.00	4.37	0.00
B _{1g}	+	4.34	0.00	4.23	0.00	4.57	0.00	4.49	0.00	4.35	0.00	4.61	0.00
B _{3u}	+	4.17	0.00	4.14	0.00	4.25	0.00	4.49	0.00	4.42	0.00	4.43	0.00
B _{2u}	-	3.58	0.17	3.55	0.12	3.64	0.23	3.42	0.18	3.35	0.15	3.41	0.19
B _{2u}	+	3.49	0.00	3.48	0.03	3.33	0.00	3.52	0.00	3.54	0.01	3.50	0.00
B _{3u}	+	3.27	0.00	3.28	0.00	3.06	0.00	3.29	0.00	3.29	0.00	3.21	0.00
A _{1g}	+	3.03	0.00	3.04	0.00	2.87	0.00	3.07	0.00	3.07	0.00	3.02	0.00
A _{1g}	-	2.90	0.00	2.87	0.00	2.87	0.00	2.32	0.00	2.38	0.00	2.32	0.00
B _{3u}	-	2.33	0.00	2.38	0.00	2.35	0.00	1.81	0.00	1.94	0.00	1.85	0.00
B _{1g}	+	2.29	0.00	2.28	0.00	2.41	0.00	2.22	0.00	2.20	0.00	2.48	0.00
B _{2u}	+	2.07	0.00	2.04	0.00	2.29	0.00	1.94	0.00	1.92	0.00	2.17	0.00
A _{1g}	+	1.83	0.00	1.79	0.00	1.95	0.00	1.72	0.00	1.64	0.00	1.81	0.00
B _{1g}	+	1.78	0.00	1.76	0.00	1.92	0.00	1.66	0.00	1.64	0.00	1.81	0.00
B _{3u}	+	1.43	0.00	1.32	0.00	1.65	0.00	1.25	0.00	1.08	0.00	1.47	0.00
B _{2u}	+	0.75	0.00	0.73	0.00	0.82	0.00	0.89	0.00	0.86	0.00	1.03	0.00
B _{1g}		0.00	Ref.	0.00	Ref.	0.00	Ref.	0.00	Ref.	0.00	Ref.	0.00	Ref.

^a According with Pariser nomenclature.¹²

0.1 are predicted. The lowest transition is long axis polarized, of the type ${}^3B_{2u} \leftarrow {}^3B_{1g}$. It appears located between 3.35 and 3.65 eV. Its oscillator strength varies between 0.11 and 0.23, depending on the calculation procedure. A second very strong transition, of the same type, is predicted between 5.46 and 6.05 eV. Its oscillator strength varies between 0.93 and 1.41. Finally, a short axis polarized transition, of the type ${}^3B_{3u} \leftarrow {}^3B_{1g}$, is located between 5.53 and 5.68 eV. Its oscillator strength is of the order of 0.30.

It is clear from these results that the theoretical predictions do not change significantly with the different models and procedures used in the evaluation of the wave functions. The spectral characteristics are practically the same when obtained either from SCF MO's minimizing the lowest triplet configuration 3V_6 energy (T procedures), or from SCF MO's minimizing the ground configuration 1V_0 energy (S procedures). The introduction (B models) of the difference $\Delta W_C' = W_6' - W_1' = 1.00$ eV, that removes the strict pairing properties, does not change the general trend of the spectrum. The oscillator strengths of the so-called "+ transitions,"¹² now not rigorously zero, remain extremely weak in general and in any case their value is larger than 0.1. The theoretical predictions are not significantly modified when Pariser-Parr Coulombic integrals are used instead of Nishimoto-Mataga ones.

The influence of the degree of configurational interaction is illustrated in Figure 5. In this figure, the results obtained for the allowed ${}^3B_{2u} \leftarrow {}^3B_{1g}$ and ${}^3B_{3u} \leftarrow {}^3B_{1g}$ transitions by the T_{AM} procedure are represented as an example. When passing from one step to the other, the number of intense transitions remains the same. The relative energy spacing between transitions is very slightly modified by the introduction of biexcited configurations. On the contrary, these configurations have a great effect on the relative and absolute values of the intense transition oscillator strengths.

C. *The $S_n^{2-} \leftarrow S_0^{2-}$ Spectrum of Biphenylene Dinegative Ion.* As predicted theoretically by Hoijtink,¹³ the electronic absorption spectra $T_n \leftarrow T_1$ of alternant hydrocarbons in their lowest triplet state look very much like the $S_n^{2-} \leftarrow S_0^{2-}$ spectra of their respective dinegative ions. Both spectra appear to have a similar number of bands, with identical polarization, and about the same relative intensities. The frequency of the $S_n^{2-} \leftarrow S_0^{2-}$ bands of the ion presents a bathochromic shift with respect to the bands in the $T_n \leftarrow T_1$ spectrum of the molecule. Using this resemblance, it is then possible to make a fairly reliable estimate of the general features of the $T_n \leftarrow T_1$ biphenylene spectrum on the

(12) R. Pariser, *J. Chem. Phys.*, **24**, 250 (1956).

(13) G. J. Hoijtink, *Pure Appl. Chem.*, **11**, 393 (1965).

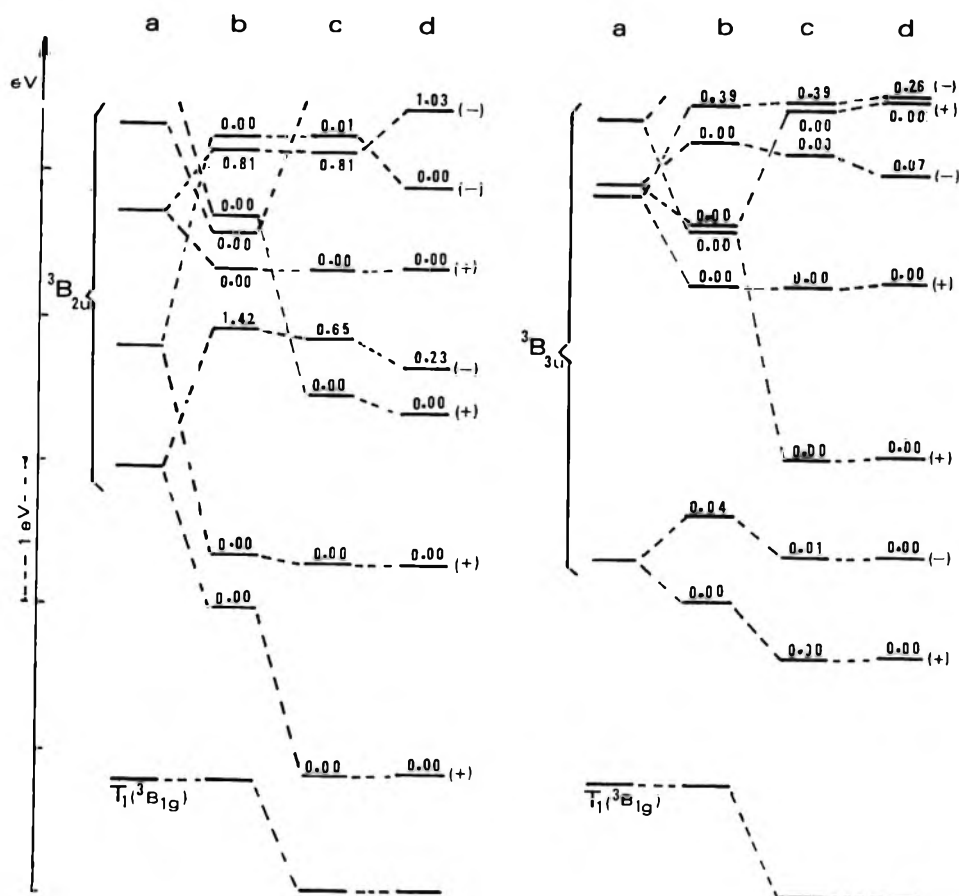


Figure 5. Steps in IC calculation. Results obtained by the T_{AM} procedure for the ${}^3B_{2u} \leftarrow {}^3B_{1g}$ and ${}^3B_{3u} \leftarrow {}^3B_{1g}$ allowed transitions. The numbers represent oscillator strength values: a, results before IC; b, first-order IC between degenerate levels; c, results after interaction with configurations monoexcited with respect to the ground V_0 configuration; d, final results, including biexcited configurations.

basis of the experimental spectrum of the dinegative ion. This can be done as a test of the previous theoretical prediction. The theoretical interpretation of the nature and properties of the observed absorption bands of the dinegative biphenylene ion are presented first.

a. Theoretical Interpretation of the Biphenylene Dinegative Ion Spectrum. The calculation procedures S_{AM} , S_{BM} , and S_{AP} , previously described, are used in this study. A new procedure, the S_{AM}^{2-} , is also utilized. In this procedure the ground and excited wave functions are built with SCF MO's obtained by minimizing the energy of the ion ground configuration ${}^1V_0^{2-}$. The interaction calculation includes all possible monoexcited configurations, together with those obtained by biexcitations from the two highest occupied to the two lowest unoccupied MO's in the ion.

Table III summarizes the excitation energies and oscillator strengths obtained by the four procedures considered. The results are compared with the experimental values. The theory gives a satisfactory explanation of the two bands observed. Both can be assigned to ${}^1B_{2u} \leftarrow {}^1A_{1g}$ transitions and are long axis polarized. A third, ${}^1B_{2u} \leftarrow {}^1A_{1g}$, short axis polarized tran-

sition is also predicted. It appears to be located about 0.25 eV higher than the strongest ${}^1B_{3u} \leftarrow {}^1A_{1g}$ band, which probably hides it. This transition is probably the origin of the weak shoulder observed on the high frequency side of the strongest absorption band.

Neither the utilization of the dinegative ion MO's, nor the distinction between secondary and tertiary carbon atoms, leads to any significant change in the theoretical interpretation of the spectrum. The relative energy level spacing and the absolute energy values are better estimated when Coulombic integrals are evaluated by the Nishimoto-Mataga procedure.

b. The $T_n \leftarrow T_1$ Spectrum of Biphenylene As Estimated from the $S_n^{2-} \leftarrow S_0^{2-}$ Spectrum of the Dinegative Ion. We shall now estimate the general features of the $T_n \leftarrow T_1$ biphenylene spectrum from the expected resemblance to the absorption spectrum of its dinegative ion. To do this it is assumed that the blue shift of the biphenylene $T_n \leftarrow T_1$ bands, with respect to the corresponding bands of the dinegative ion, is equal to 0.9 eV. This is the order of magnitude of the mean shift observed for the alternant hydrocarbons when both spectra are experimentally known.¹³ Such an estimate implies the existence, for the triplet-triplet spectrum of

Table III: Calculated $S_n^{2-} \leftarrow S_0^{2-}$ Spectrum of the Dinegative Ion of Biphenylene

State	S_{AM}		S_{BM}		Calculation procedure				Experience ^a	
	eV	f	eV	f	S_{AP}	f	S_{AM}^{2-}	f	eV	f
A_{1g}	4.98	0.00	5.12	0.00	5.14	0.00	4.82	0.00		
B_{1g}	4.79	0.00	4.48	0.00	5.09	0.00	4.37	0.00		
B_{2u}	4.24	0.26	4.13	0.26	4.09	0.23	4.25	0.23
B_{3u}	4.01	1.93	3.98	2.04	4.59	2.02	4.00	2.13	3.59	0.81
A_{1g}	3.60	0.00	3.43	0.00	3.98	0.00	3.47	0.00		
B_{3u}	2.55	0.44	2.38	0.43	2.61	0.37	2.41	0.39	2.55	0.02
B_{1g}	2.19	0.00	2.12	0.00	2.41	0.00	2.04	0.00		
A_{1g}	1.96	0.00	1.46	0.00	2.13	0.00	1.89	0.00		
B_{2u}	1.03	0.00	0.77	0.00	1.27	0.00	0.90	0.01		
A_{1g}	0.00	Ref.	0.00	Ref.	0.00	Ref.	0.00	Ref.		

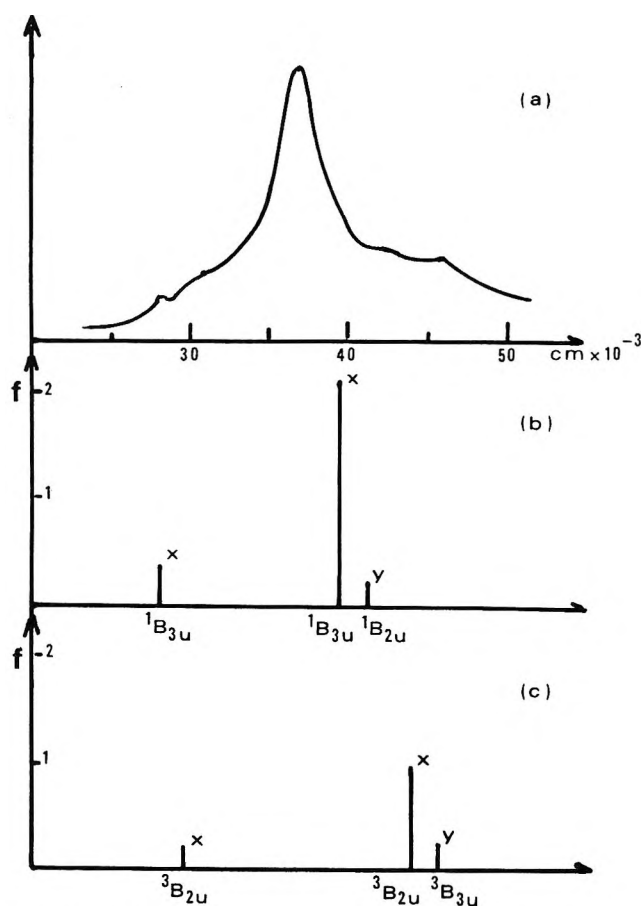
^a Reference 10.

Figure 6. Estimated $T_n \leftarrow T_1$ spectrum of biphenylene: a, the estimated spectrum, from the dinegative ion experimental spectrum¹⁰ shifted to the blue by 7200 cm^{-1} ; b, the estimated spectrum, from the theoretical dinegative ion spectrum shifted to the blue by 7200 cm^{-1} ; c, $T_n \leftarrow T_1$ spectrum of biphenylene calculated by the T_{AM} procedure.

biphenylene, of a moderately intense ${}^3B_{2u} \leftarrow {}^3B_{1g}$ transition, located at about 3.4 eV. A second, very intense, ${}^3B_{2u} \leftarrow {}^3B_{1g}$ transition, located at about 4.4 eV, is also predictable. Finally, the existence of an experimentally hidden ${}^3B_{3u} \leftarrow {}^3B_{1g}$ transition, located at about 4.7

eV, should also be expected. The general features of the $T_n \leftarrow T_1$ spectrum of biphenylene can be estimated, in a similar way, from the calculated $S_n^{2-} \leftarrow S_0^{2-}$ absorption spectrum of the ion. The results of both estimates are compared in Figure 6 with the theoretical prevision previously obtained by the T_{AM} procedure.

The three predictions are very similar. The number and nature of the transitions are the same. The relative intensities and energy range of the bands are also similar. The agreement concerning the lowest ${}^3B_{3u} \leftarrow {}^3B_{1g}$ transition is very good. It may be concluded that the lowest triplet-triplet transition is located between 3.2 and 3.6 eV. Concerning the other bands, we can assume, from these results, the existence of a ${}^3B_{2u} \leftarrow {}^3B_{1g}$ transition, approximately localized in the 5.00-eV region, about ten times as intense as the first transition. This strong transition probably hides a short axis polarized ${}^3B_{3u} \leftarrow {}^3B_{1g}$ band.

Conclusions

The theoretical location of the first triplet state of biphenylene agrees with the determination of Evans using oxygen perturbation techniques.⁵ The triplet state has ${}^3B_{1g}$ symmetry and, by consequence, the phosphorescence is symmetry forbidden. This is also the case for the fluorescence in biphenylene. Because of the central tetragonal ring, biphenylene belongs to the "symmetrically starred" D_{2h} alternant hydrocarbons group. We have proved that, for this type of hydrocarbon, transitions between ground state and any level having a V_i^{n-i+1} component configuration (n = number of π electrons) are symmetry forbidden. Our results, as well as those of Evans, are not consistent with the assignment of the two emissions observed,⁴ in boric acid solution, to biphenylene fluorescence and phosphorescence. In fact, the observed short-lived emission has not even approximate mirror symmetry with the $S_1 \leftarrow S_0$ absorption band. On the other hand, the broad band attributed to phosphorescence starts ap-

proximately at 2.60 eV with a maximum at 2.36 eV. The absorption spectrum is only slightly altered in boric acid. Then, according to Evans' results, the phosphorescence, if present, should be expected to occur at least 3000 cm^{-1} farther in the red.

The semiempirical SCF method used provides a satisfactory interpretation of all of the observed properties: the singlet-singlet absorption spectra of biphenylene¹ and of its dinegative ion, and the location of the first triplet of the molecule. The predicted properties for the triplet-triplet spectrum of biphenylene are independent of the calculation procedures used. Moreover, the predicted $T_n \leftarrow T_1$ characteristics are in agreement with those estimated from their expected similarity with the absorption spectrum of the biphenylene dinegative ion. All this allows a reasonable confidence on the predictions concerning the triplet-triplet spectrum of biphenylene and makes possible a discussion of the resulting consequences.

In the visible, no triplet-triplet transition is predicted. This is in agreement with the negative experimental results in this region.

In the uv region, the lowest observable transition is calculated between 3.2 and 3.6 eV. This band would then lie under the 1L_b band of the $S_n \leftarrow S_0$ absorption spectrum, which makes experimental measurements very difficult. The same can be said for the second transition of the ${}^3B_{2u} \leftarrow {}^3B_{1g}$ type. If, as predicted, this transition has an energy above 5.00 eV, then it is situated in the region of the very intense 1B_b band of the $S_n \leftarrow S_0$

absorption spectrum and consequently cannot be observed.

In conclusion, the only intense calculated bands are located in regions where it seems to be rather difficult to detect them; on the other hand, no significant absorption is to be expected in the experimentally accessible energy range. Since the knowledge of the triplet state lifetime is of crucial importance as regards the extent of radiationless deactivation in biphenylene, the present results should stimulate further experimental investigation in the uv with improved techniques.

In the case of other alternant hydrocarbons, direct $S_1 \rightarrow S_0$ radiationless transitions have been shown to be of minor importance, except perhaps for the case of very low-lying first singlet states. The biphenylene first singlet and triplet states are at energy locations similar to those of anthracene, for example, so that an effective radiationless deactivation process does not seem possible in terms of pure energy grounds (energy gap law). It is difficult to imagine the mechanism responsible for the absence of emission, in organic solvents at low temperature, for a biphenylene molecule remaining undeformed in the excited state. Hochstrasser pointed out several experimental facts⁶ suggesting a change of shape of the molecule after excitation. A change of geometry is generally thought to be favorable to radiationless transitions. At the present time we are working out the theoretical implications of distortion in the excited state in the deactivation of biphenylene.

A Molecular Orbital Calculation of Chemically Interacting Systems.

Bimolecular Nucleophilic Substitution

by Kenichi Fukui,* Hiroshi Fujimoto, and Shinichi Yamabe

Faculty of Engineering, Kyoto University, Sakyo-ku, Kyoto, Japan (Received February 16, 1971)

Publication costs assisted by Kyoto University

A semiempirical valence-shell molecular orbital (MO) calculation on the mode of chemical interaction in the bimolecular nucleophilic substitution reaction of methyl chloride has been carried out. The wave function of the combined system of two reacting species is derived using the configuration interaction (CI) procedure for the charge-transferred and polarized electron configurations. The wave function for each electron configuration is constructed from the antisymmetrized product of the MO's for a self-consistent field (SCF) with respect to each of the two reacting species in the isolated ground state. The interaction energy has been partitioned into the Coulomb, exchange, delocalization, and polarization terms. The Coulomb term was found to play a dominant role in the long-range interactions, while the exchange and delocalization interaction terms were calculated to grow rapidly with the progress of the reaction. The changes in the electron populations due to chemical interaction are calculated from the ground-state CI wave function. The delocalization interaction was found to be important in interpreting the intermolecular chemical bond formation as well as intramolecular chemical bond weakening.

Introduction

Some attempts have been made to interpret quantitatively the chemical interaction energy between two interacting systems by the use of wave functions obtained for the two reactants in an isolated state.¹⁻⁷ Murrell and coworkers extended the theory of long-range interaction to the region of small orbital overlap and expanded the energy as a power series in intermolecular potential and overlap integrals.¹ Although Murrell included charge-transfer energy, he suggested that the contribution of the term was rather small in comparison with the polarization term for the systems to which he would apply the theory.⁸ Discussion was also made by Murrell of approximate methods for estimating the exchange energy in terms of overlap integral and interatomic distance.⁹ To represent the deformation of the ground-state wave function of the combined system of two interacting reactants from that of the isolated state, a configuration interaction procedure was used for the initial, charge-transferred and locally excited electron configurations. The interaction energy was partitioned into Coulomb, exchange, delocalization, and polarization interaction terms, and succinct expressions of these were derived.⁵ From an examination of the magnitudes of the matrix elements, it appears that the contribution of charge-transferred states is important in interpreting the interaction energy between reactant and reagent in a majority of chemically reacting systems. As a means of elucidating the contribution of various charge-transfer and polarization interaction terms, we represented the energy difference between the initial state and a charge-transferred state and that between the initial state and

a locally excited state in terms of the ionization potentials and electron affinities of the two reactants. Studying the charge-transfer interaction terms, we arrived at the conclusion that the charge-transfer interaction between the highest occupied (HO) MO of one reactant and the lowest unoccupied (LU) MO of the other is usually the most important among the various charge-transferred configurations,¹⁰ in conformity with our previously proposed reaction model for deriving the chemical reactivity index, frontier electron density.¹¹ The important role of the charge-

(1) (a) J. N. Murrell, M. Randić, and D. R. Williams, *Proc. Roy. Soc., Ser. A*, **284**, 566 (1965); (b) J. N. Murrell and G. Shaw, *J. Chem. Phys.*, **46**, 1768 (1967).

(2) R. Rein and M. Pollak, *ibid.*, **47**, 2039 (1967).

(3) G. Klopman, *J. Amer. Chem. Soc.*, **90**, 223 (1968).

(4) L. Salem, *ibid.*, **90**, 543, 553 (1968).

(5) K. Fukui and H. Fujimoto, *Bull. Chem. Soc. Jap.*, **41**, 1989 (1968).

(6) M.-J. Hulon and P. Claverie, *Chem. Phys. Lett.*, **4**, 429 (1969), and the references cited therein.

(7) P. D. Dacre and R. McWeeny, *Proc. Roy. Soc., Ser. A*, **317**, 435 (1970), and the references cited therein.

(8) See, for instance, F. B. van Duijneveldt and J. N. Murrell, *J. Chem. Phys.*, **46**, 1759 (1967).

(9) J. N. Murrell and J. J. C. Teixeira-Dias, *Mol. Phys.*, **19**, 521 (1970). See also, M. W. Hanna, *J. Amer. Chem. Soc.*, **90**, 285 (1968); J. L. Lippert, M. W. Hanna, and P. J. Trotter, *ibid.*, **91**, 4035 (1969); E. G. Cook, Jr., and J. C. Schug, *J. Chem. Phys.*, **53**, 723 (1970).

(10) K. Fukui and H. Fujimoto, *Bull. Chem. Soc. Jap.*, **42**, 3399 (1969).

(11) (a) K. Fukui, "Molecular Orbitals in Chemistry, Physics, and Biology," P.-O. Löwdin and B. Pullman, Ed., Academic Press, New York, N. Y., 1964, and references cited therein; (b) K. Fukui, "Sigma Molecular Orbital Theory," O. Sinanoğlu and K. B. Wiberg, Ed., Yale University Press, New Haven, Conn., 1970; (c) K. Fukui *Fortschr. Chem. Forsch.*, **15**, 1 (1970).

transfer interaction between these particular orbitals in determining the favorable position and spatial direction of chemical reaction has also been confirmed by Woodward and Hoffmann,¹² Klopman,³ Salem,^{4,13} and Pearson.¹⁴ Recently, Devaquet and Salem¹⁵ and Sustmann and Binsch¹⁶ devised methods to obtain the SCF energy of the combined system of two reactants from the MO's of the two fragments by the use of perturbation theory. They obtained fair results in predicting the steric course in Diels-Alder reactions by the employment of semiempirical MO wave functions.

In the present paper, we will show how our method of calculation distinguishes the favorable path of a given reaction. The reaction chosen for illustration is the bimolecular nucleophilic substitution of methyl chloride in which the attacking base is a chloride ion, for the sake of simplicity of calculation.

Interaction Energy

We make here a brief mention of the general features of our method of calculating the interaction energy.⁵ The lowest energy state of the combined system of two interacting species, say A and B, is represented by a configuration interaction wave function

$$\psi = C_0\psi_0 + \sum_i^{\text{occ}} \sum_l^{\text{uno}} C_{i \rightarrow l} \psi_{i \rightarrow l} + \sum_k^{\text{occ}} \sum_j^{\text{uno}} C_{k \rightarrow j} \psi_{k \rightarrow j} + \sum_i^{\text{occ}} \sum_j^{\text{uno}} C_{i \rightarrow j} \psi_{i \rightarrow j} + \sum_k^{\text{occ}} \sum_l^{\text{uno}} C_{k \rightarrow l} \psi_{k \rightarrow l} + \dots \quad (1)$$

where ψ_0 represents the initial state in which neither electron transfer nor electron excitation takes place, $\psi_{i \rightarrow l}$ stands for the charge-transferred state in which one electron in the i th occupied MO of A is transferred into the l th unoccupied MO of B, and $\psi_{i \rightarrow j}$ corresponds to the state in which one electron in the i th MO is elevated to the j th unoccupied MO of A due to the interaction with B. The normalized wave functions of the combined system $\psi_0, \psi_{i \rightarrow l}, \dots$ are represented in terms of the Slater determinants, composed of orthonormal spin orbitals with LCAO MO spatial functions of A and those of B, which are made SCF with respect to the ground state of each isolated molecule. To a first approximation, we take here only monotr transferred and monoexcited electron configurations. Then, the lowest singlet interaction energy, ΔW , between two closed-shell systems is approximately given by

$$\Delta W = \epsilon_Q + \epsilon_K - D - \pi \quad (2)$$

where ϵ_Q is the Coulomb interaction energy, ϵ_K is the exchange interaction energy. The delocalization interaction energy D and the polarization interaction energy π are approximately expanded in the second-order perturbation forms, provided that the interaction is not yet very strong.

$$D = \sum_i^{\text{occ}} \sum_l^{\text{uno}} \frac{|H_{0,i \rightarrow l} - S_{0,i \rightarrow l} H_{0,0}|^2}{H_{i \rightarrow l, i \rightarrow l} - H_{0,0}} + \sum_k^{\text{occ}} \sum_j^{\text{uno}} \frac{|H_{0,k \rightarrow j} - S_{0,k \rightarrow j} H_{0,0}|^2}{H_{k \rightarrow j, k \rightarrow j} - H_{0,0}} \quad (3)$$

$$\pi = \sum_i^{\text{occ}} \sum_j^{\text{uno}} \frac{|H_{0,i \rightarrow j} - S_{0,i \rightarrow j} H_{0,0}|^2}{H_{i \rightarrow j, i \rightarrow j} - H_{0,0}} + \sum_k^{\text{occ}} \sum_l^{\text{uno}} \frac{|H_{0,k \rightarrow l} - S_{0,k \rightarrow l} H_{0,0}|^2}{H_{k \rightarrow l, k \rightarrow l} - H_{0,0}} \quad (4)$$

Calculation on Isolated Systems

A semiempirical SCF method which includes all valence electrons is employed to obtain the wave function of a system composed of methyl chloride and chloride ion. The approximations employed are almost the same as the method developed by Yonezawa and co-workers.¹⁷ The results of calculation of the MO energies are shown in Figure 1. The calculated ionization potentials of methyl chloride and chloride ion are 11.45 and 3.47 eV, respectively, in good agreement with the observed values, 11.28 and 3.75 eV (the electron affinity of atomic chlorine).¹⁸

The LUMO of methyl chloride is an antibonding MO with a_1 symmetry belonging to the C_{3v} point group, having maximum extension at the carbon atom in the direction of the carbon-chlorine bond axis. In Figure 2 are shown atomic populations of methyl chloride and chloride ion in the isolated state. The values in parentheses indicate the atomic bond populations.

Calculation of Interaction Energy

For the purpose of calculating the intermolecular interaction energy, we adopted somewhat different choices of integrals from those in isolated systems. The electron repulsion integral $(tt|uu)$ ($= \iint \int t(1)u(2)e^2/r_{12}t(1)u(2)dv(1)dv(2)$) was simply put equal to $e^2/R_{\alpha\beta}$, where $R_{\alpha\beta}$ is the distance between the two nuclei α of the system A, and β of the system B, to which the AO's t and u belong. The core attraction integral $v_{\gamma u}$ ($= \int t(1)(-Z_{\gamma}e^2/r_{\gamma 1})t(1)dv(1)$) was taken equal to $-Z_{\gamma}e^2/R_{\gamma\gamma'}$ when the AO t belongs to the nucleus γ' ($\gamma \neq \gamma'$), while it was calculated using the

(12) (a) R. B. Woodward and R. Hoffmann, *J. Amer. Chem. Soc.*, **87**, 2511 (1965); (b) R. Hoffmann and R. B. Woodward, *ibid.*, **87**, 4388 (1965); (c) R. B. Woodward and R. Hoffmann, "The Conservation of Orbital Symmetry," Academic Press, New York, N. Y., 1969.

(13) L. Salem, *Chem. Brit.*, **5**, 449 (1969).

(14) R. G. Pearson, *Theor. Chim. Acta*, **16**, 107 (1970).

(15) (a) A. Devaquet and L. Salem, *J. Amer. Chem. Soc.*, **91**, 3793 (1969); (b) A. Devaquet, *Mol. Phys.*, **18**, 233 (1970).

(16) R. Sustmann and G. Binsch, *ibid.*, **20**, 1, 9 (1971).

(17) (a) T. Yonezawa, K. Yamaguchi, and H. Kato, *Bull. Chem. Soc. Jap.*, **40**, 536 (1967); (b) H. Kato, H. Konishi, H. Yamabe, and T. Yonezawa, *ibid.*, **40**, 2761 (1967). The Wolfsberg-Helmholtz parameter K was put equal to 1.12 for the carbon 2s-chlorine 3s bond and 1.08 for others.

(18) (a) K. Watanabe, *J. Chem. Phys.*, **26**, 542 (1957); (b) T. L. Bailey, *ibid.*, **28**, 792 (1958).

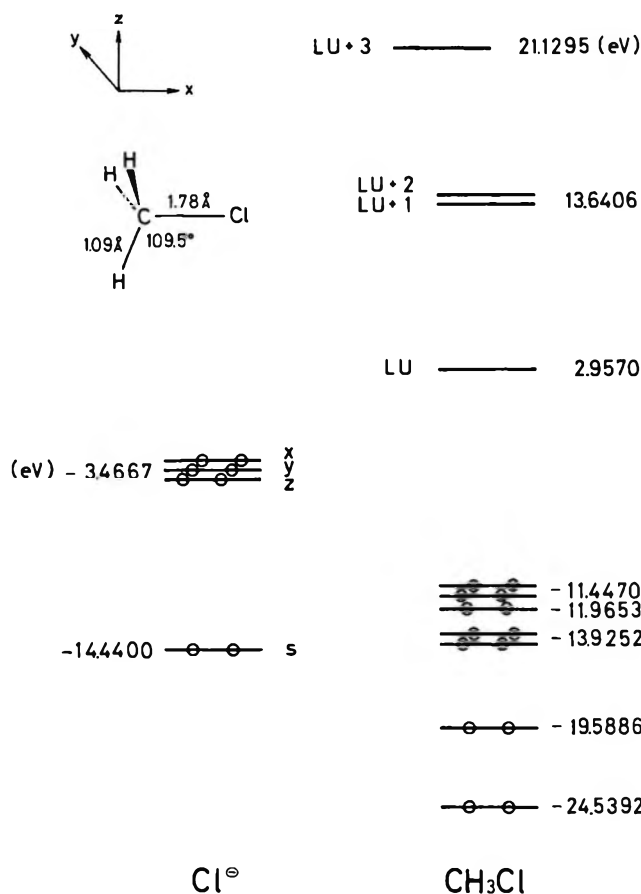


Figure 1. MO energy levels of methyl chloride and chloride ion.

Slater AO's when the center of the AO t coincided with that of the nucleus γ . With such approximated integrals, the four energy terms were calculated using the Mulliken approximation.¹⁹ In Table I are presented the results of calculation with respect to the four models shown in Figure 3. Although the models are only arbitrarily set up and the method of calculation is very crude, we can see essential features of the changes in the energy terms as the chemical reaction progresses. In the early stage of the interaction, the Coulomb interaction term ϵ_Q appears to be almost solely responsible for the stabilization. On going from model I to model III, the exchange interaction term ϵ_K rapidly increases. Thus, the stabilization due to the delocalization and polarization terms becomes increasingly important with the progress of the reaction. The polarization term appears to be less important than the delocalization term as the interaction between the reactant and the reagent becomes strong. Models III and IV can hardly be regarded as reproducing the species which are actually reacting; however, the results of our calculations seem to suggest that the inversion process must have a lower activation energy than the retention process, in general. In models I-IV the nuclear framework of methyl chloride has been kept unchanged, since the charge-transfer interaction

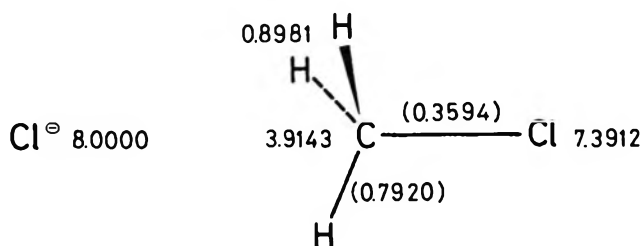


Figure 2. The atomic populations and atomic bond populations in methyl chloride and chloride ion.

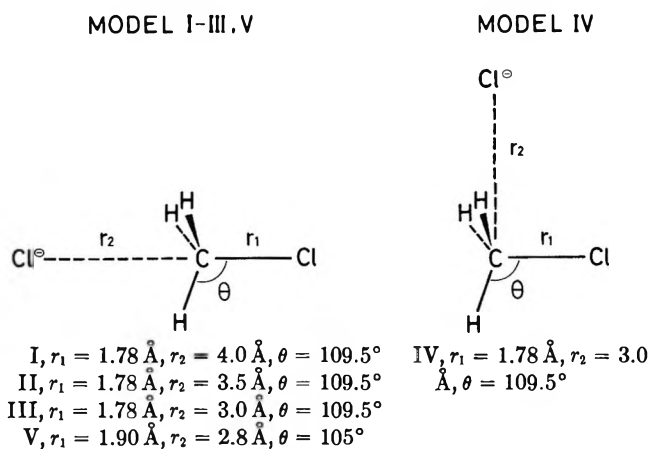


Figure 3. Assumed reaction models.

is supposed to be not yet so strong as to bring about considerable molecular deformation. In reality, the geometry of the reactant will gradually vary as the reaction proceeds. The interaction energy and the destabilization energy due to the deformation of the framework from the stationary equilibrium point will be important parts of the energy change of the system due to the interaction.

Table I: Calculated Interaction Energies

	Model I	Model II	Model III	Model IV
ϵ_Q , eV	-0.498	-0.619	-0.788 (-0.788)	-0.259
ϵ_K , eV	0.033	0.205	1.164 (0.726)	1.593
D , eV	0.027	0.150	1.053 (0.581)	0.311
π , eV	0.067	0.105	0.176 (0.176)	0.129

The way of choosing the integrals employed in this calculation is a crude one and requires further tests. We find a problem in the balance between one-center core attraction and one-center electron repulsion integrals. As mentioned before, the former was calculated nonempirically by the Slater AO's, while the

(19) R. S. Mulliken, *J. Chim. Phys.*, **46**, 497 (1949).

latter was approximated by the Pariser-Parr scheme.¹⁷ Another calculation was therefore made, modifying the one-center core attraction integral, v_{att} in such a way as to make the quantity $(v_{att} + \sum_{t'}^{\alpha} n_{t'}(t't'|t't'))$ give the same value for the semiempirically estimated electron repulsion integrals as that calculated theoretically, where $n_{t'}$ is the occupation number of the AO t' belonging to the atom α . The calculated results for model III are given in parentheses in Table I. Although ϵ_K and D decrease to some extent in comparison with the previous calculation, we see that the change in the sum of the four terms is relatively small. Murrell and Teixeira-Dias proposed some convenient methods of estimating the exchange interaction energies of two hydrogen atoms in the 2s, 2p, and hybrid valence states.⁹ In the present study, however, we evaluated all four energy terms by use of the Mulliken approximation,¹⁹ in order to be consistent with the calculations for isolated systems. The energy values presented here are unquestionably far from being quantitative. They should rather be regarded as only giving some information about the relative changes in energy with the variation in location of the attacking chloride ion.

Electron Populations

It is interesting to see how the CI wave function, eq 1, represented in terms of MO's of two isolated reactants, interprets the most characteristic phenomenon of this reaction, *i.e.*, electron transfer from the anion to methyl chloride and bond interchange due to the interaction. Here, we may tentatively neglect the polarization terms in obtaining the wave functions, since they are supposed to have little influence upon the intermolecular charge transfer. The coefficients $C_0, C_{i \rightarrow l}, \dots$, of the ground-state wave function of the combined system are given in Table II, with respect to two models. We have normalized the wave function with respect to the second order of overlap integrals of the MO's of two reactants. It seems clear in both models that the most important term except ψ_0 is the state where one electron is transferred from the $3p_x$ orbital of chloride ion into the LUMO of methyl chloride, paralleling the direction of the interaction. The increase in the magnitude of the contribution of the $\psi_{3p_x \rightarrow LU}$ state in model V in comparison with model III is mainly due to the lowering of the LUMO energy of methyl chloride, caused by the stretching of the carbon-chlorine bond from 1.78 to 1.90 Å, in conformity with our previous calculation.²⁰ The charge transfer into the LUMO, having an antibonding nature, will weaken the bond and the stretching of that bond will cause the lowering of the LUMO energy, which, in turn, will promote further mixing in of the charge-transferred state. The interaction would be self-accelerated in this manner.

Table II: The Coefficients of the Ground-State CI Wave Functions

	$C_{i \rightarrow l}$			
	LU	LU + 1	LU + 2	LU + 3
Model III, $C_0 = 0.9277$				
s	0.0769	0	0	0.0222
x	0.2968	0	0	0.0007
y	0	0.0009	0.0301	0
z	0	0.0301	0.0009	0
Model V, $C_0 = 0.8230$				
s	0.1072	0	0	0.0061
x	0.4771	0	0	0.0297
y	0	0.0005	0.0199	0
z	0	0.0199	0.0005	0

To obtain electron populations, it is convenient to get the diagonal element of the first-order spinless density matrix²¹ of ψ

$$\rho(1|1) = M \int \psi^*(1, 2, \dots, M) \times \psi(1, 2, \dots, M) d\xi_1 d\tau_2 \dots d\tau_M \quad (5)$$

where M is the total number of electrons. This is a straightforward procedure and details are not shown here. The electrons of the systems A and B can populate the intermolecular region between A and B through the overlapping of the AO t of A and the AO u of B, in the case of chemical interaction. Collecting the terms represented by an intermolecular AO pair t and u , after integrating $\rho(1|1)$ over all space, we get the AO bond population ϕ_{tu} of a bond newly formed between these two AO's.

$$\begin{aligned} \phi_{tu} \cong & \left\{ -4C_0^2 N_0^2 \sum_i^{\text{occ}} \sum_k^{\text{occ}} c_t^{(i)} c_u^{(k)} s_{tu} S_{ik} (M!) + \right. \\ & \sum_i^{\text{occ}} \sum_l^{\text{uno}} C_{i \rightarrow l}^2 N_{i \rightarrow l}^2 (-4 \sum_{i'}^{\text{occ}} \sum_k^{\text{occ}} c_t^{(i')} c_u^{(k)} s_{tu} S_{i'k} + \\ & 2 \sum_k^{\text{occ}} c_t^{(i)} c_u^{(k)} s_{tu} S_{ik} - 2 \sum_{i'}^{\text{occ}} c_t^{(i')} c_u^{(l)} s_{tu} S_{i'l} + \\ & 4c_t^{(i)} c_u^{(l)} s_{tu} S_{il}) (M!) + \\ & \sum_k^{\text{occ}} \sum_j^{\text{uno}} C_{k \rightarrow j}^2 N_{k \rightarrow j}^2 (-4 \sum_i^{\text{occ}} \sum_{k'}^{\text{occ}} c_t^{(i)} c_u^{(k')} s_{tu} S_{ik'} + \\ & 2 \sum_i^{\text{occ}} c_t^{(i)} c_u^{(k)} s_{tu} S_{ik} - 2 \sum_{k'}^{\text{occ}} c_t^{(j)} c_u^{(k')} s_{tu} S_{jk'} + \\ & 4c_t^{(j)} c_u^{(k)} s_{tu} S_{jk}) (M!) \left. \right\} + 2\sqrt{2}C_0 \left(\sum_i^{\text{occ}} \sum_l^{\text{uno}} C_{i \rightarrow l} c_t^{(i)} c_u^{(l)} s_{tu} + \right. \\ & \left. \sum_k^{\text{occ}} \sum_j^{\text{uno}} C_{k \rightarrow j} c_t^{(j)} c_u^{(k)} s_{tu} \right) \quad (6) \end{aligned}$$

(20) H. Kato, K. Morokuma, T. Yonezawa, and K. Fukui, *Bull. Chem. Soc. Jap.*, **38**, 1749 (1965). Due to the lowering of the LUMO energy, the energy difference between the ψ_0 and $\psi_{3p_x \rightarrow LU}$ states is so small in model V that the second-order expansion of the energy D is no longer realistic. MO overlap integrals are still less than 0.1.

(21) R. McWeeny, *Proc. Roy. Soc., Ser. A*, **223**, 63 (1954); **232**, 114 (1955). See also ref 7.

where N is the normalization factor, $c_t^{(i)}$ is the coefficient of the t th AO in the i th MO, s_{tu} represents the overlap integral between AO's, and S_{ik} indicates that between MO's. The first term is usually negative,²² arising from the exchange interaction between A and B, while the second term represents the AO bond population due to delocalization and is generally positive for the newly formed bond in the ground state. When the negative AO bond population of the intermolecular AO pair t and u due to the exchange interaction is overcome by the positive AO bond population originating from the mixing in of the charge-transferred states, the chemical binding between the AO's t and u becomes "bonding."

The changes in the AO bond population of the AO's t and t' of the system A, caused by the interaction with B, are given by

$$\begin{aligned} \varphi_{tt'} \cong & 2\left(-\sum_i^{\text{occ}} \sum_l^{\text{uno}} C_{i \rightarrow l}^2 c_l^{(i)} c_{l'}^{(i)} s_{ll'} + \right. \\ & \left. \sum_k^{\text{occ}} \sum_j^{\text{uno}} C_{k \rightarrow j}^2 c_k^{(j)} c_{j'}^{(j)} s_{jj'} - \right. \\ & \left. 2\sqrt{2}C_0 \sum_i^{\text{occ}} \sum_l^{\text{uno}} C_{i \rightarrow l} S_{il} c_l^{(i)} c_{l'}^{(i)} s_{ll'}\right) + O(S^2) \quad (7) \end{aligned}$$

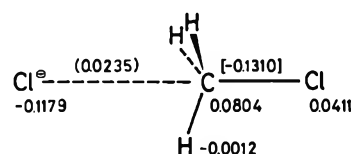
Equations 6 and 7 indicate the importance of the delocalization interaction in representing the formation of new bonds and weakening of old bonds in chemical reactions. To calculate the changes in AO populations, we may extend here the concept of the population analysis of Mulliken²³ to the intermolecular AO pair t and u . The fraction of electrons influent into the intermolecular region between A and B by means of orbital overlap interactions may be partitioned into two parts, one of which reverts to the AO t of A and the other to the AO u of B. Thus, the AO populations of t and u , in the case of chemical interaction, consist of three parts; valence-inactive population, intramolecular valence-active population, and intermolecular valence-active population, following the theory of Ruedenberg, which partitions the electrons of a molecule into valence-inactive and valence-active populations.²⁴

The changes in atomic populations and in atomic bond populations are given in Figure 4, with respect to models III, IV, and V. It is seen that the charge transfer from the attacking chloride ion can not be effective in model IV in comparison with model III. Thus, the course which leads to inversion appears to be favorable, in accordance with the results of the energy calculation.

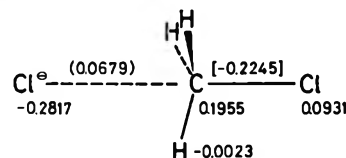
In Table III are shown the changes in the AO populations of the carbon atom. The most conspicuous change can be found in the $2p_x$ orbital.

In Table IV, the changes in the AO populations of the attacking chloride ion are presented. The dona-

MODEL III



MODEL V



MODEL IV

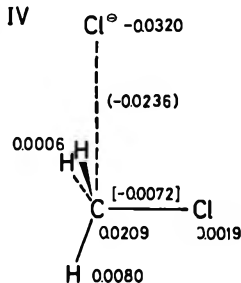


Figure 4. The changes in the atomic populations and in the atomic bond populations due to the interaction.

Table III: The Changes in the AO Populations of the Carbon of Methyl Chloride Due to the Interaction

AO	Model III	Model V
s	0.0106	0.0125
x	0.0665	0.1804
y	0.0017	0.0013
z	0.0017	0.0013

Table IV: The Changes in the AO Populations of Chloride Ion Due to the Interaction

AO	Model III	Model V
s	-0.0111	-0.0177
x	-0.1025	-0.2616
y	-0.0022	-0.0012
z	-0.0022	-0.0012

tion of electrons mainly takes place from the $3p_x$ orbital.

In Table V are given the changes in the AO bond populations of the carbon-chlorine bond of methyl chloride. The negative values indicate decreases in the AO bond populations.

(22) L. Salem, *Proc. Roy. Soc., Ser. A*, **264**, 379 (1961).

(23) R. S. Mulliken, *J. Chem. Phys.*, **23**, 1833, 1841, 2338, 2343 (1955).

(24) K. Ruedenberg, *Rev. Mod. Phys.*, **34**, 326 (1962).

Table V: The Changes in the AO Bond Populations of the Carbon-Chlorine Bond in Methyl Chloride Due to the Interaction in Model III

		C			
		s	x	y	z
Cl	s	-0.0146	-0.0288	0	0
	x	-0.0310	-0.0564	0	0
	y	0	0	-0.0001	0
	z	0	0	0	-0.0001

The AO bond populations between the AO's of the carbon atom of methyl chloride and the AO's of chloride ion are shown in Table VI, with respect to model III. It may be noted that the chemical bond is formed first between the carbon $2p_x$ and chlorine $3s$ and $3p_x$ orbitals. The carbon $2s$ orbital shows an antibonding character with the chlorine orbitals in the early stage of the reaction. This is attributed partly to the exchange interaction and partly to the delocalization interaction. The contribution of the carbon $2p_y$, $2p_z$, and hydrogen $1s$ orbitals is not important.

The mixing in of the polarized electron configurations may, conceivably, suffice to compensate partly for the AO bond populations due to the exchange interaction, since the overlap integral between ψ_0 and $\psi_{i \rightarrow j}$, for instance, is the second order of the MO overlap integrals between A and B.

Table VI: The Intermolecular AO Bond Populations between Methyl Chloride and Chloride Ion in Model III

		CH ₃ Cl				
		C _s	C _x	C _y	C _z	H ^a
Cl-	Cl _s	-0.0088	0.0057	0	0	-0.0017
	Cl _x	-0.0172	0.0468	0	0	-0.0082
	Cl _y	0	0	-0.0015	0	0
	Cl _z	0	0	0	-0.0015	0.0010

^a In x - z plane.

using the MO's obtained for these species in an isolated state. The calculation has been confined to the early stages of the reaction because of the approximations employed. This is one of the inherent limitations of the present method. To overcome this shortcoming, it is necessary to include not only monotransferred and monoexcited electron configurations but also highly transferred and highly excited ones and expand the energy by the use of accurate wave functions. It seems to be inevitable at present to introduce semi-empirical approximations to deduce some information on the chemical interaction between sizable molecules. We may hence be content with qualitative or even more semiquantitative knowledge of the interaction energy and wave functions of interacting systems. We must make mention here that the present calculation is very crude, and the exchange and delocalization interaction energies are somewhat overestimated. The models employed have been arbitrarily set up and may deviate from the species which are actually reacting. Undoubtedly, there are many factors to be taken into consideration in discussing the favorable path of chemical interaction. The present calculation has no concern with such factors, *e.g.*, the possible effect of solvent molecules. However, the comparison of models III and IV may supply us with some information on the reason why the inversion process is more favorable than the retention process in usual bimolecular nucleophilic substitution reactions. The transition state of the reaction is far beyond the approach of the present calculation, because the interaction between the reactant and the reagent grows too strong to be regarded as a weak interaction. It is our feeling that the cooperation of charge-transfer and molecular deformation mentioned before supplies a reasonable ground for extrapolating the results of calculation at the early stage to the transition state of the reaction. We believe that this approach can reveal the sources of stabilization and destabilization and the origins of the formation of new bonds and weakening of old bonds in this reaction, of which little has been disclosed in the previous calculation.²⁰

Acknowledgment. It is a pleasure to express our gratitude to the Data Processing Center of Kyoto University for generous permission to use the FACOM 230-60 computer.

Conclusion

We have made an approximate numerical calculation of the interaction energy and bond interchange in the interaction of methyl chloride with chloride ion,

Low Pressure Ultrafiltration of Sucrose and Raffinose

Solutions with Anisotropic Membranes

by R. W. Baker, F. R. Eirich,*

Polymer Research Institute, Polytechnic Institute of Brooklyn, Brooklyn, New York 11201

and H. Strathmann

Technische Hochschule, Aachen, Germany (Received October 22, 1970)

Publication costs assisted by NIH and Pharmetrics

The low pressure ultrafiltration of sugar solutions has been studied with asymmetric "Loeb-Sourirajan" type membranes. The rejection increases from zero at zero pressure to a limiting value at higher pressures. The rejection also decreases with increasing sugar concentration. The data may be explained in part by using a pore flow membrane model and calculating the effect of diffusion of the solute relative to the center of mass of motion of the liquid through the pores.

Introduction

In recent years membrane ultrafiltration has gained increasing attention as a simple and convenient technique for concentration, purification, and fractionation of macromolecular solutions. Asymmetric membrane structures developed by Loeb and Sourirajan¹ and others² in the early sixties have led to considerable improvements in the ultrafiltration process. These asymmetric membranes consist of a dense, 0.2–2 μm thick skin layer, supported by the 50–100 μm thick porous substructure,^{3,4} which has an average pore size of about 1 μm . The substructure has practically no effect on the permeability and retention characteristics of the membrane. The major advantage of the asymmetric membrane, due to the extreme thinness of the skin layer, is the high filtration rate attainable at relatively low hydrostatic pressures.

A variety of asymmetric membranes with different molecular weight cut-offs are now available.⁵ The molecular weight cut-off of a membrane indicates the minimum molecular weight of particles which will be completely rejected by this membrane. In previous papers^{6,7} the properties and uses of asymmetric membranes with molecular weight cut-offs larger than 30,000 were described. In this paper, properties of membranes intermediate between the cellulose acetate (reverse osmosis desalination) membrane described by Lonsdale⁸ and others and high-molecular-weight cut-off membranes will be discussed. These membranes are operated at pressures of 1–5 atm and have molecular weight cut-offs between 500 and 10,000. Their flux and retention characteristics show a remarkable pressure and feed solution concentration sensitivity which cannot be simply related to the osmotic pressure or concentration polarization, as in the case of the desalination membranes,⁹ or to a gel formation on the

membrane surface, as in the case of high flux pore membranes and macromolecular solutions.⁷

Membranes with molecular weight cut-offs between 500 and 10,000 are of considerable practical interest. They are routinely used in the laboratory for ion binding studies,^{10,11} protein concentration,¹² and protein desalting.¹³ The purpose of this paper is to study the relation between filtration rate, feed solution concentration, applied hydrostatic pressure, and retention of these low pressure ultrafiltration membranes and interpret the experimental results by existing theories of membrane transport mechanisms.

Experimental Section

The ultrafiltration experiments were carried out in a batch-type cell fitted with internal magnetic stirrer. The test stand is schematically shown in Figure 1. It consisted of the actual test cell, a calibrated variable

- (1) S. Loeb and S. Sourirajan, *Advan. Chem. Ser.*, No. 38, 117 (1962).
- (2) A. S. Michaels, *Ind. Eng. Chem.*, 57, 32 (1965).
- (3) B. Keilin, Office of Saline Water Research & Development Report No. 84, Jan 1964.
- (4) H. K. Lonsdale, U. Merten, and R. L. Riley, *J. Appl. Polym. Sci.*, 9, 1341 (1965).
- (5) A. S. Michaels in "Progress in Separations and Purification," E. S. Perry, Ed., Wiley, New York, N. Y., 1968.
- (6) R. W. Baker, *J. Appl. Polym. Sci.*, 13, 359 (1969).
- (7) R. W. Baker and H. Strathmann, *ibid.*, 14, 1197 (1970).
- (8) H. K. Lonsdale in "Desalination by Reverse Osmosis," U. Merten, Ed., MIT Press, Cambridge, Mass., 1966.
- (9) U. Merten, *Ind. Eng. Chem., Fundam.*, 2, 229 (1963).
- (10) W. F. Blatt, S. M. Robinson, and H. J. Bixler, *Anal. Biochem.* 26, 151 (1968).
- (11) J. A. Gordon and J. R. Warren, *J. Biol. Chem.*, 243, 5663 (1968).
- (12) W. F. Blatt, M. P. Feinberg, H. P. Hopfenberg, and C. A. Saravis, *Science*, 150, 224 (1965).
- (13) V. E. Pollak, M. Gaizutis, and J. Rezaian, *J. Lab. Clin. Med.*, 71, 338 (1968).

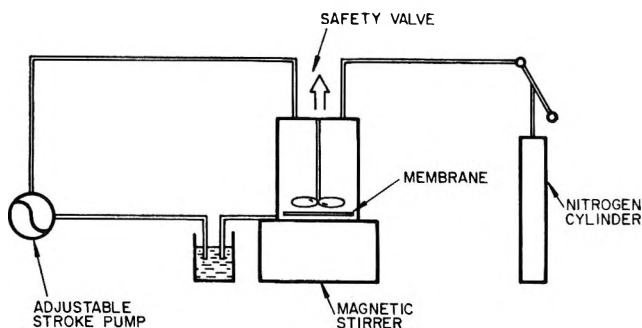


Figure 1. Schematic diagram of the ultrafiltration system.

stroke piston pump which fed the filtrate from a reservoir back into the test cell, and a nitrogen cylinder which delivered the hydrostatic pressure driving force. Membrane flux and retention data were determined under steady-state conditions; *i.e.*, the stroke setting of the pump was adjusted by a micrometer screw until the feed rate just balanced the filtration rate. The rejection coefficient, R , was calculated from the difference in the concentration of solute in the bulk solution, C_b , and the concentration of solute in the filtrate, C_f , by eq 1

$$R = 100 \left[1 - \frac{C_f}{C_b} \right] \quad (1)$$

Osmotic flow experiments were carried out in cells purchased from the Chemical Rubber Co. These cells consisted of two Lucite chambers containing the solutions separated by a membrane. Concentration polarizations at the membrane surface were counteracted by a mechanical shaker. Diaflo UM-10 membranes purchased from the Amicon Corp., Lexington, Mass., were used for the major part of the study. These membranes are made from a neutral polyelectrolyte complex.² A PM-10 membrane, also purchased from the Amicon Corp. and made from a chemically inert non-ionic polymer, was used for some of the experiments. Both membranes have an asymmetric structure⁵ similar to the Loeb-Sourirajan¹ type cellulose acetate desalination membrane.

Results

The experimental results are summarized in Figure 2 where flux and retention data for the UM-10 and PM-10 membranes with sucrose and raffinose solutions of various concentrations are plotted *vs.* the applied hydrostatic pressure. In all cases a sharp increase in retention with increasing pressure and decreasing sugar concentration is observed, contrasted with a decrease in flux with increasing sugar concentration, while the flux increases fairly linearly with the applied pressure. The raffinose rejection obtained with the PM-10 was rather low (not exceeding 10%) and showed a considerable scattering. However, the same general relation between flux retention, feed solution concentration, and

pressure as obtained with the UM-10 membrane was observed.

Discussion^{13a}

Membrane Permeation Models. Before a detailed discussion of the experimental results is possible, it is necessary to determine the transport mechanism within the membranes. Theoretical models for various transport mechanisms are described in the literature.¹⁴⁻¹⁸ Membranes which retain only macromolecules (mol wt > 30,000) are clearly best described by a pore flow model.⁷ Microsolute retentive membranes, such as the cellulose acetate desalination membrane, can be satisfactorily described by a solvent diffusion model,⁴ as well as by a pore flow mechanism,¹⁴ or a combination of both.¹⁶

Several criteria may be used to distinguish between these mechanisms. One of the most useful is the water permeability of the membrane, which in a pore flow membrane is generally several orders of magnitude larger than that of a diffusive-type membrane of the same thickness and porosity.

The volume flux, $J_{v(\text{pore})}$, of a pore flow membrane, can be described as a Poiseuille flow, *i.e.*, by eq 2^{17,18}

$$J_{v(\text{pore})} = \frac{\epsilon r^2}{8\eta_w \tau} \frac{\Delta P}{\Delta \lambda} \quad (2)$$

where ϵ is the membrane porosity, r is the pore radius, η_w the viscosity of water, τ the tortuosity factor, ΔP the pressure difference between up- and downstream membrane surfaces and $\Delta \lambda$ the membrane thickness, *i.e.*, in an asymmetric ultrafiltration membrane the skin thickness. The volume flux, $J_{v(\text{diff})}$, in terms of a diffusive model is given by^{17,18}

$$J_{v(\text{diff})} = \frac{D_w \bar{V}_w C_w}{RT} \frac{\Delta P}{\Delta \lambda} \quad (3)$$

where D_w is the diffusion coefficient for water inside the membrane, \bar{V}_w is the partial molar volume of water in the membrane, C_w the water concentration in the membrane, R is the gas constant, and T the absolute temperature.

Table I lists experimentally determined membrane fluxes and the calculated values for $J_{v(\text{diff})}$ and $J_{v(\text{pore})}$ at 50 psig for skin thickness $\Delta \lambda$ of 1 μm , a tortuosity factor of 4, and a skin porosity of 0.2. It is difficult to

(13a) NOTE ADDED IN PROOF. The constructive criticisms contributed by D. A. Michaels during his review of this paper were greatly appreciated.

(14) P. Meares, *Eur. Polym. J.*, **2**, 241 (1966).

(15) R. M. Barrer, *Trans. Faraday Soc.*, **36**, 644 (1940); **38**, 322 (1942).

(16) A. S. Michaels, H. J. Bixler, and R. M. Hodges, *J. Colloid Sci.*, **20**, 1034 (1965).

(17) R. Schlögl, "Stofftransport durch Membranen," Steinkopff Verlag, Darmstadt, 1964.

(18) U. Merten in "Desalination by Reverse Osmosis," MIT Press, Cambridge, Mass., 1966.

Table I: Experimentally Determined and Calculated Fluxes for Cellulose Acetate Diaflo, UM-10, and PM-10 Membranes Assuming a Pore Flow and a Solvent Diffusion Model^a

Membrane	~ Pore radius assuming a pore model, Å	~ Diffusion coefficient assuming a diffusive model, cm ² sec ⁻¹	$\frac{J_v(\text{pore})}{J_v(\text{diff})}$	$J_v(\text{diff})$ at 50 psig, cm sec ⁻¹	$J_v(\text{pore})$ at 50 psig, cm sec ⁻¹	$J_v(\text{exp})$ at 50 psig, cm sec ⁻¹
Cellulose acetate desalination	2-4	1×10^{-6}	2-7	25×10^{-6}	$0.9-3.4 \times 10^{-6}$	$2-4 \times 10^{-6}$
UM-10	7-15	1×10^{-6}	20-100	25×10^{-6}	$0.1-0.5 \times 10^{-3}$	$0.7-1.7 \times 10^{-3}$
PM-10	10-20	1×10^{-4}	40-170	25×10^{-6}	$0.22-0.9 \times 10^{-3}$	$1.0-2.5 \times 10^{-3}$

^a The pore size of the UM-10 and PM-10 membranes was estimated from the retention of raffinose and sucrose, whose approximate molecular radii are 10 and 5 Å, respectively.

place a value on D_w . However, Lonsdale, *et al.*,⁴ have reported a D_w of about 1×10^{-6} cm² sec⁻¹, a very high value which has been questioned by Meares.¹⁴ Even assuming this high value of D_w , the observed fluxes for the UM-10 and PM-10 membranes are *ca.* 1000 times higher than the values calculated by a diffusive model. Only the cellulose acetate membrane which is listed for comparison shows a reasonable agreement between the experimentally determined fluxes and data calculated by a diffusive model. Fluxes calculated by the pore flow model, however, are of the same order of magnitude as the experimentally determined fluxes. The water permeabilities, therefore, clearly imply a pore flow mechanism for the UM-10 and PM-10 membranes. Additional supporting evidence excluding a diffusive mechanism is given by the negligible solute rejections for microsolute species such as NaCl, KCl, and urea shown by the UM-10 and PM-10 membranes. This nonselectivity for such diverse species is not easily explained by a diffusive model.

Membrane Solute Rejection. Henderson and Sliepcevich,¹⁹ when measuring the ultrafiltration of sucrose through cellophane membranes, observed a similar though not so marked effect of pressure and concentration on membrane flux and solute retention. They attributed this to diffusion within the membrane pores which provides an additional solute flux through the membrane, leading to lower rejection coefficients. At first sight it appears unlikely that solute diffusion in the center-of-mass motion of fluid in the pore can contribute a large enough portion to the overall solute flux to explain the rejection-pressure relation observed with UM-10 and PM-10 membranes. However, in an anisotropic membrane the actual separation barrier consists only of the membrane skin which may be as thin as 0.2-2 μm, and the solute transport due to diffusion may well be a significant part of the overall solute flux, even with these high flux membranes.

In the following discussion, a theoretical model similar to that described by Schlögl¹⁷ and Merten¹⁸ is used which assumes transport of solvent and solute exclu-

sively through pores. In a real membrane there is a continuous distribution of pore sizes ranging from small pores which completely retain the solute to large pores which completely pass the solution. The retention characteristics of a given membrane for a given solute is therefore basically determined by its pore-size distribution. The pore distribution can be described by a two-pore population model in which the total volume flux J_v is given by

$$J_v = j_{v(l)} + j_{v(s)} \quad (4)$$

where $j_{v(l)}$ is the volume flux through the pores which show no rejection to the solute, while $j_{v(s)}$ is the volume flux through the pores which completely retain the solute. The volume flux through the pores, which shows no rejection to the solute, $j_{v(l)}$, can be expressed as a fraction of the total volume flux J_v by

$$j_{v(l)} = f \cdot J_v \quad (5)$$

where f is a constant ≤ 1 .

The total solute flux through the solute permeable pores, j_s , is given by

$$j_s = u \cdot C_s - D_s \frac{dC_s}{dX} \quad (6)$$

where C_s is the solute concentration in the pores, u the center-of-mass velocity in the solute permeable pores, D_s the diffusion coefficient in the center of mass system, and dC_s/dX the concentration gradient of the solute in the pores. Equation 6 describes the total solute flux through the pores as a sum of a contribution due to the center-of-mass motion of fluid given as $(u \cdot C_s)$, and another due to the diffusion of the solute in the pore with respect to the center of moving mass given as

$$-D_s \frac{dC_s}{dX}$$

The solute flux through the solute permeable pores, j_s ,

(19) W. E. Henderson and C. M. Sliepcevich, *Chem. Eng. Progr., Symp. Ser.*, 55, No. 24, 145 (1959).

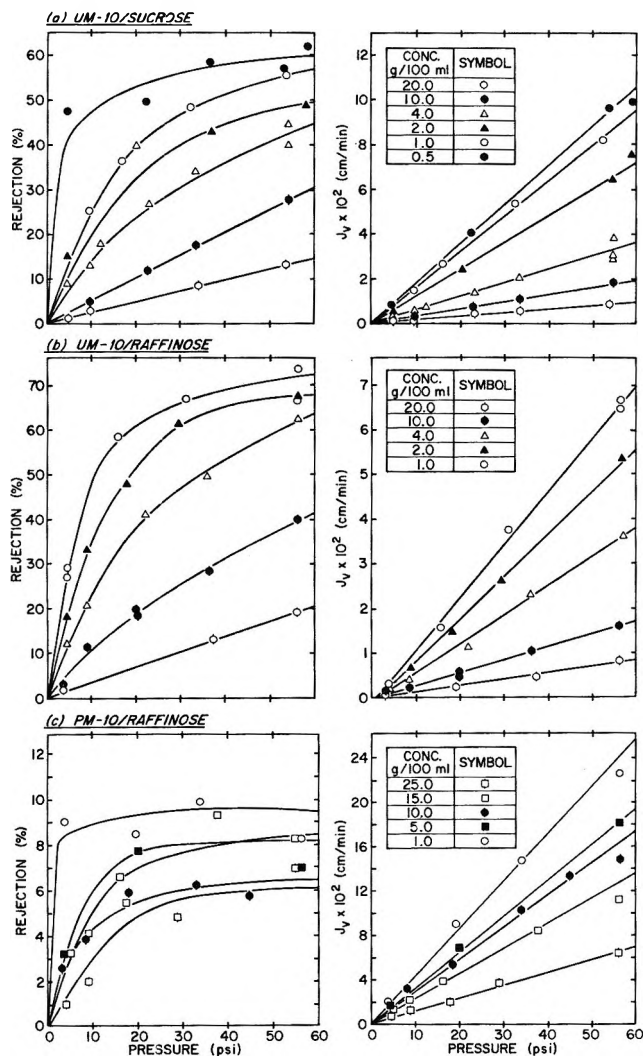


Figure 2. Membrane retention and flux data for raffinose and sucrose determined at various hydrostatic pressures and solute concentrations: a, UM-10 membrane and various sucrose solutions; b, UM-10 membrane and various raffinose solutions; c, PM-10 membrane and various raffinose solutions.

can be related to the general membrane solute flux, J_s , by

$$j_s = \frac{J_s}{\epsilon_1} \tag{7}$$

where ϵ_1 is the porosity due to the solute permeable pores.

In similar way the center-of-mass velocity, u , in the solute permeable pores can be related to the overall volume flux

$$u = \frac{j_{v(1)}}{\epsilon_1} = \frac{fJ_v}{\epsilon_1} \tag{8}$$

Introducing eq 7 and 8 into eq 6 and integrating over the length, L , of the solute permeable pores

$$\frac{f \cdot J_v \cdot C_s'' - J_s}{f \cdot J_v \cdot C_s' - J_s} = \exp\left(\frac{fJ_v L}{\epsilon_1 D_s}\right) \tag{9}$$

where C_s' is the solute concentration at $X = 0$, the upstream side of the solute permeable pores, and C_s'' that at $X = L$, the downstream side of the solute permeable pores. It is assumed that in a "well-stirred" batch cell to a first approximation

$$C_s' = C_b \text{ and } C_s'' = C_f \tag{10}$$

with C_b the solute concentration in the bulk of the feed solution and C_f that in the filtrate.

Furthermore, the total membrane salt flux, J_s , can be expressed by

$$J_s = J_v \cdot C_f \tag{11}$$

Introduction of eq 9, 10, and 11 into eq 1 gives the solute rejection as a function of the total water flux, of the solute diffusion coefficient in the solute-permeable pores and of the pore-size distribution

$$R = 100 \left[1 - \frac{f \exp\left(\frac{fJ_v L}{\epsilon_1 D_s}\right)}{f - 1 + \exp\left(\frac{fJ_v L}{\epsilon_1 D_s}\right)} \right] \tag{12}$$

It follows from eq 12 that as J_v goes to zero, the exponential term goes to unity and the rejection coefficient reduces to zero as shown in Figure 2.

The second limiting case of eq 12 occurs as J_v tends to become very large. In this case the exponential terms tend towards infinity, and the rejection coefficient approaches a limiting value, R_∞ , which is equal to $100[1 - f]$. Furthermore, since the only concentration and pressure-dependent term in eq 12 is J_v/D_s , it follows that the rejection data for each membrane and solute at all the concentrations and pressures shown in Figure 2 can be normalized onto a single line by plotting the rejection against J_v/D_s , as shown in Figure 3. The diffusion coefficients for the solutes in the pore solution

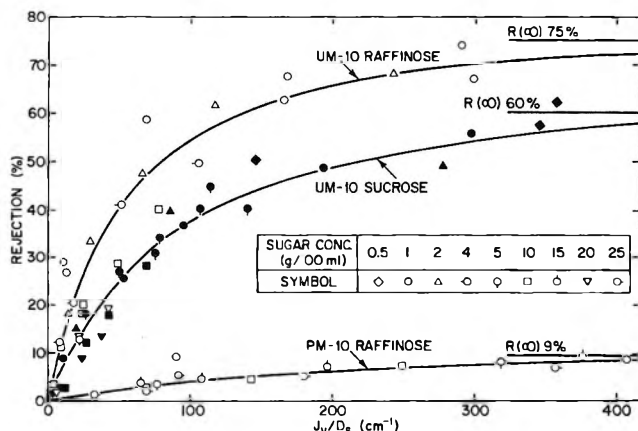


Figure 3. Normalized plot of the retention data shown in Figure 2. The lines through the experimental points were calculated from eq 12 assuming a total pore length of $5 \mu\text{m}$ and a large pore porosity ϵ_1 of 0.025 for raffinose/UM-10, 0.04 for sucroses/UM-10, and 0.1 for the raffinose/PM-10.

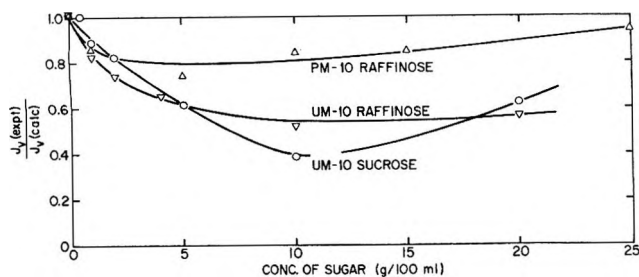


Figure 4. Ratio of experimentally determined to calculated membrane fluxes, eq 13, as a function of the concentration of the feed solution.

were taken from the "Critical Tables." The solid curve through the experimental points has been calculated by eq 12 assuming a total pore length, L , of $5 \mu\text{m}$. The fraction of the porosity due to large pores, ϵ_1 , will depend on the particular solute and membrane. The values of ϵ_1 equals 0.04 for the UM-10 sucrose system, 0.025 for the UM-10 raffinose system and 0.1 for PM-10 raffinose, which were necessary to get the good agreement between the experimental results and the calculated curve in Figure 3, appear reasonable, assuming the total porosity to be in the region of 0.1–0.3.

The Membrane Permeability. The volume flux of sugar solutions through the membranes increased linearly with increasing pressure and showed a remarkable dependence on the concentration of the sugar solution. For a pore flow membrane the calculated volume flux, $J_{v(\text{calcd})}$, of a sugar solution can be related to the volume flux of water, J_w , under the same conditions by eq 13

$$J_{v(\text{calcd})} = J_w \cdot \frac{\eta_w}{\eta_s} \left(\frac{\Delta P - \Delta \pi}{\Delta P} \right) \quad (13)$$

The term η_w/η_s takes care of the increased viscosity of the sugar solutions. The second term compensates

for the osmotic pressure difference across the membrane. The osmotic pressure data for sucrose could be found in the "Critical Tables." For raffinose, the data had to be calculated using the equation of Callender.²⁰ The water flux used in the calculation of $J_{v(\text{calcd})}$ was the mean of the fluxes measured before and after each set of sugar runs. The osmotic fluxes introduced by concentration gradients of sucrose and raffinose were measured and showed no anomalous effects.

Figure 4 shows a plot of the ratio of the experimental to the calculated sugar permeabilities *vs.* the sugar concentration. There is a considerable deviation from the admittedly simple relation expressed in eq 13, in that the experimental flux is seen to be significantly smaller than the calculated value; *i.e.*, the ratio is always smaller than 1. Furthermore, this deviation is strongly dependent on the sugar concentration and is largest at a concentration of 10–15% sugar. The discrepancy in the calculated and experimentally determined fluxes is believed to be caused by a crowding effect of the sugar molecules at the entrance of the pores by which they mutually interfere with their entrance into the membrane. This crowding will be affected by the diameter of the hydrated sugar molecules which goes through a maximum in the concentration range of sugar where the maximum deviation is observed. These second-order phenomena are not accounted for in eq 13 so that deviations are to be expected. The experimental result of this study, however, can in general be adequately described by a pore flow model.

Acknowledgment. The financial aid under a training grant from the National Institute of Dental Research, which made this study possible, is gratefully acknowledged.

(20) H. L. Callender, *Proc. Roy. Soc., Ser. A*, **80**, 466 (1908).

Standard Potential of the Ferrocene-Ferricinium Electrode in Pyridine.

Evaluation of Proton Medium Effect

by L. M. Mukherjee

Chemistry Department, Illinois State University, Normal, Illinois 61761 (Received March 3, 1971)

Publication costs borne completely by The Journal of Physical Chemistry

Behavior of biscyclopentadienyl iron(II) (ferrocene) and biscyclopentadienyl iron(III) picrate (ferricinium picrate) in pyridine has been investigated through differential vapor pressure measurements and conductance studies. Ferrocene is found to exist as stable monomers, whereas ferricinium picrate dissociates as a simple weak electrolyte. Analysis of the potentials of half-cells comprised of (equimolar) mixtures of ferrocene and ferricinium picrate accordingly at concentrations 1.0, 2.5, and 5.0 mM, against an Ag|silver picrate electrode and the Zn(Hg)|ZnCl₂(s) reference electrode yielded an average value of 0.628 V vs. a nhe in pyridine for the standard reduction potential of the ferrocene couple. Combining this result with the standard potential of ferrocene-ferricinium system in water, a value of -0.227 V is calculated for the potential of a nhe in pyridine vs. (E°_{H})_{aq} on the molal scale. The medium effect for proton ($\log_m \gamma_{\text{H}}$), on this basis, is found to be -3.85.

Introduction

Two reference electrodes, viz., Zn(Hg)|ZnCl₂(s) and Hg|HgCl₂(s), LiCl(s) and the Ag indicator electrode have already been standardized in pyridine vs. a normal hydrogen electrode (nhe) in the same solvent.^{1,2} Thus, the p_{aH} and p_{Ag} scales are already established in pyridine with reference to the standard state in the solvent itself, that is, on the assumption that the ionic activity coefficients become unity at infinite dilution in pyridine. Correlation of the pH scale so defined with the aqueous standard state would, therefore, provide a means for ascertaining the "medium effect" of transfer of a proton from water to pyridine and would permit conversion of the pyridine p_{aH} values to the unified aqueous scale. Potentiometric studies involving the ferrocene-ferricinium electrode system^{3a-c} in pyridine appeared promising in this respect. The two members of this couple are complexes of relatively large size with Fe²⁺ and Fe³⁺ sandwiched between two cyclopentadienyl ions. Moreover, the reduced form is an uncharged species and the oxidized form carries only one unit of positive charge. This would favor cancellation of the neutral component of the medium effect for the ferricinium ion with the medium effect for ferrocene; also, the residual electrostatic component can be expected to be small due to the large size of the ferricinium ion. Consequently, in the absence of any specific interactions, the standard potential of the ferrocene-ferricinium electrode can be presumed to remain constant independent of the solvent. Indeed, when referred to an aqueous nhe, i.e., (E°_{H})_{aq} in respective solvents, the E° values reported for this couple show only small variations:³ 0.400 V (water); 0.400 V (methanol); 0.340 V, 0.348 V (acetonitrile);

0.390 V (formamide). (It should, however, be pointed out in this connection that Coetzee, *et al.*,⁴ derived a substantially different value (0.577 V) for the E° of the ferrocene couple in acetonitrile vs. (E°_{H})_{aq}. The arguments advanced by them to explain the discrepancy are not too convincing as has been noted recently by Popovych.⁵ It would appear that the value of the potential of the Ag|0.01 M AgNO₃ reference electrode arrived at from the Rb potential is questionable.)

The present work consists of a study of the behavior of ferrocene and ferricinium picrate in pyridine and the determination of the standard potential of the ferrocene-ferricinium electrode vs. a nhe in the same solvent. Using the (extrathermodynamic) assumption that the E° of the ferrocene couple vs. (E°_{H})_{aq} remains the same in water as well as in pyridine, the medium effect for proton has been evaluated. Since the latter is inherently related to the definition of the standard state in the individual solvent, the p_{aH} values measured against a nhe in pyridine can now be converted to the aqueous scale.

Theory

Behavior of Ferrocene and Ferricinium Picrate. The

(1) L. M. Mukherjee, J. J. Kelly, W. Baranetzky, and J. Sica, *J. Phys. Chem.*, **72**, 3410 (1968).

(2) (a) L. M. Mukherjee, J. J. Kelly, McD. Richards, and J. M. Lukacs, Jr., *ibid.*, **73**, 580 (1969); (b) L. M. Mukherjee and J. M. Lukacs, Jr., *ibid.*, **73**, 3115 (1969).

(3) (a) H. Strehlow, *Z. Elektrochem.*, **56**, 827 (1952); (b) H. M. Koepp, H. Wendt, and H. Strehlow, *ibid.*, **64**, 483 (1960); (c) H. Strehlow, "The Chemistry of Non-Aqueous Solvents," J. J. Lagowski, Ed., Academic Press, New York, N. Y., 1966; (d) I. M. Kolthoff and F. G. Thomas, *J. Phys. Chem.*, **69**, 3049 (1965).

(4) J. F. Coetzee and J. J. Campion, *J. Amer. Chem. Soc.*, **89**, 1 (1967).

(5) O. Popovych, *Crit. Rev. Anal. Chem.*, **1**, 73 (1970).

trode and the silver electrode has been described before.^{1,9} Emf values were measured at $25 \pm 0.5^\circ$ using a Metrohm Herisau Model E388 compensator. The potentials reported in this study are considered reliable to ± 2 mV. No significant variation in the ferrocene half-cell potential was observed even over a period of several days.

Results and Discussion

The results of the present studies on the behavior of ferrocene and ferricinium picrate in pyridine are shown in Figures 1 and 2.

It is evident that the plot for ferrocene virtually coincides with that of the standard monomer 1,3-diphenylguanidine. It can, therefore, be reasonably concluded that the ferrocene molecules behave as stable species in pyridine. Ferricinium picrate, on the other hand, does seem to conform to the postulated dissociation reaction (*cf.*, eq 1). The thermodynamic dissociation constant and the limiting conductance (Λ_0) of the salt are calculated to be 4.0×10^{-4} and $71.48 \pm 0.82 \text{ ohm}^{-1} \text{ cm}^{-1} \text{ g equiv}^{-1}$, respectively. Since the limiting conductance of picrate ion is 33.7,⁷ the λ° of ferricinium ion is found to be 37.8. Comparison of this value with the $\lambda^\circ_{Ag^+}$ (34.3⁷) would, therefore, suggest that the solvated silver ion is slightly bigger in size than the ferricinium ion.

The results of emf measurements using cell I and II are summarized in Table I. The computed values

Table I: Summary of Results on Emf Measurements at 25°

Cell	Potential, V, of ferrocene half-cell		
	$5.00 \times 10^{-3} M^a$	$2.50 \times 10^{-3} M^b$	$1.00 \times 10^{-3} M^c$
I	0.5845 (0.629)		0.6035 (0.628)
II	0.5828, 0.5826 (0.627) (0.627)	0.5960 (0.631)	0.6012 (0.625)

^a $\alpha \cong 0.42$. ^b $\alpha \cong 0.50$. ^c $\alpha = 0.62$.

of the E° of the ferrocene-ferricinium couple *vs.* a nhe in pyridine are listed in parentheses under the corresponding half-cell potential. As can be seen, the E° values estimated on the basis of the two types of cells are remarkably close, the maximum variation being only about 6 mV. This agreement among the final values seems to support our original contention that the junction potentials are indeed negligible or have cancelled in the process.

Comparing the average (0.628 V) of the above E° values with the E° of the ferrocene couple obtained in water³ (0.400 V), the potential of a nhe in pyridine is

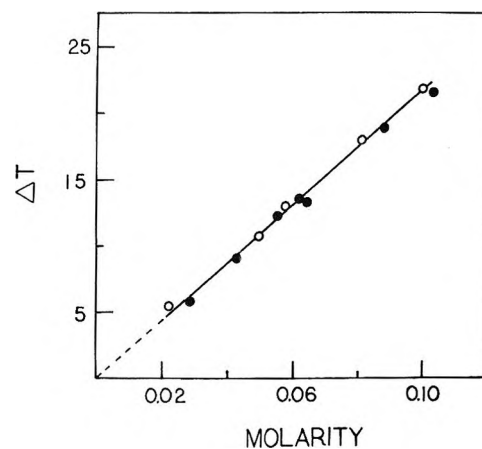


Figure 1. Differential vapor pressure measurements. Plot of ΔT *vs.* molarity: \circ , 1,3-diphenylguanidine (monomer); \bullet , ferrocene.

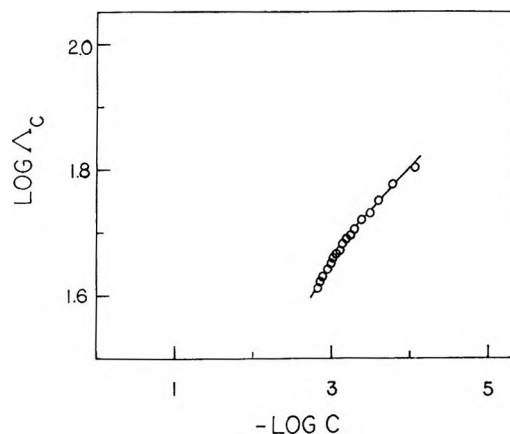


Figure 2. Plot of $\log \Lambda_c$ *vs.* $-\log C$ for ferricinium picrate (25°).

calculated to be -0.228 V *vs.* $(E^\circ_{H})_{aq}$ in the same solvent. Conversion of this potential to the molal scale leads to a value of -3.85 for the medium effect for the proton ($\log_m \gamma_H$). Accordingly, the difference between the two pa_H scales, *viz.*, $(pa_H)_{aq} - (pa_H)_{pyridine}$, is estimated to be 3.85.

It is considered worthwhile to note in this connection that the medium effects ($\log_m \gamma_H$) calculated⁵ for acetonitrile and formamide are 2.4 and -2.5 , respectively, on the molal scale based on the ferrocene assumption. The corresponding estimates on the rational scale would, therefore, be -0.373 (acetonitrile) and -5.20 (formamide) as compared with that of -6.06 for the truly aprotic¹⁰ solvent pyridine. It is somewhat interesting to observe that the proton medium effects in pyridine and formamide are so close in spite of significant differences in properties of the two solvents.

(9) S. Bruckenstein and L. M. Mukherjee, *J. Phys. Chem.*, **64**, 1601 (1960).

(10) I. M. Kolthoff, *J. Polarogr. Soc.*, **10**, 22 (1964).

A Nuclear Magnetic Resonance Study of Acid-Base Interactions for the Chloranil Electrode System in Acetonitrile

by N. F. Heffinger, R. P. T. Tomkins,* and P. J. Turner

Department of Chemistry, Rensselaer Polytechnic Institute, Troy, N. Y. 12181 (Received July 19, 1971)

Publication costs borne completely by The Journal of Physical Chemistry

In the hydrochloranil-chloranil electrode system in acetonitrile, specific hydrogen bonding interactions between solutes and solvent and between the two solutes are sufficiently weak to indicate that the activity coefficients of the electrode materials should be fairly constant. Chloranil behaves as a weaker base than either the solvent or small amounts of water in the solutions and should not interfere with acid solutions except at high dilution. Hydrochloranil has weak acid properties which may become significant in basic solutions although its restricted stability to air oxidation limits its application to acid and weakly basic solution. Proton exchange in this system is rapid.

The use of emf methods for the study of acid-base interactions in nonaqueous solutions is occasionally impeded by difficulties in obtaining a satisfactory electrode reversible to hydrogen ions. In acetonitrile, the hydrogen electrode on platinized platinum has been found satisfactory in some cases;¹ however, it is subject to interference by the solvent.²⁻⁴ Although the glass electrode shows some stability in acetonitrile,⁵ the proposed mechanisms, whereby the potential of the glass electrode depends linearly on the pH, require empirical terms to account for the asymmetry potentials; *i.e.*, each electrode must be calibrated.⁶ Electrodes of the quinhydrone type offer a possible solution to this problem; however, some basic disadvantages of these electrodes do arise from the additional activity terms in the Nernst equation and interference of the acidic and basic electrode materials with the solution under investigation.⁷ Both of these difficulties are aggravated by the generally greater solubilities of the electrode materials in nonaqueous solvents.⁸ The chloranil-hydrochloranil (tetrachlorobenzoquinone-tetrachloroquinol) system has been found satisfactory in acidic solvents where comparison with the hydrogen electrode is possible.⁹ The smaller susceptibility of this latter system to base-induced side reactions found with the benzoquinone system⁸ suggests that the chloranil electrode would be more suitable for use in less acidic solvents, *e.g.*, acetonitrile. The use of dilute electrode systems of this type is recommended to minimize anomalous solvent effects and requires some understanding of the acid-base interactions of chloranil and hydrochloranil.

It is to be expected that the most significant specific interactions in quinhydrone systems in aprotic solvents are protonation and hydrogen bonding, between dissolved species. Both should sharply influence proton activities and hence the adequate functioning of the

electrode. Since two separate activity coefficients appear in the Nernst equation for the quinhydrone electrode, the emf method provides only the relative values. It is possible to use hydroxyl proton chemical shifts to evaluate protonation of the materials independently rather than as the mixture used for emf measurements.¹⁰

The chemical shift $\Delta\nu_i$ of a proton whose concentration is C_i , in environment i , if exchanging rapidly with a set of other environments, will give a resultant chemical shift which is the mean of all the exchanging protons

$$\Delta\nu = \frac{\sum_i \Delta\nu_i C_i}{\sum_i C_i} \quad (1)$$

If a strong interaction takes place between two sites, *e.g.*, the case of hydrogen bonding, a further independent environment is added and must be included in eq 1, which now contains an additional parameter.

To examine these interactions, solutions of chloranil and hydrochloranil in acetonitrile containing perchloric

(1) I. M. Kolthoff and F. G. Thomas, *J. Phys. Chem.*, **69**, 3049 (1965).

(2) G. J. Hills, in "Reference Electrodes," D. J. G. Ives and G. J. Janz, Ed., Academic Press, New York, N. Y., 1960, p 446.

(3) C. Papon and J. Jacq, *Bull. Soc. Chim. Fr.*, 13 (1965).

(4) J. N. Butler, *Advan. Electrochem. Electrochem. Eng.*, **7**, 87 (1970).

(5) I. M. Kolthoff and M. K. Chantooni, *J. Amer. Chem. Soc.*, **87**, 4428 (1965).

(6) G. Mattock and D. M. Band, in "Glass Electrodes for Hydrogen and Other Cations," G. Eisenman, Ed., Marcel Dekker, New York, N. Y., 1967, Chapter 2.

(7) D. J. G. Ives and G. J. Janz, ref 2, p 289.

(8) P. J. Turner, M.S. Thesis, Rensselaer Polytechnic Institute, Troy, N. Y., 1970.

(9) B. O. Heston and N. F. Hall, *J. Amer. Chem. Soc.*, **56**, 1462 (1934).

(10) See, *e.g.*, E. J. King, "International Encyclopedia of Physical Chemistry and Chemical Physics," Vol. 4, I.U.P.A.C., Topic 15, "Acid-Base Equilibria," p 110.

acid as the more strongly acidic, and acetone as the more strongly basic, species have been examined at concentrations from about $10^{-3} M$ up to saturation. The use of such a weak base as acetone is preferred, as strong bases still tend to cause some polymerization of hydrochloranil in presence of oxygen.¹¹ The use of an aliphatic ketone can also give qualitative indications of hydrogen bonding between hydroquinones and quinones by making use of concentration ranges above those accessible with the quinone as solute.

Experimental Section

Materials. Chloranil (Eastman Organic Chemicals) was recrystallized from ethanol and dried for 12 hr under vacuum at room temperature.

Hydrochloranil (Eastman Organic Chemicals) was not improved by sublimation *in vacuo* or by recrystallization from 70% aqueous ethanol and was used as received, mp 236–238° (lit. mp 232°, 236°).¹²

The purification of acetonitrile (Fisher reagent grade) has been described previously.¹³ Solvent peak asymmetry in the nmr spectra indicated very slight traces of water in the acetonitrile after three distillations probably as a result of access of air to the distillate during sample preparation. Samples were therefore condensed rapidly from batches of about 50 ml which were refluxed continuously over ~5 g calcium hydride (Metal Hydrides Inc.) and led directly into the nmr tube.

Acetone (Fisher ACS reagent grade) was used as received. Perchloric acid (Baker AR grade) was used as a ~0.25 *M* stock solution in acetonitrile, prepared by weight. Analysis of the acid as received by potentiometric titration with aqueous sodium carbonate showed that the reagent contained 61.0% HClO_4 , *i.e.*, could be formulated as $\text{HClO}_4 \cdot 3.6\text{H}_2\text{O}$.

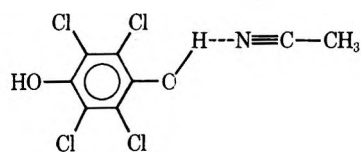
Nmr Spectra. Spectra were measured using a Varian Associates T-60 60 MHz analytical spectrometer at a sample temperature of 34°. Chemical shifts for each sample were measured relative to the main solvent band, the center of which was located by averaging the four strongest spinning bands. Uncertainty in chemical shifts obtained by this procedure is estimated as ± 1 Hz.

Results and Discussion

Chloranil itself is pmr inactive but two to four weak resonances appeared about 5 Hz downfield of the main solvent peak and are assigned to solvent impurities, possibly water, of concentration in the region of $10^{-3} M$. The shift of these relative to solvent was essentially independent of chloranil concentration, suggesting that chloranil was not very strongly solvated by the impurities.

The —OH protons of hydrochloranil appear about 314 Hz downfield of the solvent and are concentration-independent over the concentration range $10^{-2} M$ to

saturation, as shown in Table I. This implies that hydrogen bonding to the solvent, *viz.*



dominates the interactions, rather than a hydrogen bonded self-association of the type

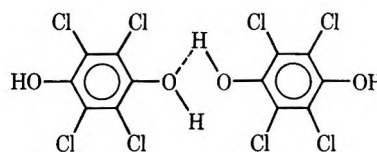


Table I: —OH Proton Chemical Shifts for Hydrochloranil Solutions in Acetonitrile

Hydrochloranil, <i>M</i>	$\Delta\nu$, Hz
0.02	312.0
0.04	314.8
0.05	314.3
0.13 (sat.)	312.5

In solutions containing both chloranil and hydrochloranil (see Table II), there is a slight tendency for the —OH peak to move upfield as the relative concentration of chloranil is increased, but this movement is only about 0.5 Hz per tenfold increase of $[\text{C}/\text{CH}_2]$, which is considerably less than the general scatter of points (~2 Hz) and can be neglected. This invariance is a strong indication that any specific interaction in solution analogous to the formation of quinhydrones is weak by comparison with solvation, and the two components do not significantly interfere with each other in dilute solution in acetonitrile.

Table II: —OH Proton Chemical Shifts for Solutions of Chloranil (C) with Hydrochloranil (CH_2) in Acetonitrile

Concn, <i>M</i>		$\text{C}:\text{CH}_2$	$\Delta\nu$, Hz
C	CH_2		
0	0.050	0	314.3
0.015	0.050	0.30	314.0
0.015	0.120	0.125	313.1
0.020	0.025	0.80	313.5
0.020	0.040	0.50	314.3
0.030	0.080	0.375	312.5

(11) R. P. T. Tomkins and P. J. Turner, unpublished results.

(12) "Beilsteins Handbuch der Organischen Chemie," 4th ed, Springer-Verlag, New York, N. Y., 1923, Vol. 6, p 851.

(13) R. P. T. Tomkins, E. J. Andalaft, and G. J. Janz, *Trans. Faraday Soc.*, 65, 1906 (1969).

The spectra of chloranil and hydrochloranil solutions containing perchloric acid are presented in Table III. The system $\text{HClO}_4\text{-H}_2\text{O}$ -hydrochloranil-acetonitrile gives a broad, concentration-dependent resonance which is assigned to the sum of -OH protons from all the solutes. These must therefore be participating in an exchange equilibrium which is fast relative to the nmr time scale ($\sim 10^{-3}$ sec).¹⁴ A second, sharp resonance, 24.0 ± 1.0 Hz downfield of the solvent, is concentration-independent and may be attributed to proton solvation by acetonitrile, *i.e.*, to methyl protons of the species $\text{CH}_3\text{-C}^+\text{NH}$. The chemical shifts for the -OH protons in a 0.016 M HClO_4 solution follow an equation of the form

$$\Delta\nu = \frac{(2n + 1)\Delta\nu_{\text{HClO}_4} \cdot C_{\text{HClO}_4} + 2\Delta\nu_{\text{CH}_2} \cdot C_{\text{CH}_2}}{(2n + 1)C_{\text{HClO}_4} + 2C_{\text{CH}_2}}$$

where n is the effective degree of hydration of a solution of $\text{HClO}_4 \cdot n\text{H}_2\text{O}$, $\Delta\nu_{\text{HClO}_4} = 130 \pm 2$ Hz, $C_{\text{HClO}_4} = 0.016$ M. It is found that the fit is not particularly good, $\pm \sim 10$ Hz, with the curve of best fit having n close to 1.5, indicating that only about half the water is apparently taking part in rapid exchange. The sharpness of the protonated acetonitrile peak suggests that a second fast exchange may be taking place which involves the remaining water but not hydrochloranil, although no resonance corresponding to NH or water could be located in these systems. The poor fit may be a result of slow oxidation of hydrochloranil by perchloric acid. These results are consistent enough to indicate that (a) perchloric acid undergoes proton exchange with aqueous impurities, and these protons exchange rapidly with those of hydrochloranil; (b) dissociation of hydrochloranil is relatively weak, as estimated from the line width which is increased somewhat on addition of hydrochloranil to the acid solution, but still sufficient to promote proton exchange.

Addition of chloranil to perchloric acid solutions in acetonitrile had a very small effect on the -OH protons, causing a 1-2 Hz downfield movement. Some interaction with acid protons is therefore to be expected, which may cause difficulties with very dilute acids. These interactions are apparently considerably weaker than those of the proton with water or comparable bases. A greater downfield movement is seen when appreciable amounts of undissolved solid are present. This may be due to adsorption of the acid by the solid phase. If this is the case, the unsaturated electrode is more suitable for precise work.

The effect of acetone on hydrochloranil solutions is shown in Table IV. The small downfield shift as acetone concentration is increased indicates a very slight increase in hydrogen-bonded interactions, either of hydrochloranil to acetone or by self-association as the solvent dielectric constant is lowered. This is approximately linear with acetone concentration and indicates

Table III: Chemical Shifts of -OH Protons and Protonated Solvent for Chloranil (C) and Hydrochloranil (CH_2) Solutions in Acetonitrile Containing Perchloric Acid and Water^a

Concn, M				$\Delta\nu$, Hz	
HClO_4	H_2O	C	CH_2	OH	Solvent
0.016	0.058	0	0	132	24
0.016	0.058	0	0	129	24
0.016	0.058	0	0	133	24
0.016	0.058	0.0256	0	134	24
		(sat)			
0.016	0.058	0.0256	0	146	24
		(sat)			
0.016	0.058	0	0.0081	166.5	24.5
0.016	0.058	0	0.0149	201	25
0.016	0.058	0	0.0493	233	25
0.016	0.058	0	0.178	273	25
			(sat)		
0	0	0	0.13	312.5	
0.095	0.34	0	0.13	246.3	23.3
0.190	0.68	0.022	0	248.8	23.3
0.057	0.205	0.022	0	202.0	24.0
0.019	0.068	0.020	0	148.8	23.8
0.190	0.68	0	0	250.0	23.5

^a Reference frequency is the methyl resonance of the bulk solvent in the same solution.

that hydrochloranil hydrogen bonds to aliphatic carbonyl groups about as well as to acetonitrile, hydrogen bonding is dictated on a probabilistic basis, and no significant shift occurs at concentrations of acetone comparable with those of hydrochloranil, or with those attainable with chloranil.

Table IV: -OH Proton Chemical Shifts for Hydrochloranil (CH_2) in Solutions in Acetonitrile Containing Acetone^a

Me_2CO , %	Concn, M		$\alpha\text{-OH}$, Hz
	Me_2CO	CH_2	
2.0	0.276	0.034	... ^b
2.0	0.276	0.090	314
20	2.76	0.11	335
33	5.55	0.20	354
50	6.90	0.12	368
0	0	0.05	314

^a Reference frequency is the methyl resonance of the bulk solvent in the same solution. ^b Signal below the limit of detection.

Acknowledgment. Helpful suggestions by Professor G. J. Janz are acknowledged with pleasure. This work was supported by the U. S. Department of Defense, Project Themis.

(14) L. M. Jackman and S. Sternhell, "Applications of NMR Spectroscopy in Organic Chemistry," Pergamon, Elmsford, N. Y., 1969, p 56.

Effect of Pressure on Charge-Transfer Complexes in Solution.

II. Complexes Formed between Ions and between Ions and Neutral Molecules

by A. H. Ewald* and J. A. Scudder

CSIRO Division of Mineralogy, North Ryde, NSW, Australia 2113 (Received August 17, 1971)

Publication costs assisted by CSIRO Minerals Research Laboratories

The effect of pressure on the charge-transfer (CT) absorption of a number of electron donor-acceptor complexes (EDAC) has been measured in solution over a range of 3 kbars and at several temperatures. The EDAC formed between an anion donor and a cation acceptor (4-methoxy-*N*-methylpyridinium iodide) showed a decrease in the stability constant and a blue shift of the CT absorption with increase in pressure. Three EDAC formed between ions and neutral molecules (sodium iodide and trinitrobenzene, tropylium tetrafluoroborate and hexamethylbenzene, and potassium pentamethoxycarbonylcyclopentadienylide and trinitrobenzene) showed little effect of pressure on the stability constant and on the CT maximum. The pressure effects found for these, and for the neutral-neutral complexes investigated earlier, are interpreted qualitatively in terms of the change of solvation of the components and the complexes brought about by the change in pressure.

Introduction

In part I¹ we measured the effect of increased hydrostatic pressure on the formation constant (K) and the charge transfer (CT) absorption energy of electron donor-acceptor complexes (EDAC) formed between π donors and π acceptors in solution and came to the conclusion that a large part of the effect could be explained by changes in the solvation of the donors, acceptors and EDAC with change in pressure. We have now extended our measurements to include EDAC formed between charged donors and acceptors and neutral molecules.

In the case of EDAC formed between ions, the polarities of the ground state and the excited state differ in the opposite sense to those in complexes formed between neutral components; the effect of pressure on these complexes should also be opposite if change in solvation is the predominant factor. For complexes formed between ions and neutral molecules little change in polarity is expected either during formation or on excitation and there should be only small solvent and pressure effects on K and λ_{CT} .

We have measured the absorption spectra of one ion-ion complex, 4-methoxycarbonyl-*N*-methylpyridinium iodide (MMPI), and three ion-neutral complexes, NaI-trinitrobenzene (I⁻-TNB), tropylium tetrafluoroborate-hexamethylbenzene (TRP⁺-HMB), and potassium 1,2,3,4,5-pentamethoxycarbonylcyclopentadienylide-trinitrobenzene (MCP⁻-TNB) over a range of pressures and at several temperatures and have evaluated formation constants and absorption coefficients from them. From the pressure effects we have calculated volume changes of formation.

MMPI was chosen for the measurements because it has been shown that the energy of its CT absorption is strongly solvent dependent² and that the CT maximum is well separated from the component absorptions and readily observed. The other systems were chosen to include a variety of ionic donors and acceptors.

Experimental Section

Materials. MMPI and NaI were prepared and recrystallized as in ref 3. 1,3,5-Trinitrobenzene (TNB) was recrystallized twice from ethanol. Hexamethylbenzene (HMB) was recrystallized from methanol. Tropylium tetrafluoroborate (TRP⁺) was prepared by the method of Dauben, *et al.*,⁴ and was obtained in good yields, mp 482-483°K; (ref 4 gives 483°K); nmr in CH₃CN: singlet at 556 cps *ex* TMS (ref 5 = 552 cps); uv λ_{max} (CH₃CN) 273.7 nm (log ϵ = 3.7) (ref 4 λ_{max} (CH₃CN) = 273.5 nm (log ϵ = 3.64)). Potassium pentamethoxycarbonylcyclopentadienylide (KMCP) was prepared by the method of Le Goff and LaCount,⁶ mp 492-493°K (ref 6 = 493°K); nmr in CH₃CN: singlet at 219 cps *ex* TMS; uv λ_{max} (MeOH) 265 and 294 nm (ref 7 = 265 and 295 nm). Acetone and 2-

(1) A. H. Ewald, *Trans. Faraday Soc.*, **64**, 733 (1968); referred to as part I.

(2) E. M. Kosower, *J. Amer. Chem. Soc.*, **80**, 3253 (1958); **83**, 3147 (1961).

(3) A. H. Ewald and J. A. Scudder, *Aust. J. Chem.*, **23**, 1939 (1970).

(4) H. P. Dauben, L. R. Honnen, and K. M. Harmon, *J. Org. Chem.*, **25**, 1442 (1960).

(5) G. Fraenkel, R. E. Carter, A. McLachlan, and J. H. Richards, *J. Amer. Chem. Soc.*, **82**, 5846 (1960).

(6) E. Le Goff and R. B. LaCount, *J. Org. Chem.*, **29**, 423 (1964); *J. Amer. Chem. Soc.*, **85**, 1354 (1963).

methylpropan-1-ol (*i*-BuOH) were purified and handled, and their physical properties were evaluated as in ref 3.

Methanol was purified and after distillation was stored and handled under dry nitrogen. Density data were obtained from Timmermans⁸ and Bridgman.⁹ Acetonitrile was distilled from CaH₂, stored in brown bottles and handled under dry nitrogen. The normal density was obtained from Timmermans⁸ and its pressure dependence was measured by a piston displacement method. The results at 303°K were fitted to the Tait equation to give

$$\frac{\Delta V}{V} = 0.229 \log \frac{P + 818}{P + 1}$$

with P in atmospheres.

The spectroscopic measurements were made as described in part I,¹ and the results were evaluated by the methods described there,¹⁰ except that we used Liptay's¹¹ method to average measurements taken at eight to ten different wavelengths, and an analogous method to select and reject those spectra which showed an anomalous pressure variation at the absorption maximum.¹² By using a criterion of 5% deviation from a mean value, this led to the rejection of 5% of the data.

For equilibria in which ions are involved it is necessary to include an activity coefficient in the definition of the equilibrium constant. For the MMPI system the equilibrium can be defined as

$${}^zK_s = \frac{x_c}{(x_0 - x_c)^2 f^2} \quad (1)$$

which assumes unit activity coefficient for the complex of concentration x_c . This leads to the equation for the evaluation of the data

$$\frac{x^0}{DV} + \frac{DV}{\epsilon^2} = \frac{1}{{}^zK_s \epsilon f^2} + \frac{1}{\epsilon} 2x^0 \quad (2)$$

where V = molar volume and D = optical density of the solution, zK_s and ϵ are the mole fraction formation constant and absorption coefficient of the EDAC, x^0 is the total concentration (in mole fractions) of MMPI, and f is the activity coefficient of MMPI calculated by the Debye-Hückel equation, using $\bar{a} = 5 \text{ \AA}$ as in the evaluation of the conductivity measurements.³ This may not be the best choice for this parameter when evaluating spectroscopic measurements as was discussed at length by Davies, Otter, and Prue¹³ and by Matheson;¹⁴ small variations in \bar{a} , however, do not alter the values of K and ϵ greatly.¹⁴

For complexes which involve only one ionic component one may assume that the activity coefficients of the complex and the ion are very similar and therefore cancel out in the expression for the equilibrium constant. The equation used for evaluation then takes the form given in footnote 10.

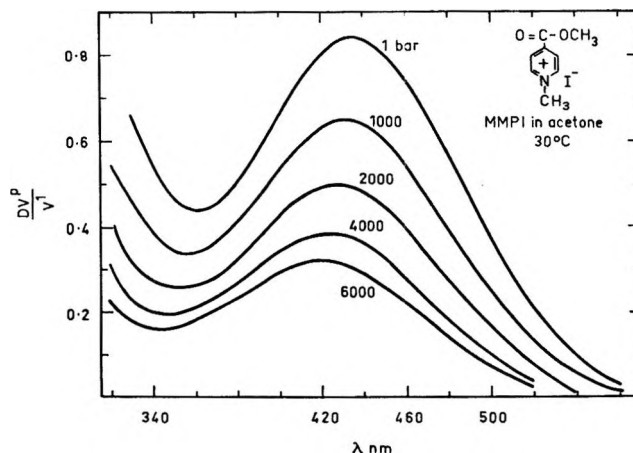


Figure 1. Charge-transfer absorption band of MMPI in acetone at 30° and various pressures. Concentration, 72.3×10^{-6} mole fraction; path length, 1.91 mm.

The evaluation of K and ϵ from spectroscopic measurements has in the last few years been shown to be very uncertain except under rather stringent conditions.¹⁵⁻¹⁷ Owing to the algebraic form of eq 2 it is very difficult to arrive at unique values of K and ϵ , although the product $K\epsilon$ can be determined with greater certainty.¹⁸

Results and Discussion

A set of spectra of MMPI in acetone at various pressures is shown in Figure 1. The broad absorption bands are typical of EDAC in solution and are one reason why quantitative determination of the absorption maximum is often difficult. In many cases the CT band overlaps the absorption of one of the components (*e.g.*, TNB) and it is necessary to correct for this before the absorption maximum can be found. When comparing spectra at different pressures and temperatures

(7) R. C. Cookson, J. Hudec, and B. Whitear, *Proc. Chem. Soc., London*, 117 (1961).

(8) J. Timmermans, "Physico-Chemical Constants of Pure Organic Compounds," Elsevier, New York, N. Y., 1950.

(9) P. W. Bridgman, "The Physics of High Pressure," 2nd ed, Bell, London, 1949.

(10) The equation given in part I omitted a factor $1/V$ in the first term. It should have read

$$\frac{x_c^0 x_d^0}{D V} + \frac{D V}{\epsilon^2} = \frac{1}{{}^zK_s \epsilon} + \frac{1}{\epsilon} (x_a^0 + x_d^0)$$

(11) W. Liptay, *Z. Elektrochem.*, **65**, 375 (1961).

(12) J. A. Scudder, M.Sc. Thesis, University of Sydney, N.S.W., Australia, 1971.

(13) W. G. Davies, R. J. Otter, and J. E. Prue, *Discuss. Faraday Soc.*, **24**, 103 (1957).

(14) R. A. Matheson, *J. Phys. Chem.*, **69**, 1537 (1965); **70**, 3368 (1966).

(15) K. Conrow, G. D. Johnson, and R. E. Bowen, *J. Amer. Chem. Soc.*, **86**, 1025 (1964).

(16) W. B. Person, *ibid.*, **87**, 167 (1965).

(17) R. A. LaBuddle and M. Tamres, *J. Phys. Chem.*, **74**, 4009 (1970).

(18) R. Foster, "Organic Charge-Transfer Complexes," Academic Press, London, 1969, p 158.

it is necessary to allow for the change in density of the solution. For the very dilute solutions used in the present work, adequate correction is obtained by multiplying the optical density by the relative volume of the solvent referred to some standard condition. Such a correction has been applied to the measurements shown in Figure 1.

Table I gives the wavelength of the CT maximum, λ_{CT} , and the energy shift of it at 3040 bars ($\delta\nu$ in cm^{-1}), as well as the equilibrium constants and absorption coefficients found at 1 bar and the volume change derived from the pressure variation of K , for the different complexes we have examined.

Table I: Equilibrium Constants, Absorption Coefficients, and CT Maxima of EDAC in Solution

Complex (solvent)	Temp, °K	λ_{CT} , nm	$\delta\nu$ (3040 bars), cm^{-1}	K , (mole fraction) $^{-1}$	ϵ , $\text{mol l.}^{-1} \text{cm}^{-1}$	ΔV , $\text{cm}^3 \text{mol}^{-1}$
MMPI (acetone)	265.2			2680 ^a		
	275.2			4180 ^a		
	293.2	427	416	3600	1060	
	303.2	429	590	3200	930	+16
	313.2	434	660	3000	1710	
MMPI (<i>i</i> -BuOH)	303.2	372	220	≤ 3000	910	+17
I ⁻ -TNB (MeOH)	298.2	360	0	87	390	0
I ⁻ -TNB (<i>i</i> -BuOH)	318.2	365	0	27	940	
I ⁻ -TNB (<i>i</i> -BuOH)	298.2	365	0	1540	575	
TRP ⁺ -HMB (<i>i</i> -BuOH)	308.2	0	0	550	340	
TRP ⁺ -HMB (CH ₃ CN)	303.2	417 ± 3	0	165	455	0
TRP ⁺ -HMB (CH ₃ CN)	313.2	413 ± 2	0	52	1180	
MCP ⁻ -TNB (MeOH)	303.2	382	0	194	1260	0
MCP ⁻ -TNB (MeOH)	313.2	385	0	73	2620	

^a From ref. 3.

Figure 2 is a plot of the values of $\log K^p/K^1$ as a function of pressure and includes¹ the neutral complex TNB-HMB for comparison. Figure 3 shows the values of $\delta\nu$ found for the complexes at various pressures. Values for TNB-HMB are again included. The pressure shift is zero within the accuracy of the measurements for all the ion-neutral EDAC and only the TRP⁺-HMB complex is shown.

We shall discuss the individual systems first and then draw some general conclusions.

MMPI. The spectra of this salt were measured in acetone at three temperatures, and in *i*-BuOH at one temperature, at five pressures between 1 and 3040 bars. The concentration range was 5 to 80 × 10⁻⁵ mole fraction MMPI.¹² The absorption band in *i*-BuOH was found at a shorter wavelength and showed less pressure shift than the band in acetone. The great sensitivity of the MMPI/CT band to solvent polarity has been attributed by Kosower² to a "dipole flip" of the complex during excitation which, due to the Franck-Condon

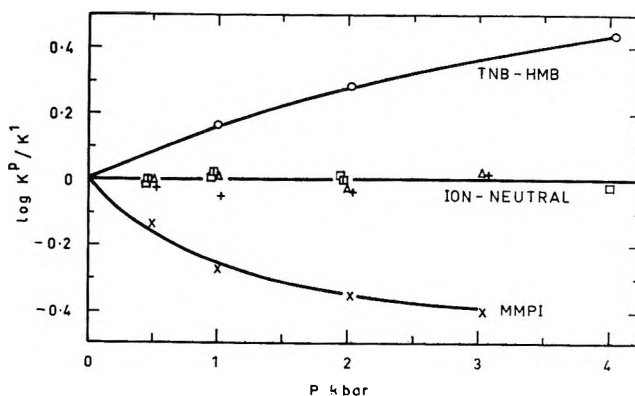


Figure 2. Effect of pressure on the relative stability of various EDAC.

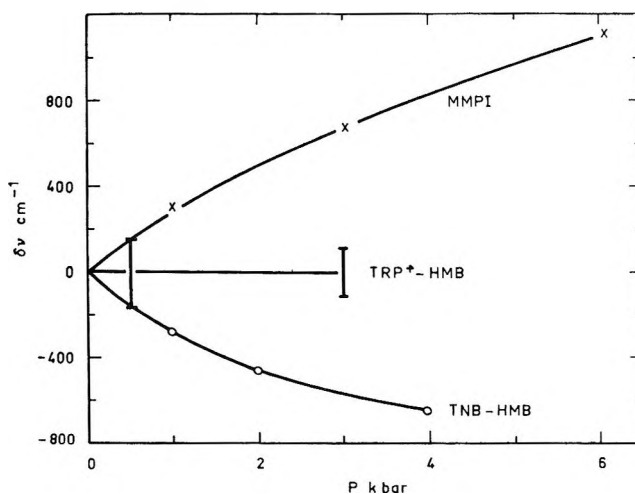


Figure 3. Effect of pressure on the energy of the CT transition of various EDAC.

effect, leads to a mismatch between the dipole field of the excited complex and the reaction field of the solvent around it. This destabilizes the excited state relative to the ground state and leads to a blue shift of the absorption band when the solvent interaction is increased by increase of pressure.

The system has been the subject of a detailed conductometric investigation³ and this led to association constants which were rather different (Table II) from those found spectroscopically and given in Table I. According to Prue's "optical marker" argument¹⁹ the two methods could give the same association constant even if not all the associated species give a CT absorption; the ϵ derived from spectroscopic measurements on such systems, on the other hand, is a weighted average of the absorption coefficient of the different associated species. We therefore carefully analyzed our present results to see whether the difference between them and the earlier results is significant.

(19) J. E. Prue in "Chemical Physics of Ionic Solutions," B. E. Conway and R. G. Barradas, Ed., Wiley, New York, N. Y., 1966, p. 170.

Table II: MMPI Association Constants at 1 bar Found Conductometrically (from Ref 3 Converted to (mole fraction)⁻¹ Units)

Temp, °K	265.2	275.2	293.2	303.2	313.2
	In acetone				
$K_\gamma \times 10^{-3}$	2.68	4.18	8.11	8.56	13.3
	In <i>i</i> -BuOH				
$K_\gamma \times 10^{-3}$	52.1	...

We used a computer to map out the standard deviation in the fit of eq 2 as a function of K and ϵ . This showed the minimum to lie in a long, narrow, approximately hyperbolic valley, along which the value of the standard deviation varies little. We calculated the 90% confidence limits for K and ϵ by applying a χ^2 test to the residual variance and found that the conductometric association constant K_γ was contained within these limits in every case. We therefore conclude that the difference between K_γ and the spectroscopically determined K_s is *not significant*. Since the conductometric measurements are inherently much more accurate ($\pm 10\%$),³ K_γ is the best estimate of the association constant in this system. For convenience we quote in Table II the values from ref 3, converted to mole fraction units as used in this paper. The values of $\log K^p/K^1$ shown in Figure 2 for this system and the values of ΔV in Table I are derived from K_γ .

The positive values of ΔV are in marked contrast with the contractions found for the EDAC formed from neutral molecules and indicate the important role of desolvation when the EDAC is formed from the component ions. The magnitude of ΔV is not as great as one would expect for completed desolvation of a pair of ions (30–40 cm³/mol, from kinetic measurements²⁰) and this, together with the solvent sensitivity of the CT energy, indicates that the EDAC is still solvated.

I⁻-TNB. The color produced when iodide solutions are added to TNB solutions has been attributed to the formation of EDAC.^{21–23} Briegleb, *et al.*,²¹ found the absorption maximum to be solvent dependent and measured the formation constant and absorption coefficient in a series of solvents using different salts as sources of I⁻ ions. He showed by infrared studies that the complexes differed from "Meisenheimer" complexes, and we confirmed this by nmr measurements.

In our measurements NaI was used as the source of I⁻ and for the measurements in methanol the concentrations ranged from 250 to 1000 $\times 10^{-5}$ mole fraction I⁻, and from 5 to 9 $\times 10^{-5}$ mole fraction TNB. In *i*-BuOH the solutions darken in the course of a few hours,²¹ but this effect can be suppressed by the addition of a small amount (*ca.* 10⁻⁴ M) of glacial acetic acid. The concentration of I⁻ in this solvent was 15 to 300 $\times 10^{-5}$ mole fraction and that of TNB 3 to 30 \times

10⁻⁵ mole fraction. The CT band was observed as a shoulder on the TNB absorption and the spectra had to be corrected for this absorption.

NaI is known to be almost completely dissociated in MeOH^{24,25} and the EDAC formation is therefore not complicated by any ion pair equilibrium. Our results show the CT energy and the equilibrium constant to be unchanged by pressure, but ϵ_{\max} was found to increase slightly with pressure.

In *i*-BuOH only 75% of NaI is dissociated³ and two different complexes can be formed, one between free I⁻ and TNB and therefore carrying a negative charge, and the other from an ion pair and TNB and carrying no charge. These cannot be distinguished in the present experiments. The results in this solvent are similar to those in MeOH except for larger values of K and a decrease of ϵ with rising temperature. This last effect could occur if the charged EDAC had a larger ϵ than the uncharged complex, since with rising temperature the ion pairing in *i*-BuOH increases³ and the observed average ϵ would thus decrease.

In both solvents K is independent of pressure and $\Delta V = 0$. Comparison between the negative ΔV found for neutral complexes¹ and the positive value for MMPI suggests that the contraction due to the formation of the CT bond is just balanced by the reduced electrostriction of the solvent due to the spreading of the ionic charge.

TRP⁺-HMB. The tropylium halides do not give stable solutions and are therefore not suitable for lengthy measurements. The tetrafluoroborate is stable in acetonitrile and was used in these measurements at concentrations between 15 and 150 $\times 10^{-5}$ mole fraction. The π - π complex formed by TRP⁺ with mesitylene²⁶ has $K = 13$ and in order to measure a larger K we used HMB as the donor at concentrations between 25 and 140 $\times 10^{-5}$ mole fraction. The solid brown complex could be obtained by evaporating the solutions and gave an ir spectrum equal to an intimate mixture of the components and a uv spectrum, as a null, similar to the EDAC in solution.

The EDAC has a very broad CT band at 417 nm and the position has been found to be solvent independent.²⁷ The pressure measurements showed that K is independent of P ($\Delta V = 0$), but ϵ increases slightly with increasing pressure. A rise in temperature caused a decrease in K and an increase in ϵ .

(20) W. J. le Noble, *Progr. Phys. Org. Chem.*, **5**, 207 (1967).

(21) G. Briegleb, W. Liptay, and R. Fick, *Z. Elektrochem.*, **66**, 851 (1962).

(22) K. M. C. Davis, *J. Chem. Soc., B*, 1128 (1967).

(23) K. M. C. Davis, *ibid.*, 1020 (1969).

(24) R. L. Kay, *J. Amer. Chem. Soc.*, **82**, 2099 (1960).

(25) R. E. Jervis, D. R. Muir, J. P. Butler, and A. R. Gordon, *ibid.*, **75**, 2855 (1953).

(26) M. Feldman and S. Winstein, *ibid.*, **83**, 3338 (1961).

(27) T. G. Beaumont and K. M. C. Davis, *J. Chem. Soc., B*, 1010 (1968).

In contrast to the invariance of the CT maximum with pressure we found that the absorption of the TRP⁺ ion at 275 nm shifted to higher energies by 230 cm⁻¹ at 2026 bars, and showed a slight increase (3%) in ϵ and a larger increase in the oscillator strength calculated from the band width as in ref 1.

MCP⁻-TNB. In contrast to the cyclopentadiene anion, the pentacarbonyl-methoxy substituted anion is stable, and its EDAC with charged acceptors⁶ and the unstable complex formed with TCNE have been studied.²⁷ We found the complex formed between the potassium salt of MCP⁻ and TNB to be sufficiently stable in methanol (less than 5% change in four hours) to make absorption measurements in our usual pressure and temperature range. The concentrations for TNB ranged from 5 to 11 $\times 10^{-5}$ mole fraction, and for KMCP from 4 to 170 $\times 10^{-5}$ mole fraction. The CT band was observed as a shoulder on the TNB absorption at ca. 385 nm and the spectrum had to be corrected for the TNB absorption.

The results show that K and ϵ are independent of pressure ($\Delta V = 0$), but that with rising temperature K decreases and ϵ increases.

General Discussion

Within the accuracy of our measurements, K and λ_{CT} for EDAC formed between ions and neutral molecules are pressure independent, but our present and earlier³ measurements indicate a pressure dependence for the ion-ion complex MMPI. Briegleb and his co-workers²¹ found λ_{CT} to be solvent dependent for I⁻-TNB, but were not able to correlate this dependence with any bulk property of the solvent and concluded that specific solvent interactions are important. Beaumont and Davis,²⁷ on the other hand, agree with our results in finding λ_{CT} to be constant for TRP⁺-HMB in most solvents, but to be strongly solvent dependent for TRP⁺-I⁻ and TRP⁺-MCP⁻.

The average thermodynamic quantities for ion-neutral complexes are given in Table III; detailed values for MMPI were reported earlier.³ The values of ΔH and ΔS are very uncertain but indicate rather large negative values, contrary to Briegleb's finding²¹ that $\Delta H \approx 0$ and ΔS is positive for I⁻-TNB. Our ΔH and ΔS values for the ion-neutral complexes have the same sign as those found for neutral-neutral complexes¹ but are about twice as big. It is difficult to account for the large negative entropy, but in the case of the neutral complexes it was found to be highly solvent dependent and, together with the solvent dependence of K for both types of complexes, this indicates the important role solvent interactions play in the stability of EDAC. Similar negative entropies and enthalpies have been observed²⁸ for the formation of "Meisenheimer" complexes between TNB and anions such as CN⁻ and EtO⁻. Although the bond formed in these complexes is differ-

Table III: Values of Thermodynamic Quantities Averaged over All Pressures for Ion-Neutral Complexes^a

	I ⁻ -TNB in MeOH (308°K)	I ⁻ -TNB in <i>i</i> -BuCH (303°K)	TRP ⁺ -HMB in MeCN (308°K)	MCP ⁻ -TNB in MeOH (308°K)
$-\Delta G$	9.9 \pm 0.6	17.3 \pm 0.6	11.8 \pm 0.7	12.2 \pm 0.4
$-\Delta S$	130 \pm 30	190 \pm 80	220 \pm 70	200 \pm 40
$-\Delta H$	50 \pm 10	80 \pm 30	80 \pm 20	70 \pm 10

^a ΔG , ΔH in kJ mol⁻¹; ΔS in J mol⁻¹ °K⁻¹.

ent, their formation involves the desolvation of the anion as for the EDAC.

The effect of pressure on the different types of EDAC is illustrated in the energy diagrams in Figure 4. These diagrams are not quantitative but are given to show the effect of pressure on the CT energy and on the free energy of formation of the EDAC. The molecular dimensions of the complexes are affected only very little by the pressures used in the present experiments and the change will have little effect on the CT energy or the stability of the complex. The solvation of the components and the EDAC is, however, changed by increase in pressure and this in turn changes the stability of the complex if it is either more or less polar than the components from which it is formed. Thus the stability of both neutral-neutral and ion-ion complexes is changed because in one the EDAC is more polar than the components while in the other it is less polar. During the combination of a large ion with a neutral molecule there is not much change in solvation, as was shown earlier²⁹ for the formation of triiodide ions, and it is not surprising that there is no pressure effect on the stability of the ion-neutral EDAC.

The energy of the CT band is affected by the change in solvation brought about by increase in pressure again

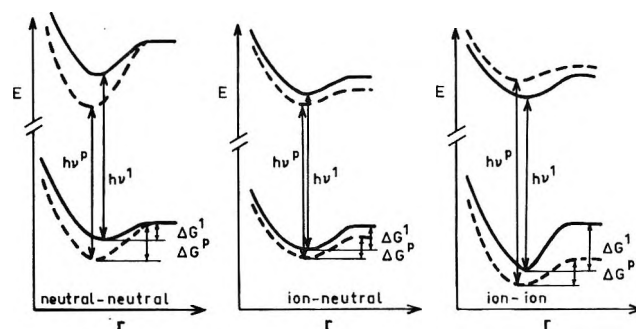


Figure 4. Schematic energy diagrams for three types of EDAC in solution, showing the effect of pressure on the stability ($-\Delta G$) and on the energy of the CT transition ($h\nu$) of the complexes. Key: —, ordinary pressure; ----, high pressure.

(28) E. Buncl, A. R. Norris, W. Proudlock, and K. E. Russell, *Can. J. Chem.*, **47**, 4129 (1969).

(29) A. H. Ewald and S. D. Hamann, *Aust. J. Chem.*, **9**, 54 (1956).

only if there is a change in polarity during excitation. This is the case in the neutral-neutral and the ion-ion complexes and in the case of MMPI it is reinforced by the change in direction of the dipole moment in the excited state. Changes in solvent polarity should on the whole parallel the changes caused by increase in pres-

sure, but the picture is often complicated by specific solvent-solute interactions.

Acknowledgments. We wish to acknowledge helpful discussions with Professor R. W. Green and Dr. S. D. Hamann and the assistance of Mr. E. S. Merritt in carrying out many of the high-pressure measurements.

Dilatometric Studies of Counterion Binding by Polycarboxylates¹

by A. James Begala² and Ulrich P. Strauss*

School of Chemistry, Rutgers University, the State University of New Jersey, New Brunswick, New Jersey 08903
(Received June 4, 1971)

Publication costs assisted by the United States Public Health Service

The volume changes associated with the binding of hydrogen and magnesium ions to three polycarboxylates in 0.2 *M* tetramethylammonium chloride were determined by dilatometry supplemented by potentiometry. The polycarboxylates were the anions of polyacrylic acid (PAA) and of the hydrolyzed copolymers of maleic anhydride with ethylene (HEMA) and vinyl methyl ether (HVMEMA). The differential volume changes, ΔV_D , observed for the interaction of hydrogen ion with the maleic acid copolymers appeared to occur in two distinct steps. The values of ΔV_D were exceptionally large for the dianionic groups and abnormally small for the monoanionic group, indicating cooperative hydrogen bonding by two adjacent carboxylate groups. Comparisons with glutaric, 4-carboxypimelic, succinic, and maleic acids showed that the highly charged poly-anions gave generally much larger effects than their low molecular weight analogues. Magnesium ion produced substantially larger volume changes with HVMEMA than with the other two polyacids, indicating that the methoxy oxygen participates in the chelation together with the adjoining carboxylate group. However, in all cases the binding of magnesium ion resulted in only partial dehydration of the participating ionic species. A few exploratory measurements suggested that barium, lithium, and potassium ion are bound in a manner similar to magnesium ion; however, silver ion produced about equal volume changes with all three polyacids, indicating insensitivity to the environment of the binding carboxylate groups.

Introduction

It has been shown that volume changes accompanying the interactions between polyanions and simple cations indicate a great degree of specificity in such interactions.³⁻⁵ The volume effects are known to arise from changes in the water structure close to the interacting ionic species. The work so far has been mainly of an exploratory nature and has dealt with comparisons involving a number of polyelectrolytes with widely different structures. It appears likely that even more can be learned about short-range interactions in polyelectrolyte systems from a comparison of polyions exhibiting only small differences in their structure. We therefore applied the dilatometric method to three weak polycarboxylic acids having the same average linear charge density but differing in the local environments surrounding the ionic groups, namely polyacrylic acid (PAA) and the hydrolyzed copolymers of maleic anhydride with ethylene (HEMA) and vinyl methyl ether (HVMEMA).

Specifically, the interactions between the polyanions of these acids in the tetramethylammonium (TMA) form and the following cations were studied by dilatometry: H^+ , Mg^{2+} , Ba^{2+} , Ag^+ , Li^+ , and K^+ . Most of our attention was devoted to the first two of these cations, for which the extent of binding was determined by potentiometry. For comparison purposes a few low-molecular weight analogues of the polyacids, namely glutaric, succinic, maleic, and 4-carboxy-pimelic acid were also included in our study.

(1) The support of this research by grants from the United States Public Health Service (Grant GM 12307) and from S. C. Johnson and Son, Inc., is gratefully acknowledged.

(2) This work constitutes a portion of a thesis presented in 1971 by A. J. Begala to Rutgers University, in partial fulfillment of the requirements for the Ph.D. degree.

(3) U. P. Strauss and Y. P. Leung, *J. Amer. Chem. Soc.*, **87**, 1476 (1965).

(4) A. Ikegami, *J. Poly. Sci., Part A*, **2**, 907 (1964).

(5) E. E. Conway, J. E. Desnoyers, and A. C. Smith, *Phil. Trans. Roy. Soc. London, Ser. A*, **256**, 389 (1964).

Experimental Section

Materials. The polyacrylic acid sample was obtained as a gift from S. C. Johnson Company. The sample of HEMA was Monsanto's Grade 21, and the HVMEMA sample was General Aniline and Film Corporation's Gantrez An-139. Since, for our purposes, the molecular weights of these polyacids were not needed, no effort at an exact determination was made. From reported viscosity results it was evident that these samples were high polymers with molecular weights of the order of 10^5 . Hydrolysis of the anhydride copolymers was accomplished by stirring in distilled water at 90° for 30 min. After filtration through a $0.22\text{-}\mu$ pore-size Millipore filter, each polyacid was exhaustively dialyzed against distilled water.

The glutaric (mp $95\text{--}96^\circ$), succinic (mp $187\text{--}189^\circ$), and maleic (mp $136\text{--}138^\circ$) acids were obtained from Matheson Coleman and Bell Co., while the 4-carboxypimelic acid (1,3,5-pentane-tricarboxylic acid, mp $112.5\text{--}114^\circ$) was obtained from K & K Laboratories. All other chemicals were reagent grade.

Ion Binding Determinations. The binding of hydrogen and magnesium ions was determined by emf measurements under nitrogen at 30° with a Radiometer Model 25 pH meter.

For hydrogen ion, glass and saturated calomel electrodes were employed. The degree of neutralization, α , of the polyacids was determined using the equation

$$\alpha = [(\text{TMAOH}) + (\text{H}^+) - (\text{OH}^-)]/C_p \quad (1)$$

where (TMAOH), (H^+), and (OH^-) are the molarities of added titrant, free hydrogen ion, and free hydroxyl ion, respectively, and C_p is the concentration of polyacid expressed in monomoles per liter. In the case of the maleic acid copolymers one monomole represents one maleic acid residue and one ethylene or vinyl methyl ether residue. For these polyacids, therefore, $\alpha = 2$ at complete neutralization. Since in several instances where comparisons between the polyacids were desired, a common range for the degrees of neutralization was convenient, a quantity α' was defined so that $\alpha' = \alpha$ for PAA and $\alpha' = \alpha/2$ for HEMA and HVMEMA, *i.e.*, so that $\alpha' = 1$ at complete neutralization for all three polyacids.

The binding of magnesium was determined using an Orion divalent ion electrode, Model 92-32, and a saturated calomel electrode. The degree of binding of magnesium ion may be defined by the expression

$$\theta_{\text{Mg}} = ([\text{Mg}^{2+}] - [\text{Mg}^{2+}]_f)/n_p \quad (2)$$

where $[\text{Mg}^{2+}]$ and $[\text{Mg}^{2+}]_f$ are the normalities of total and free magnesium ion, respectively, and n_p is the normality of total polyacid. The normality of free magnesium ion was determined from a calibration curve of the emf as a logarithmic function of the magnesium concentration in the solvent consisting of a 0.20 M tetramethylammonium chloride (TMACl)

solution. The calibration curve was linear from $3 \times 10^{-2}\text{ N}$ to $3 \times 10^{-3}\text{ N}$ magnesium ion but flattened out quite markedly below $1 \times 10^{-3}\text{ N}$ Mg^{2+} due to interference of TMA^+ . All measurements reported here were carried out above pH 5 where interference by hydrogen ion was negligible.

Dilatometry. Volume changes were measured at 30° using Linderstrom-Lang dilatometers as described previously.^{3,6} In each experiment, a given volume of solution I containing a polyelectrolyte which had been brought to dialysis equilibrium against 0.2 N TMACl at the desired pH was mixed with an equal volume of solution II containing hydrogen chloride or a metal chloride and sufficient TMACl so that the total chloride ion concentration was 0.2 N . A single solution I was used for all experiments with a given polyacid. The values of α' of PAA, HEMA, and HVMEMA were 1.00, 0.86, and 0.91, respectively, in each of these initial solutions. Complete neutralization of the maleic acid copolymers would lead to pH values above 11, necessitating an undesirably large blank correction for the neutralization of free hydroxyl ion in the experiments with hydrogen ion and also raising the possibility of undesirable hydroxyl complexes in the metal ion experiments. By keeping the pH of the initial solutions below 10, these complications were avoided.

In the experiments with silver ion, nitrate was substituted for chloride ion, and for the low-molecular-weight carboxylic acids the solution I was brought to the desired ionic strength directly without dialysis. Corrections due to dilution on mixing determined in the manner described by Strauss and Leung³ were made where necessary, but were found to be negligible in almost all cases. Those solutions II containing metal chloride were made up to pH 7 so that displacement of bound hydrogen ion by metal ion in incompletely neutralized polyacids was kept very small. The effect of such displacements on the volume changes was negligible in all cases.

Results and Discussion

Interaction with Hydrogen Ion. The volume changes observed on adding hydrogen chloride to the TMA salts of PAA, HEMA, and HVMEMA in 0.2 M TMACl are shown in Figures 1, 2, and 3, respectively. In each figure the abscissa, n_{H} , represents the moles of added hydrogen ion bound per 2.5 equiv of total polyacid. The total volume change, ΔV , represented by the ordinate, is also based on 2.5 equiv of total polyacid. The degree of neutralization, α' , is indicated by the scale on top of each of the three figures. In contrast to the PAA curve which is concave downward over the whole range of α' , the copolymer curves appear to be linear at both ends. For each copolymer,

(6) J. Rasper and W. Kauzmann, *J. Amer. Chem. Soc.*, **84**, 1771 (1962).

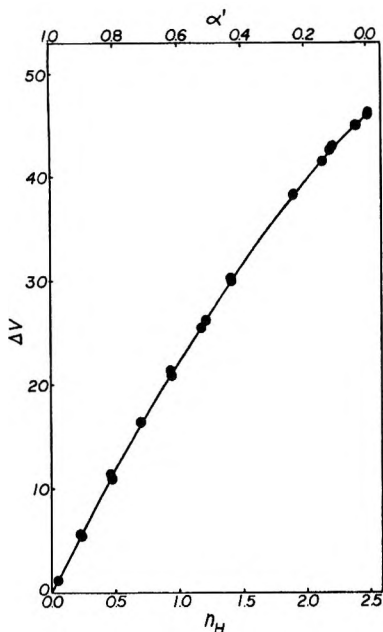


Figure 1. Volume change on the addition of hydrochloric acid to tetramethylammonium polyacrylate in 0.20 *M* TMACl at 30°. The lower abscissa, n_H , denotes moles added H^+ bound per 2.5 equiv of total polyacid. The ordinate, ΔV , denotes the volume change in milliliters per 2.5 equiv total polyacid. The upper abscissa, α' , denotes the state of neutralization of the polyacid.

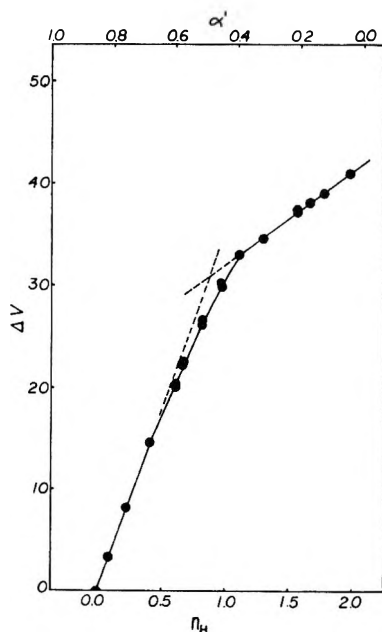


Figure 2. Volume change on the addition of HCl to the TMA salt of hydrolyzed ethylene-maleic anhydride copolymer in 0.20 *M* TMACl at 30°. Notation as in Figure 1.

the dashed lines which are extrapolated from the linear portions of the curves are seen to intersect at the half-neutralization point.

It is revealing to present these results by means of

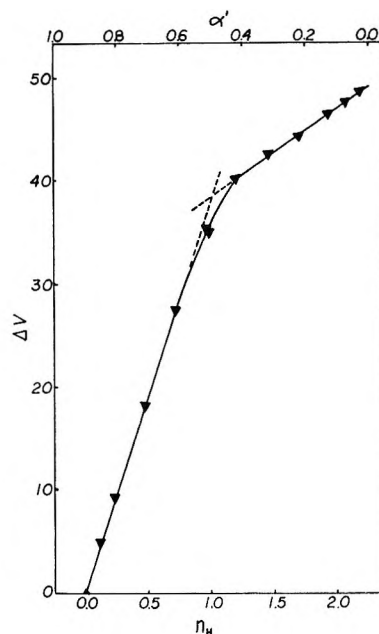


Figure 3. Volume change on the addition of HCl to the TMA salt of hydrolyzed vinyl methyl ether-maleic anhydride copolymer in 0.20 *M* TMACl at 30°. Notation as in Figure 1.

the molar differential volume change, ΔV_D , defined by the relation

$$\Delta V_D = d\Delta V/dn_H \quad (3)$$

and obtained as the slope of the curves in Figures 1-3. This quantity is a measure of the molar volume change for the reaction, $-\text{COO}^- + \text{H}^+ = -\text{COOH}$, at a given state of neutralization. In most cases ΔV_D could be obtained easily from the linear portions of the ΔV vs. n_H curves. With PAA, however, the slope varied continuously and ΔV_D was obtained by analytical differentiation of a polynomial function representing the experimental curve determined by means of a polynomial regression program for the IBM 7040 computer.

In Figure 4, ΔV_D is presented as a function of the degree of neutralization, α' , for PAA and HEMA. The difference in behavior between these two structurally isomeric polyacids shows up in a striking manner. The PAA curve increases continuously with α' , while the HEMA curve consists of two distinct levels separated by a pronounced transition about the half-neutralization point. An even sharper transition is shown by HVMEMA as seen in Figure 5. The effects observed resemble the pH behavior of these polyacids. While the pH-titration curve of PAA shows no special feature near $\alpha' = 1/2$, those of HEMA and HVMEMA exhibit a well-defined equivalence point at half-neutralization, corresponding to a ΔpK of about three units between the first and second ionization steps of the dicarboxylic acid units.^{7,8} The ΔV_D

(7) A. J. Begala, Ph.D. thesis, Rutgers University, New Brunswick, N. J., 1971.

(8) P. L. Dubin and U. P. Strauss, *J. Phys. Chem.*, **74**, 2842 (1970).

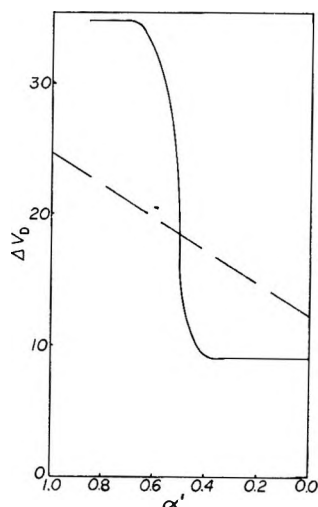


Figure 4. Differential volume changes for the binding of hydrogen ion to two isomeric polycarboxylates in 0.2 M TMACl at 30°. Dashed curve, PAA; full curve, HEMA. The ordinate, ΔV_D , in milliliters per mole of H^+ .

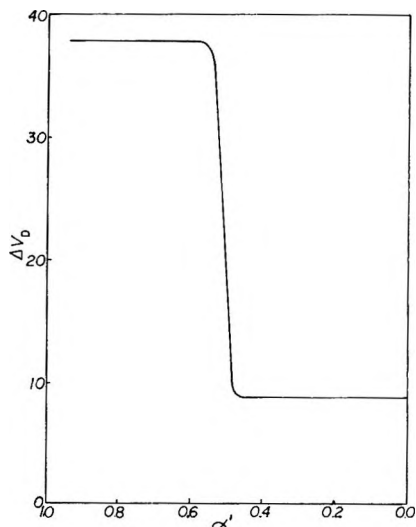


Figure 5. Differential volume change for the binding of hydrogen ion to the tetramethylammonium salt of HVMEMA in 0.2 M TMACl at 30°. Notation as in Figure 4.

results of the polyacids are summarized in Table I⁹⁻¹³ which also contains data for several di- and triprotic acids for comparison.

Viewing the glutaric and 4-carboxypimelic acids as the dimer and trimer, respectively, corresponding to polyacrylic acid, we find that ΔV_D for PAA at $\alpha = 0$ and for the first dissociable H^+ of glutaric acid has nearly identical values as one would expect. On the other hand, the corresponding value for the first H^+ of the tri-acid is slightly higher. We have no explanation for this finding at present. In general, ΔV_D appears to increase with increasing ionization for PAA as well as for its oligomers.

The striking difference in the values of ΔV_D for the first and second ionization steps of maleic acid and its

Table I: Differential Molar Volume Changes for the Interaction of Hydrogen Ion with Polyacids in 0.2 M TMACl at 30°

	α	ΔV_D	ΔV_h^a	Δn_h^b
PAA	0	12.3	7.3	4
	1	24.6	19.6	11
HEMA	0-1	9.1	4.1	2
	1-2	34.5	29.5	16
HVMEMA	0-1	8.8	3.8	2
	1-2	37.4	32.4	18
Maleic acid	0-1	6.0	1.0	0.6
	1-2	24.4	19.4	11
Succinic acid	0-1	11.6	6.6	4
	1-2	13.5	8.5	5
Glutaric acid	0-1	12.2	7.2	4
	1-2	13.7	8.7	5
4-Carboxy-pimelic acid	0-1	13.7	8.7	5
	1-2	13.7	8.7	5
	2-3	15.6	10.6	6

^a Calculated from $\Delta V_h = \Delta V_D + \bar{V}_H$, with $\bar{V}_H = -5 \text{ ml/mol}^{9-12}$ (see text). ^b Assuming the density of water of hydration = 1.1 ml/g.¹³

copolymers is most likely due to the binding of a proton to both carboxylate groups in the monoanion. Since the hydrogen bonded proton is not space filling, the resulting seven-membered ring should have the stability normally attributed to a six-membered ring. Such a chelation would account for the large value of ΔV_D when the first proton is added to the dianion since the water structure about two negative charges is disrupted. Furthermore, the chelation would explain why the values of ΔV_D for the addition of the second proton are abnormally small compared to those observed for single carboxylate groups. The single electronic charge in the hydrogen bonded dianion is distributed by resonance over a larger region than it would be in a single carboxylate group; consequently the electrostricting power would be lowered.

In contrast, succinic acid shows only a small difference between the values of ΔV_D for the mono- and dianion, indicating that with the possible rotation about the single bond between the α -methylene groups, the carboxylate groups will keep away from the cis position where their mutual repulsion is greatest.

The observation that the polydibasic acids HEMA and HVMEMA show two well-separated values for ΔV_D for the mono- and dianionic groups indicates that even in the absence of the double bond the cis position

(9) P. Mukerjee, *J. Phys. Chem.*, **65**, 740 (1961).

(10) B. E. Conway, R. E. Verrall, J. E. Desnoyers, *Z. Phys. Chem. (Leipzig)*, **230**, 157 (1965).

(11) E. Glueckauf, *Trans. Faraday Soc.*, **61**, 914 (1965).

(12) R. Zana and E. Yeager, *J. Phys. Chem.*, **71**, 521 (1967).

(13) T. Yasunaga and T. Sasaki, *Nippon Kagaku Zasshi*, **72**, 87 (1951).

of the carboxylate groups has been preserved during the hydrolysis of the anhydride form. This behavior implies absence of rotation around the single bond between the CH groups carrying the carboxylate groups, presumably due to steric hindrance by the large polymeric chains attached to these CH groups. Such steric hindrance has also been observed for nonpolymeric α, α' -dialkyl succinates.¹⁴

Of particular interest is the result that with HEMA and HVMEHA, ΔV_D for the dianion as well as for the monoanion is constant with varying α , in contrast to PAA for which ΔV_D increases linearly with α . The latter result was previously observed by Ikegami,⁴ who ascribed it to a combination of a cooperative enhancement of hydration of neighboring carboxylate groups and of an overall charge effect on the thickness of a secondary hydration region. The results for the maleic acid copolymers, on the other hand, indicate the absence of overlapping hydration of adjoining dicarboxylate groups. A comparison of the magnitude of the ΔV_D values with the corresponding ones of maleic acid is revealing. For the dianion ΔV_D is about 13 ml larger for the copolymers than for maleic acid. A comparison between fumaric and succinic acids shows that the effect of the double bond is to lower ΔV_D by not more than 2 ml for both mono- and dianions.¹⁵ Therefore, the major portion of the large increase in ΔV_D for the copolymers is likely due to an increased hydration of the dianion due to the high electrical charge on the polymer. The constancy of ΔV_D with changing α' means either that the effective overall charge does not increase beyond half-neutralization or that an increase in overall charge in this region has no further effect on the hydration of the dianion groups. For the monoanion, ΔV_D is only about 3 ml larger for the copolymers than for maleic acid. Since about 2 ml of this difference may be ascribed to the change from double to single bond, there appears to be no significant effect of polyelectrolyte overall charge in the monoanion region ($0 < \alpha' < 0.5$) where the effective charge is known to change very substantially.

To explain this difference in charge effect between the monoanion and dianion regions let us examine the number of water molecules involved in the hydration layers. The value of ΔV_D may be considered to be the sum of the volume changes of the anions and of the hydrogen ion. The contribution of the latter may be taken as 5 ml.⁹⁻¹² The values of ΔV_b , the volume change due to the anion alone, thus obtained, are given in the fourth column of Table I. If we take the density of the water of hydration as 1.1 ml g⁻¹, as estimated by ultrasonic absorption measurements,¹³ we obtain an estimate of n_b , the number of water molecules in the hydration layers of carboxylate groups, given in the last column of Table I. We note that the monoanions of the copolymers carry only two water molecules, indicating the existence of only a very small

inner hydration region. It seems not unreasonable that this inner region is not affected by the overall charge. On the other hand, the dianions are seen to carry extensive outer hydration layers. The change from the 11 water molecules in the hydration layer of the maleate to the 16 to 18 water molecules in the layers around the dianionic groups in the copolymers may well be due to the high electrical field around the polyions.

Interaction with Metal Ions. Table II summarizes the following type of experiment. Equal volumes of solution I containing the polyelectrolyte at a concentration of 0.1 N in neutralized carboxyl groups and solution II being 0.02 N in the appropriate metal chloride or nitrate at pH 7 were mixed. The ionic strength was maintained at 0.2 as described in the Experimental Section. The resulting volume increase, ΔV_t , is given in milliliters per mole of total metal ion.

Table II: Comparison of ΔV_t Values^a

Metal ion	PAA $\alpha' = 1^b$	HEMA $\alpha' = 0.86^b$	HVMEHA $\alpha' = 0.91^b$
Mg ²⁺	26.6	23.8	40.8
Ba ²⁺	33.2	28.2	44.6
Ag ⁺	20.8	18.4	18.6
Li ⁺	4.35	3.10	9.87
K ⁺	2.75	2.63	5.44

^a ΔV_t is in milliliters per mole of total metal ion. Ratio of equivalents of metal ion to equivalents of neutralized carboxyl groups was 0.2 for all data. ^b α' indicates initial degree of neutralization of polyacid. (See Experimental Section.)

All the results in Table II were obtained with a ratio of 0.2 equiv of metal ion per equivalent of neutralized carboxylate groups. At this ratio, the alkaline earth and silver ions are essentially completely bound by the polyions, and therefore ΔV_t is equal to ΔV_b , the volume increase expressed in milliliters per mole of bound metal ion. The alkali metal ions are only partly bound. Since $\Delta V_t = [(M^+)_b / (M^+)_t] \Delta V_b$, and since both $[(M^+)_b / (M^+)_t]$, the ratio of bound to total metal ion, and ΔV_b increase independently with the strength of binding, the ΔV_t values should serve as a doubly sensitive criterion for comparison of the strengths of interaction of a particular metal ion with a number of polyanions.

The results contained in Table II may be summarized as follows. First, for each alkali and alkaline earth metal ion the ΔV_t values for the isomeric PAA and HEMA polyanions are fairly close, but the values

(14) H. C. Brown, D. H. McDaniel, and O. Hefiger, in "Determination of Organic Structures by Physical Methods," Vol. I, E. A. Braude and F. C. Nachod, Ed., Academic Press, New York, N. Y., 1955 p 622.

(15) W. Kauzmann, A. Bodanszky, and J. Rasper, *J. Amer. Chem. Soc.*, **84**, 1777 (1962).

for the HVMEMA polyanion are significantly larger. Second, for the silver ion, this difference between HVMEMA and the two other polyanions is not observed. These results indicate that, unlike for the case of hydrogen ion, chelate formation of the metal ions with two adjacent carboxyl groups is of minor importance, if it occurs at all. This finding is not unexpected if we consider that seven- or eight-membered rings would be involved in such chelation phenomena for the maleic acid copolymers and the PAA, respectively. On the contrary, coordination of metal ion with an ether-oxygen and the nearest carboxylate group in HVMEMA leads to a six-membered ring, to the formation of which we ascribe the larger values of ΔV_t observed for HVMEMA with all but the silver ion. This ion is known to coordinate with two covalent bonds subtending a bond angle of 180° , and therefore cannot be made to fit into such a six-membered ring. One would expect any chelation of the silver ion to occur between carboxylate groups widely separated along the polymer chain, which would make the effect of the immediate neighborhood of the binding group to be of only minor importance, in line with our observations.

Further information about the nature of the interaction between magnesium ion and the three polyacids was obtained by measuring both the binding equilibria and the volume changes over a range of magnesium ion binding. The accessibility at the upper end of this range is limited by the appearance of a gel phase. The results are given in two forms. Figure 6 shows the total volume change observed on adding magnesium chloride to the TMA salts of the polyacids in 0.2 M TMACl. In each case, the abscissa, θ_{Mg} , represents the equivalents of magnesium ion per equivalent of total polyacid, as defined by eq 2. The ordinate, ΔV , is based on the same amount of polyacid. The quantity, ΔV_D , defined analogous to the hydrogen ion case, as

$$\Delta V_D = 2d\Delta V/d\theta_{Mg} \quad (4)$$

is a measure of the differential volume change for the binding of 1 mol of magnesium ion by a polyanion in a given state. This quantity, shown in Figure 7, is seen to decrease continuously with increasing θ_{Mg} for all three polyacids. For the maleic acid copolymers this continuous decrease is in marked contrast to the hydrogen ion effect which occurred in step-wise fashion and from which we deduced that the hydration layers of adjoining dicarboxylate groups did not overlap. The magnesium effect may be explained as follows: unlike the covalent binding of hydrogen ion, the weaker ionic binding of magnesium does not lead to complete dehydration of the participating species. As a consequence, the extent of dehydration becomes sensitive to the strength of binding which, in turn, depends on the overall charge of the polyion.

This idea is supported by the following calculation.

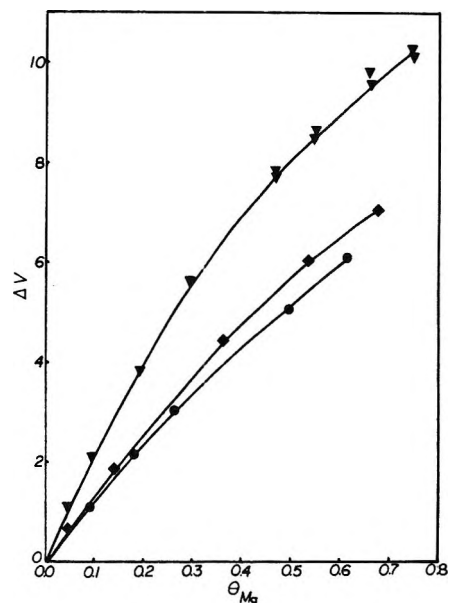


Figure 6. Volume changes on the addition of $MgCl_2$ to tetramethylammonium carboxylates in 0.2 M TMACl at 30° . The abscissa, θ_{Mg} , denotes equivalents added Mg^{2+} bound per equiv of total polyacid. The ordinate, ΔV , denotes the volume change in milliliters per equiv of total polyacid. Key: \blacklozenge , PAA; \bullet , HEMA; \blacktriangledown , HVMEMA.

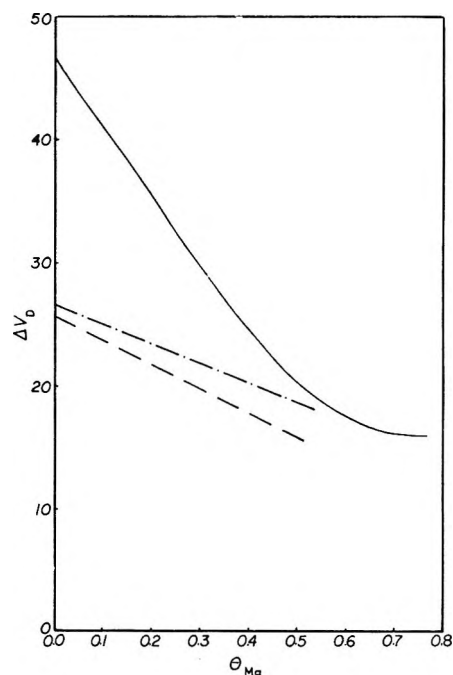


Figure 7. Differential volume changes for the binding of magnesium ion to polycarboxylates in 0.2 M TMACl at 30° . The ordinate, ΔV_D , in milliliters per mole of Mg^{2+} . Key: $-\cdot-\cdot-$, PAA; $- - -$, HEMA; $—$, HVMEMA.

From the ΔV_h values in Table I it appears that the maximum volume change for the dehydration of a dicarboxylate group is 33.6 ml/mol for HEMA and 36.2 ml/mol for HVMEMA. Various estimates have placed the maximum obtainable volume change for

magnesium ion from 30 to 42 ml/mol.^{9,12,16} Thus, complete release of water of hydration should lead to a volume change estimated between 64 and 76 ml/mol of magnesium ion for HEMA and between 66 and 78 ml for HVMEMA, whereas the largest volume changes observed by us, namely the values of the limit of ΔV_D as θ_{Mg} approaches zero, are 25.4 ml for HEMA and 46 ml for HVMEMA. These results show clearly that even under the most favorable conditions the dehydration accompanying the binding of magnesium ion by the maleic acid copolymers is incomplete. In the case of HEMA we interpret these findings to mean that one or more hydration layers separate the bound magnesium ion from the dicarboxylate group. With HVMEMA we would expect no water molecules to separate the chelated magnesium ion and the binding ligands; rather, we would expect residual water of hydration to belong to the zwitterion formed by the positive chelate consisting of the magnesium ion, one carboxylate and one ether group and by the negative carboxylate group not participating in the chelate ring. We would expect chelation to be the normal mode for

magnesium binding for HVMEMA at high α and low θ_{Mg} . As θ_{Mg} increases we visualize a gradually increasing portion of the bound magnesium ion to be unchelated and to be attracted in a manner similar to that occurring with HEMA. Such a picture is in accord with the ΔV_D curves in Figure 7, which are seen to converge at high θ_{Mg} , indicating that the mode of binding under such conditions is similar for all three polyacids.

The specificities of the polycarboxylates towards various types of cations described here demonstrate further the importance of short-range interactions in the binding of counterions by polyelectrolytes. The findings, furthermore, support the rationale of our approach in using polyelectrolytes of chemically similar structure in order to detect subtle differences in their modes of interaction with counterions.

Acknowledgment. We wish to thank the Lever Brothers Company for providing a fellowship for A. J. B. during 1967–1968. Expert technical assistance provided by Sylvia Taylor is also gratefully acknowledged.

(16) J. Padova, *J. Chem. Phys.*, **39**, 1552 (1963).

Infrared Optical Constants and Absorption Intensities of

Naphthalene Single Crystal¹

by Koji Tsuji and Haruka Yamada*

Department of Chemistry, Kwansei Gakuin University, Nishinomiya, Japan (Received February 16, 1971)

Publication costs assisted by Kwansei Gakuin University

Infrared optical constants of naphthalene single crystal have been determined along the crystal *b* axis, by measuring the ATR spectra using the perpendicular polarization. Then the absorption intensities of the fundamental bands of naphthalene have been obtained for the *b* axis components of the single crystal. The absorption intensities of the polycrystal and the oriented film have also been determined by measuring the ATR spectra of polycrystalline disks and by measuring the absorption of thin films. Comparisons of the intensities are made between the polycrystal and the single crystal. The intensity ratios obtained are in good agreement with those predicted from the oriented gas model for the B_{1u} , out-of-plane bands, but not for the B_{2u} and B_{3u} , in-plane bands. With the use of the intensities obtained the crystal splittings are discussed.

I. Introduction

The infrared absorption intensities of molecular crystals have been studied by measuring the intensities of polycrystals and by comparing the values with those of gaseous samples, in order to elucidate the intermolecular interactions in crystals, and the data have now been accumulated to a certain extent.² To develop the theoretical analysis of this problem, measurement

of the absorption intensities in single crystals is necessary, though the usual absorption measurement for most crystals is of little use.

(1) Presented at the Symposium on Molecular Structure (Chemical Society of Japan) in Tokyo, Oct 1968.

(2) See, for example, D. A. Dows, "Physics and Chemistry of the Organic Solid State," Vol. 1, D. Fox, M. Labes, and A. Weissberger, Ed., Interscience, New York, N. Y., 1963, p 657; Vol. II, 1965, p 88.

We first applied the infrared attenuated total reflection (ATR) technique to naphthalene single crystal and the polarization measurements were of great use for the determination of the assignments of molecular vibrations.³ Then we developed techniques for obtaining the optical constants and intensities for anisotropic crystals using polarized ATR. A preliminary report for the iodoform crystal was recently published.⁴

The present work reports the results of quantitative measurements on the naphthalene single crystal from the ATR technique. The most difficult point in the ATR measurements for single crystals is to make good optical contact between the ATR element and the crystalline sample. Fortunately in the case of naphthalene the contact is especially good as described earlier and caused little difficulty.^{3a} The optical constants for the *b* axis (unique crystal axis) component of the single crystal have been determined, and the absorption intensities for the *b* axis component have been calculated.

For comparison, the optical constants and intensities of the polycrystal have also been determined by the same method, using naphthalene disks made from fine powder. The intensities obtained for the disks are in good agreement with those determined from absorption measurements for thin polycrystalline films made by spraying at low temperature, justifying the above method for obtaining the absorption intensities of crystals.

Since the molecular vibrations of naphthalene have been extensively studied by polarized Raman^{5,6} as well as infrared spectra^{3a,7-11} and also by normal coordinate calculations,¹²⁻¹⁴ it seems a suitable substance for analyzing absorption intensity data.

II. Measurements of Polarized ATR Spectra for Naphthalene Single Crystal

A brief interpretation of the technique for obtaining the ATR spectra of naphthalene single crystal has already been reported.^{3a} The spectra were measured by use of a Jasco DS-402G grating double beam spectrophotometer equipped with an ATR attachment in the region 1700 ~ 400 cm⁻¹. The ATR attachment, which is constructed for single reflection and whose angle of incidence can be varied continuously over a limited range from 30 to 60°, has a hemicylindrical KRS-5 element of which the reflecting surface is 20 × 30 mm. It replaced the usual sample box and was fixed so that the reflecting beam should be parallel, as described below. The light passing through the ATR attachment was not monochromatic, and the energy was diminished to about 30% of its usual energy. The reference beam was adequately attenuated by use of a single beam attenuator. Polarized light was obtained by use of an AgCl polarizer which consists of six AgCl plates, and the efficiency was 96%. It was placed in front of the thermocouple detector, so that the

polarization effect from the spectrometer optics for the sample beam was canceled by that of the reference beam. The absorption bands located near the grating ghosts were omitted, because the observed reflectivities were less reliable than those of the other bands. The spectral slit widths used were 1.7 cm⁻¹ at 1400 cm⁻¹, 1.4 cm⁻¹ at 1200 cm⁻¹, 1.4 cm⁻¹ at 900 cm⁻¹, and 1.9 cm⁻¹ at 500 cm⁻¹. The spectra were recorded with sufficiently slow speed so that they could be confirmed to be reproducible. For the bands which overlap with those of atmospheric H₂O and CO₂, the measurements were taken after blowing out the spectrometer with air dried by passing through a molecular sieve.

The crystal structure of naphthalene is monoclinic, space group *C*_{2h}⁵-*P*2₁/*a*, with two molecules per unit cell.¹⁵ The *b* unique symmetry axis is at right angles with the *a* and *c* axes, respectively. The *c* axis makes an angle of 122° 55' with the *a* axis. The *ab* plane of naphthalene which was obtained by cleaving the single crystal was polished to optical flatness using liquid benzene. It was then fixed firmly by coinciding the crystal *b* axis with the cylindrical *z* axis of the KRS-5 element, and the *a* axis with the *x* axis, taking the reflecting surface of the KRS-5 element as *xz* plane. The direction of the *b* axis was determined by use of its double refraction. The *ab* plane as the reflecting surface was as large as that of the KRS-5 element. The upper or lower part of the cylindrical surface of the KRS-5 element was sometimes covered with a black paper band, when the reflecting surface was slightly smaller than that of the KRS-5. The light propagates in the *ac* plane, that is, the incident (or reflecting) plane, perpendicular to the *b* axis. Perpendicular polarization where the electric vectors vibrate along the *b* axis gives the ATR spectrum for the *b* axis component. The optical properties of naphthalene crystal are also known,¹⁶ one of the principal axes of the dielectric ellipsoid coinciding with the

(3) (a) H. Yamada and K. Suzuki, *Spectrochim. Acta, Part A*, **23**, 1735 (1967); (b) K. Tsuji, H. Yamada, K. Suzuki, and I. Nitta, *ibid.*, **26**, 475 (1970).

(4) K. Tsuji and H. Yamada, *Bull. Chem. Soc. Jap.*, **41**, 1975 (1968).

(5) M. Suzuki, T. Yokoyama, and M. Ito, *Spectrochim. Acta, Part A*, **24**, 1091 (1968).

(6) D. M. Hanson and A. R. Gee, *J. Chem. Phys.*, **51**, 5052 (1969).

(7) G. C. Pimentel and A. L. McClellan, *ibid.*, **20**, 270 (1952).

(8) W. B. Person, G. C. Pimentel, and O. Schnepp, *ibid.*, **23**, 230 (1955).

(9) A. L. McClellan and G. C. Pimentel, *ibid.*, **23**, 245 (1955).

(10) H. Luther, G. Brandes, H. Günzler, and B. Hampel, *Z. Elektrochem.*, **59**, 1012 (1955).

(11) E. R. Lippincott and E. J. O'Reilly, Jr., *J. Chem. Phys.*, **23**, 238 (1955).

(12) D. E. Freeman and I. G. Ross, *Spectrochim. Acta*, **16**, 1393 (1960).

(13) D. B. Scully and D. H. Whiffen, *ibid.*, **16**, 1409 (1960).

(14) J. R. Scherer, *J. Chem. Phys.*, **36**, 3308 (1962).

(15) S. C. Abrahams, J. M. Robertson, and J. G. White, *Acta Cryst.*, **2**, 233, 238 (1949).

(16) K. S. Sundarajan, *Z. Krist.*, **93**, 238 (1936).

crystal b axis and the other two axes lying in the ac plane, making an angle of 97° with each other. For the measurement of the b axis component, therefore, no elliptic polarization results.

III. Determination of Optical Constants and Absorption Intensities from the ATR Spectra

A. Calculation of Optical Constants. The optical constants, namely, refractive index, n , and attenuation index, k , can be calculated from the observed ATR spectra on the basis of Fresnel's and Snellius' formulas.

The methods for obtaining optical constants from reflectivities have been reported by several authors.¹⁷⁻²³ In the present work, a method is used which calculates n and k from the reflectivities, R_s 's, measured at two different angles θ_1 and θ_2 by use of polarized light whose electric vectors vibrate perpendicularly to the incident plane. R_s is expressed by

$$R_s = \left| \frac{\cos \theta - \sqrt{n'^2 - \sin^2 \theta}}{\cos \theta + \sqrt{n'^2 - \sin^2 \theta}} \right|^2 \quad (1)$$

Here, the complex refractive index of the absorbing sample is given by

$$n' = n - ink \quad (2)$$

For the numerical determination of n and k expressions have been derived by Fahrenfort and Visser.¹⁷ On their calculations, however, it is difficult to get accurate values of $2n^2k$ by eight-figure computation unless k is sufficiently large. Thus at the wings of absorption bands, both n and k cannot be accurate, as pointed out by Hansen.¹⁸ According to Hansen, an approximate formula

$$k = -\frac{(1 - n^2)\sqrt{\sin^2 \theta - n^2}}{4n^2 \cos \theta} \ln R_s, \theta > \theta_{\text{critical}} \quad (3)$$

should therefore be used, if k becomes less than 0.005. We thus use the method by Fahrenfort and Visser with some modification suggested by Hansen. After the calculations to obtain n 's have been completed, k 's are computed. And if the k obtained is less than 0.005 it is recalculated by use of expression 3.

The computations were performed on a FACOM 270-20 take off computer with double precision where all numbers could be effective up to 17 figures. Since the refractive index, n , calculated was the value relative to that of the KRS-5 element, the refractive index of the sample could be obtained by multiplying n by the refractive index of KRS-5 at that wave number. The refractive index of KRS-5 can be calculated by Tilton's dispersion formula.²⁴

In the computation program, R_s 's observed at two incident angles θ_1 and θ_2 , at respective wave numbers, were taken as input data, and n , k , and Lambert's α

$$\alpha = \frac{4\pi nk}{\lambda} \quad (4)$$

are obtained as outputs. A subprogram to plot n , k , and α vs. wave number by use of a X-Y plotter was inserted. The absorption intensity, A , is given by

$$A = \frac{1}{c} \int \alpha d\nu \quad (5)$$

where c is the density of naphthalene crystal in moles per liter unit ($c = 9.11_3 \text{ mol l.}^{-1}$ calculated from the density 1.152). Integration was taken over a region three times as wide as half-width.

B. Parallelism of Incident Beam. For the determination of optical constants from ATR spectra, it is required that the beam passing through the KRS-5 element and then irradiating the sample should be parallel.¹⁷ It was fortunately achieved by moving the ATR attachment, originally designed to have its focus point at the reflecting surface, towards the monochromator from the usual location by about 2 cm. The light energy entering the monochromator was hardly diminished by this change. Because of the hemicylindrical element, there might be possibility of errors in the results due to convergence in the z axis direction. It must be tested by use of liquid samples.

C. Determination of the Angles of Incidence. For the determination of optical constants, it is also required to know the angles of incidence accurately. Although the ATR attachment had an angle scale on it, it was not precise enough for the present purpose. We determined the angles of incidence using a small He-Ne laser (University Laboratories Co., 0.6 mW) as follows. The sharp laser light was introduced into the ATR attachment from the entrance or exit, and the light reflected at the reflecting surface of the KRS-5 element was run on a white paper horizontally fixed on the ATR attachment. The angle between the reflected light and the reflecting surface plane of the KRS-5 element was measured with a protractor on the paper. By repeating this procedure, the angles of incidence could be determined within an accuracy of 0.1° .

D. Selection of Incident Angles θ_1 and θ_2 . For the measurement of R_s , θ_1 and θ_2 should be chosen so as

(17) J. Fahrenfort and W. M. Visser, *Spectrochim. Acta*, **18**, 1103 (1962).

(18) W. N. Hansen, *ibid.*, **21**, 209 (1965).

(19) J. Fahrenfort and W. M. Visser, *ibid.*, **21**, 1433 (1965).

(20) A. C. Gilby, J. Burr, Jr., W. Krueger, and B. Crawford, Jr., *J. Phys. Chem.*, **70**, 1525 (1966).

(21) P. A. Flournoy, *J. Chem. Phys.*, **39**, 3156 (1963).

(22) T. Hirshfeld, *Spectrochim. Acta*, **22**, 1823 (1966).

(23) N. J. Harrick, "Internal Reflection Spectroscopy," Interscience, New York, N. Y., 1967.

(24) L. W. Tilton, E. K. Plyler, and R. E. Stephens, *J. Res. Nat. Bur. Stand.*, **43**, 81 (1949).

to minimize the errors appearing in n and k . Error analysis was carried out by Fahrenfort and Visser¹⁷ and also by others.^{20,25} Following their suggestion, the R_s curve was first recorded at a higher angle, θ_1 , than the critical angle, θ_{critical} , where the R_s curve resembled the usual absorption curve, then at a lower angle, θ_2 ($\theta_2 < \theta_{\text{critical}}$), where the R_s curve appeared as that of anomalous dispersion, the difference between the two angles being $\theta_1 - \theta_2 \approx 10^\circ$.

E. Correction for the Incompleteness of the Contact between the KRS-5 Element and the Sample. For crystal-line samples the contact between the KRS-5 element and the sample cannot be as good as for the case of liquid samples. A method of measuring optical constants of single crystals by the ATR technique, however, has already been reported by us,⁴ and the optical constants were determined for the iodoform crystal. In the present work the same technique has been used. The observed reflectivity can be corrected for the incompleteness of the contact between the KRS-5 element and the sample crystal. If any appreciable energy is detected as reflectivity for parallel polarization, R_p , at the principal angle, θ_p , in a nonabsorbing region, we ascribe it to the energy due to the lack of optical contact, since R_p should go down to zero at the principal angle, θ_p . Measuring R_p at θ_p in a region where the sample does not show any absorption, we can obtain the true R_s corrected for the incompleteness of the contact

$$R_s(\text{true}) = R_s(\text{obsd}) - R_p(\text{at } \theta = \theta_p, k = 0) \quad (6)$$

As we described previously^{3a} the contact between the KRS-5 element and the naphthalene was so good that the correction of R_s for incompleteness of the contact was hardly needed, though the correction was determined in every case.

IV. Measurements of Intensities for Polycrystalline Naphthalene

For the comparison of the intensities of single crystal with those of polycrystal, we have determined the intensities of the polycrystal by two methods.

A. Absorption Measurements of Polycrystalline Films. The polycrystalline film of naphthalene was obtained by subliming the vapor onto a cold substrate (KRS-5) in a cold cell at -160° . The absorption spectra were measured by the same spectrometer as described above, with the narrower slit widths than those for the ATR measurements. The spectral slit widths were 1.4 cm^{-1} at 1400 cm^{-1} , 1.2 cm^{-1} at 1200 cm^{-1} , 1.0 cm^{-1} at 900 cm^{-1} , and 1.5 cm^{-1} at 500 cm^{-1} , which were smaller than the observed half-widths, about 4–5 cm^{-1} . During the slow deposition of naphthalene the transmitted energy was recorded at 4000 cm^{-1} to form interference fringes, which enabled us to determine the thickness of the film.²⁶ The thicknesses were 3.12 to 3.30 μ , and the intensities were obtained

as usual. By this method the film deposited was not always polycrystal but was preferentially oriented film where the ab plane was largely perpendicular to the incident beam. The film orientation could be determined by comparing the absorption spectrum of the powder with the polarized ATR spectra of the single crystal previously reported.^{3a} The oriented film thus obtained was transformed to polycrystal by annealing. Figures 8 and 9 show the spectra of polycrystal and the ab -oriented film, respectively. Most of the film obtained showed the spectra intermediate between these two. The films were then annealed carefully, observing the remarkable changes in the B_{3a} bands, such as those at 1504 and 1212 cm^{-1} . To prevent loss of the sample due to sublimation, the annealing process was done for the narrow range of temperatures.

The absorption intensities have been determined for both the polycrystal and the ab plane component of oriented film at -160° .

B. ATR Method for Naphthalene Disk. Since the intensities of single crystal have been determined by the ATR method at room temperature, it is preferable to compare these with polycrystalline intensities determined also from the ATR method at room temperature, if possible. To achieve this, naphthalene disks were made by the usual method for KBr disks. With powder of large particle size, a disk obtained was not isotropic. Completely isotropic disks were obtained when the particle size of the powder was less than 300 mesh. The optical constants were obtained by use of such an isotropic disk. The optical contact of the naphthalene disk with the KRS-5 element was so good that the correction for incompleteness of contact was almost negligible. The calculation was the same as that described for the single crystal. From the optical constants the intensities were obtained.

We also tried to make polycrystalline blocks by pouring fused naphthalene into a flat glass vessel and cooling it. The naphthalene block thus obtained was anisotropic, and the reflecting surface was almost the ab plane. We also tried pouring fused naphthalene onto the KRS-5 element directly, but the reflecting plane was almost parallel to the ab plane and the optical contact between the KRS-5 element and the naphthalene block was rather incomplete.

V. Results

A. Single Crystal. Some of the reflectivity curves obtained for the b axis component of the single crystal are shown in Figures 1 and 2, where the two incident angles were 54.6 and 44.2° . From the R_s curves, n and k are calculated. Figures 3–7 are obtained by plotting n and k vs. wave number. The absorption

(25) W. N. Hansen, *Spectrochim. Acta*, **21**, 815 (1965).

(26) J. L. Hollenberg and D. A. Dows, *J. Chem. Phys.*, **37**, 1300 (1962).

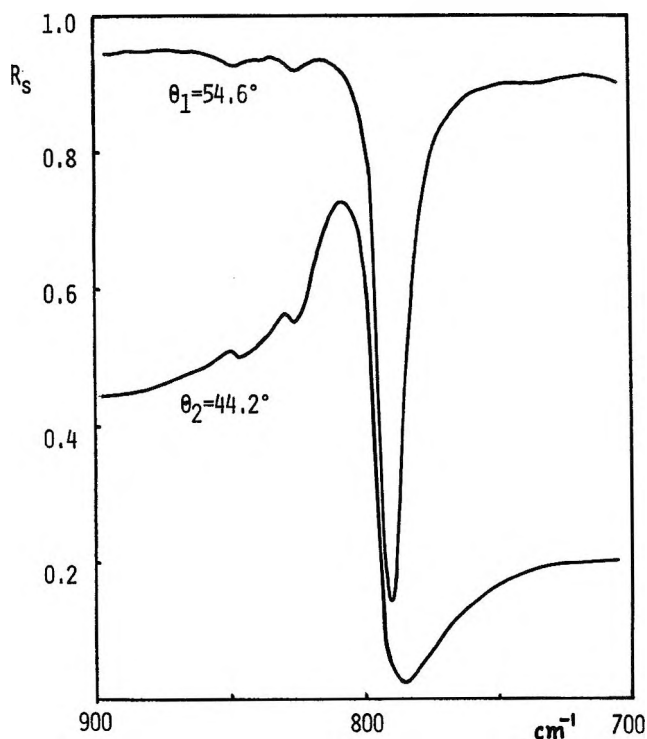


Figure 1. Reflectivity curves obtained for b axis component of single crystal.

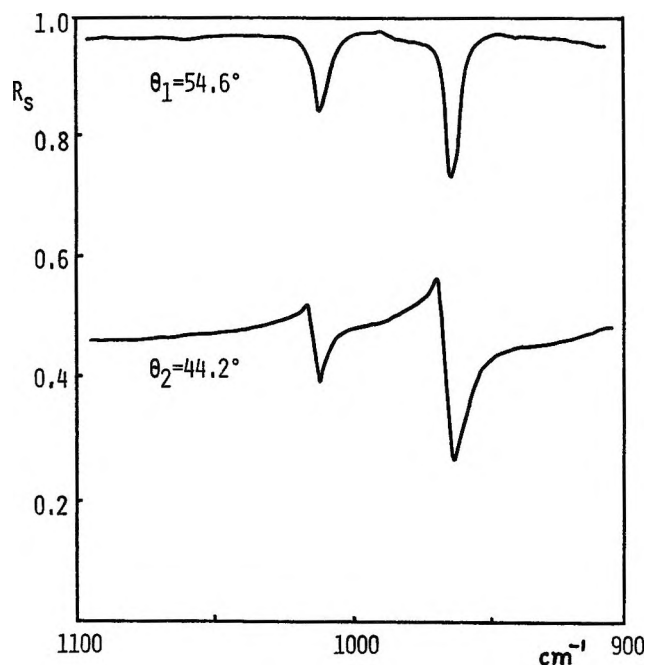


Figure 2. Reflectivity curves obtained for b axis component of single crystal.

intensities defined by (4) could be determined using the n and k values here obtained. In Table I the intensities measured for the b axis component are listed together with the frequencies and the assignments for all infrared-active fundamentals. The spectra of polycrystalline and ab -oriented film are shown in Figures 8 and 9.

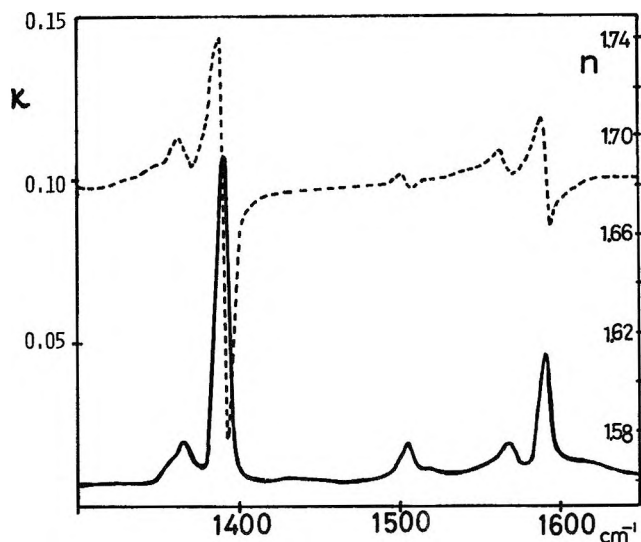


Figure 3. Optical constants along b axis obtained from ATR measurements of single crystal; n by dotted line, k by solid line.

Table I: Frequencies of Infrared-Active Fundamentals and Absorption Intensities for b Axis Components of Single Crystal

Symmetry	ν , cm^{-1}	A_b , darks	Assignments
B_{1u}	960	660 ^a	CH bend
	780	8770 ^b	CH bend
	480	1820 ^c	CC distort
	(176)		Wig-wag
B_{2u}	3065		CH stretch
	3054		CH stretch
	1593	710 ^a	CC stretch
	1390	1600 ^a	CC stretch
	1274	940 ^a	CH bend
	1126	850 ^{a,d}	CH bend
	820		Skele. distort
	(362)		Skele. distort
B_{3u}	3090		CH stretch
	3005		CH stretch
	1504	280 ^a	CC stretch
	1365	350 ^a	CC stretch
	1212	290 ^a	CH bend
	1135	850 ^{a,d}	CH bend
	1008	390 ^a	Skele. distort
616		Skele. distort	

^a 10% error. ^b 20% error. ^c 5% error. ^d Including 1126- and 1135- cm^{-1} peaks.

B. Polycrystal and Oriented Film. The n and k curves obtained for the polycrystalline disks are shown in Figures 10–12. The intensities for the polycrystal are obtained from the n and k values, and also from the absorption measurements of the thin films. The results are summarized in Table II as A_{poly} . For the 480 cm^{-1} (B_{1u}) band, the intensity obtained from the ATR measurements is 2580 darks, being in good agreement with 2620 darks obtained from the absorption measurements. The average values from these

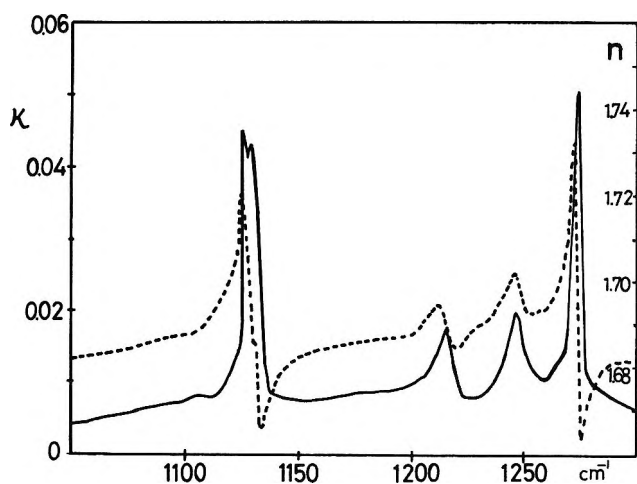


Figure 4. Optical constants along b axis obtained from ATR measurements of single crystal; n by dotted line, k by solid line.

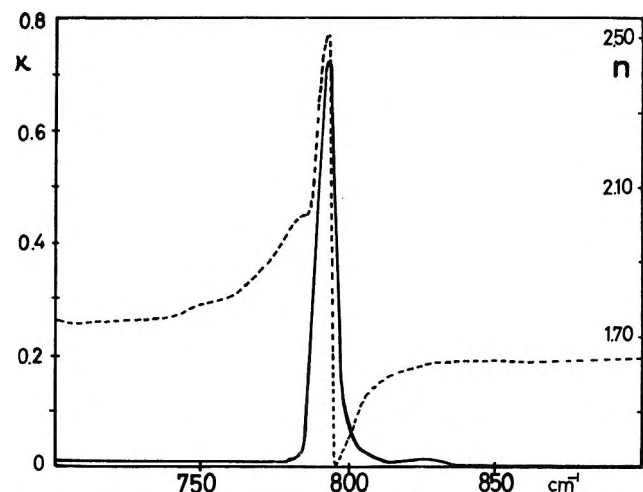


Figure 6. Optical constants along b axis obtained from ATR measurements of single crystal; n by dotted line, k by solid line.

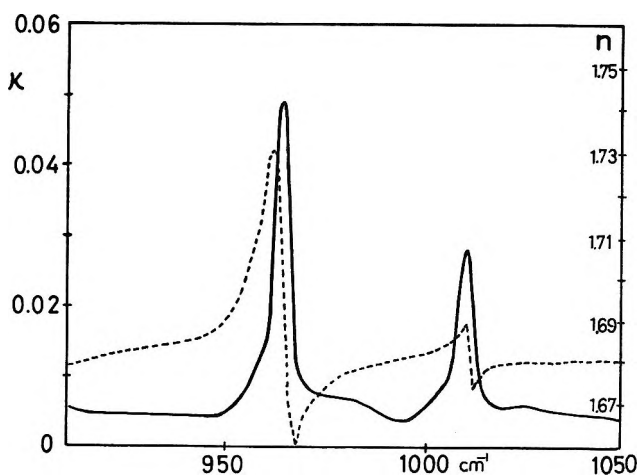


Figure 5. Optical constants along b axis obtained from ATR measurements of single crystal; n by dotted line, k by solid line.

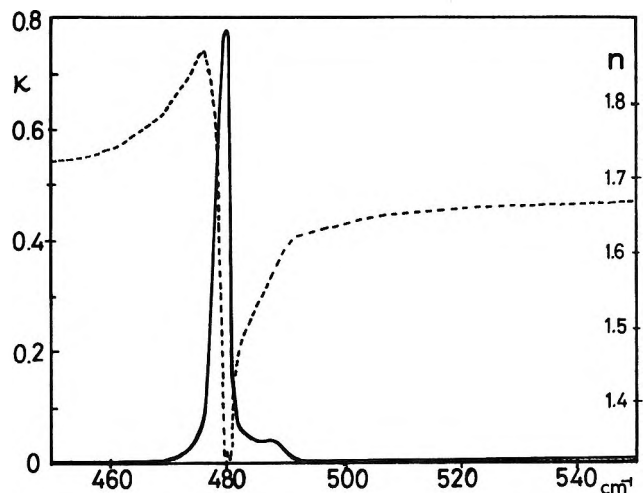


Figure 7. Optical constants along b axis obtained from ATR measurements of single crystal; n by dotted line, k by solid line.

Table II: Absorption Intensities of Polycrystal and ab Plane Component of Oriented Film

Symmetry	ν , cm^{-1}	$A_{\text{poly, darks}}$			$A_{\text{ab, darks}}$
		ATR	Absorption	Average	
B_{1u}	960	900 ^b	840 ^b	870	1100 ^c
	480	2580 ^c	2620 ^a	2600	3190 ^c
B_{2u}	1390	1060 ^b	1020 ^b	1040	1150 ^c
	1274	680 ^b	640 ^b	660	610 ^c
B_{3u}	1212	700 ^b	600 ^b	650	
	1008	970 ^b	810 ^b	890	440 ^c

^a 5% error. ^b 10% error. ^c 20% error.

two methods are also given in Table II, though for the weaker bands other than the 480-cm^{-1} band the intensities are less accurate.

In Table II, A_{ab} represents the intensities in the ab plane component which were obtained from absorp-

tion spectra of the ab -oriented films, with unpolarized light, where the ab plane was parallel to the window surface and perpendicular to the light beam.

VI. Accuracy of Optical Constants and Absorption Intensities

To determine the optical constants by the ATR method, the beam parallelism, the accuracy of incident angles, the efficiency of the polarizer, the optical contact between sample and ATR element, as discussed above, should all be considered. The validity of the apparatus and the computation method here used could be checked by determining optical constants of liquids which have already been determined. For the 1035-cm^{-1} band of liquid benzene, the refractive index (mean value) obtained by our method was 1.463, compared with 1.462 by Fahrenfort, *et al.*,¹⁷ 1.454 by Crawford, *et al.*,²⁰ and 1.450 by Thompson, *et al.*²⁷ The

(27) G. M. Irons and H. W. Thompson, *Proc. Roy. Soc., Ser. A*, **298**, 160 (1967).

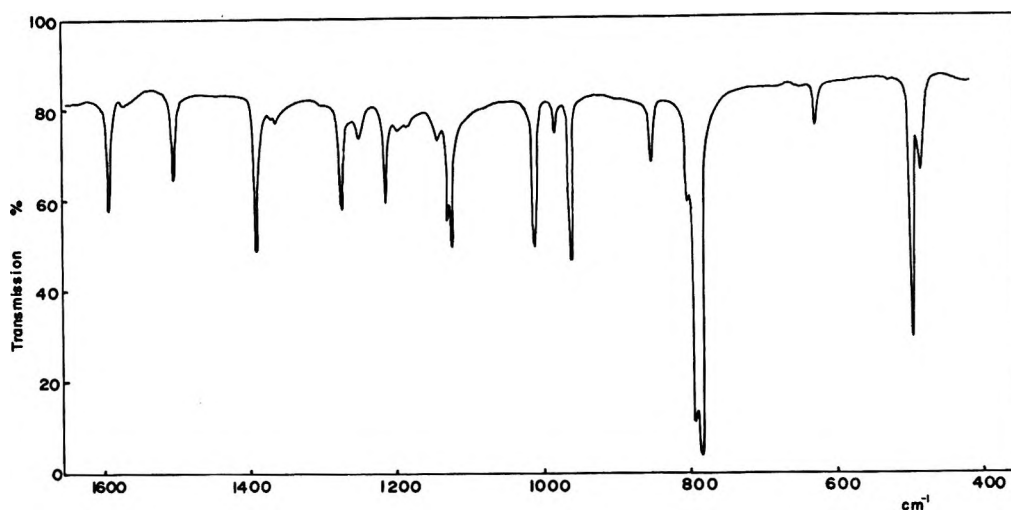


Figure 8. Absorption spectrum of polycrystalline film at -160° ($l = 3.30 \mu$).

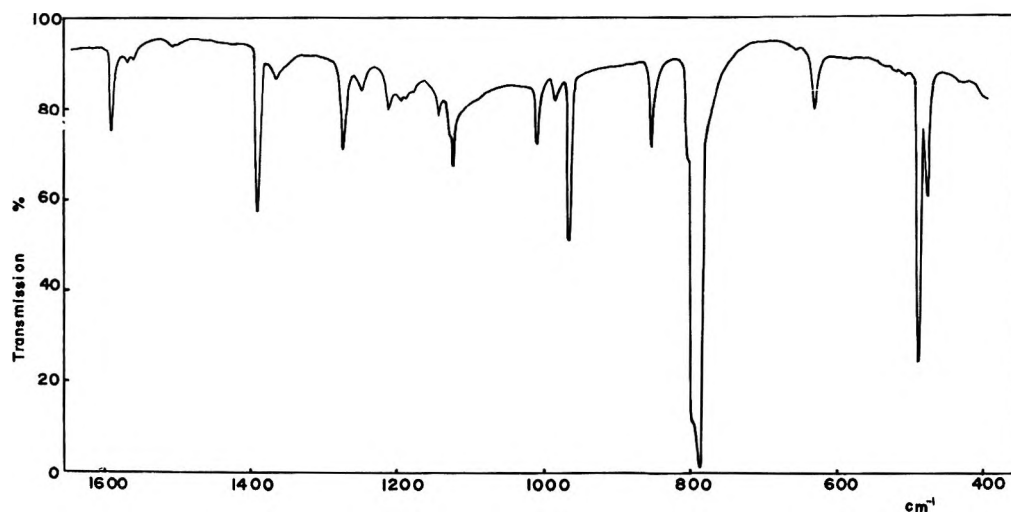


Figure 9. Absorption spectrum of *ab*-oriented film at -160° ($l = 3.12 \mu$).

absorption intensity of this band, $A \times 10^{-3}$ darks, was 1.23, compared with 1.23 by Fahrenfort, *et al.*,¹⁷ 1.29 by Crawford, *et al.*,²⁰ 1.5 by Thompson, *et al.*,²⁷ and 1.12 by Flournoy.²¹ Besides liquid benzene, measurements were made on chloroform, methylene halides, etc. For the bands which had been already studied the values obtained were in good agreement with those reported. Some new data on liquids will be published elsewhere.

It can be seen that the present technique may be satisfactory for liquid samples. For crystalline samples the difficulty of making optical contact should be added. Applying this technique, we already reported the result of a crystalline sample, iodoform. If a comparison is made for the cases of iodoform and naphthalene, the optical contact between the sample and the ATR element is much better for naphthalene than for iodoform.

Although the calculated n and k actually fluctuate with the observed R and θ values, the α values, how-

ever, are little affected by such changes. The accuracy of absorption intensity depends on not only the method and the sample used but also the values of intensity and width of the band concerned. From our experiences, we might say that bands with intensity from 100 to several thousand darks are suitable, and the most accurate intensity is obtained for a band of about 2000 darks, if the ATR method with KRS-5 element is used. The best value here obtained for the 480-cm^{-1} band might include experimental and calculated errors up to 5%, which value is about the same as that for the absorption intensity of the film.²⁶ For the other bands the errors must be larger than 5%. The estimated errors are shown in the footnotes to the tables.

VII. Discussion

The ATR spectra of naphthalene single crystal, the band splittings and the dichroic properties have already been described and the qualitative results

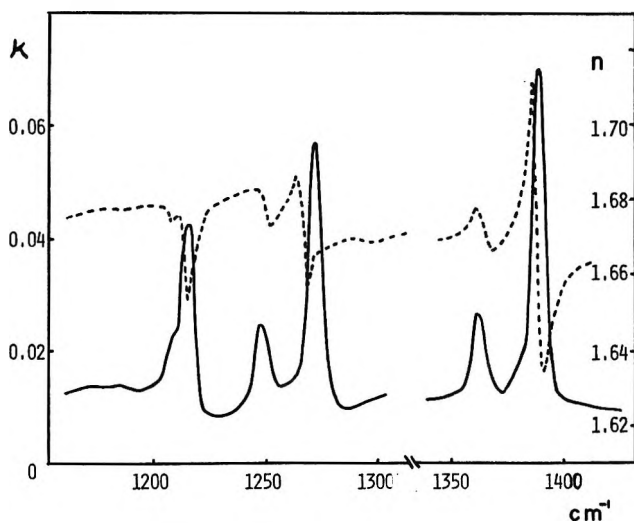


Figure 10. Optical constants for naphthalene disk obtained from ATR measurements; n by dotted line, k by solid line.

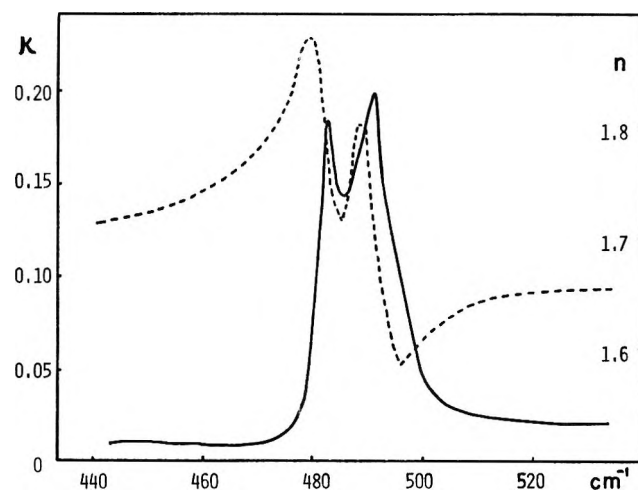


Figure 12. Optical constants for naphthalene disk obtained from ATR measurements; n by dotted line, k by solid line.

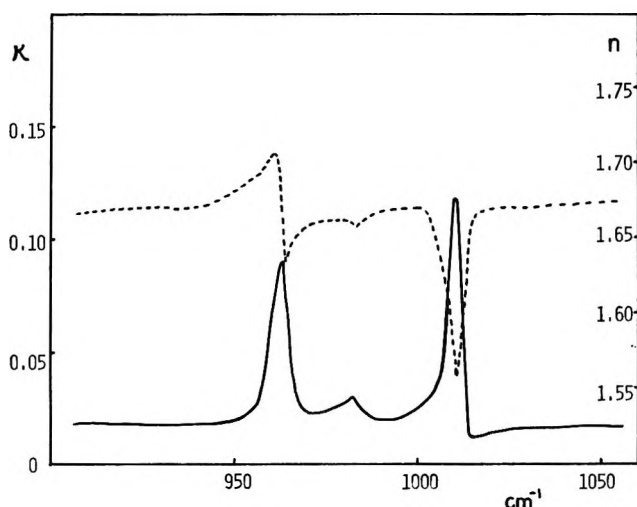


Figure 11. Optical constants for naphthalene disk obtained from ATR measurements; n by dotted line, k by solid line.

obtained here are identical with those obtained previously.^{3a} We now discuss the quantitative results.

The refractive indices obtained for the b axis show anomalous dispersion at the absorption, and the mean values over the respective bands are 1.67–1.70, a little smaller than the value, 1.722, along the b axis at the Na D line.¹⁶ The n and k curves at 1130-cm⁻¹ band are still double for the b component of the single crystal. It is explained as the b axis component of the 1143-cm⁻¹ (B_{3u}) band and the b axis component of 1126-cm⁻¹ (B_{2u}) band, as described earlier.^{3a}

Tables I and II compare the absorption intensities between the single crystal and the polycrystal. In Table III the intensity ratio, A_b/A_{poly} , indicates the ratio of the intensity of the b axis component of single crystal to that of the polycrystal, A_{ab}/A_{poly} the intensity ratio between the ab component of the oriented film and the polycrystal, and A_b/A_{ab} the intensity

ratio between the b axis component of single crystal and the ab component of oriented film.

The intensity ratios along the crystal axes have been calculated from the crystal structure,^{8,15} using the oriented gas model. The ratios ($a:b:c$) are 3.6:1:0.20 for B_{1u} bands, 0.14:1:0.025 for B_{2u} bands and 4.2:1:23.2 for B_{3u} bands, where c axis indicates the actual crystal c axis and not the c' (orthorhombic) axis.

The calculated values for A_b/A_{poly} , A_{ab}/A_{poly} , A_b/A_{ab} are obtained by taking into account the directions of electric vectors which were used in the measurements. The ratio A_b/A_{poly} is calculated as $b^{1/3}(a+b+c)$, and similarly A_{ab}/A_{poly} and A_b/A_{ab} as $1/2(a+b)^{1/3}(a+b+c)$ and $b^{1/2}(a+b)$, respectively.

For the bands belonging to the B_{1u} symmetry species, the observed intensity ratios are in good agreement with the calculated values, that is, the predictions from the oriented gas model.

On the other hand, for the bands belonging to B_{2u} and B_{3u} the agreements between calculation and observation are rather poor, for any ratio, A_b/A_{poly} , A_{ab}/A_{poly} , or A_b/A_{ab} . However, the bands belonging to a symmetry species behave in the same way; A_b/A_{poly} observed for one band is almost equal to that of the other band belonging to the same species. The intensity behaviors can thus be classified by the symmetry species to which the bands belong.

The b axis components of the B_{2u} bands are weaker than predicted from the oriented gas model, while the b axis components of the B_{3u} bands are stronger than predicted. The B_{2u} bands originally have the strongest components in the b axis, while the B_{3u} bands have the weakest components. Consequently, the deviations from the oriented gas model appear to be such that the strongest components grow weak and the weakest components become strong. Similarly for the c axis components, the B_{3u} bands are smaller than predicted and the B_{2u} bands larger.

Table III: Comparison of Intensity Ratios between Observation and Calculation

Symmetry species	ν , cm^{-1}	A_b/A_{poly}		$A_{\text{ab}}/A_{\text{poly}}$		A_b/A_{ab}	
		Obsd	Calcd	Obsd	Calcd	Obsd	Calcd
B_{1u}	480	0.70	0.63	1.23	1.44	0.57	0.43
	960	0.76	0.63	1.27	1.44	0.55	0.43
B_{2u}	1274	1.42	2.58	0.92	1.47	1.54	1.75
	1390	1.54	2.58	1.11	1.47	1.39	1.75
B_{3u}	1008	0.44	0.11	0.50	0.27	0.89	0.38
	1212	0.45	0.11				

Measurements of intensities in solution are given in Table IV. The intensities of the B_{1u} bands in solution are close to those in polycrystal, while the intensities of B_{2u} and B_{3u} bands are quite different from those in the crystal. The bands at 1392 cm^{-1} (B_{2u}) and at 1209 cm^{-1} (B_{3u}) in solution are quite different in intensity from those in polycrystal. Since there cannot be found any reason why the errors in these bands are especially large, these are probably due to the condensation effects. It is noticed that the B_{1u} , out-of-plane vibrations behave quite normally again, since the field corrections are not much different between the solution and the crystal.

Table IV: Absorption Intensities of Fundamental Bands in Solution

Symmetry species	ν , cm^{-1}	A_{soln} , darks	Solvent	A_{poly} , darks
B_{1u}	956	950 ± 5	CS_2	870
	780	$15,300 \pm 500$	CS_2	$12,500^a$
	476	$2,400 \pm 240$	CS_2	2,600
B_{2u}	1595	860 ± 60	CHBr_3	
	1392	570 ± 20	CCl_4	1,040
	1265	500 ± 20	CS_2	660
	1127	$1,030 \pm 30^b$	CS_2	
B_{3u}	1505	$1,070 \pm 30$	CHBr_3	
	1364	110 ± 10	CCl_4	
	1209	210 ± 10	CS_2	650
	1012	700 ± 20	CS_2	890

^a Calculated from A_b , see text. ^b Including the peak at 1137 cm^{-1} .

Unfortunately the results for the C-H stretching bands have not been obtained, because the ATR method used did not give rise to accurate intensities for the C-H stretching region.

Taking into account the field effects for the ellipsoidal molecules in condensed media,²⁸ the relative increase in apparent intensities in crystal from the gaseous values should be in the order of $B_{1u}(z) > B_{2u}(Y) > B_{3u}(X)$. Then the increases in the b axis component should be $B_{2u} > B_{3u}$, that is, the increases in intensity are expected to be greater for the B_{2u} bands than for the B_{3u} bands. This is not the actual case. Conse-

quently, the deviation from the prediction is certainly caused by an effect other than the field effect.

We present merely the experimental results at this time, but it is very probable that the electronic states perturb the vibrational intensities in the crystal as discussed by Brown.²⁹ There are two low electronic transitions at 2200 \AA ($A_g \rightarrow B_{3u}$) and 2750 \AA ($A_g \rightarrow B_{2u}$) which give rise to Davydov splittings in the crystal,³⁰ and so vibronic coupling could be expected for the B_{2u} and B_{3u} bands and not for the B_{1u} bands.

Among the absolute infrared intensities of some fundamental bands which we have measured, the out-of-plane bands at 780 and 480 cm^{-1} , assigned to the C-H deformation and the skeletal distortion vibrations, respectively, are the strongest. The observed crystal splittings are 20 cm^{-1} for the 780-cm^{-1} band and 9 cm^{-1} for the 480-cm^{-1} band, and they are considerably larger than those observed for the other bands. The splittings of fundamental bands and the lattice vibrational frequencies in the crystal have been studied by Harada and Shimanouchi³¹ and by Rich and Dows.³² Their calculations are based on assumed intermolecular interactions between two molecules, composed of central forces acting between pairs of atoms, one on each molecule. For the lattice vibrations, Harada and Shimanouchi found good agreement between observed and calculated values, by taking into account the interactions in the H-H and H-C pairs. On the other hand, the splittings of the bands, especially at 780 and 480 cm^{-1} , could not be fully interpreted in terms of the H-H interactions, even when the H-C interactions were additionally considered.

As shown in Table II these two bands causing the large splittings are the strongest in the b axis component of the single crystal. Although the 780-cm^{-1} band is too strong for measuring the absorption intensity of the polycrystal, we can predict its value because the B_{1u} bands show the same intensity ratios in the

(28) O. F. Kalman and J. C. Decius, *J. Chem. Phys.*, **35**, 1919 (1961).

(29) T. L. Brown, *ibid.*, **43**, 2780 (1965).

(30) D. P. Craig and J. R. Walsh, *ibid.*, **24**, 471; **25**, 588 (1956); *J. Chem. Soc.*, 1613 (1958).

(31) I. Harada and T. Shimanouchi, *J. Chem. Phys.*, **44**, 2016 (1966).

(32) N. Rich and D. A. Dows, *Mol. Cryst. Liquid Cryst.*, **5**, 111 (1968).

oriented gas model. For the 780-cm⁻¹ band we calculated the polycrystalline intensity as 12,500 ± 1,500 darks. For the 480-cm⁻¹ band, the polycrystalline intensity is calculated as 2890 or 2200 darks, using A_b or A_{ab} , respectively, and the average is obtained as 2550 ± 350 darks, in agreement with the observed value of 2600 darks.

If we assume transition dipole-transition dipole interactions between the molecules in the crystal,² the ratio of the splittings between these two bands should be

$$\frac{\frac{1}{\nu_{780}} \left(\frac{\partial \mu}{\partial Q} \right)_{780}^2}{\frac{1}{\nu_{480}} \left(\frac{\partial \mu}{\partial Q} \right)_{480}^2} = \frac{\Delta \nu_{780}}{\Delta \nu_{480}} = 2.9$$

compared with the observed value 20/9 = 2.2. The assumption of atom-atom interactions gives rise to the ratio of the splittings of 2.4/12.6 from the Kitaigorodski potential, while the value 8.4/0.2 is obtained from the deBoer potential, these calculated splittings being far from the observed values.³² Thus it is clear that the transition dipole-transition dipole interactions play an important role in the splitting of the intense bands, such as 780- and 480-cm⁻¹ bands of naphthalene, even when the behavior of most weak bands and the lattice vibrations could be well interpreted as due to the atom-atom interactions.

Acknowledgment. The authors wish to thank Mr. T. Inoue for his assistance in making the disks and also in measuring the absorption intensities in solutions.

Mass Spectrometric Study of the Reaction of Dicyanoacetylene with Oxygen Atoms¹

by Clifford W. Hand*

University of Alabama, University, Alabama 35486

and Ralph H. Obenauf, Jr.

Carnegie-Mellon University, Pittsburgh, Pennsylvania 15213 and the University of Alabama, University, Alabama 35486
(Received June 29, 1971)

Publication costs assisted by the University of Alabama

The reaction of dicyanoacetylene with oxygen atoms was studied in a discharge-flow reactor coupled to a time-of-flight mass spectrometer. The second-order rate constant at room temperature is 1.1×10^{-16} cm³/(molecule sec) (standard deviation 0.3×10^{-15}). In the presence of O₂ the stoichiometric factor is 1.2, increasing to 5.5 oxygen atoms consumed per dicyanoacetylene molecule in the absence of molecular oxygen. Initial attack is believed to be at the acetylenic bond, and stable end products are CO, NO, CO₂, and C₂N₂. CN, OC₃N, OC₂N, and C₂N were observed as important intermediates, and the presence of the intermediate C₂O is inferred. First mass spectrometric evidence of the species OC₂N₂ has been obtained.

Introduction

The reaction of dicyanoacetylene (DCA) with ground-state oxygen atoms has recently been investigated by Meyer and Setser² in a discharge-flow apparatus. The reaction is chemiluminescent, emitting both the (A → X) and (B → X) bands of CN, and it was the observation of this emission which enabled Meyer and Setser to measure a rate constant and to outline the general course of the reaction. We report here the results of a mass spectrometric investigation of the same reaction, with a determination of the second-order rate constant over the pressure range 0.75 to 5.0 Torr. Ad-

ditional products and intermediates have been identified, and the overall stoichiometry of the reaction was found to be critically dependent on the presence of molecular oxygen.

Experimental Section

Experiments were conducted in a discharge-flow reactor with mass spectrometric detection, as shown in

(1) Submitted to the faculty of Carnegie-Mellon University by R. H. O. in partial fulfillment of the requirement for the Ph.D. degree.

(2) J. A. Meyer and D. W. Setser, *J. Phys. Chem.*, **74**, 3452 (1970).

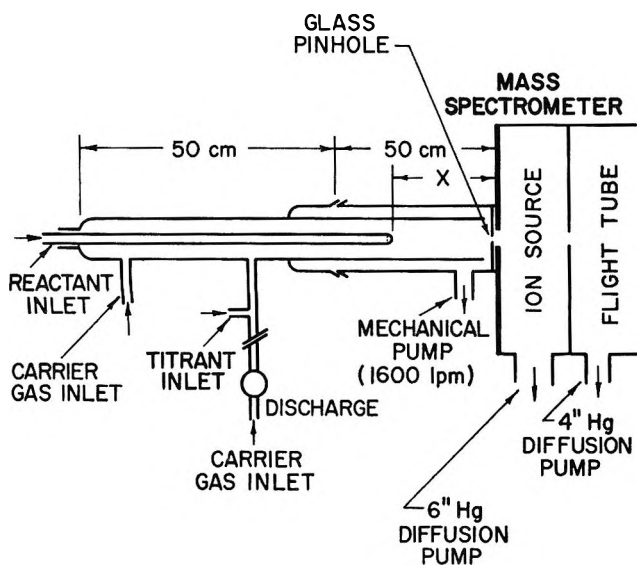


Figure 1. Discharge flow system.

Figure 1. The mass spectrometer was a Bendix Model 12 time-of-flight, modified by the substitution of a Model 14 ion source and a John Fluke high-voltage power supply. Oxygen atoms were produced in a microwave discharge (2.45 GHz; Kiva 125-W generator with Evenson cavity) in molecular oxygen diluted by inert carrier gas or, alternatively, by the nitric oxide titration of active nitrogen.³ The latter method produces O atoms relatively free of molecular oxygen (*vide infra*).

The stable reactant DCA, sometimes diluted in inert carrier, entered through a movable, axially mounted probe (6-mm Pyrex tubing). The probe entered through an extension tube which was continuously flushed with undischarged carrier gas.⁴ This was found to greatly reduce nonreproducibility associated with what we have come to call "probe effects," and which presumably are due to atoms coming into contact with fresh, unpoisoned surfaces created when the probe position is changed. The probe had six radially positioned 0.5-mm diameter holes to afford good mixing with a minimum of back diffusion of atoms into the probe. Carrier gas flow rates were measured within 1% by calibrated capillary flow meters,⁵ two of which were used to permit introduction of 5–10% oxygen diluted in a helium carrier. Reactant and titrant gas flow rates were measured to an accuracy of 0.5% by monitoring the pressure drop from a known volume with Dynasciences Model P7D-0.1PSID differential pressure transducers, which in turn were calibrated against a MKS Baratron Type 144 capacitance manometer. When flow rates of less than 10^{-8} mol/sec were required, the reactant was diluted in inert carrier gas.

The reactor was constructed from 22-mm Pyrex tubing with a cross-sectional area of 2.80 ± 0.02 cm². Pressure in the reactor was monitored (through the

probe with no gas flowing through the probe) with the Baratron manometer and found to be invariant $\pm 1\%$ along the 50-cm length of the reactor. The wall was poisoned with 5% HF and rinsed with distilled water, a treatment which extended also to the connecting lines, upstream to and somewhat beyond the discharge region. The efficiency of the poisoning was periodically checked by measurement at room temperature of the rate of heterogeneous oxygen atom recombination; a typical value for the rate constant was 1.5 sec^{-1} , corresponding to a surface recombination coefficient, γ , of 3.5×10^{-5} . High pumping speed was provided by an Edwards ED1SC1500 (1600 l./min) pump; the linear flow velocities in the reactor were varied by means of a throttle valve.

A sample of the reacting mixture was expanded directly into the TOF ion source, through pinholes of 0.05–0.50 mm diameter depending on the reactor pressure. These pinholes were constructed by HF etching of microscope cover slips (25 mm diameter by 0.3 mm thick) so that discharged gas would contact only Pyrex surfaces prior to sampling. This procedure produced uniform pinholes of 0.05 mm diameter, from which larger orifices were made by careful grinding with a flame-sharpened tungsten needle. An Edwards ED6M3A Hg diffusion pump was used in the differential pumping system. Maximum sensitivity varied somewhat with experimental conditions, but for most of the work reported here was about 10^{12} particles/cm³ in the flow reactor.

Oxygen atom concentration was determined by several means, depending on the experiment; for those runs in which molecular oxygen was discharged, atom concentration was determined by titration with NO₂.⁶ The visual end point, that is, the extinction of the air afterglow, occurred about 10% beyond the instrumental end point (defined as the point at which $m/e = 16$ is reduced to background). Atom concentration could also be determined by observing the decrease in $m/e = 32$ peak height when the discharge was turned on, a method which consistently yielded O-atom concentrations within 5% of those obtained by titration to the instrumental end point; the latter was used in all rate constant calculations. For those runs in which O atoms were produced by the titration of active nitrogen with NO, the visual end point was found to lie about 5% short of the instrumental; here again the instrumental end point was used in calculations.

Nitric oxide was purified by passage through 50% aqueous KOH to remove NO₂, then through anhydrous P₂O₅ and subsequent trap-to-trap distillation. Nitro-

(3) R. Brown and C. A. Winkler, *Angew. Chem., Int. Ed. Engl.*, **9**, 181 (1970).

(4) H. Niki, E. Daby, and B. Weinstock, *Symp. Combust.*, **12th**, 277 (1969).

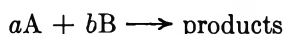
(5) B. A. Thrush, *J. Chem. Educ.*, **41**, 429 (1964).

(6) F. Kaufman, *Progr. React. Kinet.*, **1**, 1 (1961).

gen dioxide was mixed with oxygen to react with NO impurity, then passed through P_2O_5 and distilled. Dicyanoacetylene was prepared according to the procedure given by Byrd.⁷ Acetylenedicarboxamide (2.5 g; Eastman), P_2O_5 (21 g), and sand (42 g) were thoroughly mixed under vacuum, and the temperature suddenly raised to 215° by immersion in an oil bath. The mixture was continuously stirred, and the crude product was collected in a trap at -196°. The reaction was complete (ca. 30% yield) in about 30 min, and the product was purified by distillation. Analysis by mass spectrometry showed no impurities. Matheson ultra-pure oxygen and prepurified nitrogen were used without further purification. The carrier gas, helium or nitrogen, was passed through a Pyrex wool-packed liquid nitrogen trap upstream of the discharge, and for those runs in which the main objective was the identification of products and intermediates, helium was passed through a titanium sponge furnace at 600° to remove trace impurities.

Results

Determination of the Rate Constant. All values for rate constants were obtained under pseudo-first-order conditions at room temperature with at least a 15-fold excess of one reactant. Determinations were made with each reactant in excess, and although differing in method, both types measured the rate of removal of one species. For the reaction stoichiometry



the measured rate is dA/dt or dB/dt , which are related by

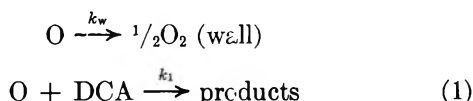
$$\frac{1}{a} \frac{dA}{dt} = \frac{1}{b} \frac{dB}{dt}$$

therefore, measurement of both rates yields the ratio of the stoichiometric coefficients

$$\frac{\frac{dA}{dt}}{\frac{dB}{dt}} = \frac{a}{b}$$

This ratio is usually referred to as the stoichiometric factor.

When DCA is the reactant in excess, two reactions must be considered



With the reactant inlet probe fixed at a distance, x , from the pinhole, and a constant linear flow velocity, LFV , the integrated rate expression becomes

$$\ln \frac{[O]}{[O]_x} = -\frac{(k_1)(x)}{LFV} [\text{DCA}] - \frac{(k_w)(x)}{LFV}$$

where $[O]_x = [O]$ at the point of mixing, *i.e.*, immediately upstream of the probe tip. The quantity is never measured, but as shown below its value is not required for a determination of k_1 .

If $[O]_0$ is equal to $[O]$ at the mass spectrometer pinhole when $[\text{DCA}] = 0$

$$\ln \frac{[O]_0}{[O]_x} = -\frac{(k_w)(x)}{LFV}$$

and thus

$$\ln \frac{[O]}{[O]_0} = -\frac{(k_1)(x)}{LFV} [\text{DCA}]$$

The slope of a plot of $\ln [O]$ vs. $[\text{DCA}]$ is proportional to k_1 , the second-order rate constant, provided that the slope is evaluated in the pseudo-first-order region of the graph. To eliminate instrumental errors such as back diffusion of atoms into the probe or stagnation at the pinhole, the slopes were determined at two different probe positions and the equations solved simultaneously for the rate constant. Typical results are shown in Figure 2.

When O atoms were in excess, the concentration of DCA was measured as a function of probe position; the data were corrected for any change in atom concentration, which was monitored throughout. The instrument sensitivity for O atoms was calibrated daily by O-atom titration at the midpoint of the reactor. Typical results from these runs are shown in Figure 3, where the rate constant is obtained from the slope, m , of the plot by

$$k_1 = \frac{(m)(LFV)}{[O]}$$

The results are collected in Table I, and with O atoms in excess the rate constant was $1.1 \pm 0.3 \times 10^{-15} \text{ cm}^3/(\text{molecule sec})$,⁵ and invariant over the pressure range 0.75–5.0 Torr. With DCA in excess the average rate constant was $1.4 \pm 0.4 \times 10^{-15} \text{ cm}^3/(\text{molecule sec})$, also invariant with respect to pressure. The stoichiometric factor, that is, the moles of O atoms consumed per mole of DCA consumed, is thereby determined as 1.2 ± 0.4 . However, when using "molecular oxygen free" atoms and DCA in excess a rate constant of $3.0\text{--}6.0 \times 10^{15} \text{ cm}^3/(\text{molecule sec})$ was obtained, giving a stoichiometric factor of 2.7–5.5.

To check the accuracy of our procedures the rate constant and stoichiometric factor of the widely studied reaction $O + C_2H_2$ were determined. The average value of the second-order rate constant determined in other laboratories by several different techniques^{9–14}

(7) N. R. Byrd, NASA Corp. Report N6420601 (1964).

(8) This and all subsequent errors are the standard errors derived from first-order regression analysis of data.

(9) A. A. Westenberg and N. deHaas, *J. Phys. Chem.*, **73**, 1181 (1969).

(10) J. O. Sullivan and P. Warneck, *ibid.*, **69**, 1749 (1965).

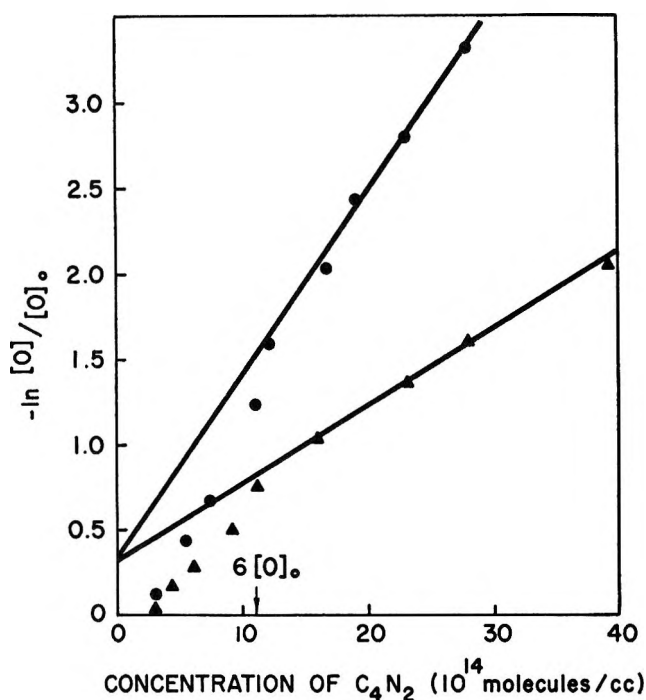


Figure 2. Fixed probe method: the rate of removal of O atoms, measured at two different probe positions, as a function of [DCA]. Linear flow velocity = 62.8 cm/sec; total pressure = 5.05 Torr; O₂/He discharge; ●, 40 cm; ▲, 15 cm.

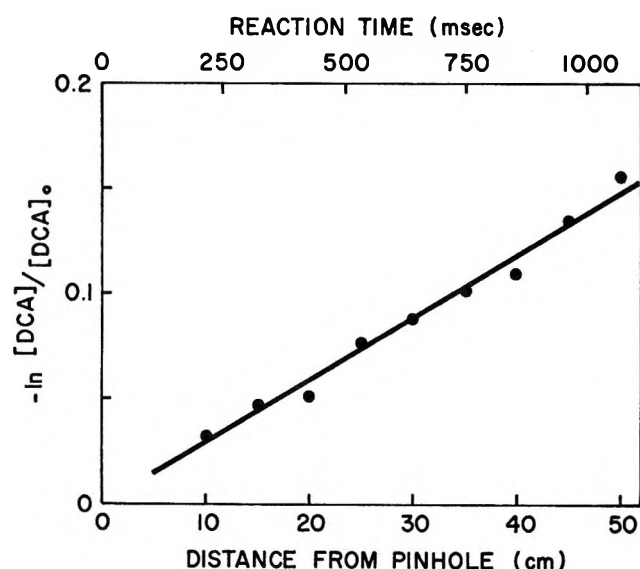


Figure 3. Rate of removal of DCA by O atoms; [DCA] vs. time; linear flow velocity = 46.7 cm/sec; total pressure = 4.95 Torr; O₂/He discharge; [O] = 6.20 mTorr.

is $1.5 \pm 0.2 \times 10^{-13}$ cm³/(molecule sec) at room temperature, in agreement with our value of $1.0 \pm 0.3 \times 10^{-13}$ cm³/(molecule sec) determined with O atoms in excess. With C₂H₂ in excess, and using the fixed probe technique described above, a value of $2.0 \pm 0.3 \times 10^{-13}$ cm³/(molecule sec) was obtained yielding a stoichiometric factor of 2.0 ± 0.4 in agreement with literature values.^{9,11,13}

Table I: O + DCA Second-Order Rate Constants Obtained under Various Conditions at 298–301°K

Pressure, Torr	Species in excess	Pressure of species in excess, mTorr	Discharged gas	$k_1 \times 10^{14}$, cm ³ /(molecule sec)
0.76	O	3.03	O ₂ /He	1.1 ± 0.2
0.74	O	3.12	O ₂ /He	1.3 ± 0.3
0.75	DCA	≤ 42.8	O ₂ /He	1.7 ± 0.3
1.00	O	4.25	O ₂ /He	1.4 ± 0.1
1.10	O	4.37	O ₂ /He	1.5 ± 0.2
1.00	O	3.73	O ₂ /He	1.1 ± 0.2
0.97	DCA	≤ 73.1	O ₂ /He	1.2 ± 0.2
3.10	O	5.82	O ₂ /He	0.9 ± 0.1
2.97	O	6.79	O ₂ /He	0.8 ± 0.1
2.93	DCA	≤ 137.3	O ₂ /He	0.9 ± 0.1
5.00	O	6.01	O ₂ /He	0.7 ± 0.1
4.95	O	6.20	O ₂ /He	0.7 ± 0.1
5.05	DCA	≤ 100.8	O ₂ /He	1.7 ± 0.2
1.05	O	2.92	N ₂	2.0 ± 0.4
1.02	DCA	≤ 43.0	N ₂	3.0 ± 0.5
1.03	DCA	≤ 28.6	N ₂	6.0 ± 0.3

Identification of Products and Intermediates. Dibeler, *et al.*,¹⁵ have reported appearance potentials of fragment ions from DCA and C₂N₂, and the least of these was 17.3 V. All of our experiments were, therefore, run at an ionizing voltage of less than 16.5 V, to eliminate the possibility of incorrectly identifying as an intermediate what was actually a fragment ion from reactant or end product. Furthermore, the complete absence of ions at higher masses supports our assignment of mass peaks to parent rather than fragment ions. Peaks corresponding to CO₂, C₂N₂, NO, CO, NO₂, OC₂N, and OC₂N₂ were observed in the O₂ discharge experiments. The appearance potential of the $m/e = 28$ peak was 14.2 ± 0.2 V, indicating it to be primarily CO rather than N₂. The major products were CO₂, CO, and NO, while C₂N₂ and NO₂ were formed to a lesser extent, and OC₂N₂ and OC₂N were observable only at maximum sensitivity.

When the reaction was run in the "molecular oxygen free" system, the intermediates CN, OC₃N, and C₂N were observed in addition to OC₂N and OC₂N₂, and in comparable amounts. No conclusions can be drawn concerning CO and NO, since their contributions to the peaks at $m/e = 28$ and 30 would be overwhelmed by N₂ carrier and NO titrant. Cyanogen was present in a greater proportion to CO₂ than in the runs with

(11) C. A. Arrington, W. Brennen, G. P. Glass, J. V. Michael, and H. Niki, *J. Chem. Phys.*, **43**, 525 (1965).

(12) G. S. James and G. P. Glass, *ibid.*, **50**, 2268 (1969).

(13) J. M. Brown and B. A. Thrush, *Trans. Faraday Soc.*, **63**, 630 (1967).

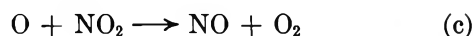
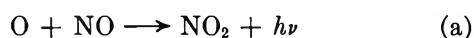
(14) K. Hoyerman, H. G. Wagner, and J. Wolfrum, *Z. Phys. Chem. (Frankfurt am Main)*, **55**, 72 (1967).

(15) V. H. Dibeler, R. M. Reese, and J. L. Franklin, *J. Amer. Chem. Soc.*, **83**, 1813 (1961).

O₂ present, and NO₂, which was observed as a minor product in the O₂ discharge runs, was not observed. The reaction was accompanied by an intense violet chemiluminescence which was not observed in the oxygen discharge system.

Discussion

In the present work we have determined the room temperature rate constant for the reaction of DCA with oxygen atoms to be $1.1 \pm 0.3 \times 10^{-15}$ cm³/(molecule sec), in rather sharp contrast to the value of $3.6 \pm 0.7 \times 10^{-14}$ cm³/(molecule sec) obtained by Meyer and Setser.² There are two possible factors contributing to this discrepancy. First, Meyer and Setser measured the reaction rate by monitoring O-atom concentration in the absence of molecular oxygen. Although their result is reported as a rate constant, it is actually the product of the rate constant and the stoichiometric factor; the true bimolecular rate constant is obtained by dividing their value by the number of O atoms consumed per DCA molecule. Our results indicate that this stoichiometric factor is critically dependent on the concentration of molecular oxygen. Apparently O₂ efficiently quenches the further consumption of atoms by secondary radicals (*vide infra*). This is demonstrated in the present work by a stoichiometric factor of 1.2 in the O₂ runs and a stoichiometric factor of 2.7–5.5 when O₂ is not present. It should be pointed out in this regard that it is virtually impossible to produce O atoms truly free of molecular oxygen. First, one must slightly overtitrate with nitric oxide to ensure that N atoms are consumed, and hence oxygen can be formed *via*

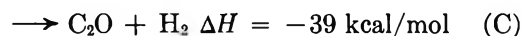
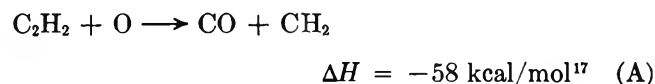


These reactions proceed with rate constants $k_a \cong 1 \times 10^{-17}$, $k_b \cong 5 \times 10^{-32}$ (M = N₂), and $k_c > 1 \times 10^{-13}$, all in molecular units.⁶ At 3 Torr [N₂] $\cong 10^{17}$ molecules/cm³ giving a second-order rate constant $k_b' \cong 5 \times 10^{-15}$ cm³/(molecule sec). If the titration is deliberately stopped well short of the end point, the result will be a mixture of O and N atoms. Even in this case, the reaction system (a–c) is important near the nitric oxide input where mixing occurs and particularly important inside the injector tip due to back-diffusion of nitrogen atoms into the stream of pure nitric oxide. We have tried several different injectors, the most successful being a 0.5-mm capillary tip approximately 5 mm long. Even here, however, the air afterglow extended about 2 cm past the capillary upstream into the NO supply line. Second, wall recombination of O atoms occurs from the point of titration on, becoming more important at slower linear flow velocities. On the basis of these considerations it is not at all un-

likely that the [O₂] can be up to 10% of the [O] in the "O₂-free system." Since the stoichiometric factor for O + DCA is clearly a function of the O₂ concentration our value of 2.7–5.5 should be regarded as a lower limit.

The second reason for the discrepancy in k_1 can be seen by referring to Figure 2, in which the plot becomes linear only when [DCA]/[O] > 6. The sharp downward break, beginning anywhere from six- to tenfold excess, was evident in all of our fixed probe runs. The most likely explanation of this behavior is the failure of the assumption of pseudo-first-order kinetics. The value of k_1 reported by Meyer and Setser was obtained at a three- to sixfold excess; working up our data in this concentration region, assuming a first-order rate law, gives rate constants about twice that which we report in Table I.

Mechanism. The reaction O + DCA should have many points of similarity to the reaction of oxygen atoms with acetylene, for which the initial attack is believed to be^{9,16}



The analogous possibilities in the O + DCA reaction are

Table II: Selected Heats of Formation

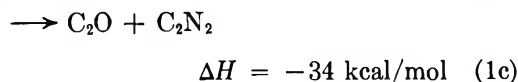
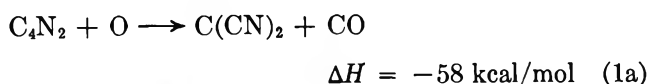
Substance	ΔH_f , kcal/mol	Reference
C ₄ N ₂	127	2
O	60	a
NO	23	a
NO ₂	8	b
CO	-25	a
C ₂ N ₂	154	a
CN	≤103	c
C ₂ O	79	2
C ₂ N ₂	74	21
NCO	16	21
C ₂ N	184	2
CO ₂	-94	b
C ₂ H ₂	58	a
CH ₂	85	a
N	113	a

^a D. R. Safrany and W. Jaster, *J. Phys. Chem.*, **72**, 3305 (1968).

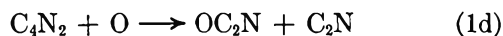
^b F. D. Rossini, D. D. Wagman, W. H. Evans, S. Levin, and I. Jaffe, *Nat. Bur. Stand. (U. S.), Circ.*, **500** (1952). ^c D. W. Setser and D. H. Stedman, *J. Chem. Phys.*, **49**, 467 (1968); V. H. Dibeler and S. K. Liston, *ibid.*, **47**, 4548 (1967).

(16) D. G. Williamson and K. D. Bayes, *J. Phys. Chem.*, **73**, 1232 (1969).

(17) This and all subsequent heats of reaction have been calculated on the basis of the values given in Table II.

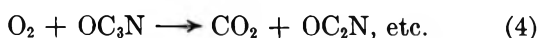
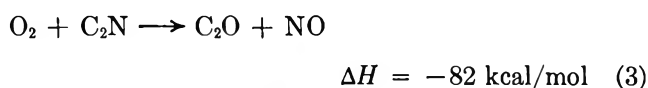
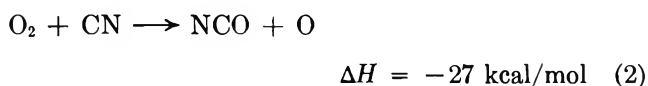


Although several reactions could account for the small quantities of OC_2N observed in all runs



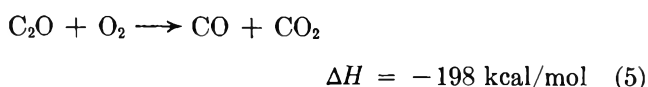
we regard reaction 1d as the most important for three reasons. First, since the concentration of OC_2N is about the same with and without molecular oxygen, reaction D is unimportant. Second, C_2N is observed in the "O₂-free" runs. Third, the stoichiometric factor was 1.2 (in the presence of O₂), while significant contribution by reaction E would require a larger stoichiometric factor.

The intermediates CN, C_2N , and OC_3N were not observed with molecular O₂ present, and thus could be quenched by



Reaction 2 is fast¹⁸ ($k_2 = 7 \times 10^{-12} \text{ cm}^3/(\text{molecule sec})$ at 687°K) with very low activation energy, and in our system, where $[\text{O}_2] \cong 10^{13} \text{ molecules/cm}^3$, can easily account for removal of CN. Reaction 3 accounts for the absence of C_2N in the O₂ discharge runs, and reaction 4 could account for part of the CO₂ production as well as OC_2N .

The C_2O radical was not observed; nevertheless it is a frequently invoked intermediate¹⁶ and could undergo reactions 5 or 6

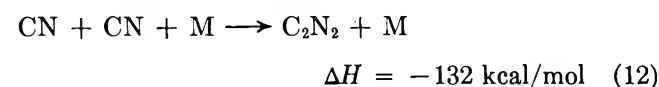
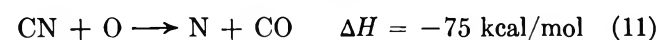
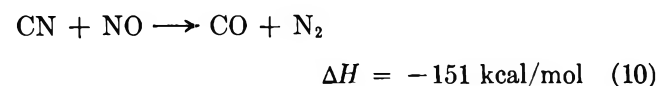
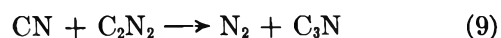


Reaction 5 could be the major step by which CO and CO₂ are formed, since CO₂ production is reduced relative to C_2N_2 in the O₂-free runs. However, if reaction 5 is sufficiently fast it would still produce appreciable amounts of CO₂, since the concentration of molecular oxygen is about $10^{13} \text{ molecules/cm}^3$ even in the "O₂-free" runs. It is unlikely that CO₂ could be produced to any extent by



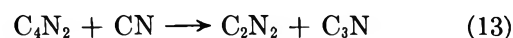
Reaction 7 is slow¹⁹ ($k_7 = 2 \times 10^{-20} \text{ cm}^3/(\text{molecule sec})$) at room temperature, as is reaction 8. Baulch reports¹⁹ $k_8 \cong 3 \times 10^{-34} \text{ cm}^6/(\text{molecule}^2 \text{ sec})$ and at 1 Torr, where $[\text{M}] \cong 3 \times 10^{16} \text{ molecules/cm}^3$, $k_8' \cong 1 \times 10^{-17} \text{ cm}^3/(\text{molecule sec})$, assuming nitrogen has an average third-body efficiency.

In addition to reaction 2 several reactions can account for CN removal



Paul and Dalby have obtained a value of $k_9 = 4 \times 10^{-15} \text{ cm}^3/(\text{molecule sec})$ ²⁰ from flash photolysis experiments near room temperature, and hence reaction 9 should be of minor importance with respect to reactions 2 and 11 ($k_2 = 7 \times 10^{-12} \text{ cm}^3/(\text{molecule sec})$, $k_{11} = 2 \times 10^{-12} \text{ cm}^3/(\text{molecule sec})$ ¹⁸). Also, the concentrations of O and O₂ are much greater than those of the products C_2N_2 and NO, and since our measurement of the $m/e = 28$ appearance potential indicates that very little N₂ is formed, reaction 10 is probably negligible as well.

Several reactions can account for cyanogen production in addition to reactions 1c and 12, namely



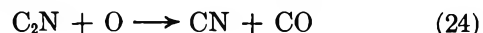
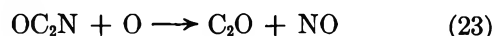
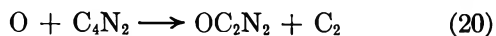
Setser and Thrush²¹ predicted the formation of a "long-lived activated adduct" in the reaction of cyanogen with oxygen atoms; we have indeed observed a peak at $m/e = 68$, corresponding to the species OC_2N_2 . Formation could occur by three reactions in this system

(18) J. C. Boden and B. A. Thrush, *Proc. Roy. Soc., Ser. A*, **305**, 107 (1968).

(19) D. L. Baulch, D. D. Drysdale, and A. C. Lloyd, "High Temperature Reaction Rate Data," Vol. I, The University of Leeds, 1968.

(20) D. E. Paul and F. W. Dalby, *J. Chem. Phys.*, **37**, 592 (1962). The value reported was simply for the disappearance of reactants, with the nature of the products unspecified.

(21) D. W. Setser and B. A. Thrush, *Proc. Roy. Soc., Ser. A*, **288**, 275 (1965).

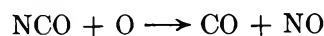
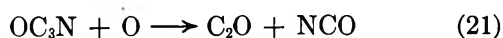


Infrared absorption bands due to two distinct species have been observed in the flash photolysis of $\text{O}_3 + \text{C}_2\text{N}_2$ mixtures,²² and attributed to the insertion and addition products of C_2N_2 with $\text{O}(^1\text{D})$ and $\text{O}(^3\text{P})$, respectively.

In the present work $\text{O}(^3\text{P})$ is the reacting species, thus reaction 19 would yield only the addition product; however, reaction 18 could form either of the two. It is unlikely that reaction 20 leads to appreciable formation of OC_2N_2 , as the other evidence indicates that the initial attack is on the central carbons of DCA.

Several reactions can be written for NO_2 formation from NO , O , and O_2 . Since their rate constants and thermochemistry are well known,²³ and as they are not associated directly with $\text{DCA} + \text{O}$, we do not discuss them here.

In the absence of molecular oxygen additional radical-O atom reactions can occur resulting in the formation of stable products



Conclusion

The rate constant for reaction between oxygen atoms and dicyanoacetylene is $1.1 \pm 0.3 \times 10^{-15} \text{ cm}^3/(\text{molecule sec})$. In the presence of molecular oxygen the stoichiometric factor is 1.2, which can be accounted for if the major pathway is reactions 1b, c, and d followed by reactions 2, 3, 4, 5, and 12. The stoichiometry is critically dependent on the concentration of molecular oxygen, the ratio of O atoms consumed to DCA molecules consumed increasing as the $[\text{O}_2]$ is reduced. Although this ratio did not exceed 5.5 in any of our experiments, appreciable amounts of O_2 were present at all times; the ratio could be considerably higher than 5.5 in a system truly free of O_2 . The higher stoichiometric factor is explained by reactions 6, 11, 21, 22, 23, and 24 becoming more important in the O_2 -free system.

Acknowledgment. We thank the Research Grants Committee of the University of Alabama for a Grant-in-Aid to C. W. H.

(22) C. W. Hand and R. M. Hexter, *J. Amer. Chem. Soc.*, **92**, 1828 (1970).

(23) D. L. Baulch, D. D. Drysdale, and A. C. Lloyd, "High Temperature Reaction Rate Data," Vol. V, The University at Leeds, 1970.

Transitions in Mesophase-Forming Systems. III. Transformation

Kinetics and Textural Changes in Cholesteryl Nonanoate¹

by Fraser P. Price* and Joachim H. Wendorff

Polymer Science and Engineering, University of Massachusetts, Amherst, Massachusetts 01002 (Received April 19, 1971)

Publication costs assisted by National Institutes of Health

The equilibrium density-temperature behavior of carefully purified (0.6 mol % impurities) cholesteryl nonanoate has been studied between room temperature and 95°. The transition temperatures were 78.8, 91.6, and 75.3°, the pretransition ranges on the low temperature sides of the transition were 4.8, 3.6, and 0.5°, and the volume changes were 5.1, 0.3, and 0.08% for the solid-cholesteric, cholesteric-isotropic, and the smectic-cholesteric transitions, respectively. No pretransition effects were observed on the high temperature side of any of these transitions. The transformation kinetics of the smectic-solid and the isotropic-cholesteric transformations were interpreted by the Avrami equation to yield n 's of 4.0 and approximately 1.8, respectively. The former indicates sporadic nucleation of spheres. The meaning of the latter is not clear. The smectic-solid transformation exhibits homogenous nucleation below 60°. The isotropic cholesteric transformation was too rapid to measure at supercoolings greater than 2°. Within the cholesteric phase three textures were observed. The transformations among these textures are reversible with temperature. This is the second documented case of thermally reversible textural transitions, the first being that observed in cholesteric cholesteryl myristate.

Introduction

The aliphatic esters of cholesterol constitute a series of compounds exhibiting mesophase behavior.² That is, they transform from the crystalline solid to the isotropic liquid not in a single transition as is usually the case, but in a series of transitions. Each transition represents a loss of some kind of order, and the phases existing above and below a given transition are always at least stable enough in a thermodynamic sense to be observable. Compounds whose molecules are either nearly equidimensional, *viz.* camphor, or approximately rodlike, *viz.* linear aliphatic acids, lose rotational order in a stepwise fashion and exhibit transitions below the final transition to the isotropic liquid. The liquid crystal formers have molecules which are lathlike, and they disorder stepwise by loss of positional order.

In previous papers in this series, we have described investigations of the equilibrium properties of the various phases of cholesteryl myristate³ and cholesteryl acetate.⁴ We have also described the kinetics of transformation among the various phases. Since one of our ultimate goals is to delineate the effect of structure upon the behavior of mesophases, the study described here is concerned with the nonanoate.

One interesting and unexpected outcome of our studies of cholesteryl myristate was the observation of a textural change within the cholesteric state that is reversible with temperature.³ The density measurements indicated only one state between 78.1 and 83.8°. However, optical studies showed a transparent blue texture visible between 83.8 and 83.0°. This texture, when cooled at a rate of 1°/hr could be supercooled to around 79° before it transformed to a turbid texture

which persisted down to 78.1°. With extremely slow stepwise cooling the transformation takes place only very slightly below 83°. Between 83 and 80° the transformation from clear blue to turbid is facilitated by stirring and shaking. Upon very slow stepwise heating the turbid state transformed to the blue state at 83.0°. While various textures within the cholesteric state have long been recognized, to our knowledge, this was the first report of a textural transition that is reversible with temperature. It possibly could result from reorganization of networks of thermally induced defects. It has been proposed by Frank⁵ that the various textures observed in mesophases result from "disinclination" lines which are, in effect, various aggregates of defects. The various arrays of differing energy into which these lines arrange themselves are observable as textural differences. It seems probable that with increased temperature, increasing concentration of defects would be reflected in increasing numbers of high energy defect arrays. It is difficult to envision, however, how the small changes in temperature could produce sufficient changes in the number of defects and why, even if sufficient changes did occur, the transition should be as abrupt as it seems to be.

We describe herein studies of the equilibrium density of the solid, smectic, cholesteric, and isotropic cholesteryl

(1) This work was supported by Grant No. HE13188 from the National Institutes of Health.

(2) (a) G. W. Gray, "Molecular Structure and Properties of Liquid Crystals," Academic Press, New York, N. Y., 1962; (b) G. H. Brown and W. C. Shaw, *Chem. Rev.*, **57**, 1049 (1957).

(3) F. P. Price and J. H. Wendorff, *J. Phys. Chem.*, **75**, 2839 (1971).

(4) F. P. Price and J. H. Wendorff, *ibid.*, **75**, 2849 (1971).

(5) F. C. Frank, *Discuss. Faraday Soc.*, **25**, 19 (1958).

teryl nonanoate. Also, we present the results of kinetic studies of the isotropic-cholesteric and the smectic-solid transformations. In addition we present observations of reversible textural changes on heating and cooling the cholesteric phase.

Experimental Section

Materials. The cholesteryl nonanoate used was Lot No. 701 from the Eastman Kodak Co., Rochester, N. Y. The mercury was ACS reagent grade obtained from Sargent Welch Co., Boston, Mass.

The cholesteryl nonanoate was purified by recrystallizing three times from 1-pentanol and washed and dried as described in the first publication of this series. This material was introduced into a dilatometer and outgassed under high vacuum (10^{-4} Torr) by several cycles of pumping, melting, and freezing. When no further outgassing was observed on melting, the sample was frozen under vacuum and the mercury was introduced.

Methods. The experimental procedures and computational techniques employed are described in the first paper of this series.³

As in previous investigations, it was found necessary to hold the sample for some time above its melting point in order to get reproducible results. This is presumably due to the presence of persistent heterogeneous nuclei which must be destroyed. In the present case of the nonanoate, annealing at 98° for an hour was sufficient to ensure reproducible results.

The dilatometric techniques employed here have a sensitivity of one part in 10^4 to 10^6 . The precision of the measurements is comparable. Whereas, the changes in density or specific volume have an accuracy equal to their precision, the absolute values of the density or specific volume over the observed temperature range have a much smaller accuracy. This is due to the lack of sufficiently precise determination of the sample weight in the dilatometer. The weight of the dilatometer itself is so great that it could be measured only to ± 5 mg. This introduces an uncertainty into the sample weight of about 0.2%. Thus, even though the densities of the cholesteryl esters are determined pycnometrically at three temperatures to a 0.02% accuracy, the volume of the sample in the dilatometer is known to only about 0.2%.

Results and Discussion

Equilibrium Studies. The results of the equilibrium density-temperature behavior study are summarized in Table I and displayed in Figures 1 and 2.

The values of 78.8 , 75.3 , and 91.6° for the solid-cholesteric, the cholesteric-smectic, and the cholesteric-isotropic transitions are in good agreement with those determined by other investigators by various methods.⁶

Figure 1 shows the behavior of the solid crystalline nonanoate. It was found that this behavior was dis-

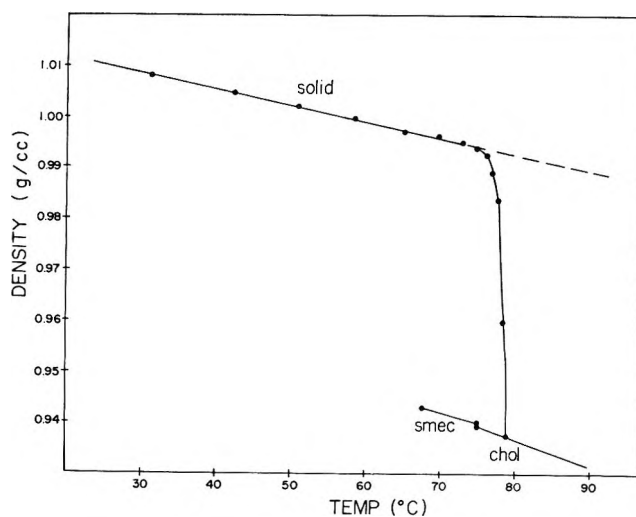


Figure 1. Plot of equilibrium density vs. temperature for the solid-cholesteric transition in cholesteryl nonanoate.

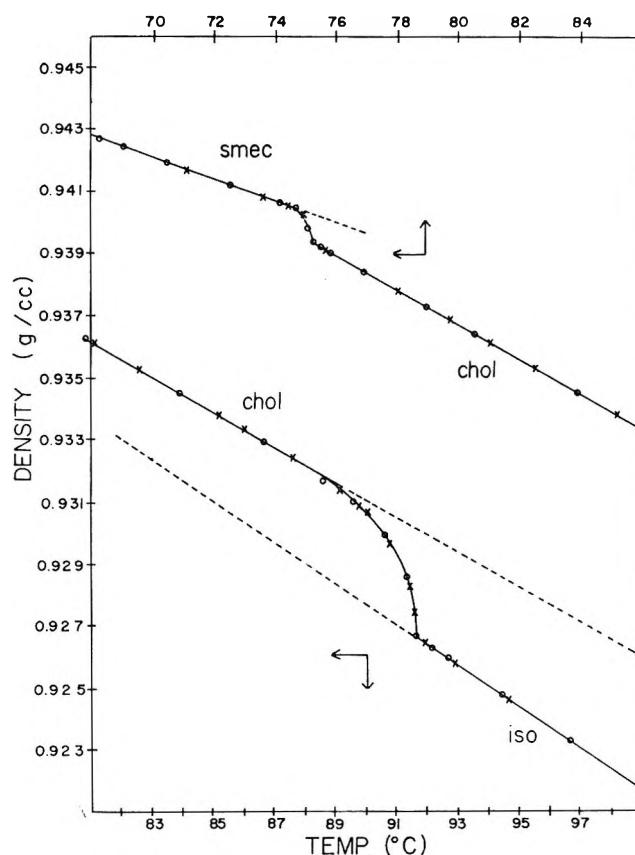


Figure 2. Plot of equilibrium density vs. temperature for the smectic-cholesteric and the cholesteric-isotropic transitions in cholesteryl nonanoate: ●, temp decreasing; ×, temp increasing.

played by all samples regardless of the crystallization temperature. The density decreases approximately linearly with temperature up to about 74° and then significant downward curvature is exhibited. The

(6) G. J. Davis, R. S. Porter, and E. M. Barrall, II, *Mol. Cryst. Liquid Cryst.*, 11, 319 (1970).

Table I: Summary of Equilibrium Volume-Temperature Relations for Cholesteryl Nonanoate

Temp, °C	State	Transition volume change	α , °C ⁻¹	A/R, °K	T ₀ , °C
$T \leq 74$	Solid	...	3.0×10^{-4}
$74 \leq T \leq 78.8$...	5.1%	...	1.56×10^6	78.8
$75.3 \leq T \leq 88$	Chol	...	6.2×10^{-4}
$88 \leq T \leq 91.6$...	0.3%	...	1.04×10^3	91.6
$91.6 \leq T$	Iso	...	7.2×10^{-4}
$T \leq 74.8$	Smec	...	3.8×10^{-4}
$74.8 \leq T \leq 75.3$...	0.08%	...	7.0×10^6	75.3

samples melt over about a 5° range. This melting behavior is not consistent with the van't Hoff equation. However, the initial slope combined with a value of $\Delta H = 11.4$ cal/g indicates an impurity content of about 0.6 mol %. As a check on this impurity content, we have made calorimetric measurements of this transition using a differential scanning calorimeter. The calculation made according to published procedures⁷ yielded impurity contents of between 0.6 and 0.8 mol %. The agreement between the two methods is satisfactory.

Some previous investigators^{6,8} have obtained indications of a transition in the solid cholesteryl nonanoate between 73 and 79°. However, the evidence presented is not compelling and in fact one set of authors⁸ attributed the observed effects to pretransition effects. We have carefully examined the density of our material between 64 and 79°. Below 73° temperature intervals of 1° were used and above 73°, intervals of 0.5° were employed. We detected no evidence of a solid-solid transition in this region.

As noted in previous papers^{3,4} in this series, it is possible to have a premelting where the order (positional or rotational) continuously becomes smaller in the region just below the transition temperature. In such a situation it is reasonable that the fraction F of the high temperature phase should depend on temperature, T , as

$$F = \exp\left[-(A/R)\left(\frac{1}{T} - \frac{1}{T_0}\right)\right]$$

where A is an energy and T_0 is the melting point of the pure compound. In fact, the data displayed in Figure 1 do fit such an equation, and the resultant values of A/R are listed in the fifth column of Table I. For the cholesteric-solid transition the value of A calculated therefrom is 310 kcal/mol. This is so absurdly large that we can offer no reasonable explanation. We merely list the values for A/R for this and the other transitions as a means of describing the volume-temperature behavior in the transition regions. In the cases listed, the slopes of the lines were determined using five to seven points. The variances of the calculated from the observed values of F were about 0.008. The solid melting range of the nonanoate is about the same

as that of the myristate but is very much smaller than that of the acetate, which is 20°.

The cholesteric state shows an essentially linear density-temperature behavior between 75.3 and 91.6°. The breadth of the cholesteric-isotropic transition is surprisingly large (3.6°). The other cholesteryl esters we have studied show a range of about 0.5° for this transition. In the cholesteric phase of this compound the coefficient of thermal expansion is slightly smaller than that of the isotropic liquid. This situation also is in contradistinction to the behavior of most other cholesteric phases whose expansion coefficients are significantly greater than those of their isotropic liquids.

In cholesteryl nonanoate the smectic phase is monotropic. It is attained by cooling the cholesteric phase below 75.3°. The smectic phase also shows a linear density-temperature behavior over most of its existence range. This phase has a small (0.5°) transition region. The volume change for the smectic-cholesteric transition is small compared to the cholesteric-isotropic transition in this cholesteryl ester. The change is also small compared to the smectic-cholesteric transition in cholesteryl myristate.³ The coefficient of expansion of the smectic phase in conformity with the behavior of other cholesteryl esters is less than that of the cholesteric phase but significantly greater than that of the solid phase. It is worth noting that here, as in the case of the cholesteryl acetate and myristate, there are no detectable pretransition effects on the high temperature side of the transitions.

Kinetic Studies. The transformation kinetics were studied by the techniques described in the first paper of this series.³ The results of the isothermal transformations were interpreted in terms of the Avrami equation^{9,10}

$$F(t) = \exp[-Kt^n] \quad (1)$$

where n is a constant dependent on the modes of nuclea-

(7) G. J. Davis and R. S. Porter, *J. Therm. Anal.*, **1**, 449 (1969).

(8) L. S. Goldberg and J. M. Schnurr, *Appl. Phys. Lett.*, **14**, 306 (1969).

(9) M. Avrami, *J. Chem. Phys.*, **7**, 1103 (1939); **8**, 212 (1940).

(10) U. R. Evans, *Trans. Faraday Soc.*, **41**, 365 (1945).

tion and growth of the transforming regions, K is a constant dependent on the mode of nucleus injection and the shape of the transforming regions, and $F(t)$ is the volume fraction untransformed at time t . The form of eq 1 implies that plots of $F(t)$ vs. $\log t$ should have a fixed shape for a given n .

We are aware of the assumptions implicit in eq 1 and of the restrictions imposed thereby.¹¹ Nevertheless, we choose to use it because it is the most convenient technique for correlating data on transforming systems.

The transformation to the solid state will be discussed first. Here it was found that on quenching from 98 to above 60° no transformation occurred over a period of 24 hr. Below 60° the crystallization started essentially immediately with no perceptible induction period. In both cholesteryl acetate and cholesteryl myristate there was always an appreciable temperature range in which was observed an induction period which decreased sharply with decreasing temperature. Regardless of the reason for the odd behavior of the cholesteryl nonanoate, it seems quite probable that 60° represents the upper limit of the homogeneous nucleation region.^{12,13} Further, it should be noted that, since both the isotropic-cholesteric and the cholesteric-smectic transformations are very rapid below 60°, the transformation to the solid always takes place from the smectic state. This is the same situation that prevailed with cholesteryl myristate. In Figure 3 are displayed plots of $F(t)$ vs. $\log t$ for this transformation. These plots have all been shifted to a temperature of 48.8° (30° supercooling). The shift factors are given. The quantitative aspects of Figure 3 are given in Table II.

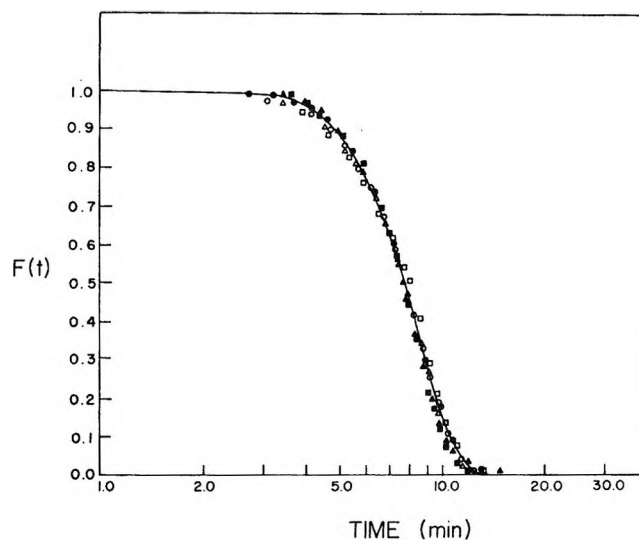


Figure 3. Plots of $F(t)$ vs. \log (time) for smectic-solid transition. Data shifted to 30.0° supercooling; shift factor in brackets: ●, 55.0° [0.46]; ▲, 48.8° [1.00]; ■, 44.7° [1.50]; ○, 38.5° [2.05]; △, 31.5° [2.27]; □, 26.0° [2.60].

Thus the isotropic-cholesteric transition will be next considered. In Figure 4 are plots of the time course of this transformation. It is seen that the curves are of dubious superposability. Below 90° the transformation was too rapid to be measured. All the runs shown in Figure 4 were at temperatures within the transition region of the cholesteric-isotropic transition.

The Avrami equation was applied to the data shown in Figure 4, in spite of the questionable validity of such application. The runs made at 91.25, 91.08, 90.55, and 90.00° yielded respectively values of n of 1.83, 1.78, 1.82, and 1.84, and values of K (min^{-n}) of 5.5×10^{-1} , 9.2×10^{-1} , 1.3, and 2.7. In view of the significant deviation of n from 2.0 in addition to the reservations noted above, it is not deemed worthwhile to attempt interpretation of the temperature dependence of the K 's in the same frame of reference that was established for the transition in the myristate.

Visual Observations of the Cholesteric State. It has long been known that the cholesteric state of the cholesteryl esters has several different appearances.^{14,15} Friedel correctly recognized these appearances as various textures of the same basic structure. However, previous investigators have been concerned with the visual appearances of the various textures, usually in very thin specimens of indeterminate thickness, when observed upon cooling or heating at undefined rates.

We, on the contrary, are here concerned with the

Table II: Avrami Constants for the Smectic-Solid Transition in Cholesteryl Nonanoate

$T, ^\circ\text{C}$	$\Delta T, ^\circ\text{C}$	n	K, min^{-n}
55.0	23.8	3.9	1.4×10^{-5}
48.8	30.0	4.1	1.5×10^{-4}
44.7	34.1	4.2	6.7×10^{-4}
38.5	40.3	3.9	4.0×10^{-3}
31.5	47.3	3.9	6.7×10^{-3}
26.0	52.5	4.0	9.2×10^{-3}
Av		4.0	

In the present case, as in the transformation to the solids of the other cholesteryl esters, $n = 4.0$. This indicates sporadic nucleation of spheres. In the present case also the interpretation of the temperature dependence of K is hampered by a lack of independent information about the influence of temperature upon either the nucleation or growth rates of the spheres. Thus no attempt will be made here to interpret the behavior of the K 's.

The cholesteric-smectic transition has such a small volume change that kinetic studies were not made.

(11) F. P. Price, *J. Appl. Phys.*, **36**, 10 (1965).

(12) F. P. Price, "Nucleation," A. C. Zettlemoyer, Ed., Marcel Dekker, New York, N. Y., 1970, Chapter 8.

(13) D. Turnbull and J. C. Fischer, *J. Chem. Phys.*, **17**, 71 (1949).

(14) O. Lehmann, "Flüssige Kristalle," W. Engelmann, Leipzig, 1904.

(15) G. Friedel, *Ann. Phys.*, **18**, 274 (1922).

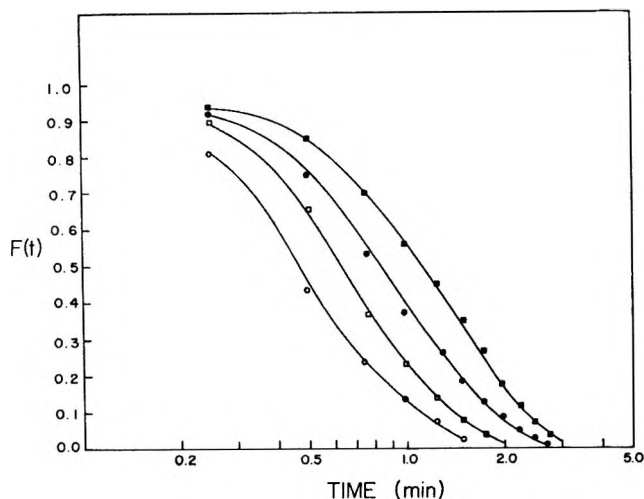


Figure 4. Plots of $F(t)$ vs. $\log(\text{time})$ for the isotropic cholesteric transition: ■, 91.25°; ●, 91.08°; □, 90.55°; ○, 90.00°.

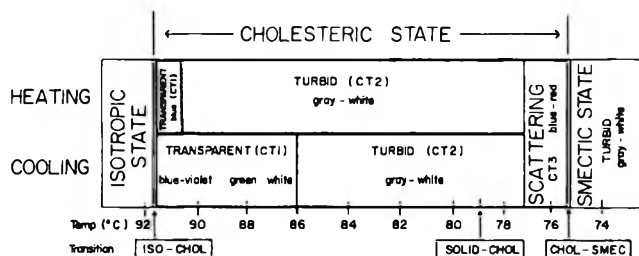


Figure 5. The textures of the cholesteric phase of cholesteryl nonanoate and their temperature behavior.

range of existence and rate of appearance of these textures under well-defined heating and cooling rates as well as with the rate of appearance of the textures under isothermal conditions after quenching. Further, the fact that we have used thick specimens (dilatometric) tends to minimize the wall effects which certainly played a role in the observations of previous investigators.

We observe, as others have,¹⁴⁻¹⁶ three textures in the cholesteric state of cholesteryl nonanoate. These textures we call CT1, CT2, and CT3. Texture CT1, the homeotropic one described by others, ranges in color from violet to red (with decreasing temperatures), appears in thicknesses of 2-5 mm in the dilatometer, and is similar to those observed in cholesteryl myristate³ and acetate.⁴ Texture CT2 is the turbid, gray-white focalconic described by Friedel.¹⁵ The rate of development of CT2 from CT1 in cholesteryl myristate is currently being studied by others.¹⁷ Texture CT2 develops from CT1 by a process of nucleation and growth, and some details of this process in the nonanoate are given below. Texture CT3 develops instantaneously without induction from CT2 on cooling, and clearly is the helical structure discussed by others.^{18,19} This texture exists in cholesteryl acetate in which CT1 and CT2 are absent. Both textures CT1 and CT3 undergo a bathochromic shift with decreasing temperature.

Figure 5 is an attempt to summarize these findings. The transformation from the isotropic state to CT1 takes place in only a few minutes and at 90° is complete in 1.5 min. Texture CT1 persists over a wider temperature range on cooling than on heating. This indicates that the transformation CT1 → CT2 is controlled by nucleation and growth. That this is not the case for the CT2 → CT3 transformation is indicated by the essentially instantaneous nature of the transformation and by its reversibility at 77° upon heating. Texture CT2 upon extremely slow heating reverts at 90.5° to CT1. All these observations indicate that the textures CT1, CT2, and CT3 are thermodynamically stable in the ranges 91.6-90.5, 90.5-77, and 77-75.3°, respectively.

Semiquantitative observations were made of the kinetics of the isothermal transformation of CT1 to CT2. This transformation is characterized by an induction time which decreases rapidly with decreasing temperature. In the dilatometer, this induction time was observed visually, as was the time required for the transformation to become complete. These times ranged between 30 sec and 3 hr. It was found that in the temperature range from 83 to 89°, the data for both the induction and the transformation time fitted the equation.

$$\ln t = A + BT \quad (2)$$

where t is the time in minutes, T is the temperature in °K, and A and B are constants. The values of A and B are -238.5 and $+0.67$, respectively, for the induction period and -119.0 and $+0.47$, respectively, for the transformation time. The variance of $\ln t$ was 0.03 for the data sets for both the induction and the transformation times. Both data sets contained eight pairs of points.

All these visual observations point to a remarkable situation of thermally reversible textural transitions. It is the reversibility of these transitions that is the unique aspect of the present work, for to our knowledge, with the exception of our observations on cholesteryl myristate,³ such reversibility has never before been reported.

Acknowledgment. The authors wish to express their gratitude to Professor R. S. Stein and Professor R. S. Porter for much helpful discussion during the course of this study. Thanks are also due to Mr. Saleh Jabarin for making available to us the preliminary results of his study of the textural transformation in the cholesteric phase of cholesteryl myristate.

(16) I. G. Chistyakov and L. A. Gosakova, *Sov. Phys.-Crystallogr.*, **14**, 132 (1969).

(17) R. S. Stein and S. Jabarin, private communication.

(18) H. L. DeVries, *Acta Crystallogr.*, **4**, 219 (1951).

(19) F. F. Knapp and H. J. Nicholas, "Liquid Crystals and Ordered Fluids," J. F. Johnson and R. S. Porter, Ed., Plenum Press, New York, N. Y., 1970, p 147.

NOTES

Carbon-13 Nuclear Magnetic Resonance Relaxation in Hemimellitene and Isodurene

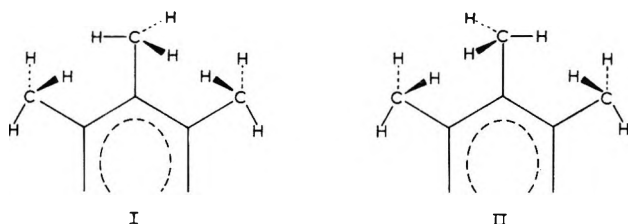
by Terry D. Alger,* David M. Grant,
and Robin K. Harris

Departments of Chemistry, Utah State University, Logan, Utah 84321
and University of Utah, Salt Lake City, Utah 84112
(Received July 9, 1971)

Publication costs assisted by the National Science Foundation

It is generally accepted that an isolated methyl group such as that in toluene is essentially a free rotor (≈ 0 kcal for this sixfold barrier), while the adjacent methyls in *o*-xylene have a threefold barrier to rotation of about 2 kcal/mol.^{1,2} This is supported by pmr and cmr (carbon-13 magnetic resonance) spin-lattice relaxation studies^{3,4} which demonstrate that the proton³ and carbon-13⁴ relaxations of a lone methyl group have substantial contributions from spin-rotation effects, while carbon-13 relaxations of the rotationally restricted methyl groups in *o*-xylene are dominated by the dipolar mechanism.⁴

In the 1,2,3-trisubstituted methylbenzenes, hemimellitene (1,2,3) and isodurene (1,2,3,5), an additional structural feature arises which affects the rotation rates of the methyl at C-2. According to previous results² there are two equivalent low-energy conformers for the 2-methyl groups which give rise to a sixfold rotation barrier. These conformations are demonstrated for the 1,2,3-trimethyl interactions as



The 1-CH₃ in conformer II and the 3-CH₃ in conformer I are in minimum energy configurations relative to the 2-CH₃ and have threefold energy profiles with 1.5–2 kcal/mol barriers for rotation.^{1,2} The 1-CH₃ in conformer I and the 3-CH₃ in conformer II also are governed by a threefold barrier to rotation but now the magnitude exceeds 2 kcal/mol by a considerable amount due to the orientation of the 2-methyl. On the other hand, the 2-methyl will possess the same steric energy in both forms because of symmetry giving rise to the expected sixfold barrier. As sixfold barriers to

rotation are generally much lower than threefold barriers, one may expect the 2-methyl carbon relaxation to exhibit spin-rotational effects. Kuhlmann, *et al.*,⁵ predict significant carbon-13 spin-rotation effects for methyls with barriers ≤ 400 cal/mol. On the other hand, the 1 and 3 methyls could be sufficiently restricted in their rotation that the dipolar relaxation mechanism should again dominate.

The cmr relaxation data given in Table I for hemimellitene and isodurene substantiate the above anticipated results. Both the 2-CH₃ in hemimellitene and the 2- and 5-CH₃'s in isodurene have substantial contributions ($T_{10} = 20$ sec, and $T_{10} = 21$ and 24 sec, respectively) to their relaxations from mechanisms other than dipolar processes. Decreases in these values of T_{10} with temperature confirm that these contributions are from spin rotation mechanisms. On the other hand, the relaxations of the 1 and 3 methyls are dominated by dipolar processes ($T_{1D} = 14$ sec, $T_{10} = 98$ sec for hemimellitene; $T_{1D} = 12$ sec, $T_{10} \geq 100$ sec for isodurene). The nuclear Overhauser effect (NOE) data in Table I were used to separate dipolar contributions, T_{1D} , from the proton-decoupled relaxation times, T_1 ($\eta = 2T_1/T_{1D}$);⁶ the contributions from all relaxation processes, T_{10} , other than dipolar were then determined from the reciprocal additivity relationship of relaxation times ($1/T_1 = 1/T_{1D} + 1/T_{10}$).

Carbon-13 relaxation theory^{4,5} predicts that the dipolar relaxation contribution for a rapidly rotating methyl group should be three times the dipolar contribution of a ring carbon with an attached proton in a slowly reorienting molecule. Thus, the values of $T_{1D} = 28 \pm 4$ for the 2-CH₃ and $T_{1D} = 9 \pm 2$ for the 5- and 4,6-ring carbons in trimethylbenzene confirm that the 2-CH₃ is essentially a free rotor. The data for the 2- and 5-CH₃'s in tetramethylbenzene compared with C-4,6 in the ring likewise confirm that these methyls are also free rotors. Theory also predicts that T_{1D} for a rigid CH₃ group whose correlation time is that of the entire molecule in an isotopic tumbler will be $1/3$ that of T_{1D} for a ring carbon with a single attached proton^{4,5}

(1) W. G. Fateley, F. A. Miller, and R. E. Witkowski, Technical Documentary Report No. ML-TDR-64-158, Part I, June 1964.

(2) (a) W. R. Woolfenden and D. M. Grant, *J. Amer. Chem. Soc.*, **88**, 1496 (1966); (b) W. R. Woolfenden, Thesis, University of Utah, 1965.

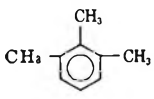
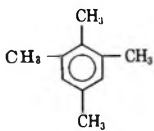
(3) D. K. Green and J. G. Powles, *Proc. Phys. Soc.*, **85**, 87 (1965).

(4) K. F. Kuhlmann and D. M. Grant, *J. Chem. Phys.*, in press.

(5) K. F. Kuhlmann, D. M. Grant, and R. K. Harris, *ibid.*, **52**, 3439 (1970).

(6) T. D. Alger, S. C. Collins, and D. M. Grant, *ibid.*, **54**, 2820 (1971).

Table I: Carbon-13 NOE and T_1 Data for 1,2,3-Trimethylbenzene and 1,2,3,5-Tetramethylbenzene at $36 \pm 2^\circ$

Compound	Carbon	Frequency, MHz	η , NOE-1	T_1 , sec	T_{1D} , sec	T_{10} , sec
	1,3-CH ₃	15.1	1.75 ± 0.15	12.0 ± 2	14 ± 3	98 ± 20
	2-CH ₃	15.1	0.85 ± 0.15	11.8 ± 2	28 ± 4	20 ± 5
	1,3-Ring	15.1	0.60 ± 0.15	55.0 ± 10	180 ± 20	80 ± 25
		25.1	0.55 ± 0.15	45.0 ± 10	154 ± 20	60 ± 15
hemimellitene	2-Ring	15.1	0.75 ± 0.15	55.0 ± 10	150 ± 20	85 ± 25
		25.1	0.70 ± 0.15	45.0 ± 10	130 ± 20	65 ± 15
	4,6-Ring	15.1	1.90 ± 0.15	8.3 ± 1	9 ± 2	≥ 80
	5-Ring	15.1	1.75 ± 0.15	7.9 ± 1	9 ± 2	≥ 80
	1,3-CH ₃	15.1	1.80 ± 0.15	11.0 ± 2	12 ± 3	≥ 100
	2-CH ₃	15.1	0.90 ± 0.15	11.4 ± 2	25 ± 5	21 ± 7
	5-CH ₃	15.1	0.95 ± 0.15	11.5 ± 2	24 ± 5	22 ± 7
	1,3-Ring	15.1	0.90 ± 0.15	50.0 ± 10	110 ± 15	90 ± 25
		25.1	0.85 ± 0.15	40.0 ± 10	95 ± 15	65 ± 15
	2-Ring	15.1	0.95 ± 0.15	50.0 ± 8	105 ± 15	95 ± 25
		25.1	0.85 ± 0.15	40.0 ± 7	95 ± 15	65 ± 15
	5-Ring	15.1	1.00 ± 0.15	50.0 ± 10	100 ± 15	100 ± 25
		25.1	0.90 ± 0.15	40.0 ± 10	90 ± 15	65 ± 25
4,6-Ring	15.1	1.85 ± 0.15	6.9 ± 1	8 ± 2	≥ 100	

due to the threefold increase of hydrogens in the methyl groups. Obviously, the data $T_{1D} = 14 \pm 3$ sec for the 1,3-CH₃ and $T_{1D} = 9 \pm 2$ sec for the 5- and 4,6-ring carbons of hemimellitene illustrate that the 1- and 3-CH₃'s are not completely restricted in their rotation. It is possible, therefore, under certain assumptions to use these data to estimate the barrier to rotation for the 1- and 3-CH₃'s. In order to characterize the internal motion of the methyls it is first necessary to separate this dynamic feature from the overall molecular rotation. Unfortunately, there are insufficient data to uniquely fit the three rotational diffusion constants describing the motion of molecules of low symmetry. It was assumed, therefore, that the motion in these molecules was isotropic. Calculations of the moments of inertia about axes in the plane of the molecule and about an axis perpendicular to the plane indicate that this assumption is reasonable ($I_x = I_y \approx I_{z/2}$). Thus, using standard formulas³⁻⁶ for calculation of intramolecular dipole relaxation with isotropic motion ($R_{eff} = n\gamma_C^2\gamma_H^2\hbar^2 T_{1D}/6r_{C-H}^6$), values of $R_{eff} = 3.0 \times 10^{10}$ sec⁻¹ and $R_{eff} = 2.6 \times 10^{10}$ sec⁻¹ were obtained for hemimellitene and isodurene, respectively, from the ring carbon T_1 values. If one uses the Woessner, *et al.*,⁷ formulation which assumes that the methyl motion can be described by the diffusion constants and a methyl jump rate, ρ , values of $\rho = 1.31 \times 10^{12}$ sec⁻¹ and 1.2×10^{12} sec⁻¹ can be obtained for hemimellitene and isodurene, respectively, from the methyl T_1 values. The methyl rotational barriers can then be calculated from the energy dependence of the rate equation, $\rho = \rho_0 e^{-V/RT}$. The constant, ρ_0 , is $^{3/2}$ times the total jump rate of a freely rotating methyl group from any of its three positions in either of two

directions⁷ ($\rho_0 = ^{3/2}(kT/I)^{1/2} = 1.33 \times 10^{13}$ radians/sec at 40°).^{8,9}

For $R_{\perp} = R_{\parallel}$, the Woessner, *et al.*,⁷ formula for methyl rotation reduces to

$$1/T_{1D}^M = 3\gamma_C^2\gamma_H^2\hbar^2/r_{C-H}^6 \left[\sum_i^{A,B,C} \frac{B_{i_1}}{6R} + \frac{B_{i_2} + B_{i_3}}{6R + \rho} \right]$$

This resulted in predicted values of $V = 1.45$ and $V = 1.55$ kcal/mol, respectively, for hemimellitene and isodurene in good agreement with values expected from other estimates.^{1,2}

Values of T_1 and η were determined for all carbons in the two methylbenzenes at 15.1 and 25.1 MHz, but the results were equivalent in all cases except for the ring carbons without attached protons (the 1-, 2-, and 3-ring carbons of hemimellitene and the 1-, 2-, 3-, and 5-ring carbons of isodurene). In the cases of these quaternary carbons, η , T_1 , and T_{10} were found to decrease slightly with an increasing field. Such evidence is indicative of a minor chemical shift anisotropic relaxation mechanism, T_{1a} . Since $T_{1a} \propto 1/\omega^2$, this mechanism can be tested. The ratio, ω^2 (25.1 MHz)/ ω^2 (15.1 MHz) = 2.8, whereas T_{10} (15.1 MHz)/ T_{10} (25.1 MHz) = 1.5 ± 1.0 . Thus, it would appear that a contribution to T_{10} from chemical shift anisotropy ought to be on the order of 160 sec. A contribution of this magnitude obviously cannot affect significantly the value of the relaxation times of carbons with protons attached since they are on the order of 10–20 sec.

(7) D. E. Woessner, B. S. Snowden, and G. H. Meyer, *J. Chem. Phys.*, **50**, 719 (1969).

(8) W. T. Huntress, Jr., *ibid.*, **48**, 3524 (1968).

(9) A. A. Maryott, T. C. Farrar, and M. S. Malmberg, *ibid.*, **54**, 64 (1971).

Acknowledgments. This research was supported by grants from the National Institutes of Health (GM-

08521) and the National Science Foundation (GP 18436).

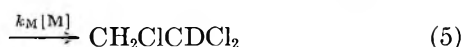
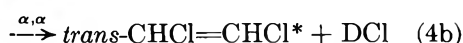
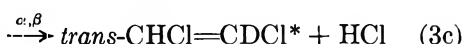
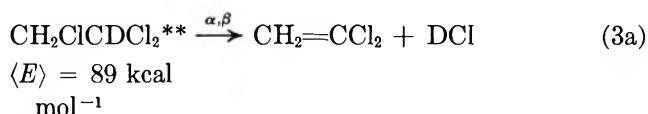
COMMUNICATIONS TO THE EDITOR

Rate Constants, Threshold Energies, and Energy Partitioning for Three and Four Centered Hydrogen Chloride Elimination Reactions of 1,1,2-Trichloroethane-1-*d*₁

Publication costs assisted by the National Science Foundation

Sir: We wish to report observations from the unimolecular reactions of chemically activated 1,1,2-trichloroethane-1-*d*₁, which shows that both α,α and α,β elimination of hydrogen chloride occurs; the threshold energy and the energy partitioning pattern also are reported. Previously α,α elimination has only been reported in competition with α,β elimination from CD₃-CHF₂.¹

The experiments consisted of photolyzing ketene-*d*₀ with chloroform-*d*₁ at room temperature and monitoring the yields of products as a function of pressure. Although other reactions were observed, the following are of current interest.



The α,α elimination is followed by rapid rearrangement of the carbene to give the olefin. Product analysis was done by gas chromatography; the chlorinated olefins were trapped from the He effluent and analyzed for isotopic content with a mass spectrometer. The α,α and α,β elimination reactions of chemically activated CD₃CHF₂ were studied by cophotolysis of (CD₃)₂CO and (CHF₂)₂CO. The results were similar to those

found by Perona and Pritchard¹ and will not be discussed.

The total α,β and α,α elimination rate constants were found by the usual² plots of decomposition product yield/stabilization product yield *vs* pressure⁻¹. The half-quenching pressures were 9.5 and 1.8 Torr for the α,β and α,α channels, respectively. The rate constant values for 3a:3b:3c were 1.5:4.8:3.2. These values take precedence over an earlier report³ from this laboratory, and no evidence was found for any *direct* formation of olefins from reaction of CHCl₂ with either CH₂Cl or CH₃.³ Converting the above half-quenching pressures to rate constants in sec⁻¹ units and fitting the magnitudes of the rate constants to RRKM calculated results using the calibrated four-centered transition state models² gave *E*₀ values of 57 and 59 kcal mol⁻¹ for the α,β and α,α process, respectively. Correction for isotope effects would lower the *E*₀ for α,α elimination of HCl from CH₂ClCHCl₂ to ~58 kcal mol⁻¹. Fitting the CD₃CHF₂ rate constants to RRKM calculations showed that the *E*₀ for the α,α process was about 2 kcal higher than for the α,β processes. The halogen substituent stabilizes the carbene through π bonding between the halogen and the vacant p orbital of the carbene.⁴ This increased thermodynamic stability has the effect of lowering the activation energy for the α,α elimination relative to the α,β elimination; the methyl carbene itself is unstable with respect to hydrogen migration.⁵

An asterisk was maintained on the *cis*- and *trans*-dichloroethenes to indicate the possibility of retention of sufficient internal energy for further unimolecular

(1) M. J. Perona, J. T. Bryant, and G. O. Pritchard, *J. Amer. Chem. Soc.*, **90**, 4782 (1968).

(2) (a) J. C. Hassler, and D. W. Setser, *J. Chem. Phys.*, **45**, 3246 (1966); (b) K. Dees and D. W. Setser, *ibid.*, **49**, 1193 (1968); (c) K. Dees, D. W. Setser, and W. G. Clark, *J. Phys. Chem.*, **75**, 2231 (1971); (d) W. G. Clark, D. W. Setser, and K. Dees, *J. Amer. Chem. Soc.*, **93**, 5328 (1971).

(3) J. C. Hassler and D. W. Setser, *J. Chem. Phys.* **45**, 3237 (1966). Some unidentified experimental error for the work of this reference resulted in faulty data for the 1,1,2-C₂H₃Cl₃ studies. The results for 1,1-C₂H₄Cl₂ are thought to be approximately correct.

(4) J. F. Harrison, *J. Amer. Chem. Soc.*, **93**, 4112 (1971).

(5) (a) C. L. Kibby and G. B. Kistiakowsky, *J. Phys. Chem.*, **70**, 126 (1966); (b) D. P. Chong and G. B. Kistiakowsky, *ibid.*, **68**, 1793 (1968); (c) A. W. Kirk and E. Tschuikow-Roux, *J. Chem. Phys.*, **51**, 2247 (1969).

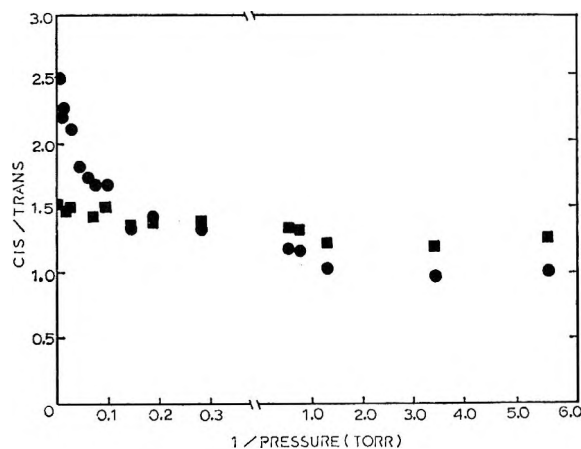


Figure 1. The *cis*-1,2-dichloroethene/*trans*-1,2-dichloroethene product yields as a function of pressure⁻¹. Key: ●, α,α process ($C_2H_2Cl_2$); ■, α,β process (C_2HDCl_2).

reaction. The threshold energy for *cis*-*trans* isomerization is 56 kcal,⁶ and the elimination of HCl is only 9.5 kcal mol⁻¹ endothermic.⁷ Thus, depending upon the energy partitioning pattern and upon the initial formation of nonequilibrium proportions of the *cis* and *trans* isomers, subsequent *cis*-*trans* isomerization may occur. The data are shown in Figure 1. The results from the α,α process are decisive and show that sufficient energy was retained for isomerization. Unfortunately the α,β process only slightly favors the *cis* isomer, in contrast to the α,α process which strongly favored the *cis* isomer. Furthermore the *cis*- C_2HDCl_2 only partially isomerized to the *trans*- C_2HDCl_2 which indicates that some of the molecules were formed with energies below 56 kcal mol⁻¹. These two features combine to give only a small change in the *cis*- C_2HDCl_2 /*trans*- C_2HDCl_2 ratio over the whole pressure range. The general conclusion is that the α,α process followed by rearrangement partitions a much larger fraction of the energy to the olefin than does the α,β process.

A quantitative fit of calculated rate constants to the experimental data for the isomerization of *cis*-CHCl-CHCl is shown in Figure 2. The calculated rate constants were obtained by combining the RRKM calculated⁸ *cis*-*trans* isomerization specific rate constants with an assumed energy distribution, which was obtained from the sum of statistical partitioning⁹ of *excess energy* between DCl and CH₂ClCCl plus the energy re-

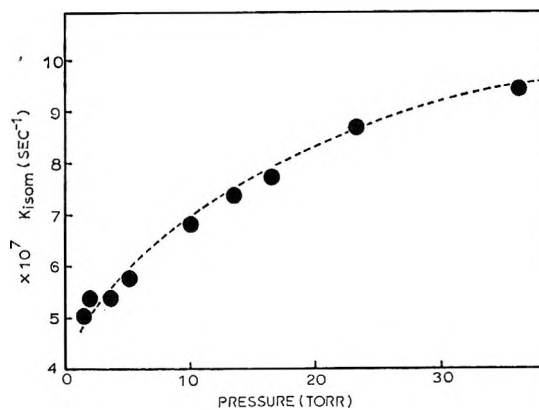


Figure 2. The experimental and calculated values of k_a (*cis*-*trans*) for *cis*- $C_2H_2Cl_2$ as a function of pressure. The broken line is the calculated curve.

leased by rearrangement of CH₂ClCCl to CHClCHCl. These data thus provide stronger evidence¹⁰ that the reverse of the α,α elimination reactions, *i.e.*, carbene + HCl, have nearly zero activation energy and that this unimolecular reaction partitioned the excess energy in a statistical manner.⁹ The energy partitioning pattern found for the α,β process is consistent with previous results.^{2b,10,11} Apparently $<2/3$ of the total available energy is released to the internal degrees of freedom of the olefin.

Acknowledgments. This work was supported by the National Science Foundation under Grants G.P.-27536X and -16743.

(6) L. D. Hawton and G. P. Semeluk, *Can. J. Chem.*, **44**, 2143 (1966).

(7) See reference 2c, P. Goldfinger and G. Martens, *Trans. Faraday Soc.*, **57**, 2220 (1961), and S. Furuyama, D. M. Golden, and S. W. Benson, *J. Amer. Chem. Soc.*, **91**, 7564 (1969) for summaries of the thermochemical data.

(8) See K. S. Pitzer and J. L. Hollenberg, *ibid.*, **76**, 1493 (1954) for fundamental frequencies used for the RRKM calculation of *cis*-*trans* isomerization.

(9) Y. N. Lin and B. S. Rabinovitch, *J. Phys. Chem.*, **74**, 1769 (1970).

(10) H. W. Chang, D. W. Setser, and M. J. Perona, *J. Phys. Chem.*, **75**, 2070 (1971).

(11) P. N. Clough, J. C. Polanyi, and R. T. Taguchi, *Can. J. Chem.*, **48**, 2919 (1970).

CHEMISTRY DEPARTMENT
KANSAS STATE UNIVERSITY
MANHATTAN, KANSAS 66502

K. C. KIM
D. W. SETSER

RECEIVED OCTOBER 29, 1971

Reprints from Chemical & Engineering News

On orders of \$10 or less please remit check or money order

Keeping broadly informed challenges every person today. If you missed these features from recent issues of C&EN, you can still get copies by filling in the coupon below.

Population

A 2-part feature
David M. Kiefer, C&EN
Oct. 7 & 14, 1968 **75¢**

Mr. Kiefer finds that population is growing unchecked in much of the world, and that U.S. population will expand 50% in the next 30 years or so. Social as well as technological innovation is needed to thwart this advance. **10148**

Computers in Chemical Education

Dr. Frederick D. Tabbutt
Reed College
Portland, Oregon
January 19, 1970 **50¢**

A number of experiments with computers in education have been undertaken in the past few years. Some of the approaches to computer-assisted education now show promise as useful adjuncts as surrogate teachers. **11970**

Arthritis

A 3-part feature
Howard J. Sanders, C&EN
July 22, 29, & Aug. 12, 1968 **75¢**

Causes of arthritis are still a mystery, although more and more evidence points to infection as a possible trigger. Mr. Sanders discusses and examines the possible causes and the past, present, and future of treatment. **07228**

Industrial Research Careers

Howard Reiss
University of California
Los Angeles
June 29, 1970 **50¢**

A major concern of those beginning careers in science is, of course, where to carry out their careers—in a university, private industry, a foundation or wherever. An industrial research career can be a rewarding one, both professionally and financially. **62970**

Public Policy and the Environment

February 9, 1970 **50¢**

Speaking at the 158th ACS National Meeting, Lee DuBridge, Herbert Doan, and Barry Commoner urged cooperation among government, industry, and university in tackling environmental improvement. **02970**

Pollution Control Instrumentation

Michael Heylin, C&EN
February 15, 1971 **50¢**

Efforts to control air and water resources intelligently depends on the ability to detect and to monitor pollutants. The challenge to produce better instrumentation for this purpose is now receiving intense attention from industry and government researchers. **21571**

Allergy

Howard J. Sanders, C&EN
May 11, 1970 **50¢**

Although hay fever, bronchial asthma, and other allergies will not be conquered, they will be better understood and better treated. The expanding study of these diseases in fundamental scientific terms, using the latest research techniques, allergic disorders will yield more and more of their secrets that only a few years ago seemed almost unfathomable. **51170**

Food Additives

Howard J. Sanders, C&EN
October 10, 1966 **75¢**

Makers of food additives are keeping their eyes on the spectacular growth of new foods and the shifting moods of regulation-minded Washington. An array of chemicals enhances the wholesomeness, attractiveness, convenience, and nutritional value of American foods. **10176**

Technology Assessment

David M. Kiefer, C&EN
October 5, 1970 **50¢**

Technology assessment is an attempt—still halting and uncertain—to establish an early-warning system to control, direct, and, if necessary, restrain technological development so as to maximize the public good while minimizing the public risks. **10570**

Chemistry and the Atmosphere

Howard J. Sanders, C&EN
March 28, 1966 **75¢**

The earth's atmosphere is a vast, churning mixture of gases and trace quantities of liquids and solids. Held to the earth by the pull of gravity, it is the transparent envelope without which life on earth would cease to exist. **32866**

Career Opportunities The New Priorities

March 8, 1971 **50¢**

C&EN's annual career guide for chemists and chemical engineers. In the search for new priorities, new opportunities are emerging. Here C&EN looks at three such areas—food, shelter, and health. **03871**

Chaos in Science Teaching

Dr. Conrad E. Ronneberg
Professor Emeritus, Denison University
June 1, 1970 **50¢**

To many people familiar with the situation in teaching introductory science courses, both in high school and college, the situation is utter chaos. To place attempts to improve science teaching in proper perspective requires a brief review of the progress of science teaching since World II. **06170**

Artificial Organs

A 2-part feature
Howard J. Sanders, C&EN
April 5 and 12, 1971 **75¢**

The implanting of a total artificial heart in a human has been the most dramatic single advance to date in the field of artificial organs. In recent years, however, many other artificial organs have also been developed, and scientists foresee a vast increase in the number of body parts that, in the years ahead, will be replaceable by mechanical devices. **04571**

Scientific Societies and Public Affairs

K. M. Reese, C&EN
May 3, 1971 **50¢**

Scientific and engineering societies for many years have fostered research, published papers, and sponsored meetings without great regard for the world beyond their particular disciplines. Only in the past decade or so have the learned societies edged into the realm of public affairs. **05371**

1 to 49 copies—single copy price 50 to 299 copies—20% discount

Prices for larger quantities available on request

<input type="checkbox"/>	<input type="checkbox"/>	<input type="checkbox"/>	
10148	11970	07228	
<input type="checkbox"/>	<input type="checkbox"/>	<input type="checkbox"/>	
62970	02970	51170	
<input type="checkbox"/>	<input type="checkbox"/>	<input type="checkbox"/>	<input type="checkbox"/>
21571	10176	10570	32866
<input type="checkbox"/>	<input type="checkbox"/>	<input type="checkbox"/>	<input type="checkbox"/>
03871	06170	04571	05371

TO: REPRINT DEPARTMENT

ACS Publications
1155 Sixteenth St., N.W.
Washington, D.C. 20036

FROM:

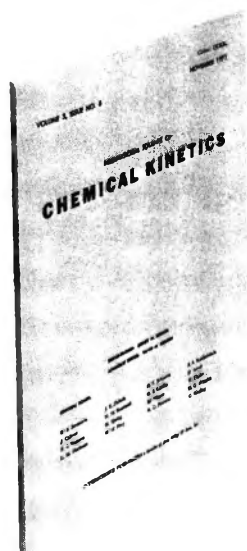
Name _____

Street _____

City _____

State _____ Zip Code _____

Amount enclosed \$ _____



INTERNATIONAL JOURNAL OF CHEMICAL KINETICS

Editor in Chief: Sidney W. Benson, *Stanford Research Institute*

Associate Editor: David Mark Golden, *Stanford Research Institute*

Editorial Board: R. B. Bernstein. J. Calvert. F. S. Dainton. L. M. Dorfman. N. M. Emanuel. H. Eyring. H. M. Frey. H. J. Johnston. K. J. Laidler. M. Magat. R. G. Pearson. B. S. Rabinovitch. H. Schiff. H. G. Wagner. C. Walling.

Here is a collection of research results and data from the field of chemical kinetics. Original research papers examine the quantitative relationship between molecular structure and chemical reactivity, covering areas in reaction mechanisms, inorganic, organic, and biochemical kinetics. The section on "Communications to the Editor" fea-

tures letters which report on preliminary results of immediate interest, information on new or unusual developments in related fields, and observations and comments on work reported in the journal. The wide scope of topics covered in each volume will inform scientists of the latest events in their own field of interest as well as in related fields.

A selection of forthcoming articles to be published in the International Journal of Chemical Kinetics—

- The Pyrolysis of Neopentane at Small Extents of Reaction—*F. Baronnet, M. Dzierzynski, G. M. Côme, R. Martin, and M. Niclause*
- Computer Simulation of Cage Processes and Some Difficulties with Present Models—*Cheves Walling and Arthur R. Lepley*
- Some Aspects of Theory and Experiment in the Ethane-Methyl Radical System—*E. V. Waage and B.S. Rabinovitch*
- Roatating Sector Study of the Gas-Phase Photolysis of the Carbon Tetrachloride-Cyclohexane System—*Merle L. White and Robert R. Kuntz*
- Chemically Activated 1,1-Dimethylcyclopropane from Photolysis of Isobutene-Neopentane-Diazomethane-Oxygen Mixtures—*G. W. Taylor and J. W. Simons*
- The Reactions Between SO_2 and C_2H_2 (and C_2H_4) at Elevated Temperatures: A Single-Pulse Shock Tube Investigation—*R. Fifer, R. Moreau, and S. H. Bauer*
- The Kinetics and Thermochemistry of the Gas-Phase Reaction of Cyclopentadiene and Iodine—

Shozo Furuyama, David M. Golden, and Sidney W. Benson

- On the Use of Activation Parameters as a Test for Concerted Decomposition of Initiators—*William A. Pryor and Kennedy Smith*
- Abstraction of Hydrogen by Methylene—*J. R. McNesby and R. V. Kelly*
- Quenching Cross Sections for the Deactivation of Metastable Mercury—*J. M. Campbell, S. Penzes, H. S. Sandhu, and O. P. Strausz*
- Reactions of HO_2 in the High Temperature Pyrolysis of H_2O_2 in Presence of H_2 —*H. Kijewski and J. Troe*

Volume III—Bimonthly
Subscription Price: \$20.00
Foreign Postage: \$2.00
Back volume prices on request

Department # 093-820

Available from your bookstore or from Dept. 093—

WILEY-INTERSCIENCE

a division of JOHN WILEY & SONS, Inc.
605 Third Avenue, New York, N.Y. 10016
In Canada: 22 Worcester Road, Rexdale, Ontario

wiley